

Spatio-temporal mRNA dynamics in Stress Granules and Processing Bodies

Inauguraldissertation

zur
Erlangung der Würde eines Doktors der Philosophie
vorgelegt der
Philosophisch-Naturwissenschaftlichen Fakultät
der Universität Basel

von

Johannes Wilbertz

aus Aachen, Deutschland

Basel, 2018

Genehmigt von der Philosophisch-Naturwissenschaftlichen Fakultät

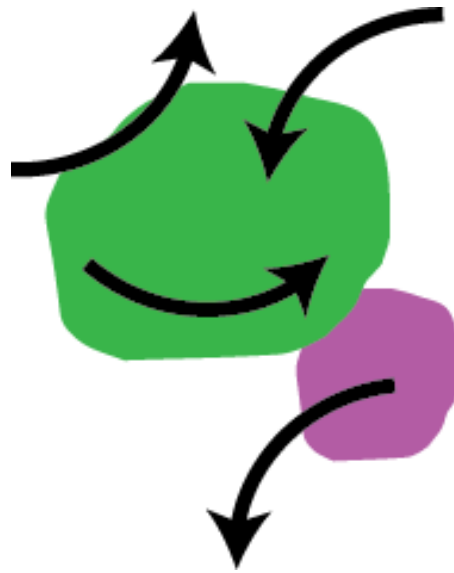
auf Antrag von

Prof. Dr. Susan Gasser, Dr. Jeffrey Chao, Dr. Georg Stoecklin

Basel, den 22.05.2018

Prof. Dr. Martin Spiess (Dekan)

Spatio-temporal mRNA dynamics in Stress Granules and Processing Bodies



Johannes Wilbertz

PhD Thesis

Supervised by Dr. Jeffrey Chao

Friedrich Miescher Institute for Biomedical Research, Basel, Switzerland

University of Basel, Switzerland

Basel, 2018

You can't say A is made of B
or vice versa.
All mass is interaction.

Richard Feynman

For my parents.

Table of contents

Thesis overview and contributions	6
Summary for non-biologists	8
Zusammenfassung für Nicht-Biologen	10
Chapter 1: mRNA localization & expression regulation during the cellular stress response	12
1.1 Gene expression regulation on the post-transcriptional level shapes the proteome	13
1.1.1 mRNA export	16
1.1.2 mRNA localization & transport	18
1.2 mRNA translation regulation	21
1.2.1 Canonical mRNA translation initiation	21
1.2.2 Non-canonical modes of translation initiation	25
1.2.3 The integrated stress response	35
1.2.4 Translational down-regulation during stress	40
1.2.5 Selective translation during stress	44
1.3 The dynamic nature of stress-induced mRNP granules	46
1.3.1 Translation initiation block and early SG formation	47
1.3.2 SG dynamics: Phase separation, docking and fusion	49
1.3.3 Disassembly of SGs	51
1.4 mRNP granules and localized mRNA biology	54
1.4.1 mRNA-centered evidence for translation regulation inside of mRNP granules	54
1.4.2 mRNA-centered evidence for mRNA decay inside of mRNP granules	56
1.4.3 mRNA-centered evidence for localization, storage and protection of mRNAs inside of mRNP granules	57
1.5 mRNP granules and disease	58
1.6 Functional mRNA dynamics during stress are unknown – an experimental approach	61

Chapter 2: Single-molecule RNA imaging in living cells reveals the function of stress granule and processing bodies during the integrated stress response	80
2.1 Introduction	81
2.2 Results	84
2.3 Summary and discussion	96
2.4 Material and methods	100
2.5 Supplementary figures	108
Chapter 3: Several small molecules negatively modulate stress granules and decrease cell viability	118
3.1 Introduction	119
3.2 Results	123
3.3 Summary and discussion	135
3.4 Material and methods	137
Chapter 4: mRNAs are translationally repressed inside of processing bodies during stress relief	144
Chapter 5: Protocol for single-molecule imaging with the TRICK translation biosensor	150
Chapter 6: Thesis summary and future research perspectives	186
Acknowledgements	192
Curriculum vitae	194

Thesis overview and contributions

Chapter 1 introduces post-transcriptional gene regulation and the composition, formation, dynamics and assumed functionality of stress-induced RNA-protein granules. Current research and insights are summarized and integrated into a testable working model. The scientific need for the application of single molecule RNA imaging in living cells to understand RNA-protein granule biology is highlighted.

Chapter 2 describes how *cis*-acting elements direct mRNA localization and how mRNA behave relative to stress-induced RNA-protein granules. Stress granules do not seem to be required for mRNA localization into processing bodies, although mRNA movement between the two is possible. The *trans*-acting protein factor LARP1 is identified as regulator of mRNA presence in stress-induced mRNPs and the effects of mRNA localization on translation and decay are tested. This chapter is a manuscript in preparation, deposited online on the bioRxiv pre-print server (doi: <https://doi.org/10.1101/332502>). I designed experiments for Fig. 1-6 and performed experiments and analyzed data for Fig. 1-4 and 6. I designed, performed experiments and analyzed data for all supplementary figures.

Chapter 3 summarizes findings of a screen utilizing a small molecule library with known mode-of-actions in order to identify molecules, which are able to negatively influence stress granule formation or stability. Several molecules were identified which do not affect eIF2 α -phosphorylation, processing body integrity or translation and uncouple stress granule presence from translation regulation. The identified molecules negatively affect cell viability, presumably through apoptosis upregulation. Being able to modulate stress granule presence might be interesting in a number of disease contexts. This chapter is a manuscript in preparation. I designed experiments for Fig. 2-9 and performed experiments for Fig. 2 and 4-9. I analyzed data for Fig. 2 and 4-8.

Chapter 4 focuses on the results obtained with an RNA-based biosensor to study the localization and the first round of translation of a single mRNA molecule inside of living cells (TRICK reporter) in different biological contexts. Relevant for this thesis is the finding that a subclass of mRNA molecules specifically localizes to processing bodies during the cellular stress response and remains translationally repressed there, even if translation in the surrounding cytoplasm is re-initiated. This work serves as an example for mRNP granule-modulated sub-cellular translation regulation. This chapter was published as an original research article with me as shared first author (Halstead et al., 2015). I performed experiments and analyzed data for Fig. 2, and participated in writing the paper.

Chapter 5 describes the design of a TRICK reporter. A protocol is provided to generate cell lines, which fulfill all requirements to perform RNA imaging. In addition, technical requirements and data analysis approaches are discussed. This chapter was published as methodological article with me as shared first author (Halstead et al., 2016). I co-wrote the article with a focus on the microscopy and data analysis sections.

Chapter 6 serves as a summary of the work described in this thesis and provides a refined working model, which describes mRNA localization during cellular stress. In addition, remaining open questions are discussed and potential experimental approaches to address these questions are presented.

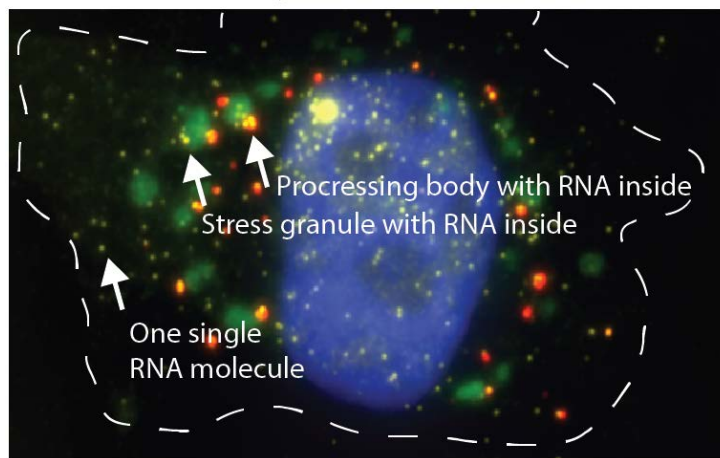
Summary for non-biologists

Every living organism consists of cells. All cells contain molecules that encode the building blocks of the cell. These molecules are called DNA and contain many genes. To retrieve this genetic information, a DNA molecule is converted into RNA molecules and RNA molecules are then TRANSLATED INTO PROTEINS. Proteins are the workhorses of the cell and perform most functions. However, one gene can give rise to many identical RNA molecules and even more proteins. This process is called GENE EXPRESSION. It has to be tightly controlled, because it is important for a cell to always have the right amount of proteins. Not too many and not too little. GENE EXPRESSION REGULATION becomes especially important when the environment of a cell changes, for example through heat, starvation, lack of oxygen, certain chemicals and many more things. Such a change of the environment is called CELLULAR STRESS. Cells need to adapt their GENE REGULATION during stress to survive. Sometimes, when the cell is very badly stressed, it can be better for the organism that some cells die so that other cells are protected. For example, when doctors treat a tumor using chemotherapy, this causes a lot of stress for the tumor cells with the aim that they die. To understand how cells change their GENE EXPRESSION during CELLULAR STRESS is therefore a very important question.

During the last few years I studied GENE EXPRESSION during CELLULAR STRESS. However, this is a very big field of science. I concentrated mainly on the question how RNA molecules are translated into proteins during CELLULAR STRESS. When cells encounter stress they often do two things. First, they stop to produce proteins from RNA molecules. Second, they form little clumps inside of themselves that contain RNA molecules and proteins. These clumps are called STRESS GRANULES and PROCESSING BODIES (picture below). Researchers do not understand very well how STRESS GRANULES and PROCESSING BODIES are connected to blocking translation of RNA into protein during periods of cell stress. For example, it is not clear where in a cell RNA molecules are blocked exactly and how this is regulated. Is RNA maybe blocked inside of STRESS GRANULES and PROCESSING BODIES during stress? Or do STRESS GRANULES and PROCESSING BODIES protect RNA so that it can be reused when the stress is over?

RNA molecules are very small. To study where RNA molecules are in a cell, how they move, and how they make proteins is not easy. You need very good microscopes and techniques to attach very bright other molecules to the RNA so that you can see them. You also need computer programs that help you to analyze if all the RNA molecules are inside or outside of STRESS GRANULES and PROCESSING BODIES. Together with other researchers, I used all of these techniques. I learned that when a cell is stressed some RNA molecules go into STRESS GRANULES and PROCESSING BODIES, but the translation of RNA into protein is off everywhere in the cell. It does not matter where the RNA is exactly. It gets more interesting when the cell recovers from the stress. Under such conditions, RNAs that are bound to PROCESSING BODIES cannot translate, but all RNAs outside can be translated into protein very well. I also observed that RNAs are still stable in the cell and that the cell does not get rid of them because they might be damaged.

This is a microscopy image of one human cancer cell



In summary, my work improved the knowledge about what RNA molecules do during cell stress and recovery from cell stress. Interestingly, I observed that not all RNA molecules are always inside of STRESS GRANULES and PROCESSING BODIES (picture). Does that mean that STRESS GRANULES and PROCESSING BODIES also have another role for some other processes that we do not know about? I did all of my experiments in human cancer cells, but STRESS GRANULES and PROCESSING BODIES have also been observed in nerve cells of patients with serious neurological diseases. What exactly do they do there? In science, answering one questions always leads to many more.

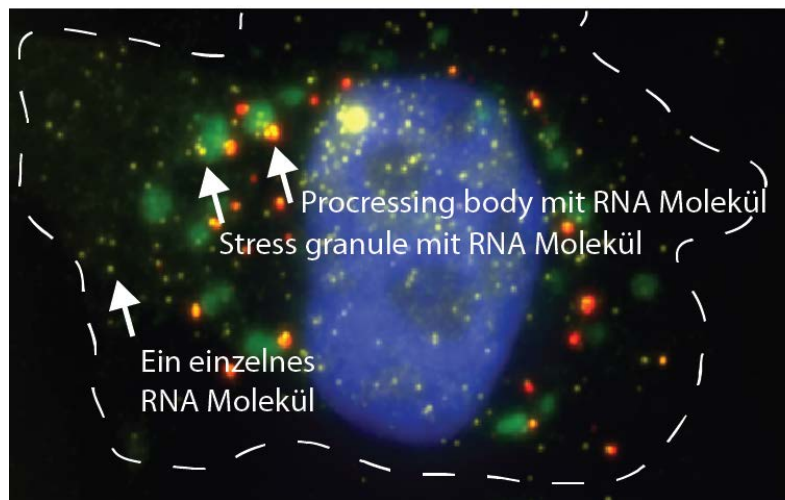
Zusammenfassung für Nicht-Biologen

Jeder lebende Organismus besteht aus Zellen. Alle Zellen enthalten Moleküle, welche die Baupläne der Zelle enthalten. Diese Moleküle heißen DNA und enthalten viele Gene. Um diese genetischen Information zu erhalten, werden DNA-Moleküle in RNA-Moleküle umgewandelt. RNA-Moleküle werden dann in Proteinen übersetzt. Proteine sind die Arbeiter der Zelle und erfüllen viele Aufgaben. Ein Gen kann jedoch viele identische RNA-Moleküle und noch mehr Proteine erzeugen. Dieser Prozess wird GENEXPRESSION genannt. Er muss streng kontrolliert werden, weil es für eine Zelle wichtig ist, immer die richtige Menge an Proteinen zu haben. Nicht zu viele und nicht zu wenige. Die Regulation der GENEXPRESSION ist besonders wichtig, wenn sich die Umgebung einer Zelle ändert, zum Beispiel durch Hitze, zu wenige Nährstoffe, Sauerstoffmangel, bestimmte Chemikalien und vieles mehr. Eine solche Veränderung der Umwelt wird ZELLSTRESS genannt. Zellen müssen ihre GENEXPRESSION während des Stresses anpassen, um zu überleben. Manchmal, wenn eine Zelle sehr stark gestresst ist, kann es für den Organismus besser sein, dass einige Zellen sterben, sodass andere Zellen geschützt werden. Zum Beispiel, wenn Ärzte einen Tumor mit Chemotherapie behandeln, verursacht dies natürlich eine große Belastung für die Tumorzellen mit dem Ziel, dass sie absterben. Zu verstehen, wie Zellen ihre GENEXPRESSION während ZELLSTRESS verändern, ist daher eine sehr wichtige Frage.

In den letzten Jahren habe ich die GENEXPRESSION während ZELLSTRESS untersucht. Dies ist jedoch ein sehr großes Feld der Wissenschaft. Ich konzentrierte mich daher hauptsächlich auf die Frage, wie RNA-Moleküle während ZELLSTRESS in Proteine übersetzt werden. Gestresste Zellen tun oft zwei Dinge: Zuerst hören sie auf, Proteine aus RNA-Molekülen zu produzieren. Zweitens klumpen RNA-Moleküle und Proteine zusammen. Diese Klumpen heißen STRESS GRANULES und PROCESSING BODIES (siehe Bild unten). Wir verstehen im Moment nicht gut, wie STRESS GRANULES und PROCESSING BODIES mit der Blockierung der Übersetzung von RNA in Protein während Zellstress verbunden sind. Zum Beispiel ist nicht klar, wo in einer Zelle RNA-Moleküle genau blockiert und wie dies reguliert wird. Kann RNA direkt innerhalb von STRESS GRANULES und PROCESSING BODIES blockiert sein? Oder schützen STRESS GRANULES und PROCESSING BODIES die RNA, damit sie nach dem Stress wieder verwendet werden kann?

RNA-Moleküle sind sehr klein. Es ist nicht einfach zu untersuchen, wo sich RNA-Moleküle in einer Zelle befinden, wie sie sich bewegen und wie sie Proteine bilden. Man benötigt sehr gute Mikroskope und Techniken, um sehr helle andere Moleküle an die RNA zu binden, sodass man die RNA sehen kann. Man benötigt außerdem Computerprogramme, mit denen man analysieren kann, ob sich alle RNA-Moleküle innerhalb oder außerhalb von STRESS GRANULES und PROCESSING BODIES befinden. Zusammen mit anderen Forschern habe ich all diese Techniken genutzt. Ich habe herausgefunden, dass in einer gestressten Zelle, einige RNA Moleküle in STRESS GRANULES und PROCESSING BODIES wandern, aber die Übersetzung von RNA in Protein überall in der Zelle blockiert ist. Dafür spielt es keine Rolle, wo genau die RNA ist. Es wird interessanter, wenn sich die Zelle vom Stress erholt. Unter solchen Bedingungen können RNAs, die in PROCESSING BODIES gebunden sind, nicht in Protein übersetzt werden, aber alle RNAs außerhalb können das sehr wohl. Ich habe auch beobachtet, dass RNAs in der Zelle nach dem Stress immer noch stabil sind und, dass die Zelle sie nicht los werden will, weil sie anscheinend nicht beschädigt sind.

Mikroskopische Aufnahme einer menschlichen Krebszelle



Zusammengefasst, verbesserte meine Arbeit das Wissen darüber, was RNA-Moleküle während des Zellstress und der Erholung von Zellstress genau machen. Interessanterweise beobachtete ich, dass nicht alle RNA-Moleküle sich immer in STRESS GRANULES und PROCESSING BODIES befinden (siehe Bild oben). Bedeutet dies nun, dass STRESS GRANULES und PROCESSING BODIES auch eine Bedeutung für andere Prozesse haben, von denen wir noch nichts wissen? Ich habe alle meine Experimente in menschlichen Krebszellen durchgeführt, aber STRESS GRANULES und PROCESSING BODIES wurden auch in Nervenzellen von Patienten mit schweren neurologischen Erkrankungen beobachtet. Was machen sie da genau? In der Wissenschaft führt die Beantwortung einer Frage immer zu vielen neuen Fragen.

Chapter 1: mRNA localization & expression regulation during the cellular stress response

This chapter introduces post-transcriptional gene regulation with a focus on translation in absence and presence of stress. Further, the composition, formation, dynamics and assumed functionality of stress-induced mRNP granules are described. Current research and models explaining how cells react to stress are summarized. This chapter concludes with a working model addressing unresolved questions concerning mRNA dynamics and regulation during the stress response. The scientific need for the application of single molecule RNA imaging in living cells to understand mRNP granule biology is highlighted.

1.1 Gene expression regulation on the post-transcriptional level shapes the proteome

The expression of a gene from its DNA template into the final non-coding RNA or protein product is highly variable. Differentiated cell types are defined by their gene expression profiles, while at the same time gene expression can change drastically during certain biological processes for example stem cell differentiation, in response to environmental stimuli, such as a viral infection, or disease states, for example in tumor cells. The compartmentalization of eukaryotic cells into a nucleus and a cytoplasm allows gene expression to be regulated on several levels since certain proteins and their catalytic processes are localized to specific locations within the cell. As a result, a high degree of gene expression specificity and plasticity occurring at the same time can be achieved.

In the nucleus gene expression regulation is achieved on the (pre-)transcriptional level. DNA packaging and modifications determine the accessibility of a gene to transcription factors and enhancers, while their interplay in combination with other proteins such as RNA polymerase II define the kinetics of transcription initiation and transcript elongation. In addition, co-transcriptional splicing and alternative splicing of the pre-mRNA occurs in the nucleus and gives rise to product variability originating from a single gene.

Without doubt, gene expression regulation on the transcriptional level is essential for life and is highly regulated. Despite this, there is evidence that the correlation between mRNA and protein abundance is often poor. These observations imply that post-transcriptional gene expression regulation is an important mechanism to control biological processes and to specify cell identities. Early work by Aebersold and colleagues concentrated on the correlation between protein and mRNA abundance in yeast by comparing mass-spectrometry data to the yeast transcriptome. In total, the authors compared the expression levels of 106 genes and found Pearson correlations between 0.935 and 0.356, depending on whether the mRNA transcripts were expressed at high or low copy numbers, respectively (Gygi et al., 1999).

Schwanhäusser *et al.* measured absolute mRNA and protein abundance and turnover by parallel metabolic pulse labelling for more than 5,000 genes in mouse fibroblasts. They found that protein and mRNA half-lives are not correlated ($R^2 = 0.02$) while mRNA copies and protein copies only correlate poorly ($R^2 = 0.41$). This especially seemed to be the case for mRNAs expressed with less than 100 copies

per cell. Using a modelling approach they conclude that protein levels are best explained by translation rates, followed by transcription rates, mRNA degradation rates and protein degradation rates (Schwanhäusser et al., 2011).

A study by Grün *et al.* quantifying mRNA and protein levels during the development of two evolutionary distant nematode species identified a high degree of correlation variability between transcript and protein abundances. Pearson correlation was highest during the embryonic-larval stage transition (0.41). Very weak correlation was observed during all subsequent larval transitions (0.03-0.11) and subsequently increased to a modest correlation of 0.3 during the late L4/young adult stage. The authors conclude that, except for the embryonic stage, strong positive and negative transcript expression changes are dampened by posttranscriptional regulation (Grün et al., 2014). Comparing mRNA abundance to ribosome profiling data during the L1 larval stage Stadler & Fire narrowed the posttranscriptional regulation mechanism responsible for the poor correlations down to mRNA translation (Stadler and Fire, 2013) confirming both the conclusions of the above described studies of Grün *et al.* and Schwanhäusser *et al.*

Taken together, the evidence obtained by the studies described above and several others, points into the direction that mRNAs itself are highly regulated. RNA export, transport and localization, mRNA stability and decay, and translation regulation all contribute to post-transcriptional gene expression (Fig. 1). All of these processes add a significant regulative layer on top of transcriptional control. Except for mRNA export, most post-transcriptional gene expression regulation occurs in the cytoplasmic compartment, highlighting the importance of compartmentalization for fundamental biological processes (Fig. 1). A good example for the high degree of interconnection between the different steps of post-transcriptional regulation is the *Saccharomyces cerevisiae* ASH1 mRNA. While still in the nucleus, the locosome complex forms on the ASH1 transcript. The proteins Puf6 and She2 bind already co-transcriptional to ASH1 (Gu et al., 2004; Shahbadian et al., 2014) while nuclear pore protein Nup60 binds during export (Powrie et al., 2011). In the cytoplasm, these and other locosome proteins are then required to bring the ASH1 mRNA to the bud tip via directed transport (see section 1.1.2) while keeping it translationally silent. In the newly forming daughter cell, ASH1 translates and plays an important role during the inhibition of mating type switching. Like all mRNAs, ASH1 is eventually degraded.

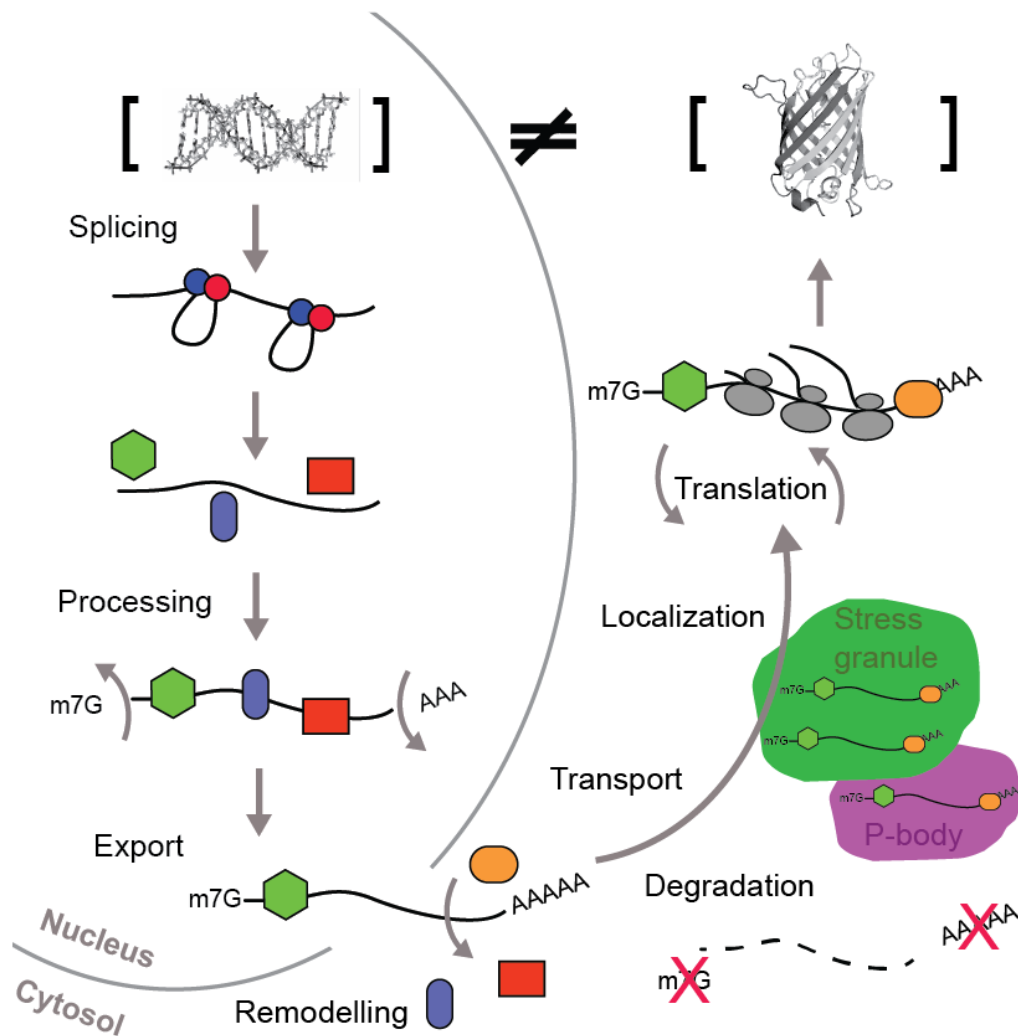


Fig. 1: Gene expression is regulated through the compartmentalization of the RNA lifecycle. Transcribed genes are immediately bound by RNA-binding proteins (RBPs) depending on the presence of *cis*-acting elements and spliced. The nuclear RNA interactome can be remodeled and RNAs undergo processing including the addition of a cap to 5'-end and a poly(A) tail to the 3'-end. Neither translation nor decay occurs in the nucleus. The nuclear RNA interactome determines how efficiently RNAs are exported. In the cytoplasm the RNA interactome is remodeled again and determines the rate at which RNAs are degraded, transported, localized and translated. To what extent transport and localization are coupled with translation and decay is an important question in cell and RNA biology. This PhD thesis addresses localization effects on RNA regulation.

RNA export, transport and localization, as well as translation regulation are introduced in the first part of this introductory chapter. mRNA decay along with transcription and nuclear export, is the third determinant of transcript abundance in the cytoplasm (Fig. 1), but will not be specifically introduced here. Instead, mRNA stability is the focus of section 1.4.2 dealing with the debated role of mRNP complexes for mRNA decay. Nonetheless, mRNA stability is crucial for post-transcriptional gene

expression. Increasing evidence points into the direction that translation and decay are coupled processes (Pelechano et al., 2015). Possible mechanisms involve codon bias or a direct binding of decay factors to the ribosome. Codon bias can lead to decreased elongation rates and slowly moving ribosomes might be more prone to the binding of proteins such as yeast Dhh1 which can trigger mRNA decay (Hanson and Collier, 2018). In addition, the cryo-EM based observation of a direct interaction between the Ski-complex and the elongation competent 80S ribosome provides a mechanistic explanation for the coupling of translation and mRNA decay. In particular, the Conti laboratory observed that mRNA 3'-ends exiting the 40S ribosomal subunit can directly enter the helicase channel of Ski2 (Schmidt et al., 2016). The Ski complex is a known exosome binding partner. Although not formally demonstrated, their interaction on the 80S ribosome could be a mechanistic explanation for the observed 3'-5' mRNA degradation during translation. At present, it is not clear how these observations fit into the picture of anti-correlated translation and decay rates.

All post-transcriptional processes play important roles during the life of an mRNA molecule and offer regulative potential during changing conditions, such as biological, chemical, or physical stresses that a cell may face. In this PhD thesis, especially research describing mRNA localization and translation regulation during the eukaryotic stress response is described.

1.1.1 mRNA export

An mRNA is bound by a plethora of protein factors representing the current stage of its life. Increasing evidence indicates that the formation of mRNP complexes immediately after transcription already shapes the fate of an mRNA with regard to its export efficiency, localization, and eventually translation and degradation (Wickramasinghe and Laskey, 2015).

The mRNA interactome forms for the first time when a nascent transcript is spliced and the exon junction complex (EJC) is deposited upstream of the splice site. The EJC serves as scaffold for serine and arginine-rich (SR) proteins and the transcription export complex (TREX) together forming a mature mRNP complex (Singh et al., 2012). At the same time poly(A) binding proteins (PABPs) can access the poly(A)-tail, which especially seems to regulate export during the stress response (details see below). Next, an export-competent mRNP is formed by the binding of nuclear export factor 1 (NXF1) and its cofactor p15. The transport of the export-competent mRNP from the site of transcription to the nuclear

periphery is the rate-limiting step of mRNA export and requires several minutes in metazoan cells. Once the NXF1-p15 dimer of the mRNP complex can directly interact with nuclear pore complex (NPC) components the actual mRNA export occurs (Bachi et al., 2000; Fribourg et al., 2001; Grant et al., 2002). Interestingly, this step is not rate limiting and occurs in less than 500ms. Single molecule mRNA imaging was crucial to obtain this knowledge (Grünwald and Singer, 2010; Mor et al., 2010; Siebrasse et al., 2012). Next to this canonical export mechanism, several selective mRNA export factors exist which are required for the export of subsets of mRNAs involved in several biological processes making mRNA export an important post-transcriptional gene expression regulatory step. Selective export to control gene expression involves transcripts such as RAD51 or CHEK1 playing a role in genome duplication and repair and is regulated through the interaction of the ALY or IPMK proteins with TREX (Wickramasinghe et al., 2013). Interaction of THOC2 or THOC5 with TREX influences the export rates of NANOG, SOX2, and KLF4 mRNAs and therefore plays an important role for the maintenance of pluripotency (Wang et al., 2013). Other biological processes influenced by selective mRNA export are translation (RPS23 mRNA), cell proliferation and survival (cyclin D1 and Myc mRNAs), and the immune response (MHCI, MHCII, CDK6 mRNAs) (Wickramasinghe and Laskey, 2015).

Next to regulation the biological processes described above, mRNA export is also an important post-transcriptional regulation step during the cell's response to stress. Early work describes this mechanism in *Saccharomyces cerevisiae* during heat shock or membrane insult by ethanol (Saavedra et al., 1996). By *in situ hybridization* the authors show that most poly(A)⁺ mRNAs are retained within the nucleus, while the heat-inducible mRNAs SSA1 and SSA4 can still be exported. Expressing other mRNAs from the heat inducible SSA4 promoter was not sufficient for export, while cloning sequences from the 5' and 3' parts of SSA4 was sufficient to generate export competent mRNAs during heat shock. While it is still under debate how stress-responsive transcripts are specifically exported during the stress response, it is becoming clearer how the remaining transcripts are retained in the nucleus during stress. The nucleocytoplasmic shuttling protein poly(A)-binding protein 1 (PABP1) is known to accumulate in the nucleus during heat shock, UV irradiation or viral infection (Burgess et al., 2011; Harb et al., 2008; Ma et al., 2009) and seems to be responsible for mRNA retention (Kumar and Glaunsinger, 2010). Recent work in human cell lines shed more light on the transcript retention mechanism during nutrient starvation (Shan et al., 2017). The authors describe a nutrient sensing cascade involving the kinase AMPK activating SIRT1 which then deacetylates the nucleus-enriched PABP1 leading to its dissociation from poly(A)-tails. As a result, the PABP1-depleted transcripts seem to be export incompetent during stress which in turn reduces translation rates and conserves energy.

Under non-stress conditions and after the successful export from the nucleus, mRNPs are remodeled on the cytoplasmic face of the NPC by the ATP-dependent RNA helicase DBP5 and its cofactors. Rapid remodeling prevents re-entry into the nucleus and allows the mRNA to bind factors allowing immediate translation or transport.

1.1.2 mRNA localization & transport

The advent of subcellular mRNA imaging technologies through *in situ hybridization* in the 1980s (Akam, 1983) and in the late 1990s through live cell imaging (Bertrand et al., 1998) made it possible to study mRNA localization beyond nuclear/cytoplasmic fractionation experiments. Biological processes in which mRNA localization has been found to play a crucial role include axonal and dendrite plasticity, embryonic patterning, cell polarization and asymmetric division (Buxbaum et al., 2015; Jung et al., 2012; Medioni et al., 2012). Indications that these and probably more biological processes are connected to mRNA localization also in a single organism comes from a study by Lécuyer *et al.* in *Drosophila* embryos (Lécuyer et al., 2007). Of 2314 transcripts analyzed by *in situ hybridization*, more than 70% revealed a distinct localization pattern, making it highly likely that at least in *Drosophila* mRNA localization plays a role in almost every biological process.

Linked to the mRNA localization is the question how mRNAs can locally concentrate in a non-random manner to fulfill tasks such as for example local translation. Next to localized protection from degradation and diffusion-coupled local entrapment, the directed transport along a polarized cytoskeleton is an important mechanism to localize transcripts (Medioni et al., 2012). One of the longest cells in the human body is the sciatic nerve. It spans about one meter from the posterior end of the spine to the big toe. Equation (1) can be used to approximately calculate the diffusing time t of a molecule over a distance x with diffusion coefficient D .

Equation (1)
$$t \approx \frac{x^2}{2D}$$

Assuming for simplicity reasons that diffusion occurs only in one dimension, the neuron's nucleus and the most distant synapse in the toe are 1 meter apart, and that the mRNA molecule is diffusing with fast $1 \mu\text{m}^2/\text{s}$ it would need almost 16,000 years to reach the synapse. Transporting mRNA as cargo in a directed manner is therefore highly favorable over diffusion as soon as cells have a polarized structure and distances of $100\mu\text{m}$ or more are present. Further, the specific localization of

mRNAs rather than proteins has several advantages (Medioni et al., 2012): First, transport costs are reduced since one mRNA can be the template for several proteins. Second, mRNA localization prevents protein activity at inappropriate sites before the destination is reached. Third, local translation aids the formation of high local protein concentrations, which can lead to the formation of macromolecular complexes or phase separations. Fourth, mRNA localization contributes to gene expression in a spatio-temporal manner. For example, different splice variants of the same gene can be localized differently or localized translation can be activated through biochemical signals such as during fertilization, the release of guiding cues or neurotransmitters (Besse and Ephrussi, 2008).

Most molecular details of the mRNA transport process stem from work on *Saccharomyces cerevisiae* ASH1 mRNA. During cell division ASH1 mRNA localizes to the bud tip of the daughter cell (Bertrand et al., 1998) where its protein product represses the transcription of the homothallic switching (HO) endonuclease. Consequently, mating type switching is inhibited in the daughter cell, but not the mother cell due to the lack of ASH1 mRNAs (Long et al., 1997; Takizawa et al., 1997). Both *cis*- and *trans*-acting factors have been identified. The *cis*-acting elements within the ASH1 mRNA are also known as “zipcodes” and are all sufficient to specifically localize reporter mRNAs. One zipcode is present in the 3'UTR while three more have been identified in the coding region (Chartrand et al., 1999). Except for a CGA-base triplet, surprisingly little sequence consensus can be found between the four zipcodes (Olivier et al., 2005). Despite this, secondary structure predictions of all four zip-code elements indicate the presence of stem loops (Chartrand et al., 1999; Niedner et al., 2014). The two proteins She2 and She3 act in *trans* to control ASH1 localization. She2p is able to bind each zipcode and requires She3p as an adaptor to bind to the myosin motor protein Myo4p (Böhl et al., 2000), which then transports the ASH1 cargo along the actin skeleton to its destination in the bud tip.

Another well-studied case of mRNA transport is β -actin transport into cellular filopodia. β -actin contains a 54-nt *cis*-acting element zipcode in the 3'UTR, immediately adjacent to the stop codon. This RNA element is both necessary and sufficient for β -actin transport (Kislauskis et al., 1994), when bound to the *trans*-acting zipcode binding protein 1 (ZBP1). ZBP1 contains six RNA-binding domains (two RNA recognition motifs (RRMs) and four hnRNP K-homology (KH) domains) (Nielsen et al., 1999), of which the KH3 and KH4 didomain binds directly to the spacer-dependent recognition elements within the zipcode (Chao et al., 2010; Nicastro et al., 2017). ZBP1 associates with β -actin in the perinuclear space and orchestrates mRNA movement to the leading cell edge. This directed transport process is likely achieved by the microtubule motor KIF11 in a ZBP1-dependent manner (Song et al., 2015). Importantly, the β -actin mRNP is kept translationally silent during transport. Only at its destination, Src kinase

phosphorylates the Tyr₃₉₆ residue of ZBP1 causing its release from β -actin and allowing translation in fibroblasts (Hüttelmaier et al., 2005) and by a presumably similar mechanism in hippocampal neurons (Wu et al., 2015). The resulting local increase in β -actin concentration causes actin polymerization and leads to cellular remodeling and migration, while a loss of ZBP1 can lead to impaired filopodia formation, an aberrant cytoplasm, and weakened cell adhesion (Vikesaa et al., 2006).

The extensive molecular details of the *cis*- and *trans*-acting factors controlling ASH1 and β -actin biology, have made both genes *bonna fide* examples for mRNA transport. Despite this, the transport of other mRNAs might function differently. Especially, a lack of known *cis*-acting localization elements impairs studying mRNA transport. Common sequence elements even of mRNAs localizing to the same cellular destination are difficult to identify. This might be due to the challenges to accurately predict RNA structures or the possibility that mRNAs contain several *cis*-acting elements which are redundant or can function differently in combination with so far unknown *trans*-acting adaptor proteins (Medioni et al., 2012). The concept of sequence-based zipcodes which universally “address” different mRNAs to the same cellular location might therefore be an oversimplification.

Distinct mRNA localization patterns have also been observed during the response to stress. This often correlates with altered gene expression and has been observed in many different eukaryotic organisms ranging from yeast during nutrient deprivation to human tumors during chemotherapeutic treatment and protein aggregation-related neurological diseases (see section 1.5). Since the regulation and biological function of mRNA localization during the stress response is still not well understood and both constitute the main research questions of this PhD thesis, these aspects of mRNA biology are discussed in more detail in section 1.4.

1.2 mRNA translation regulation

1.2.1 Canonical mRNA translation initiation

The translation process is the most energy demanding cellular process. Approximately 30% of the energy consumption of a differentiating mammalian cell and 50% of a rapidly growing bacterial cell can be attributed to translation (Buttgereit and Brand, 1995; Russell and Cook, 1995). This energy demand is mainly due to the hydrolysis of several molecules of GTP and ATP per translation initiation event, during ribosome displacement on the mRNA and tRNA incorporation, as well as polypeptide release during translation termination (Leibovitch and Topisirovic, 2018), but also due to tRNA synthase activity. Cap- and ribosome scanning-dependent translation initiation at AUG start codons is the most efficient way eukaryotic cells produce peptides and seems to account for most proteins present in a cell at a given time (Ingolia et al., 2011; Kears and Wilusz, 2017). The molecular details of canonical eukaryotic mRNA translation are important in order to understand alternative modes of translation that can occur during biological processes such as mitosis or the stress response. These alternative modes of translation are introduced in section 1.2.2.

Initiation

Most cap-dependent translation occurs through ribosomal scanning from the cap through the 5'UTR to the first start codon (Hinnebusch, 2014). Scanning requires formation of the 43S pre-initiation complex (PIC) (Fig. 2). The 43S PIC contains the following three components: the small 40S ribosomal subunit, eukaryotic translation initiation factors (eIF) 1, 3, 5, and the ternary complex (TC) which is composed of eIF2-GTP and tRNA^{Met}. The 43S PIC is recruited to the mRNA by the eIF4F cap-binding complex (Fig. 2). eIF4F consists of eIF4A (DEAD box helicase), eIF4E (cap-binding protein), and eIF4G (scaffold connecting eIF4A and E). The interaction of eIF4F and 43S PIC allows the newly formed 48S PIC complex to undergo scanning (Fig. 2). eIF4E is left behind at the mRNA cap.

Secondary structures in the mRNA 5'UTR have to be removed during scanning. This is achieved by the scanning 48S PIC component eIF4A at the expense of ATP. Upon binding to the start codon, eIF2-GTP becomes hydrolyzed causing its own dissociation and in addition the release of eIF1, 3 and 5. eIF2-GDP is then recycled by eIF2B. Next, the large 60S ribosomal subunit can bind to the previously scanning 40S subunit, a process that is stimulated by eIF5B-GTP (Fig. 2). In a final step, the 60S-bound eIF5B-GTP is

hydrolyzed and released. The 40S and 60S subunits remain on the mRNA and together form the elongation competent 80S ribosome (Fig. 2). In total this eukaryotic mode of translation initiation requires two GTPs for TC recycling and 80S ribosome formation and one ATP for mRNA activation through the eIF4F complex (Leibovitch and Topisirovic, 2018). mRNAs that are packaged into larger mRNPs and contain more secondary structures in their 5'UTR require several rounds of activation through eIF4F which is more energy demanding (Merrick, 2015).

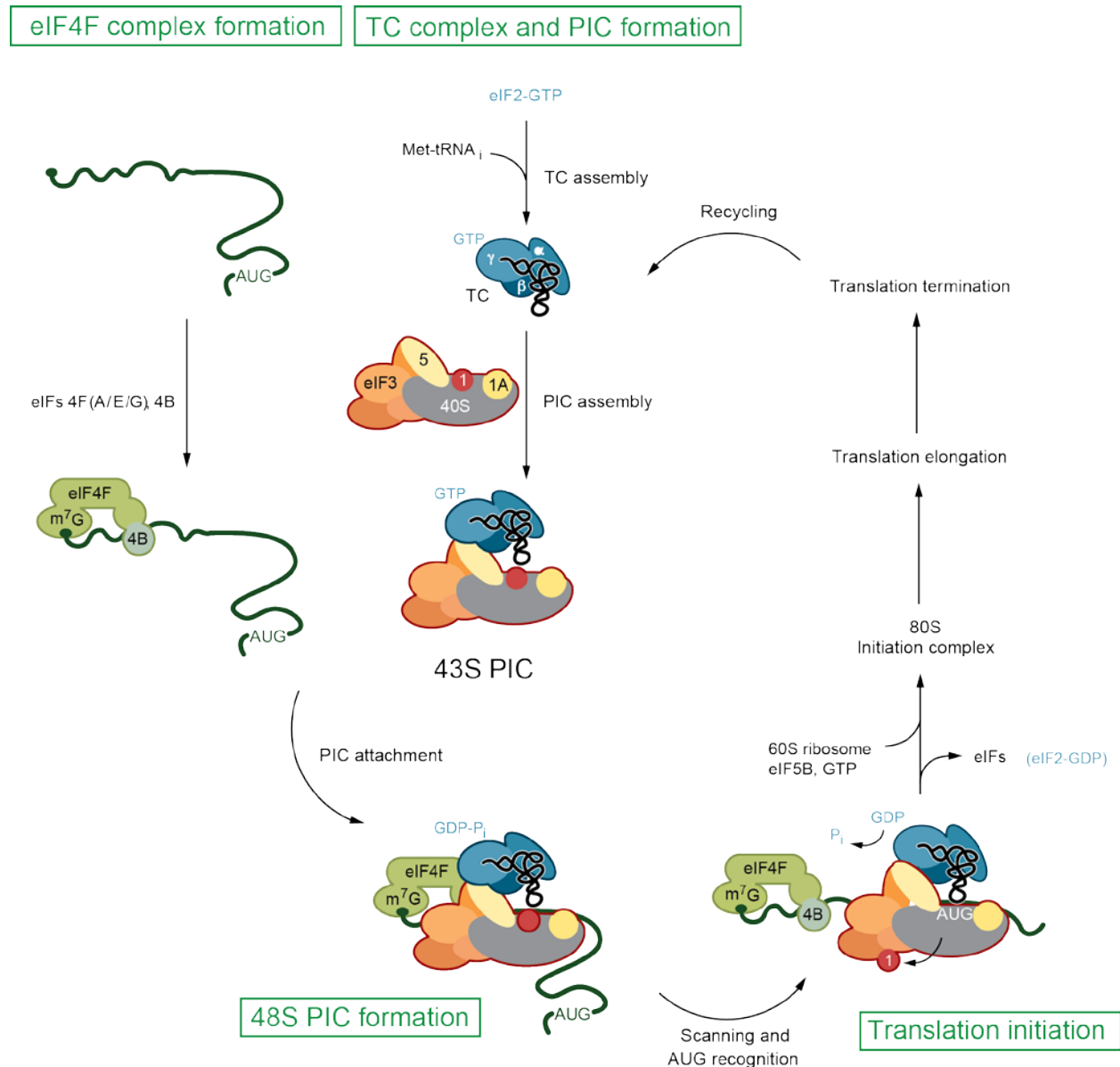


Fig. 2: Canonical mRNA translation initiation depends on protein binding to the RNA cap, pre-initiation complex (PIC) formation and scanning for the first start codon. mRNA is bound by the eIF4F complex (eIFs A/E/G) on its 5'-cap structure. In parallel, eIF2-GTP and tRNA^{Met} form the ternary complex (TC), and bind to the small 40S ribosomal subunit together with eIFs

1, 3, and 5. The assembled 43S PIC can now bind to eIF4F on the mRNA, forming the 48S complex. Secondary mRNA structures are removed and the 43S complex initiates scanning. Scanning stops once the 43S PIC binds to a start codon. The large 60S ribosomal subunit joins the 48S PIC, eIFs are remodeled and the elongation-competent 80S ribosomal complex forms. The initiation process is followed by elongation, termination and recycling. Non-canonical translation often does not require a cap-structure or relies on “leaky” scanning of the 43S complex to reach secondary open reading frames downstream of the first start codon (scheme uses graphical elements from Hinnebusch et al., 2016)).

Elongation

In eukaryotes elongation of the first methionine and all subsequent amino acids located at the ribosomal P-site starts when eukaryotic elongation factor (eEF) 1A-GTP delivers the next amino-acyl tRNA to the ribosomal A-site. Once the correct codon is recognized, eEF1B hydrolyzes the eEF1A bound GTP and a new peptide bond is formed. eEF1A and 1B are then released from the ribosome (Dever and Green, 2012).

Ribosome translocation to the next codon is mediated by eEF2 and is GTP dependent. Translocation frees the A-site and moves the uncharged tRNA from the P-site to the E-site where it dissociates. The tRNA is recycled by the amino acyl synthetase complex which requires two steps of ATP hydrolysis to AMP (Dever and Green, 2012). Elongation is by far the most energy-demanding step during translation, requiring the equivalent of two ATPs and two GTPs per incorporated amino acid. From an evolutionary perspective, it is therefore not surprising that most translation regulation occurs at the initiation step before elongation begins.

Termination & Recycling

Release of the nascent polypeptide chain occurs when the ribosome reaches the end of the coding sequence and a stop codon enters the A-site. Eukaryotic release factors (eRF) 1 and 3 catalyze this termination process. At its N-terminus eRF1 has a tRNA-like shape which can recognize stop codons through a mechanism similar to codon:anticodon interactions (Song et al., 2000). The eRF1 C-terminus can interact with the second release factor eRF3-GTP (Merkulova et al., 1999). eRF3 accelerates peptide release and increases termination efficiency in a GTP-dependent manner, although its exact functioning is not entirely understood (Dever and Green, 2012). Together both release factors form the eRF1:eRF3:GTP ternary complex. Only when the termination ternary complex is present within the ribosomal A-site, eRF1-stimulated GTP hydrolysis can occur (Alkalaeva et al., 2006). GTP hydrolysis leads to the dissociation of eRF3-GDP and allows the binding of ABCE1 to the remaining eRF1. eRF1 then stimulates hydrolysis of the peptidyl tRNA present in the P-site causing the release of the peptide chain from the ribosome (Dever and Green, 2012).

The release of the peptide chain is coupled to the first step of ribosome recycling, where the 80S ribosome is separated into the 60S subunit and the 40S subunit still bound to deacylated tRNA and mRNA. This process is likely mediated by eRF1-bound ABCE1 in an ATP dependent manner involving two hydrolysis steps (Pisarev et al., 2010; Young et al., 2015). The remaining 40S-tRNA-mRNA complex is then further recycled by eIF1 and eIF3 so that the free 40S subunit becomes available again to form the 43S preinitiation complex for the next round of translation (Pisarev et al., 2007). In addition, recent work has shown that ABCE1 remains bound to the 40S subunit and might facilitate downstream translation initiation (Simonetti et al., 2016). This likely occurs through the formation of a novel preinitiation complex containing the initiation factors eIF2 and eIF3, the 40S ribosomal subunit and ABCE1-AMP (Heuer et al., 2017). Recycling and subsequent initiation are therefore highly coordinated processes.

In total, each translation termination and recycling event in a eukaryotic cell requires the equivalent of one GTP and two ATPs. Together with a comparable energy demand for each initiation event and the enormous energy requirements during elongation, it is evident that cells benefit from translational down regulation in situations during which nutrients are limited or catabolic processes are inhibited.

Importantly, this energy demand does not yet include the energy costs for the biosynthesis of amino acids or tRNAs. For a single amino acid, these energy requirements are in the range of 9.5 (glutamate) to 75.5 (tryptophan) high-energy phosphate bonds (Craig and Weber, 1998; Wagner, 2005). The synthesis of ribosomes is costly as well. It has been known for a long time that an increased growth rate correlates with increased ribosomal fractions and vice versa (Schaechter et al., 1958). Interestingly, all ribosomal proteins and elongation factors are encoded by mRNAs containing a terminal oligopyrimidine (TOP) sequence in their 5'UTR adjacent to the cap and all show a growth-associated translational regulation (Iadevaia et al., 2008; Meyuhas and Kahan, 2014; Schibler et al., 1977). Next to the regulation of translation initiation, also the direct regulation of cellular TOP mRNAs therefore has a significant effect when energy becomes limiting. TOP mRNA biology and translation regulation during stress was specifically studied during this PhD project and will be introduced in more detail in section 1.2.4.

1.2.2 Non-canonical modes of translation initiation

Next to cap- and ribosome scanning-dependent translation initiating at AUG start codons within a single open reading frame (ORF), biological systems also utilize a wide range of non-canonical translation modes. They enable cells to selectively express genes during specific physiological conditions such as mitosis, infection, stress, or apoptosis. Alternative translation modes require distinct mRNA sequence architectures ranging from secondary structure elements and overlapping ORFs to start codon sequence contexts and alternative start codons.

IRES-mediated translation

Internal ribosome entry sites (IRESs) are *cis*-acting RNA elements which enable the formation of elongation competent ribosomes in a 5'-cap and 3'-end independent manner. IRES-driven translation has been extensively characterized in positive strand RNA virus families, helping the virus to overcome general cap-dependent and PKR-mediated translation repression during infection. The structural diversity of IRESs is large. Based on their sequence conservation and structural elements at least four different functional classes (Type I-IV) can be distinguished. Each IRES type has distinct requirements for translation initiation factors leading to different modes of AUG codon recognition by the elongation competent ribosome (Yamamoto et al., 2017).

In brief, IRES translation of type I requires the binding of IRES *trans*-acting factors (ITAFs) to the IRES structural elements which recruits eIF4A, eIF4B and protease truncated eIF4G. Importantly, cap-binding eIF4E is *not* involved in IRES-mediated translation. The IRES-bound factors serve as the base for 43S PIC assembly, which scans in an eIF4A helicase-dependent manner until it reaches a downstream start codon, where then 60S joining and the formation of elongation-competent 80S ribosome takes place. Type II is similar to type I, but does not involve 43S PIC-scanning. Instead, the pre-assembled factors on the IRES structural elements guide the 43S PIC directly to the start codon. Type III IRES translation starts by direct binding of the 40S subunit to the IRES structure and the start codon. Only then, the required eIFs bind. Finally, type IV is similar to type III in that the 40S subunit directly binds to the IRES, but requires a "pseudo translocation" event by eEF2 to position the start codon inside of the ribosomal A-site.

It is currently under debate whether IRES translation occurs also for transcripts of cellular rather than viral origin (Komar and Hatzoglou, 2011; Yamamoto et al., 2017). Most translation events of cellular

genes attributed to an IRES-like mechanism have been identified to “hidden” cap-dependent initiation events. These originated from cryptic/unknown promoters, truncated templates or unknown splice sites (Jackson, 2013; Shatsky et al., 2014). Despite these findings, evidence is increasing that at least for a small number of genes IRES-mediated translation is possible. One such case is DAP5 (also known as eIF4G2 or NAT1). DAP5 belongs to the eIF4G family, but lacks a binding site for the cap-binder eIF4E, raising the possibility that it is involved in IRES translation as an initiation factor regulating its own translation. DAP5 was found to fulfill requirements that define IRES translation (Henis-Korenblit et al., 2000). Later, it was also shown that the autoregulatory DAP5 IRES is preferentially utilized during conditions under which cap-dependent translation is compromised, such as apoptosis or ER stress (Lewis et al., 2008). Further, DAP5 interacts with known IRES translation factors and seems to stimulate presumed IRES-dependent translation of some cellular mRNAs (Lieberman et al., 2015). In addition to such single cases, a recent study identified thousands of putative IRES elements in the human genome which seem to be able to drive cap-independent translation (Weingarten-Gabbay et al., 2016). The authors selected candidate sequences from genomic 5'UTRs, cloned them in between a GFP and a RFP in a bicistronic reporter and performed FACS-seq. Reporters expressing GFP were driven by cap-dependent translation, while RFP expression and follow-up sequencing indicated that certain cellular nucleotide sequences seem to be able to initiate cap-independent translation. Stringent follow-up studies will have to show if the discovered sequences fulfill all requirements for true IRES translation also in their genomic context. Although a compelling case, recent evidence points toward the possibility that DAP5 might not fulfill all of these requirements. Instead, DAP5 translation could be controlled by a non-AUG start codon (Tang et al., 2017). This mode of translation initiation can indeed be cap-independent, but does not necessarily require an IRES. How very long and highly structured 5'UTRs of cellular transcripts are translated therefore remains an open question.

uORF-mediated translation through reinitiation

IRES-driven translation is special in its ability to proceed under conditions during which cap-dependent translation is inhibited i.e. during eIF2 α -phosphorylation or eIF4F complex inhibition. It is therefore surprising that IRES translation is not more widespread in eukaryotic cells. Instead, eukaryotic cells have evolved translation systems that rely on translation re-initiation within overlapping open reading frames (ORFs) that are partially or fully localized upstream of the main ORF (mORF) and are therefore termed uORFs. uORFs provide an important layer of repression, mediated by the titration of initiating ribosomes away from the downstream mORF. Several different types of uORF-mediated regulation exist and two of them will be described here (Fig. 3):

The simplest form are uORFs that contain a cognate or near-cognate start codon in a poor sequence context, and that are in frame with the downstream mORF (Fig. 3A). Two translational options are possible within this system: First, the scanning 43S PIC fully initiates and translates the uORF as elongation competent 80S ribosome, but fails to reinitiate at the following mORF due to the short spacing between the two ORFs. The other option is that the 43S PIC “leaky scans” the uORF due to its poor start codon and sequence context and therefore does not initiate translation at the uORF. The 43S PIC now continues scanning and receives the chance to initiate at the mORF, producing the main peptide. Cells can inhibit “leaky scanning” by increasing the expression of eIF5 resulting in more efficient joining of the 60S to the 40S subunit. Increased formation of elongation competent 80S subunits then prevents leaky scanning and mORF expression (Hinnebusch et al., 2016).

A second type of uORF architecture (Fig. 3B) is used to control the expression of stress response genes such as yeast GCN4 (Hinnebusch, 2005) or mammalian ATF4 (Lu et al., 2004; Vatter and Wek, 2004), CHOP (Palam et al., 2011) and GADD34 (Lee et al., 2009). This uORF system is functionally somewhat more complicated than the one described first. Here, at least two uORFs (uORF1 and uORF2) precede the mORF. uORF1 is short and does not overlap with any of the other ORFs. Closely downstream follows uORF2 which is longer and overlaps in frame with the mORF (Fig. 3B). Counterintuitively, this uORF architecture ensures the expression of the mORF under stress conditions only. The molecular mechanism is assumed as follows: Under non-stress conditions, uORF1 is always translated. At the stop codon, the 60S subunit dissociates. However, the distance between uORF1 and uORF2 is so small that the 40S subunit together with TC and the relevant eIFs can immediately reinitiate at uORF2. Since uORF2 overlaps in frame with the mORF, no correct mORF product is synthesized under unstressed conditions. In contrast, cellular stress conditions lead to a different uORF usage resulting in a higher chance for mORF expression: Stress ultimately leads to eIF2 α phosphorylation, which drastically reduces the availability of TC. Reduced TC makes fast translation reinitiation events between uORF1 and uORF2 unlikely. As a result, the 40S subunit completely dissociates from the mRNA and does not reinitiate at uORF2. If still some TC is present, this now opens the possibility for translation initiation at the mORF start codon. Although, mORF expression efficiency might not be extremely high, the relative likelihood of its expression is strongly increased under conditions preventing uORF2 translation initiation.

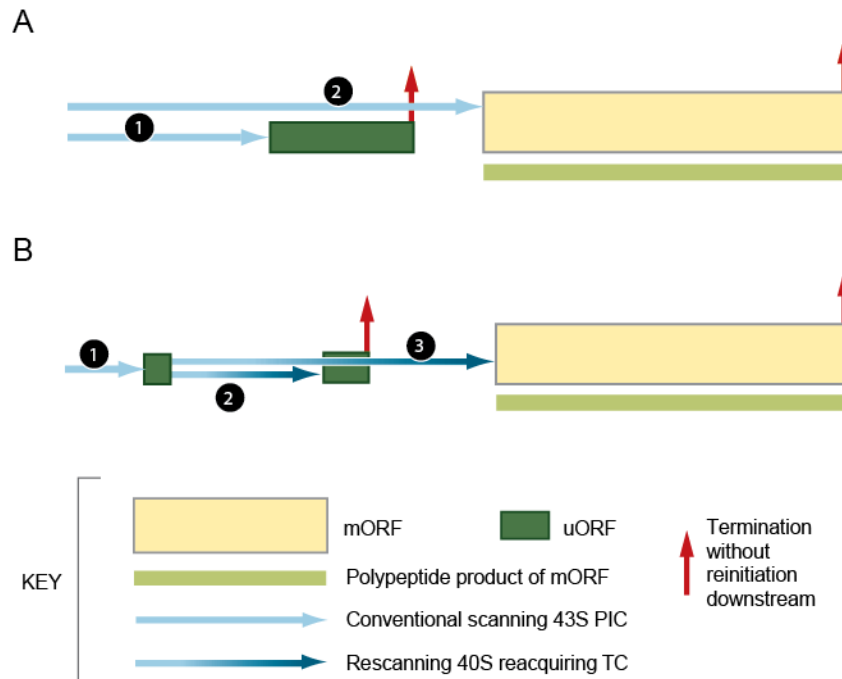


Fig. 3: Upstream open reading frame (uORF)-dependent translation relies on ribosomal scanning efficiency and successful reinitiation. (A, 1) Under normal conditions, the scanning 40S ribosome complex can initiate on the uORF and translate, but fails to reinitiate on the mORF, which is in frame with the previous uORF. (A, 2) Due to poor start codon context and reduced ternary complex (TC) levels during stress conditions, the scanning 40S ribosome complex fails to initiate at the uORF, but continues scanning and receives a second chance to reinitiate at the mORF. (B, 1) During normal conditions uORF1 is always translated and (B, 2) the scanning 40S ribosome complex can reinitiate on uORF2 which represses the mORF. (B, 3) During stress, the short distance between uORF1 and uORF2 and low levels of TC make reinitiation unlikely and the scanning 40S ribosome complex does not continue scanning and dissociates. Instead, the chance for a full reinitiation event at the mORF increases (adapted from Hinnebusch et al., 2016).

A related and interesting, but seemingly understudied aspect of uORF biology is the role of the short peptides encoded by uORFs. Only a small number of studies addressed this question so far. Peter Walter's lab recently developed a system to systematically detect unannotated peptides (Starck et al., 2016). First, cells are supplied with DNA vectors containing presumably noncoding RNA elements, such as 5'UTRs. The cells will then proteolytically cleave any synthesized peptides and present the fragments on their cell surface through major histocompatibility complex class I (MHC I). The peptide epitope can then be detected by a T cell which recognizes the "novel" non-self antigen. In addition, the T cell expresses β -galactosidase upon recognition of the peptide-MHC I complex, thus allowing the use of a colorimetric assay to monitor under which conditions and how much peptide is translated. This method has the potential to aid the discovery of a wide range of novel peptides, which could then be analyzed

more systematically for their function. Early work by Jousse *et al.* concentrated on a peptide encoded by a uORF localized in the CHOP 5' leader sequence (Jousse *et al.*, 2001). Mutational analysis showed that this 31 amino acid long peptide inhibits the expression of CHOP from the downstream mORF which partially explains why CHOP is so lowly expressed in unstressed cells. Unfortunately, the mechanisms involved to explain the inhibitory effects of the uORF-derived peptide on translation are still not understood. With the advent of next-generation sequencing and ribosome profiling, which together can map the positions and relative amounts of ribosomes on mRNA (Ingolia *et al.*, 2009, 2011; Johnstone *et al.*, 2016), it is becoming increasingly clear that the majority of mammalian mRNAs contain uORFs and that there might actually be more of them than classical mORFs. In the past, uORFs had often escaped computational annotation as coding sequences due to their short length or overlap with an already described mORF. In addition, uORFs frequently use alternative (non-AUG) start codons sometimes even without being in a Kozak sequence context (Ingolia *et al.*, 2011), which further complicated their computational detection. Further, the small size of uORF peptides makes their detection by mass spectrometry challenging (Slavoff *et al.*, 2013). This knowledge combined with novel detection algorithms will likely lead to the identification of many new and completely uncharacterized small peptides (Samandi *et al.*, 2017) and novel insights into uORF biology.

Translation initiation by alternative start codons

It has been known for several decades that mRNA translation can initiate at codons other than AUG (Zitomer *et al.*, 1984). Most of these codons resemble the canonical AUG, differing only at one base position and are consequently referred to as near-cognate start codons. Especially under non-mitotic and unstressed conditions, this mode of translation is much less predominant than AUG translation initiation. Still non-AUG initiation codons have differing efficiencies when compared to each other. CUG seems most efficient, followed by GUG, ACG, and AUU (Kearse and Wilusz, 2017). It is important to note that although translation initiation from these codons is not highly efficient; these events are not simply AUG recognition mistakes. Several transcripts are derived exclusively from non-AUG start codons.

DAP5, already introduced above in the context of IRES translation, is one such case. DAP5 translation was found to occur only from GUG start codons in mouse and human cells (Takahashi *et al.*, 2005; Tang *et al.*, 2017). Other genes, such as the yeast tRNA synthetases GRS1 and ALA1, depend similarly on non-AUG codons (Kearse and Wilusz, 2017). In addition, genome-wide techniques to study the ribosomal presence on transcripts have provided evidence that non-AUG translation is very common in mammalian cells. Ribosome profiling identified that $\approx 30\%$ of intra ORF translation and

≈75% of upstream ORF translation is controlled by near-cognate start codons (Ingolia et al., 2011). It is important to note that these findings do not mean that non-AUG translation is more common in absolute terms. Translation initiation at canonical AUGs is at least a magnitude more efficient than non-AUG translation and contributes the majority of synthesized peptides (Kearse and Wilusz, 2017).

Considering the widespread nature of alternative start codons, still surprisingly little is known about their recognition to initiate the binding of elongation competent ribosomes. Assuming that the 43S PIC (composed of 40S subunit; eIFs 1, 3, 5; ternary complex) scans the mRNA as it does for AUG-initiated translation, non-AUG start codon recognition could occur in two ways. First, through changes of initiation factor binding affinities or second, through alternative ternary complexes containing non-classical tRNA^{Met}. There is currently evidence for both mechanisms:

It is becoming increasingly clear that the start codon's context nts (for example the "Kozak sequence") and context secondary structures are differentially bound by eIF1, eIF1A, and eIF3. Together these initiation factors influence the overall conformation of the PIC, which in turn dictates the stringency of start codon recognition (Hinnebusch, 2017). A structurally altered PIC might therefore be able to recognize non-AUG codons without the need for additional protein factors. Next to this option, also an alternative ternary complex, normally containing eIF2-GTP and tRNA^{Met}, could recognize non-AUG codons. Despite this, early and recent work indicates that reporter and endogenous mRNAs containing alternative start codons give rise to full length peptides in a eIF2-tRNA^{Met} dependent manner (Kearse and Wilusz, 2017). These observations argue more for non-AUG recognition through an altered PIC structure rather than modified ternary complexes. Interestingly, the discovery of eIF2A and eIF2D as initiators on non-AUG codons challenges this view (Kearse and Wilusz, 2017). eIF2A (not equal to eIF2α) can bind a multitude of tRNAs and not just tRNA^{Met}. There are indications that eIF2A can bind to tRNA^{Leu} to drive initiation at CUG and UUG codons (Starck et al., 2012). Also eIF2D can bind multiple tRNAs and has been shown to initiate at GUG codons with tRNA^{Val} (Dmitriev et al., 2010).

Despite some molecular understanding how non-AUGs are recognized, it is still not fully understood under which biological conditions this mode of initiation becomes more attractive than canonical initiation. Ribosome profiling indicates that this could be the case during meiosis when ≈30% of ribosome footprints mapped outside of annotated ORFs (Brar et al., 2012). In addition, the cellular stress response seems to create conditions under which non-AUG translation becomes favorable. This was shown for heat shock and the unfolded protein response, for example for the protein BiP. BiP is an ER chaperone and important for protein folding homeostasis. BiP translation during stress is dependent

on the two codons UUG and CUG located in uORFs of the BiP gene based on a mechanism already described in the above section on *uORF-mediated translation*. In addition, BiP expression is eIF2A dependent, further highlighting the possibility that eIF2A-tRNA^{Leu} is responsible for the alternative start codon recognition (Starck et al., 2016). Interestingly, eIF2A itself is upregulated during various stresses including ER stress, viral infections and tumor growth increasing the relative contribution of non-AUG translation to the proteome (Kearse and Wilusz, 2017).

Translation initiation by repeat-associated alternative codons

Several genetic diseases, mostly affecting the nervous system, are characterized by massive expansions of short hexanucleotides (i.e. G₄C₂) inside of coding sequences, introns, or 5'- and 3'UTRs. The two most studied examples are amyotrophic lateral sclerosis (ALS) and frontotemporal dementia (FTD) in which repeat expansion occurs mainly in the chromosome 9 open reading frame 72 gene (*C9ORF72*) (DeJesus-Hernandez et al., 2011; Renton et al., 2011). The size of the repeats within *C9ORF72* correlates with disease severity and onset age (Gijssels et al., 2016). This is a relevant finding because abnormal disease-specific repeat proteins seem to be synthesized from both sense and antisense transcripts stemming from the *C9ORF72* repeat expansions and have been detected in brain tissues of patients with ALS and FTD (Ash et al., 2013; Mori et al., 2013; Xu et al., 2013). The detected repeat proteins are produced by an unconventional translation mechanism called repeat associated non-AUG (RAN) translation. During RAN translation initiation can occur in any of the three reading frames within expanded repeats and in all known cases non-AUG start codons are used. In addition, RAN translation might occur internally within the transcript (Xu et al., 2013). RAN translation products are toxic by blocking the ubiquitin-proteasome system, influencing ribosomal RNA synthesis, and impairing nuclear import of proteins which might subsequently aggregate (Cleary and Ranum, 2017).

Little is known about the initiation mechanism of RAN translation. Most insights stem from experiments performed with CGG repeats originating from expansions in the 5'UTR of *FMR1* (Kearse et al., 2016). In a HeLa cell expressed reporter system RAN translation was several orders of magnitudes less efficient than canonical translation and preferentially utilized ACG and GUG as start codons. RAN translation might also utilize ribosomal scanning, as it is cap-, eIF4E-, and eIF4A-dependent (Kearse et al., 2016). Others have found that initiation rates are strongly influenced by repeat length (Mori et al., 2013; Xu et al., 2013). Together these results argue for a secondary structure dependent initiation mechanism which is distinct from IRES translation because it is cap-dependent. Other kinds of repeat expansions might use different initiation mechanisms. In such cases, the presence of secondary mRNA

structures could inhibit PIC scanning and thereby promote the observed usage of downstream alternative start codons. To assess how different RAN translation is from the previously described and relatively well-characterized near-cognate start codon- or IRES-mediated translation it will be necessary to compare RAN translation dynamics in different repeat contexts and perform ribosome profiling to learn more about structure induced ribosome stalling and distribution on the repeat mRNAs.

Cap-dependent, but scanning-free translation initiation

Canonical translation involves mRNA cap recognition and ribosomal scanning, but there is evidence that mRNAs with extremely short or highly complex 5'UTRs can undergo cap-dependent, but scanning-free translation initiation. Prokaryotic mRNAs which only contain the Shine-Dalgarno sequence (AGGAGGU) in their 5'UTR can be translated *in vitro* by the eukaryotic translation system, suggesting the presence of a conserved scanning-free initiation mechanism also in eukaryotes (Grill Sonja et al., 2000). One explanation how scanning-free translation is achieved could lie in the sequence context around the start codon. Computational analysis of proximal promoter motifs lead to the identification of the Translation Initiator of Short 5'UTR (TISU) element (Elfakess and Dikstein, 2008). The TISU element contains 12 nucleotides including a start codon (C/GAAC/GAUGGCGGC). It is present in 4.5% of protein-encoding genes, is enriched in transcripts bearing short 5'UTRs with a 12 nucleotide median length and was shown to drive their translation. Although there is some overlap with the Kozak sequence, the Kozak sequence alone is not able to drive translation from short 5'UTRs (Elfakess and Dikstein, 2008). Ribosome interaction with the TISU element is cap dependent and involves AUG downstream nucleotides that seem to compensate for the absence of upstream UTR contacts. In addition, translation from TISU elements is eIF1- and eIF4A-independent, which led to the hypothesis that ribosomal scanning is not necessary for TISU containing mRNAs (Elfakess et al., 2011). This idea was further confirmed by the finding that the A-site ribosomal proteins RPS3 and RPS10e act as TISU binding proteins, directly recruiting the 80S ribosome to the start codon without the need for scanning (Haimov et al., 2017). It is currently unclear how frequently and efficiently TISU translation is used by cells. Potentially, conditions that limit canonical scanning-dependent translation, such as energy stress, enhance the likelihood for TISU translation. Recent findings indicate that TISU translation is more resistant to eIF4E inhibition through mTOR regulated 4EBP during glucose starvation than canonical translation. The eIF4E-containing eIF4F complex is released from the mRNA cap upon formation of the 48S ribosome on the TISU element (Sinvani et al., 2015). As a result, this might make subsequent 80S ribosome formation and TISU translation initiation less dependent on eIF4F and increase its relative contribution to overall translation during the stress response (Tamarkin-Ben-Harush et al., 2017).

Despite these findings, especially the molecular details of TISU translation are under debate. Important work by Kozak *et al.* showed that AUG start codons within a favored sequence require a 5'UTR of at least 20 nt for accurate translation initiation (Kozak, 1991). The possibility of TISU-driven translation is in conflict with Kozak's results. In particular, it is not clear how a ribosome with a footprint of approximately 30-35 nt (Ingolia *et al.*, 2009) could bind the AUG within the 12-nt TISU element to its P-site in order to initiate translation. Even if downstream nucleotides or secondary structures compensate for the missing upstream contacts (Elfakess *et al.*, 2011), the four nucleotides and the cap upstream of the TISU start codon do not provide enough space for ribosome binding. It remains a possibility that TISU translation can function in short (> 20 nt), but not extremely short (< 20 nt) 5'UTRs.

Codon optimality and translation

The 64 possible base triplet mRNA codons encode for "only" 20 amino acids and 3 stop codons. In principle, this redundancy should lead to a random distribution and usage of codons encoding for the same amino acid. Instead, a codon bias has been observed throughout multiple domains of life. Codon bias is the concept of a non-random codon distribution in the coding regions of genes. It is well established that codon bias correlates with tRNA levels in prokaryotes and eukaryotes, including humans. Functionally, an optimal codon usage could therefore speed up translation through a faster ribosome translocation since the fitting tRNA is readily available for each codon. How this is achieved exactly and whether "faster" ribosome translocation results in more protein product per transcript is under intense debate (Hanson and Collier, 2018; Novoa and Ribas de Pouplana, 2012; Quax *et al.*, 2015). The discussion mainly revolves around the two concepts of "elongation rate" and "translational efficiency" which are not equal (Hanson and Collier, 2018). The elongation rate describes the number of amino acids that are incorporated into the nascent peptide chain per time interval. An approximation for this measure is the number of used codons per second. Translation efficiency, on the other hand, denotes how much protein is made per transcript in a given time. For example, a block of translation initiation decreases translation efficiency to zero, but leaves the ribosomal elongation rate unaffected.

That codons could affect elongation rates had been suspected for several decades and was first shown by radio-labeled amino acid incorporation assays (Sørensen and Pedersen, 1991). It came as a surprise that the first genome-wide ribosomal profiling study did not confirm the initial findings. No clear correlation between tRNA abundances and ribosomal densities was found (Ingolia *et al.*, 2009). However, a recent meta-analysis of several ribosome profiling studies showed that the cycloheximide treatment commonly used for such experiments does not immediately stall ribosome at their respective

location, but allows them to translocate further in many cases (Gerashchenko and Gladyshev, 2014; Hussmann et al., 2015). Ribosome distributions stemming from cycloheximide experiments therefore seem to dilute codon bias effects. Since then, three technically distinct experimental approaches have proven that an optimal codon distribution leads to increased elongation rates (Hanson and Collier, 2018). First, ribosomal profiling performed with filtration and flash-freezing instead of cycloheximide treatment indicated that codons matching rare tRNAs are more slowly translated (Weinberg et al., 2016). Secondly, an experiment with an *in vitro* translated mRNA showed that optimal codons enhance the rate of translation elongation, whereas non-optimal codons slow elongation. Importantly, these experiments were not only performed as end-point measurements, but both effects were also observed within the tested mRNA (Yu et al., 2015). Lastly, evidence for codon-influenced translation rates comes from single mRNA molecule SunTag imaging. Here, small GFP-linked antibodies bind to nascent peptide epitopes and provide a read out for translation based on fluorescence intensity. The authors found that codon-optimized mRNA allows the ribosome to elongate at a rate of 4.9 codons/second versus 3.1 codons/second in a non-optimized control (Yan et al., 2016). Despite these findings, it could be a mistake to focus too much on single codons since the ribosome binds more than one codon at a time. At least in yeast, evidence exists that codons can act in concert to influence ribosome dynamics (Gamble et al., 2016).

How important codon bias is for translation efficiency or essentially the protein output per time is less clear. Codon bias is highest in strongly expressed genes and evolutionary codon conservation is more pronounced in such genes. Further, it is known that codon optimization improves heterologous expression, i.e. the expression of human genes in *E. coli*. Despite evidence for a relationship between codon-optimality and translation efficiency, there is no clear causal proof for the same effect when translation efficiency is directly measured for genes in their endogenous context (Hanson and Collier, 2018). How can it be that optimal codons clearly influence elongation rates, but not always translation efficiency? The problem is that many factors could evolutionary control codon usage. Those factors might negatively influence the multifaceted translation process as whole, but not necessarily the relatively isolated step of elongation. Several factors are currently under investigation that might explain this seemingly contradictory effect: Translation initiation is regarded as the rate-limiting step during the translation process. This means that any increase in elongation rate does not lead to more initiation, but only to faster ribosome run-off and would therefore not change the translation efficiency of a transcript. On the other hand, decreased elongation can result in a ribosomal "traffic jam" due to unchanged initiation rates and thereby block the space for newly initiating ribosomes. As a result, non-

optimized codons could have a negative effect on translation efficiency, but medium-well optimized codons would have the same effect as highly optimized codons (Hanson and Collier, 2018). Another factor are secondary structures in the 5'-end of the coding sequence. They have to be weak and therefore AT-rich in order to allow for efficient translation initiation. In *E. coli* it was demonstrated that these structural requirements can coincide with non-optimal codons (Goodman et al., 2013). Non-optimized codons might therefore even be beneficial for translation initiation, while confirming the correlation with decreased elongation rates.

Next to these rather theoretical considerations, strong evidence exists that cells can utilize codon biases to translate or repress specific mRNAs under specific conditions. In yeast cells exposed to oxidative stress, the Trm4 methyltransferase methylates specifically tRNAs encoding leucine at the wobble position. This increases the proportion of leucine tRNAs with CAA anticodon. tRNA^{CAA} can then bind to the TTG codon-enriched mRNAs of ribosomal protein RPL22A which selectively upregulates this protein and helps the cell to survive oxidative stress. RPL22A's paralogue RPL22B is not enriched for TTG codons and does not become upregulated (Chan et al., 2012). In HEK cells amino acid deprivation was shown to lower the charging of some tRNAs with amino acids, while not affecting other tRNAs. This increased the relative translation contribution of rare codon-containing ubiquitin-proteasome mRNAs (Saikia et al., 2016). Although mechanistically it is not entirely clear how codon bias influences the proteome, it becomes increasingly clear that codon optimality in concert with tRNA availability is a powerful way for cells to alter their posttranscriptional gene expression.

1.2.3 The integrated stress response

In response to external and internal chemical, physical or biological stressors, cells of all domains of life react by dramatically altering their gene expression. In eukaryotic cells, the nature of gene expression change is multifaceted and can involve many biochemical pathways. The best-studied reaction pattern of eukaryotic cells to stressors involves the integrated biochemical sensing of the stressor and subsequent translation-mediated transcriptional reprogramming to induce survival or apoptosis. This biological cascade is known as the integrated stress response (ISR) (Fig. 4A). The ISR involves several well-studied and stress-specific parallel pathways, which all converge to phosphorylate eIF2 α at Ser51. In turn, this phosphorylation event leads to the broad cellular translation down-regulation, but can also translationally up-regulate a number of genes, many of which are transcription

factors, such as ATF4. Upon re-localization to the nucleus ATF4-mediated transcriptional reprogramming leads to the expression stress response genes, such as GADD34, which binds to phosphatase 1 (PP1), the catalytic subunit of the GADD34-PP1 complex. GADD34 can reduce eIF2 α -phosphorylation levels to restore homeostasis (Fig. 4A). Very severe or chronic stressors result in prolonged eIF2 α -phosphorylation and can ultimately lead to apoptosis (Pakos-Zebrucka et al., 2016). The most important upstream players of the ISR are the four stress-sensing kinases heme-regulated inhibitor (HRI), PKR-like endoplasmic reticulum kinase (PERK), protein kinase R (PKR), and general control non-depressible 2 (GCN2). All four kinases autophosphorylate their respective kinase domain and dimerize prior to being able to phosphorylate eIF2 α (Pakos-Zebrucka et al., 2016) (Fig. 4A).

In metazoans, HRI expresses mainly in erythrocytes where it senses low heme levels due to iron deficiency and translationally represses globin-encoding mRNAs to prevent toxic aggregations (Han et al., 2013). In addition, HRI senses several other cytoplasmic stresses and in particular, sodium arsenite (SA) induced oxidative stress, which was mainly used in the work for this PhD thesis (McEwen et al., 2005; Suragani et al., 2012). How oxidative molecules activate HRI is currently unknown. However, HRI is the only stress-responsive kinase required for translational inhibition and SG formation during SA treatment in mouse embryonic fibroblasts (McEwen et al., 2005).

Endoplasmic reticulum (ER) stress, caused by unfolded proteins on the ER membrane, energy depletion or distorted ER calcium homeostasis, is sensed by the ER-localized PERK kinase. The classical model for PERK activation involves the displacement of BiP (also known as GRP78) from PERK during the unfolded protein response (UPR) allowing PERK to dimerize (Harding et al., 1999). An alternative model proposes the direct binding of unfolded proteins to the ER luminal protein IRE1 in order to activate it (Gardner and Walter, 2011). In yeast, activated Ire1 induces transcription factor Hac1 by unconventional splicing of its mRNAs. Hac1 then up-regulates the protein-folding machinery to resolve ER stress (Sidrauski and Walter, 1997).

PKR is a stress-responsive kinase able to detect viral infections by means of double-stranded RNA (dsRNA) binding leading to its dimerization and activation (Lemaire et al., 2008). Independent of dsRNA, PKR can also be activated by several other stresses, such as oxidative and ER stress, growth factor deprivation, cytokines or bacterial infection (Pakos-Zebrucka et al., 2016).

Amino acid deprivation ultimately leads to increased levels of deacylated tRNAs which can directly bind GCN2 through a tRNA synthetase-like domain (Aldana et al., 1994). Several other stresses are also linked to GCN2 activation, but often seem to have secondary effects resulting in amino acid

depletion. Similar masking effects have also been observed for the other three stress-activated eIF2 α -targeting kinases. Next to one kinase reacting to several stimuli, some studies have specifically investigated whether one kinase's function can be complemented by another one if the classical stressor is kept. Knocking out both alleles of PERK and GCN2, respectively, showed that GCN2 can fulfill PERK function during ER stress and vice versa during amino acid deprivation (Hamanaka et al., 2005; Lehman et al., 2015).

The described unspecificity to classical stimuli and complex interplay between the known four ISR kinases led to the hypothesis that other eIF2 α -targeting kinases might exist. A recent study found evidence that this is at least very unlikely. The authors used CRISPR-Cas9 to delete all four kinases simultaneously in mouse embryonic fibroblasts known to phosphorylate eIF2 α . Then they stressed the knockout cells in 14 different ways and never observed any eIF2 α phosphorylation. They conclude that no additional kinases exist that can directly phosphorylate eIF2 α (Taniuchi et al., 2016).

The formation of stress-induced mRNP complexes such as stress granules (SGs) and processing (PBs) often accompanies the ISR, but it is not fully understood whether such complexes are the cause or consequence of translational reprogramming during stress. In addition, SGs can be induced by eIF2 α phosphorylation-independent mechanisms, which makes them not a required hallmark of the ISR.

Small-molecular modulation of the ISR

Considerable effort has been undertaken to develop PERK and PKR inhibitors due to their potential relevance for protein-misfolding during neurodegenerative diseases or the regulation of translation during viral infection. In addition, an HRI activator has been described inhibiting cancer cell proliferation (Chen et al., 2011). Such compounds and their mode of action are discussed in detail elsewhere (Pakos-Zebrucka et al., 2016). Instead, here the focus will be on recently discovered compounds that modify the ISR independently of the four upstream kinases HRI, PERK, PKR and GCN2.

Kinase-independent compounds that drastically prolong and intensify the ISR include molecules that actively prevent the dephosphorylation of eIF2 α . Salubrinal (Boyce et al., 2005), guanabenz (Tsaytler et al., 2011), and Sephin1 (Das et al., 2015) bind to GADD34 and prevent its binding to PP1. As a result, GADD34-PP1 inhibition leads to higher eIF2 α phosphorylation levels. Despite this attractive mode of action model, all three compounds seem to have additional targets. In addition to GADD34, salubrinal also prevents the binding of the constitutively expressed phosphatase subunit cAMP response element binding protein (CREB) to PP1. Broad inhibition of two PP1 subunits has several

non-ISR related effects (Boyce et al., 2005). Guanabenz does not target CREB, but has also additional targets besides GADD34. As agonist for adrenergic receptor, Guanabenz is an FDA-approved drug to treat hypertension in humans. In a mouse model for systemic lupus erythematosus (SLE) Guanabenz has also been shown to inhibit Toll-like receptor 9 (TLR9) which reduces the autoimmune response (Perego et al., 2018). Of all three GADD34 inhibitors, Guanabenz-derivate Sephin1 is the highest affinity binder (Das et al., 2015). Proteolytic cleavage experiments showed that Sephin1 binds to GADD34 and leads to conformational changes presumably preventing the binding of PP1 and eIF2 α substrate recruitment (Carrara et al., 2017). Despite the insights into the molecular mechanism of Sephin1, its exclusive specificity for GADD34 has been questioned recently and even its inhibitory function as whole is under scrutiny. *In vitro* Sephin1 (and Guanabenz) was not able to decrease the stability of the GADD34-PP1 complex and showed no effect on the complex' ability to dephosphorylate eIF2 α . Further, the previously described effect of Sephin1 to restore protein folding during ER stress (Reid et al., 2016) is independent of GADD34 and eIF2 α as shown by double knockout and a phosphorylation resistant mutation, respectively (Crespillo-Casado et al., 2017). In follow-up experiments the same group of authors demonstrates that the observed discrepancies *do not* stem from non-physiological protein and inhibitor concentrations or time regimes. Further, GADD34-PP1 is most active and insensitive to Sephin1 when in complex with globular actin (G-actin) presumably forming a tripartite G-actin-GADD34-PP1 holoenzyme (Crespillo-Casado et al., 2018). G-actin had been observed before to increase cellular ability to handle the ISR (Chambers et al., 2015; Chen et al., 2015). Taken together, the authors conclude that Sephin 1 and Guanabenz have no measurable effect on the rate of eIF2 α dephosphorylation in cells, but that the compound-induced changes in gene expression during the ISR are likely due to non-GADD34 effects.

Next to molecules that prolong and intensify the ISR, recently the Integrated Stress Response InhiBitor (ISRIB) has received attention (Fig. 4A). ISRIB was discovered in an attempt to identify PERK signaling inhibitors from a library containing 106,281 compounds and was found to reverse the effects of eIF2 α phosphorylation while interestingly not affecting the phosphorylation itself (Sidrauski et al., 2013). In the primary screen under ER stress-inducing thapsigargin treatment, ISRIB inhibited ATF4 uORF-mediated Firefly luciferase reporter expression which is normally upregulated during conditions of reduced eIF2-GTP-tRNA^{Met} ternary complex availability (see also section 1.2.2). In addition, the authors found that ISRIB abrogated the presence of SGs, but did not alter the number of PBs (Sidrauski et al., 2015a). The guanine exchange factor (GEF) eIF2B was subsequently identified has an ISRIB target (Sekine et al., 2015; Sidrauski et al., 2015b) (Fig. 4A). eIF2B consists of the five α , β , γ , δ , and ϵ subunits and acts

as a dimer. eIF2B accelerates the exchange of guanosine 5'-diphosphate (GDP) for guanosine 5'-triphosphate (GTP) in the eIF2 complex. eIF2 α phosphorylation normally blocks eIF2B's GEF activity and thereby leads to translational arrest under stress. Mutational analysis showed that ISRIB binds to the two eIF2B δ subunits and thereby hyperactivates eIF2B, even in the presence of phosphorylated eIF2 α (Sekine et al., 2015; Sidrauski et al., 2015b). Recently, two crystal structures of ISRIB-bound eIF2B have confirmed the previous findings that ISRIB binds the two δ subunits and presumably fuses them more tightly together (Tsai et al., 2018; Zyryanova et al., 2018). Despite this, no further insights have been attained into the mechanism of eIF2B. In particular, it would be important to directly demonstrate the binding of eIF2B-ISRIB to eIF2 α -Ser51(phos). Further, ISRIB's disassembly effect on SGs cannot be explained by translation upregulation during stress alone. During my work for this PhD thesis, I have found that SA-induced oxidative stress represses translation even in the presence of ISRIB, while SGs can still dissolve. ISRIB can therefore uncouple the presence of SGs from translational regulation. Further, ISRIB acts only as SG disassembly promoter, but not formation inhibitor (see also Chapter 3, Fig. 1). It is therefore likely that ISRIB has at least one secondary target which directly influences SG integrity. One option would be the interference with phase separation of SG proteins containing low complexity domains (LCDs). Secondly, ISRIB might be able to block nucleo-cytoplasmic shuttling of SG proteins (Zhang et al., 2018). The goal of the screening approach described in Chapter 3 was to identify molecules that act similar to ISRIB. Extending this screen or combining a similar screen with ISRIB will likely yield insights into non-eIF2B targets of this molecule.

ISRIB is also a good example for the potential medical relevance of ISR modulators. Using a hidden platform in a water maze, already the first report on ISRIB described an enhancement of cognitive memory in mice treated with ISRIB (Sidrauski et al., 2013). Later it was found that ISRIB-mediated translation reactivation could prevent neurodegeneration in mice without any measurable side effects (Halliday et al., 2015). These observations were extended by the finding that cognitive decline in mice with traumatic brain injury can be reversed by ISRIB (Chou et al., 2017). A potential explanation for these effects could be the translation-mediated increased strength and persistence of neuronal connections upon ISRIB treatment (Placzek et al., 2016).

1.2.4 Translational down-regulation during stress

In principle, translation can be down-regulated by affecting the levels or interactions of its three most fundamental players: mRNA, tRNA, and ribosomes. The ISR and eIF2 α -phosphorylation lead to reduced levels of eIF2-GTP-tRNA^{Met} ternary complex which makes the binding of tRNA to start codons in mRNA less likely. Next to tRNA-based regulation, translation during stress can be downregulated by the reduction or sequestration of mRNAs, the prevention of initiation/elongation-competent ribosome formation on mRNA, or the reduction of the amount of ribosomes themselves. (mTOR inhibition, phosphorylation of eIF2 α , interference with eIF4F complex)

Reduced mRNA availability

Although mRNA decay is often dependent on active translation, translation itself can also be down-regulated by reduced mRNA availability during the stress response. This can be achieved in two ways: Either by increased mRNA decay or sequestration of mRNAs making them unavailable for translation initiation. An example for stress-specific mRNA decay is rapid IRE1-dependent decay (RIDD) (Han et al., 2009; Hollien et al., 2009). As explained above, one model describing the activation of the unfolded protein response during ER stress involves the direct recognition of unfolded proteins by the ER membrane protein IRE1. During RIDD, IRE1 uses its endonuclease domain to cleave the mRNAs of ER-translated secreted proteins. Importantly, RIDD contrasts the generally observed stabilization of mRNA during the stress response.

Secondly, the local sequestration of mRNAs in structures such as PBs and SGs might reduce mRNA availability during stress. However, this mechanism is debated since it could just be a consequence of arrested decay, but not a separate mechanism to repress translation. Nevertheless, mRNAs can most likely exit PBs and undergo translation during the recovery from stress (Bhattacharyya et al., 2006; Brengues et al., 2005; Halstead et al., 2015). mRNA sequestration and potential decay in PBs will be discussed in section 1.4 in more detail.

Prevention of ribosome binding

Nutrient starvation leads to an inactivation of the mTOR kinase complex (Fig. 4B). A well-studied effect of mTOR inhibition is the loss of eIF4E-BP phosphorylation. Unphosphorylated eIF4E-BP binds to eIF4E and prevents the formation of the cap-bound eIF4F complex. The absence of the eIF4F complex prevents the binding of the small ribosomal subunit-containing 43S PIC to the mRNA in order to initiate

scanning. Next to nutrient starvation, the eIF4F complex is disrupted in many other biological scenarios. For example, certain viruses have developed strategies to prevent the formation of eIF4F through inhibition of its subunits eIF4A, E, or G. Since some viruses depend only on IRESs to initiate their translation, a functional host eIF4F complex is not required for their life cycle (McCormick and Khapersky, 2017). Further, some chemotherapeutic agents can target eIF4F complex members (Anderson et al., 2015) (Fig. 4B), an aspect discussed in more detail in section 1.5.

Recently, it was also reported that human tumor cells, containing mutant KRAS, can block eIF4F complex formation. In addition, these cells contain high number of SGs (Grabocka and Bar-Sagi, 2016). The mechanism leading to these observations involves the lipid signaling molecules 15-deoxy-delta 12,14 prostaglandin J2 (PGJ2) which is secreted by mutant KRAS cells. PGJ2 can bind to eIF4A and thereby inhibits eIF4F (Kim Woo Jae et al., 2007). Importantly, PGJ2 is also able to block translation and induces SGs independent of eIF2 α in cells lacking the KRAS mutation (Grabocka and Bar-Sagi, 2016).

Reduced levels of ribosomal proteins and translation factors through TOP mRNA regulation

A third fundamental way to block translation independently of eIF2 α phosphorylation involves the decreased expression of ribosomal proteins, all translation elongation factors, and some translation initiation factors (Fig. 4B). All of these proteins are encoded by mRNAs that contain a short stretch 4 to 15 pyrimidines bases in their 5'UTR directly adjacent to the cap (Iadevaia et al., 2008; Meyuhas and Kahan, 2014). These mRNAs are referred to as 5' terminal oligopyrimidine (5'TOP) mRNAs and are conserved in all vertebrates. 5'TOP-element containing mRNAs have been shown to localize to SGs (Damgaard and Lykke-Andersen, 2011) while at the same time being strongly repressed by mTOR/mTORC1 inactivation (Hsieh et al., 2012; Thoreen et al., 2012) which can occur during different kind of stresses including oxidative stress (Heberle et al., 2015; Sfakianos et al., 2018). To investigate whether local sequestration during stress has a direct effect on translation, mRNAs containing TOP elements were used in the mRNA imaging experiments leading to this PhD thesis. 5'TOP mRNAs will be specifically introduced here with a focus on recent advances concerning their translational regulation.

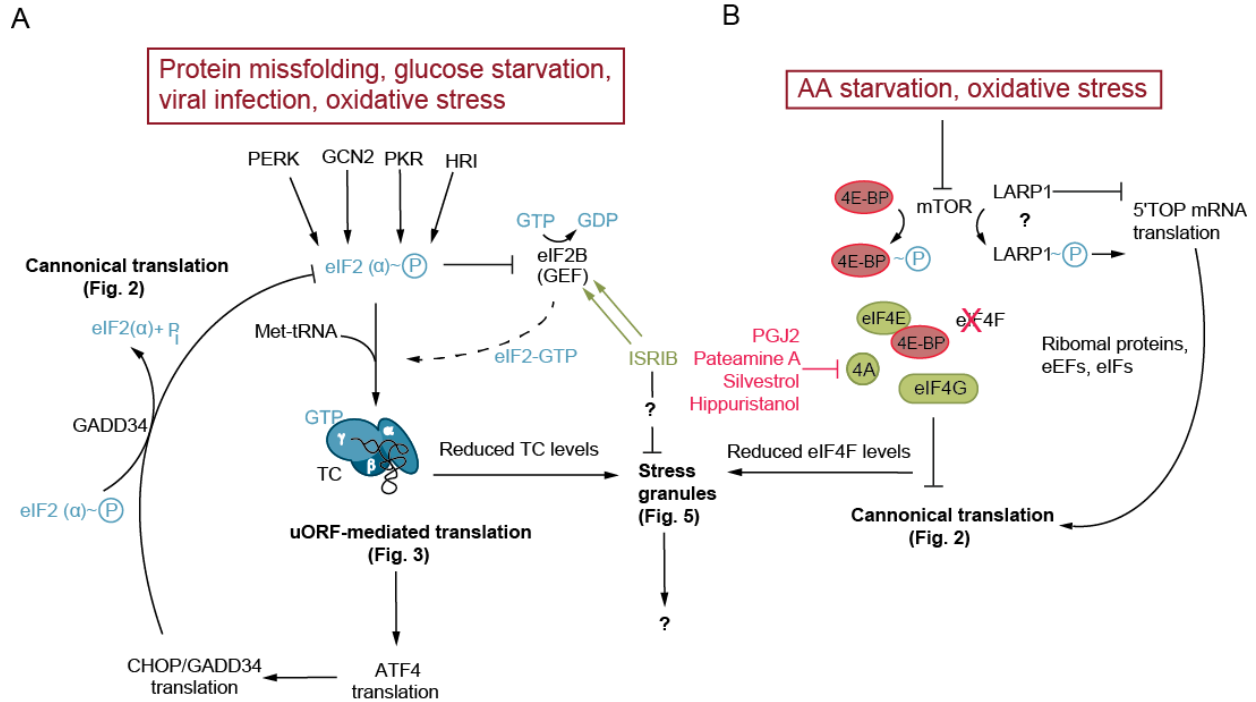


Fig. 4: Different stresses repress canonical translation initiation mainly via eIF2 α -phosphorylation and eIF4F complex assembly inhibition. (A) Stress-activated kinases phosphorylate eIF2 α leading to reduced ternary complex (TC) levels which represses canonical translation, but increases uORF-mediated translation, leading to a reduction eIF2 α -phosphorylation via ATF4/CHOP induced GADD34 phosphatase. The Integrated Stress Response Inhibitor (ISRIB) can desensitize cells against eIF2 α -phosphorylation and dissolves stress granules (SG). (B) mTOR inhibition leads to loss of the deactivating phosphorylation on 4E-BP, which can then bind to eIF4E and prevents the assembly of eIF4F. As a result, canonical translation initiation is inhibited and stress granules form. mTOR inhibition also leads to loss of phosphorylation on LARP1 which presumably represses terminal oligo pyrimidine (TOP)-element containing mRNAs and in turn reduces the expression levels of translation machinery components. Several inhibitors can block eIF4F formation directly, independent of mTOR.

Although classical TOP elements are not present in yeast, nearly 50% of its RNA polymerase II transcription is devoted to production of ribosomal proteins (Warner, 1999). In mammalian cells, ribosome-encoding TOP mRNAs are thought to contribute 20% of all transcripts present in cells (Hornstein et al., 2001; Iadevaia et al., 2008). The concerted regulation of such mRNAs has therefore a strong effect on the abundance of the translation machinery proteins and cellular translation activity as a whole (Meyuhas and Kahan, 2014; Tang et al., 2001).

Early “polypyrimidine tract” mRNA-involving experiments with the cell cycle arrest-inducing chemical compound rapamycin indicated that this class of mRNAs is subject to mTOR regulation (Jefferies et al., 1994), although the existence of mTOR had not been formally demonstrated at the time. Later, the concept of “TOP mRNAs” and their common translation regulation was further formalized

(Avni et al., 1997). mTOR and its downstream S6 kinase were identified as the first proximal kinase regulator of TOP mRNA translation (Jefferies et al., 1997) and also kinases upstream of mTOR such as phosphatidylinositol 3-kinase (PI3K) were considered as regulators (Tang et al., 2001). Using Torin1 as a more potent mTOR inhibitor than rapamycin, two genome wide ribosome profiling studies confirmed the role of mTOR/mTORC1 in 5' TOP control, but instead proposed eIF4E-BP as the most downstream TOP regulator (Hsieh et al., 2012; Thoreen et al., 2012). These findings, however, were in contrast with a previous study, which had found that eIF4E overexpression alone is not able to rescue TOP mRNA translation repression (Shama et al., 1995).

Recently, detailed insights have been gained into La-related protein 1 (LARP1) as *trans*-acting factor connecting TOP mRNA translation regulation with stress sensing through mTORC1 (Fig. 4B). However, there is controversy over the point whether LARP1 is a direct translation repressor, activator of constitutively repressed TOP mRNAs, or stabilizer of TOP transcripts. LARP1 was first identified as a TOP mRNA regulator in a quantitative proteomic screen to identify proteins that associate with the mRNA 5' cap in an mTOR-dependent manner (Tcherkezian et al., 2014). Although a direct binding to the TOP element was not demonstrated, the authors showed that LARP1 stimulates the presence of TOP reporter mRNAs in polysomes via interactions with PABP and eIF4E. Two other studies also observed a positive effect of LARP1 on TOP mRNA gene expression, but interestingly via mRNA stabilization instead of translation regulation. Both groups observed that LARP1-deficient cells have reduced TOP mRNA levels and they relate these effects to LARP1 binding to the poly(A) tail and the 40S ribosomal subunit, respectively, although the precise mechanism is not known (Aoki et al., 2013; Gentilella et al., 2017).

Also translationally repressive functions have been attributed to LARP1. Fonseca *et al.* found that when mTORC1 is inactive LARP1 is released from mTOR complex member RAPTOR. Under such conditions, LARP1 can bind the TOP motif to repress translation via competition with the scaffolding protein eIF4G, inhibiting the formation of the eIF4F complex required for translation initiation (Fonseca et al., 2015). Another study also identified the binding of LARP1 to RAPTOR under non-stress conditions, but found that that LARP1 can inhibit eIF4E cap-binding (Lahr et al., 2015). The resulting inhibition of eIF4F formation is identical to Fonseca *et al.* results. A high-resolution crystal structure of the human LARP1 DM15 region in complex with a TOP motif and a capped cytidine (m⁷GpppC) showed convincingly for the first time how TOP mRNAs bind to LARP1. Although, the capped cytidine binds LARP1 physically isolated from the TOP motif in the crystal structure, importantly, the binding of both structures to the DM15 region confirms the model that LARP1 is a translation repressor by preventing cap-access of eIF4E (Lahr et al., 2017). The repressive activity of LARP1 is directly regulated through

stress-sensing by mTORC1 through phosphorylation, which allows LARP1 to be released from TOP RNAs (Hong et al., 2017). Another recent study was able to demonstrate a molecular connection between all important components of TOP mRNA regulation: LARP1 cap/TOP-binding, mTORC1 regulation, and translation repression. In a cell-free luciferase translation assay the authors show that LARP1's DM15 region is essential for TOP element- and cap-mediated repression. The sequence identity of the TOP motif with adjacent pyrimidines in immediate proximity to the cap are essential for LARP1-mediated regulation. In the same *in vitro* assay, LARP1 also shows an increased repressive activity when mTOR is inhibited by Torin1. In addition, the authors identify a previously unknown 200 amino acid regulatory region N-terminally adjacent to the DM15 region (Philippe et al., 2018). It remains therefore a possibility that mTORC1 can modify LARP1 at multiple sites or that another unidentified factor contributes to LARP1 regulation.

Taken together, the recent functional and mechanistic insights into LARP1 and TOP mRNA regulation provide a compelling model how a general stress-induced reduction in protein synthesis can be coupled with increased repression of TOP mRNA encoded translation of ribosomal proteins at the same time. Since LARP1 specifically localizes to SGs during translation initiation inhibition it remains a possibility that LARP1-mediated repression might have a localized component during the stress response. This option is specifically addressed in Chapter 2 of this PhD thesis.

1.2.5 Selective translation during stress

As discussed in the previous section, canonical cap-dependent translation is inhibited on multiple levels during stress. Cells therefore utilize non-canonical modes of translation (see section 1.2.2) to allow translation specifically during the stress response. One of the best studied examples of selective translation involves the transcription factor ATF4 by a uORF-mediated mechanism. The translation during stress of its transcriptional targets such as CHOP and GADD34 follow similar rules as ATF4 translation (Pakos-Zebrucka et al., 2016). The relevance of the ATF4-CHOP-GADD34 axis for the ISR has been already highlighted (section 1.2.3). In general terms, uORF-mediated translation seems to be the most important translation pathways for mammalian cells to allow continued translation during stress (Andreev et al., 2015; Gao et al., 2015). Using ribosome profiling in HEK293T treated with sodium arsenite, a 5.4-fold general reduction of translation activity has been observed. Almost all repression resistant transcripts possessed at least one efficiently translated uORF in their 5'-leader, repressing

translation of the mORF under control conditions. Many of the discovered translating transcripts play an active role during the ISR (Andreev et al., 2015).

IRES-dependent translation represents a second cellular strategy to specifically allow translation during the stress response, but its occurrence and significance in cells is not clear (see section 1.2.2). Transcripts that are thought to be translated by IRES- elements during stress and which also seem to require ITAFs include for example the hypoxia response factors HIF-1 α and VEGF and the apoptosis regulator XIAP (Spriggs et al., 2010). Hypoxia-inducible factor (HIF-1 α) mRNA is a good example for the challenging identification of IRES-mediated translation of stress-responsive genes (Spriggs et al., 2010). Initially, HIF-1 α was shown to contain an IRES allowing efficient translation during hypoxia and control conditions (Lang et al., 2002). Later, it was discovered that HIF-1 α can also become translated by an IRES-independent mechanism, presumably due to cryptic promoter activity producing scanning-competent HIF-1 α transcripts (Bert et al., 2006; Young et al., 2008). In addition, it was observed that several HIF-1 α ITAFs not only bind to the IRES element, but also to the HIF-1 α 5'UTR which makes a scanning-related translation mechanism more likely (Schepens et al., 2005; Spriggs et al., 2010). Such findings are in line with other observations that next to cryptic/unknown promoters, truncated templates or unknown splice sites contribute to the translation of transcripts thought to contain IRES elements (Jackson, 2013; Shatsky et al., 2014). An interesting remaining option is that IRES-mediated repression resistance might require the translation of a uORF since this would prevent the helicase-induced melting of the IRES structure during the ribosomal scanning process (Andreev et al., 2015). In principle, the two main cellular translation initiation options during the stress response could therefore be more closely related than previously thought.

1.3 The dynamic nature of stress-induced mRNP granules

Various non-membranous messenger ribonucleoprotein (mRNP) complexes exist in eukaryotic cells and presumably catalyze mRNA metabolism in a localized manner (Banani et al., 2017). Some mRNP complexes increase in size and number when cells face an altered homeostasis for example during the cell cycle or the encounter with external biological, chemical, or physical stressors (Panas et al., 2016; Protter and Parker, 2016). The two most prominent representatives of stress-induced mRNP complexes are stress granules (SGs) and processing bodies (PBs).

SG formation was first described as a consequence of stress-induced translational arrest during which mRNAs are released from disassembled polysomes, bind aggregation prone proteins and from cytoplasmic foci (Kedersha et al., 1999). Recently developed proximity labelling approaches and elaborate lysis and centrifugation protocols have allowed the in-depth characterization of the SG and PB proteomes and transcriptomes. It is now known that SGs are composed of more than 300 proteins that probably assemble in a two-step process first forming a dense and stable core, followed by the phase separation of a surrounding shell structure (Jain et al., 2016; Wheeler et al., 2016). SGs can dramatically vary in their composition, depending under which conditions they form. This has been demonstrated in detail for single candidate proteins in yeast and human cells (Aulas et al., 2015; Buchan et al., 2008) and recently also proteome-wide in human cells (Markmiller et al., 2018). Using G3BP1-APEX proximity labelling, this study showed that 20% of a SG's protein composition is stress or cell-type dependent. SGs in *Drosophila* neurons show a particularly complex assembly of chaperones and autophagy factors (Markmiller et al., 2018).

While almost all expressed mRNAs can be detected in SG cores, only 10% of the total cellular amount of mRNA is present in SG cores. Interestingly, the recruitment efficiency per transcript varies from less than 1% to more than 95% (Khong et al., 2017). The presence of an AU-rich element (ARE), long coding sequence (CDS), long untranslated region (UTR) or poor translation efficiency were identified as broad determinants for transcript targeting to SGs (Khong et al., 2017; Namkoong et al., 2018).

Recent FACS-based purification of PBs led to an increased understanding of their protein and RNA composition. For example, 125 proteins were significantly enriched in PBs of which the majority was PB-specific compared to the SG core proteome. Interestingly, coding mRNAs were found to be more enriched in PBs than non-coding RNAs (Hubstenberger et al., 2017). Already before this study, the

presence of many components of the mRNA decay machinery inside of PBs, such as DCP1a and XRN1, had led to the idea that PBs represent centers for RNA decay (Decker and Parker, 2012). Others proposed that PBs function as sites for mRNA storage or protection from which mRNAs can return to polysomes (Bhattacharyya et al., 2006; Brengues et al., 2005). In Chapter 4, findings obtained by translation imaging of single mRNA molecules are described, which imply a translation repression function of PBs during stress recovery (Halstead et al., 2015). In addition, a dual role for mRNA storage and decay has been proposed (Aizer et al., 2014), while another recent study by our group did not detect any direct degradation events inside of PBs (Horvathova et al., 2017).

The relevance of both PBs and SGs for mRNA dynamics (Chapter 2), cell survival (Chapter 3), and localized regulation of translation (Chapters 4 and 5), during stress have been studied during this PhD project. This section aims to give an overview about the dynamical nature of mRNP complexes, with a focus on SGs. Compared with SGs, only little information is currently available on formation and disassembly mechanisms of PBs (Franks and Lykke-Andersen, 2008). Several lines of evidence obtained during the last two decades supports the view that PBs and SGs are transient and dynamical structures whose formation and disassembly is regulated by several redundant pathways.

1.3.1 Translation initiation block and early SG formation

During stress, the phosphorylation of eIF2 α inhibits the GEF activity of eIF2B and thereby depletes TC (eIF2-GTP-tRNA^{Met}) required for translation initiation. While the eIF4F complex (eIF4A/E/G) is present on the mRNA cap, the depletion of TC prevents the proper formation of the 43S PIC. This leads to a non-canonical stalled 48S PIC on the mRNA containing most of the canonical components such as eIF3, eIF4A/E/G, the 40S ribosomal subunit and PABP, but no large 60S ribosomal subunit (Kedersha et al., 2002; Kimball et al., 2003). All of these components are detectable in SGs. Block of translation initiation via mTOR inhibition prevents the formation of the eIF4F complex and forms SGs in an eIF2 α -independent manner. Consequently, the composition of mTOR-induced SGs differs from eIF2 α -dependent SGs. Fig. 5 depicts schematically how translation initiation blocking can lead to SG formation. Small molecules targeting eIF4A such as pateamine A, hippuristanol and PGJ2 also lead to eIF4F complex inhibition and SGs that resemble SGs after mTOR inhibition (Panas et al., 2016). Following blocked translation initiation, elongating ribosomes run off the mRNA molecule and the mRNA becomes accessible for the binding of RBPs with low complexity domains (LCDs) such as G3BP1, TIA1

and others (Fig. 5). Presumably, due to their LCDs, these proteins can self-oligomerize on the mRNA and thereby seed early SGs (Kedersha et al., 2013).

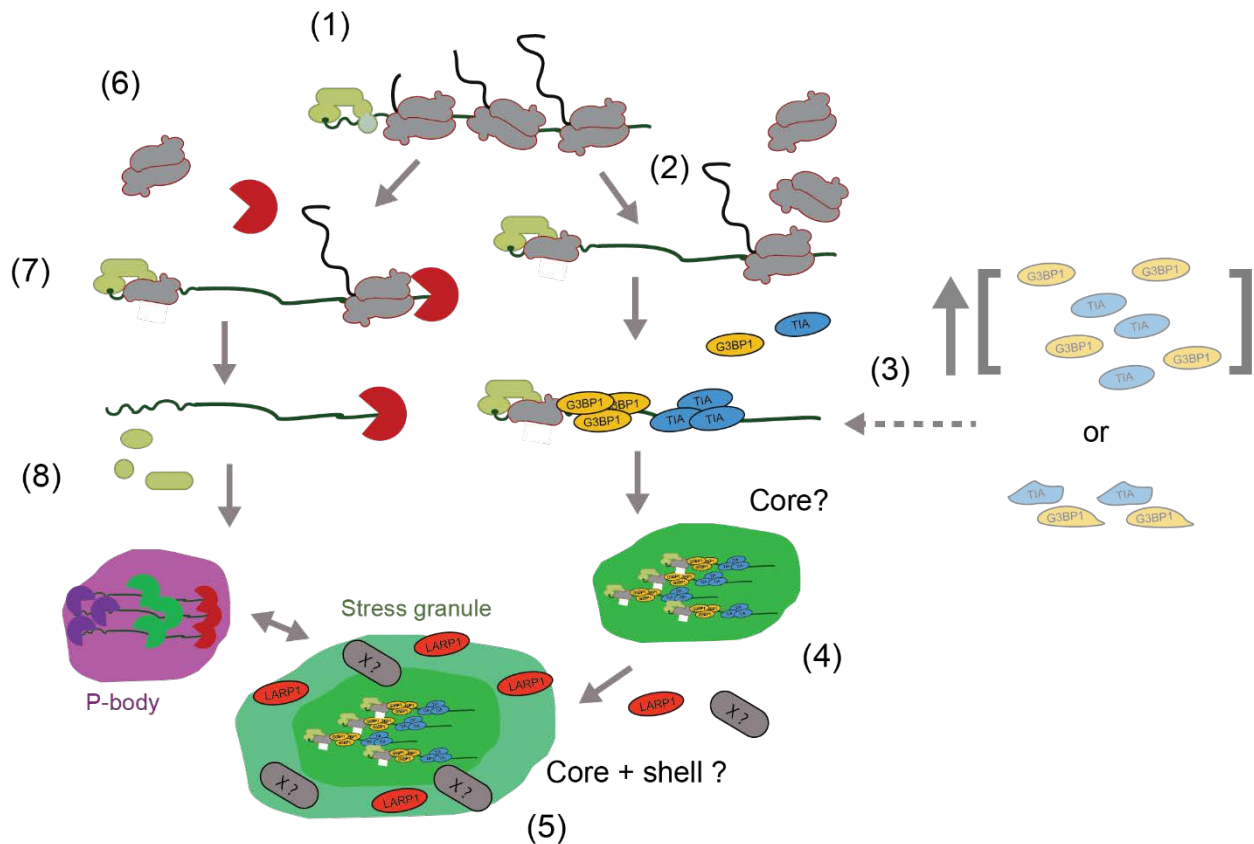


Fig. 5: Block of translation initiation and binding of aggregation-prone proteins to RNA initiates the formation of stress-induced RNA-protein granules. (1) Translation initiation block can be induced by stress or various small molecules. (2) Ribosome continue to elongate and run-off the mRNA. (3) mRNAs become susceptible to the binding of aggregation-prone stress granule (SG) proteins. In addition, the overexpression of such proteins or mutations during disease can cause SG formation independently of translation initiation block. (4) Several mRNAs bound by aggregation-prone proteins might assemble into early SG structures, referred to as cores, (5) followed by the phase separation driven formation of a shell structure which presumably contains a different proteome. (6) Processing bodies (PBs) also start to form after ribosome run-off (7) due to increased susceptibility to RNA decay factors. (8) Continued loss of translation factors and increased binding of more decay machinery components seeds PB formation. PBs can interact dynamically with SGs. Why some RNAs seed PBs while others seed SGs is not completely understood. The dynamic interactions of single mRNA molecules with PBs and SGs was specifically studied during this PhD project.

Translation initiation blocking and SG formation are not necessarily linked processes. eIF3 subunit depletion or the pharmacological inhibition of 60S subunit joining prevent SG formation while also inhibiting translation (Mokas et al., 2009; Ohn et al., 2008). The inverse is true as well and SG

formation can be inhibited downstream of translation initiation, for example through the binding of USP10 to the SG component G3BP1 (Kedersha et al., 2016). In addition, certain stresses can uncouple SG presence and translation. During the recovery from cold shock in human COS7 cells, SGs disassembled within minutes whereas polysomes fully reassembled only after 6 hours (Hofmann et al., 2012). In addition, mRNA-dependent SGs or SG-like structures can be nucleated by the overexpression of certain LCD-containing proteins such as TIA1 (Gilks et al., 2004; Kedersha et al., 1999), G3BP1 (Tourrière et al., 2003), Caprin1 (Solomon et al., 2007), DDX3 (Shih et al., 2012), or TTP (Stoecklin et al., 2004) (Fig. 5). In summary, it is unlikely that SGs directly regulate translation. Instead, it is more probable that certain aspects of cellular translation regulation also lead to the formation of SGs.

1.3.2 SG dynamics: Phase separation, docking and fusion

Over the last 20 years, several translation-dependent and –independent pathways to form SGs have been identified. However, the molecular and biophysical mechanisms that lead from stalled translation initiation complexes via the intrinsically disordered domains of RBPs and phase separation to mature SGs have only been understood since recently (Protter and Parker, 2016). In brief, phase separation, also called liquid-liquid unmixing, occurs when molecules form a network of weak interactions strong enough for those molecules to concentrate into a separate phase within the preexisting environment. Phase separated structures are temperature dependent, do not contain a membrane and exhibit liquid like behavior, which means that two spherical structures can fuse into a single spherical structure with twice the volume. SGs and PBs fulfill most of these characteristics. The well-established concept that translationally stalled mRNAs provide a scaffold and require aggregation-prone RBPs such as TIA1 and G3BP1 to form SGs fits into the phase separation theory of SG formation. In addition, live cell microscopy has provided evidence that SGs exhibit liquid-like behaviors and frequently fuse with each other (Fujimura et al., 2009; Wheeler et al., 2016). Mutational studies have shown that LCDs in SG-resident proteins are necessary for SG formation. Despite this, it is currently unclear if such intrinsically disordered domains can form a network of multivalent interactions required to fulfil the classical definition of phase separation or whether another unknown mechanism is responsible for LCD-driven SG formation (Alberti et al., 2017; Protter and Parker, 2016).

Next to their formation, the ultrastructure of SGs has been intensely studied in the recent past. Specific cell lysis and centrifugation approaches allowed the partial purification of SG components (Jain

et al., 2016). Together with high resolution imaging studies of different SG-resident proteins, the picture emerged that SGs are composed of a relatively solid and stable core part, which is surrounded by a liquid-like shell which is in dynamic exchange with the cytoplasm (Niewidok et al., 2018; Souquere et al., 2009; Wheeler et al., 2016). The evolved biochemical knowledge of SG components together with recent imaging insights has led to the core-shell model of sequential SG formation (Protter and Parker, 2016) (Fig. 5). Aggregation-prone RBPs are thought to condense on non-translating “naked” mRNAs into stable core structures, followed by the formation of a dynamic surrounding shell via high local concentrations of other secondary SG-resident proteins through phase separation. Currently, the core-shell model has still several weaknesses and leaves important questions unanswered. First, the biophysical basis of protein aggregation in the context of SGs for phase separation is only incompletely understood. In particular, it is not clear how the LCDs of SG-resident proteins result in phase separation. Secondly, there is currently only little evidence for the existence of a shell structure. Although recent imaging studies (Niewidok et al., 2018; Wheeler et al., 2016) found evidence for a bipartite SG architecture, the liquid-like properties of SGs make it difficult to purify complete SGs. This would allow the biochemical characterization of cores and shells separately from each other. It is likely that the shell consists of a different proteome. Some known SG components, such as LARP1, were not identified in the core proteome. Consequently, they might be present in the shell structure. Recently used G3BP1-based APEX proximity labelling and subsequent proteomic analysis (Markmiller et al., 2018) might contribute to a better characterization of the SG shell. A third problem is that the core-shell model can currently not explain the observed phase separation-related formation of other mRNP complexes such as P-granules in *C. elegans* or PBs in human cells (Banani et al., 2017; Hubstenberger et al., 2017; Schütz et al., 2017).

In stressed human cells PBs are often grouped around SGs and in close proximity to them (Kedersha et al., 2005; Wilczynska et al., 2005). A considerable proteomic overlap between both structures exists which has been detected early on by several immunofluorescence-based studies. Although SG composition is generally variable, proteins such as CPEB, hnRNPQ, Roquin, DDX3, TTP and others can be found in PBs and SGs (Buchan and Parker, 2009). Some of these proteins, such as TTP, enhance the interaction between PBs and SGs when overexpressed (Kedersha et al., 2005). Mostly observed in yeast, the overexpression or knock-down of some PB components has been observed to lead to the relocalization of other PB components into SG-like structures, indicating that the development of one structure into the other one might be possible (Buchan and Parker, 2009). Based on the intriguingly close association of PBs and SGs and the shared presence of proteins and reporter

mRNAs in both structures, it has been proposed that mRNAs are sorted between SGs and PBs to undergo translational repression or decay, respectively. mRNA trafficking between SGs and PBs is also known as the “mRNA triage model” (Anderson and Kedersha, 2008; Kedersha et al., 2005). However, mRNA sorting is a disputed idea. With a combination of RNA MS2-MCP labelling and FRAP, Mollet *et al.* found that RNA residence times in SGs are only brief, compared to their total residence time in the cytosol. Consequently, the researchers regarded it as more likely that RNA transfer to PBs occurs mainly through the cytosol and not through SGs (Mollet et al., 2008). In addition, PBs and SGs remain distinct structures as shown by electron microscopy (Souquere et al., 2009) and recent proteomic studies (Hubstenberger et al., 2017; Jain et al., 2016). Despite this, mRNA sorting between SG and PBs is a frequently cited idea in the scientific literature, although experiments specifically testing mRNA transfer between both structures, using high resolution imaging, have not been performed. During my PhD project, I specifically tested the possibility of mRNA triage with a set of experiments described in Chapter 2.

1.3.3 Disassembly of SGs

First indications how SG might disassemble came from experiments with the translation inhibitor cycloheximide. Cycloheximide specifically inhibits the ribosomal translocation step during translation elongation and leads to ribosomal stalling on the mRNA without subsequent disassembly. Kedersha *et al.* showed that the addition of cycloheximide to stressed cells disassembles SGs (Kedersha et al., 2000). The addition of cycloheximide seemed to trap SG components in cytosolic polysomes outside of SGs. The researchers therefore proposed a model in which SGs are in a dynamic equilibrium with polysomal mRNAs. During the recovery from stress, the out-rates of SG-trapped stalled translation machinery components and their re-binding to mRNAs might be higher than during stress. Ultimately, this might lead to SG disassembly and translation re-initiation. Although SGs are indeed highly dynamical structures, the frequently cited conclusions obtained by the original cycloheximide experiment have some caveats. First, the classical model of SG formation requires ribosomes to run off the mRNA in order for it to become accessible for aggregation-prone RBPs. Therefore, the existence of polysomes outside of SGs during the stress response is unlikely and would not allow the exchange of any components. Second, only translation incompetent PICs are present in SGs, either lacking TC or eIF4F. It is unclear how such incompletely formed initiation complexes could bind to mRNA. Third, although not impossible, the rebinding of ribosomal components to mRNAs during the ongoing stress response

is unlikely due to the strong inhibition of translation initiation in the presence of stress. Taken together, the model that SGs are in constant exchange with polysomes in the surrounding cytosol might be an oversimplification. Despite this, it is indeed likely that this exchange can occur once cells are starting to recover from stress. Under such conditions, functional translation initiation complexes are forming, and the number of polysomes is increasing. Also small molecules like ISRIB (section 1.2.3) have been implicated in translation-dependent disassembly of SGs (Sidrauski et al., 2013), although the exact mechanism is currently unclear and might involve secondary unidentified targets next to eIF2B.

In addition to the classical translation-centered model, other SG disassembly models have been proposed. For example, post-translational modifications on key stress granule components could lead to their disassembly. This has for example been demonstrated for G3BP1 by reversible phosphorylation on Ser149 (Tourrière et al., 2003). Phosphorylation seems to impair G3BP1's ability to multimerize and form SGs. Recently, casein kinase 2 (CK2) has been described to regulate G3BP1 phosphorylation on Ser149 (Reineke et al., 2017). Another kinase implicated in SG and PB disassembly is DYRK3. When DYRK3 is active, it allows stress granule dissolution, releasing mTORC1 from SGs (Wippich et al., 2013). Activated mTORC1 might then contribute to translation initiation and further promote SG disassembly. Furthermore, the methylation of RGG motifs, a loss of O-Glc-Nac glycosylation or acetylation have been implicated in SG disassembly (Protter and Parker, 2016). A third model for SG disassembly highlights the need for ongoing ATP-hydrolysis in order to maintain SGs actively as phase separated entities in the cellular environment (Jain et al., 2016). The proteomic analysis of SG cores identified several ATPases which might regulate SG stability. ATP-dependent HSP40/70 chaperonins, dead-box helicase DDX3, and VCP/Cdc48 ubiquitin segregase have all been found to regulate SG core proteins by chaperoning or post-translational modifications. In particular, the ATPase VCP/Cdc48 might provide a link to SG clearance via autophagy. Inhibition of VCP/Cdc48 function in eukaryotic cells resulted in the accumulation of SG, while the activated enzyme led to SG targeting to vacuoles where autophagy can occur (Buchan et al., 2013). Interestingly, VCP/Cdc48 activity seemed to be important for both SG and PB disassembly. Considering that autophagy allows the orderly degradation and recycling of unnecessary or dysfunctional cellular components, this PB and SG disassembly model is a very attractive one.

Another recent report specifically addressed the disassembly of PBs involving a small 7-kDa human protein the authors called NoBody (D'Lima et al., 2017). NoBody colocalized with PBs and its expression levels anticorrelated with the presence of PBs. Tagged versions of NoBody were able to pull-down protein enhancer of decapping 4 (EDC4) which is a PB-resident protein. Whether the

interaction of NoBody with EDC4 is relevant for its PB-disassembly function is currently not clear. Taken together, the large variability of translation-dependent and –independent SG disassembly mechanisms make it unlikely that one single mechanism serves as the major regulator. It is more probable that SGs disassemble in a stress-, cell type- and disease-specific manner.

1.4 mRNP granules and localized mRNA biology

Based on the above-described protein-biology centered observations, mRNP complexes seem to be highly dynamic and offer several potential entry points to regulate mRNA fate during the stress response. Despite this, it is currently an open question whether the mRNAs within a cell automatically follow the large number of RBPs which are present inside of PBs and SGs. In addition, there is only little mRNA-centered evidence, which roles mRNP complexes perform during the stress response and how these roles might be executed. Here, the focus therefore lies on findings that have been obtained by studies directly investigating the fate of mRNAs in PBs and SGs.

1.4.1 mRNA-centered evidence for translation regulation inside of mRNP granules

Translation repression within SGs has been proposed due to the striking correlation of the assembly of visible mRNP-complexes with general translation initiation repression and the presence of several eIFs, (eIF2, 3, 4A/E/G/B) inside of SGs (Decker and Parker, 2012; Stoecklin and Kedersha, 2013). In addition, the presence of inhibitory proteins, miRNAs or the steric block of ribosomal assembly have been implicated in repressing mRNA translation locally inside of SGs (Buchan, 2014). Only a small number of studies specifically concentrated on the translational fate of mRNAs inside of PBs or SGs.

Early work by Brengues *et al.* showed that in yeast, several overexpressed mRNA species visualized by the binding of a fluorescent fusion protein to their 3'UTRs exit PBs in a translation-dependent manner and are present in polysomal fractions (Brengues *et al.*, 2005). The authors conclude that in eukaryotic cells translating and nontranslating pools of mRNAs are spatially segregated in the cytosol. Work by Bhattacharyya *et al.* extended these findings to human cells and showed that cationic amino acid transporter 1 (CAT-1) mRNA can be relieved from microRNA-induced translational repression during the stress response (Bhattacharyya *et al.*, 2006). In particular, the authors show that Renilla luciferase reporters bearing the 3'UTR of CAT-1 become derepressed during starvation, protein folding and oxidative stress in Huh7 cells. Further, the binding of HuR to the CAT-1 3'UTR positively regulates the observed stress-induced derepression. Using RNA FISH against CAT-1 mRNAs the authors observed that the derepression of CAT-1 mRNA is accompanied by its release from PBs and was present

in the polysomes, consistent with translational reactivation. HuR was also observed to localize from the nucleus into the cytosol during stress. As a model, the authors propose that higher cytoplasmic levels of HuR shift the PB-to-cytosol equilibrium of repressed mRNA thereby inducing their translation. Together the studies of Brengues *et al.* and Bhattacharyya *et al.* find for the first time indications that PB localization of mRNAs could cause their spatial translation repression. However, from a current standpoint, technical limitations at the time might make it necessary to reconsider their conclusions. First, both studies make use of overexpressed reporters which could have led to artificially high PB localization. Second, both used mRNA imaging approaches have a low resolution and likely only detect mRNAs that are localized in PBs due to their locally higher concentration. The majority of mRNAs outside of PBs are not detected and are not considered for the conclusion on local translation repression. Third, the observations of a coupling between mRNA release from PBs and translation onset are strictly speaking only of a correlative nature. Detection of derepressed mRNA translation through luciferase assays or polysome profiling does not necessarily imply that exactly those mRNAs have been localized and repressed in PBs before. Despite this, the important observation of PB-induced translation repression might still hold true under some conditions and for a sub-fraction of mRNAs. Work performed during this PhD project using the TRICK single molecule translation sensor showed that during recovery from stress mRNAs that are localized inside of PBs are translationally repressed, while freely diffusing mRNAs in the cytosol are undergoing translation (Halstead et al., 2015).

mRNA-centered evidence for mRNA translation repression inside of SGs has been obtained for mRNAs bearing a 5'TOP element (Damgaard and Lykke-Andersen, 2011). Using an RNA immunoprecipitation assay, TIA-1/TIAR proteins were found to negatively regulate the translation of 5'TOP element-containing reporter mRNA in luciferase assays and polysomal fractions. TIA-1/TIAR is also a SG-nucleating protein and 5'TOP mRNAs were found to localize to SGs during amino acid starvation by RNA FISH. This mechanism could in principle lead to a systemic control of protein synthesis through sequestration and repression of 5'TOP-encoded translation and ribosome biogenesis factors. However, also this study has several technical limitations preventing a thorough conclusion about SGs as hubs for localized 5'TOP mRNA translation repression. The authors find that GCN2 kinase activation and inactivation of mTOR signaling is required for 5'TOP mRNA translation repression, while their RNA FISH imaging has only sufficient resolution to detect the high local concentration of 5'TOP mRNAs inside of SGs, but not in the cytosol. The authors did not quantify the localization ratio between the two compartments. Taken together, it is therefore likely that translation repression of 5'TOP mRNAs occurs in a decentralized manner in the cytosol and not just inside of SGs.

1.4.2 mRNA-centered evidence for mRNA decay inside of mRNP granules

Localized mRNA decay has mainly been implicated with PBs due to their high local concentration of RNA decay factors. In a landmark study, Sheth and Parker report that specifically aberrant mRNAs are targeted to PBs for nonsense-mediated decay (NMD) and undergo rapid decay (Sheth and Parker, 2006). Specifically, the authors show that the deletion of yeast NMD factor Upf1 prevents the targeting of U1A-fluorescently labelled mRNA reporters with pre-termination stop codons to PBs. Interestingly, this Upf1-deletion phenotype excludes the excess localization of mRNAs to PBs even under low resolution RNA imaging conditions. Although it is possible that NMD occurs in PBs, Sheth and Parker do not demonstrate that Upf1-mediated NMD cannot occur outside of PBs. Such an experiment would be required to show that NMD or RNA decay in general is specific to PBs. The MS2-MCP mRNA imaging system in combination with FRAP was used in living human cells to deduce RNA decay in PBs (Aizer et al., 2014). The researchers assumed that decay in PBs leads to a local depletion of mRNAs inside of PBs and therefore should result in fast mRNA-signal recovery rates after bleaching. Indeed, knockdown of DCP2, a PB-resident decapping protein, slowed RNA fluorescence recovery after PB-bleaching compared to control conditions. Despite these interesting results, a slowed fluorescence recovery is only weak evidence for direct mRNA decay inside of PBs. In addition, the used method lacked a readout to distinguish between degradation inside and outside of PBs.

Next to the RNA imaging studies described above, arguing in favor of localized RNA decay in PBs, evidence is increasing that decay occurs predominantly outside of PBs. Using mRNA reporters with viral pseudoknots that stabilize decay intermediates, Horvathova *et al.* succeeded for the first time in the direct imaging of RNA decay in fixed and living cells. However, decay was only observed in the cytosol and not in PBs, even under conditions with enhanced RNA recruitment into PBs, such as stress or the use of ARE-containing mRNA reporters (Horvathova et al., 2017). The recently described purification of PBs from unstressed human cells by a FACS-like approach, allowed for the first time reporter-independent and transcriptome wide conclusions about RNA decay in PBs (Hubstenberger et al., 2017). Although, the purified structures might not include all components of PBs, RNA sequencing of the protein-bound transcripts delivered interesting insights. PB-positive RNA species were not less abundant overall when the total cellular mRNA content was assessed. Further, mRNA half-lives only poorly correlated with localization in PBs and no decay intermediates could be identified. Taken

together, these findings indicate that decay in PBs does not occur at all or only to a relatively small extent. Most mRNA decay therefore probably occurs outside of PBs.

1.4.3 mRNA-centered evidence for localization, storage and protection of mRNAs inside of mRNP granules

Oxidative damage or other chemical modifications during the stress response can have severe consequences for RNA half-lives or translation fidelity (Nunomura et al., 2017; Simms et al., 2014). Assuming that stress-induced mRNPs can protect RNAs from harmful conditions through a chaperoning effect, it is surprising that RNA imaging studies show that generally only between 1% and 10% of cellular RNAs localize to PBs and SGs (Sheinberger and Shav-Tal, 2017; Stöhr et al., 2006). Although some exceptions exist, these findings were generally confirmed by the recent partial purifications and transcriptomic analysis of PBs and SGs (Hubstenberger et al., 2017; Khong et al., 2017).

Aizer *et al.* used the MS2-MCP mRNA imaging system in living human cells and showed that mRNAs accumulate inside of PBs during amino acid starvation (Aizer et al., 2014). Using a FRAP approach they show that during the ongoing stress response mRNA exchange kinetics with the surrounding cytosol are slow and that a large immobile fraction exists. mRNAs cleared gradually from PBs after stress is over. Although the majority of mRNA molecules in their experiments did not localize to PBs, the authors argue that the release of mRNAs from PBs during the relief from stress indicates a storage function for PBs. Currently, no published live cell data is available which clearly shows that mRNA localization to PBs or SGs significantly increases RNA half-life compared to their unbound counterparts. In Chapter 2, translation and decay RNA imaging experiments are presented which call a protective role of PBs and SGs into question.

1.5 mRNP granules and disease

Through local enrichment of biomolecules stress-induced mRNPs are thought to influence the cellular biochemistry in two ways. First, the recruitment of catalytically active molecules into mRNP complexes results in a high local concentration. As a consequence, reaction equilibria are driven towards bound states, that can specifically enhance or block a reaction. Second, mRNP complexes can reduce molecular interactions in the cytosol through sequestration and physical separation of two binding partners. Experimental evidence exists for both models which are not mutually exclusive, but highly depend on the recruited molecules and the physiological situation (Protter and Parker, 2016). Connected to the above-described conceptual physiological roles, stress-induced mRNPs also seem to play roles in various human diseases. Here, the focus will mainly be on SGs rather than PBs since their relatively well-studied link with mRNA translation has led to large body of evidence connecting this granule type with altered cell physiology.

SGs in neurological diseases and cancer

Recently, SGs-like structures have been related to human neurodegenerative disorders defined by the presence of toxic insoluble protein aggregates. This link is strongest for amyotrophic lateral sclerosis (ALS) and frontotemporal dementia (FTD), where several disease-causing mutations also influence the dynamics of SGs. Mechanistic insights have not been obtained in great detail, but disturbed phase separation induced by LCDs of the proteins FUS and TDP-43 are increasingly in the focus (Haeusler et al., 2016). In addition, translation regulation can be severely disturbed the ALS/FTD context (see section 1.2.2 on RAN translation). SGs also frequently occur inside of solid tumors, presumably induced by nutrient starvation or hypoxia. In addition, several different types of eIF2 α and eIF4F targeting chemotherapeutic agents have been shown to induce SGs (Anderson et al., 2015). What might seem an unimportant secondary effect could cause a severe resistance to cancer therapy. Chemotherapeutic drugs can induce apoptosis through the stress-activated p38 and JNK/MAPK (SAPK) pathways. Importantly, Arimoto *et al.* show that SGs negatively regulate the SAPK apoptotic response. Mechanistically, the signaling protein RACK1 becomes sequestered inside of SGs and cannot fulfill its SAPK-activating function anymore. As a result, apoptosis induction is inhibited (Arimoto et al., 2008). A similar discovery was recently made in tumor cells bearing a KRAS mutation. Here, the signaling prostaglandin molecule PGJ2 is produced in excess by the mutant cells, disrupts eIF4F complex formation and induces SGs, resulting in increased and unwanted tumor fitness (Grabocka and Bar-Sagi,

2016). On the other hand, several chemotherapeutic reagents have been shown to induce eIF2 α phosphorylation leading specifically to the stimulation of the immune system, which might help to counteract tumor formation (Bezu et al., 2018). Considering the large amount of correlative disease data on cancer and SGs (Anderson et al., 2015), it is surprising that relatively few published studies exist trying to identify unbiased or at least multidimensional ways to target SG integrity. The discovery of the molecule ISRIB is a notable exception and highlights the enormous scientific and therapeutic potential when existing chemical compound libraries are combined with a very specific stress response relevant readout (see also section 1.2.3 and Chapter 3).

SGs in viral infections

While excess SG formation might be harmful for cancer patients, some evidence points towards that boosting SG presence might be effective against viral infections. SG targeting and inhibition by viruses during their life cycles has been documented extensively (McCormick and Khapersky, 2017). Since the discovery that dsRNA causes activation of PKR and the induction of the ISR including translational repression, viruses have been studied in the context of SGs. Considering the large variations in viral structure, genome organization and replication strategies, it is surprising that all virus classes have been shown to be able to alter SG dynamics. Interestingly, viral SG suppression often occurs downstream of PKR and stress-induced translation arrest and strongly suggests that SGs have antiviral properties (McCormick, Nat Rev Immu, 2017). The most prominent role for SGs during viral infections could be the block of viral gene expression through translation inhibition, although not necessarily in a localized manner. Several viruses block PKR activation to prevent their detection. For example, Zika virus inhibits eIF2 α -dependent SG assembly upstream eIF2 (Amorim et al., 2017) and also picornavirus has been shown to regulate SG formation via its protease 2A to specifically enhance the translation of its own mRNAs (Yang et al., 2018). Further, SGs have been shown to sequester antiviral factors which might make them a preferred target for viruses (McCormick and Khapersky, 2017). The viral block of SG formation can be surprisingly robust. HIV-1 Gag blocks SG assembly irrespective of eIF2 α phosphorylation (SA & patermine A were tested) and even when SG assembly is forced by overexpression of G3BP1 or TIAR (Valiente-Echeverría et al., 2014). Interestingly, cells can form anti viral granules (AVGs) upon viral infection that resemble SGs, but are not identical to them. AVGs are for example positive for the SG marker proteins TIA1 and G3BP1, but do not contain 40S ribosomal subunits and are cycloheximide resistant (Rozelle et al., 2014). Whether AVGs are the effect of an arms race between host cells and viruses, battling for SG stability, is currently unclear. In line with such a theory are findings by Ruggieri *et al.* The researches find that SG presence in human cells can oscillate upon

infection with dsRNA (Ruggieri et al., 2012). Potentially, this represents a mechanism for cells to minimize opportunities for viruses to downregulate SGs. Several translation-targeting antiviral approaches involving eIF4A helicase inhibitors exist. However, understanding the anti-viral role of SGs independently of translation might help to use the active and forced induction of SGs as an antiviral therapy without the need to disturb translation with all of its side effects for the host. Taken together, the clearly demonstrated activities of viruses to block SG formation or to promote their disassembly are one of the strongest overall indications that SGs have important functions for cellular homeostasis during the stress response. Which functions exactly, remains an open question.

1.6 Functional mRNA dynamics during stress are unknown – an experimental approach

Research on stress-induced mRNP complexes has come a long way since the discovery was made that translation repression is linked to SG formation (Kedersha, JCB, 1999). Knowledge about the transcriptomic and proteomic composition of PBs and SGs has dramatically increased (Hubstenberger et al., 2017; Jain et al., 2016; Khong et al., 2017; Markmiller et al., 2018; Namkoong et al., 2018). Also the dynamics and architecture of proteins within PBs and SGs have been characterized in detail recently (Niewidok et al., 2018; Wheeler et al., 2016). Further, the macroscopic interaction of PBs and SGs is well documented (Decker and Parker, 2012; Stoecklin and Kedersha, 2013). Despite these recent advances, two important aspects of PB and SG biology have not been assessed in detail so far.

mRNA dynamics relative to PBs and SGs are unknown

Direct observations and quantification of mRNA interactions with stress-induced mRNPs at high resolution in living cells have not been performed. As a result, it is only incompletely understood during which phases of the stress response mRNAs enter PBs and SGs. Further, it is not known whether subpopulation of the same mRNA species interact differently with granules, i.e. what is the fraction of granule-bound mRNA compared to their unbound counterparts during the stress response. In addition, it is not clear whether these dynamics are differing between transcripts of different genes and which *cis*- and *trans*-acting elements could be responsible for their recruitment. It has also not been demonstrated at high resolution to what extent mRNA interactions differ between PBs and SGs.

RNA regulation inside and outside of PBs and SGs has not been quantified

It is unlikely that all mRNA regulation occurs in a granule-dependent manner, while the intriguing clustering of mRNA-binding proteins inside of granules points towards some localized regulation. Due to the lack of high-resolution insights into the localization pattern of mRNAs relative to PBs and SGs, it has not been possible to assess in detail to what extent both structures contribute to mRNA biology.

Experimental requirements for the study of localized mRNA regulation

The reason for the lack of direct evidence for localized mRNA regulation during the stress response seems to be mainly of a technical nature. Requirements for the study of localized mRNA biology are

complex. Such experiments involve the sequential performance of imaging, quantification (detection, tracking and colocalization), and functional assessment of RNAs relative to their localization in real-time. To understand mRNA regulation relative to stress-induced mRNPs in a high-resolution and mRNA-centered manner, the following experimental requirements are obligatory:

- 1) Direct imaging of mRNAs is required instead of focusing on mRNA-regulating RBPs and inferring automatically linked mRNA dynamics.
- 2) Dynamic information is required and therefore imaging in living cells is necessary.
- 3) mRNA localization assessment requires a high resolution; consequently single molecule imaging is obligatory. Currently, the MS2-MCP/PP7-PCP imaging systems offer the best trade-off between high imaging throughput, small cellular perturbation, and sufficient brightness and stability for live cell single molecule imaging.
- 4) mRNAs, PBs and SGs need be imaged in the same cell and at the same time to draw causal conclusions about localized regulation. This requires triple-color imaging involving high-quality fluorescent proteins and dyes as well as a suitable microscope setup with three parallel imaging channels.
- 5) Thorough quantification approaches to study the spatio-temporal distribution of mRNA are important. A combination of semi-automated mRNA tracking and automated PB/SG image segmentation with automated 2D mRNA coordinate-based colocalization has proven to be useful.
- 6) Functional sensitivity to detect relevant events in RNA biology, such as translation or decay, is necessary. The development of an mRNA imaging-based translation sensor is specifically described in this PhD thesis (Chapter 4 and 5, Halstead et al., 2015, 2016). Approaches developed by others have been used as well (Horvathova et al., 2017; Voigt et al., 2017; Yan et al., 2016).
- 7) To infer effects of mRNP granules on mRNA biology, approaches are required which correlate functional imaging observations (**6**) to the previously determined spatio-temporal mRNA

localization patterns **(5)**. However, functional mRNA single-molecule imaging with a high-spatio temporal resolution is only possible for short time frames (< 1 minute). mRNA processing potentially occurs over longer periods of time. Correlation of mRNA localization to functional effects is therefore still a challenge, which I address in the discussion in Chapter 6.

Others have skillfully developed most of these above-described individual approaches during the last years. The main contribution of the work leading to this PhD thesis is the demonstrated combination of all of the above-described experimental requirements yielding a description of dynamic mRNA localization and regulation in stressed human cells.

References

- Aizer, A., Kalo, A., Kafri, P., Shraga, A., Ben-Yishay, R., Jacob, A., Kinor, N., and Shav-Tal, Y. (2014). Quantifying mRNA targeting to P bodies in living human cells reveals a dual role in mRNA decay and storage. *J. Cell Sci.*
- Akam, M.E. (1983). The location of Ultrabithorax transcripts in *Drosophila* tissue sections. *EMBO J.* 2, 2075–2084.
- Alberti, S., Mateju, D., Mediani, L., and Carra, S. (2017). Granulostasis: Protein Quality Control of RNP Granules. *Front. Mol. Neurosci.* 10.
- Aldana, C.R.V. de, Wek, R.C., Segundo, P.S., Truesdell, A.G., and Hinnebusch, A.G. (1994). Multicopy tRNA genes functionally suppress mutations in yeast eIF-2 alpha kinase GCN2: evidence for separate pathways coupling GCN4 expression to unchanged tRNA. *Mol. Cell. Biol.* 14, 7920–7932.
- Alkalaeva, E.Z., Pisarev, A.V., Frolova, L.Y., Kisselev, L.L., and Pestova, T.V. (2006). In vitro reconstitution of eukaryotic translation reveals cooperativity between release factors eRF1 and eRF3. *Cell* 125, 1125–1136.
- Amorim, R., Temzi, A., Griffin, B.D., and Moulard, A.J. (2017). Zika virus inhibits eIF2 α -dependent stress granule assembly. *PLoS Negl. Trop. Dis.* 11, e0005775.
- Anderson, P., and Kedersha, N. (2008). Stress granules: the Tao of RNA triage. *Trends Biochem. Sci.* 33, 141–150.
- Anderson, P., Kedersha, N., and Ivanov, P. (2015). Stress granules, P-bodies and cancer. *Biochim. Biophys. Acta BBA - Gene Regul. Mech.* 1849, 861–870.
- Andreev, D.E., O'Connor, P.B.F., Fahey, C., Kenny, E.M., Terenin, I.M., Dmitriev, S.E., Cormican, P., Morris, D.W., Shatsky, I.N., and Baranov, P.V. (2015). Translation of 5' leaders is pervasive in genes resistant to eIF2 repression. *ELife* 4, e03971.
- Aoki, K., Adachi, S., Homoto, M., Kusano, H., Koike, K., and Natsume, T. (2013). LARP1 specifically recognizes the 3' terminus of poly(A) mRNA. *FEBS Lett.* 587, 2173–2178.
- Arimoto, K., Fukuda, H., Imajoh-Ohmi, S., Saito, H., and Takekawa, M. (2008). Formation of stress granules inhibits apoptosis by suppressing stress-responsive MAPK pathways. *Nat. Cell Biol.* 10, 1324–1332.
- Ash, P.E.A., Bieniek, K.F., Gendron, T.F., Caulfield, T., Lin, W.-L., DeJesus-Hernandez, M., van Blitterswijk, M.M., Jansen-West, K., Paul, J.W., Rademakers, R., et al. (2013). Unconventional translation of C9ORF72 GGGGCC expansion generates insoluble polypeptides specific to c9FTD/ALS. *Neuron* 77, 639–646.
- Aulas, A., Caron, G., Gkogkas, C.G., Mohamed, N.-V., Destroismaisons, L., Sonenberg, N., Leclerc, N., Parker, J.A., and Velde, C.V. (2015). G3BP1 promotes stress-induced RNA granule interactions to preserve polyadenylated mRNA. *J. Cell Biol.* 209, 73–84.
- Avni, D., Biberman, Y., and Meyuhas, O. (1997). The 5' terminal oligopyrimidine tract confers translational control on TOP mRNAs in a cell type- and sequence context-dependent manner. *Nucleic Acids Res.* 25, 995–1001.
- Bachi, A., Braun, I.C., Rodrigues, J.P., Panté, N., Ribbeck, K., von Kobbe, C., Kutay, U., Wilm, M., Görlich, D., Carmo-Fonseca, M., et al. (2000). The C-terminal domain of TAP interacts with the nuclear pore complex and promotes export of specific CTE-bearing RNA substrates. *RNA N. Y.* N 6, 136–158.
- Banani, S.F., Lee, H.O., Hyman, A.A., and Rosen, M.K. (2017). Biomolecular condensates: organizers of cellular biochemistry. *Nat. Rev. Mol. Cell Biol.* 18, 285–298.
- Bert, A.G., Grépin, R., Vadas, M.A., and Goodall, G.J. (2006). Assessing IRES activity in the HIF-1alpha and other cellular 5' UTRs. *RNA N. Y.* N 12, 1074–1083.

- Bertrand, E., Chartrand, P., Schaefer, M., Shenoy, S.M., Singer, R.H., and Long, R.M. (1998). Localization of ASH1 mRNA particles in living yeast. *Mol. Cell* 2, 437–445.
- Besse, F., and Ephrussi, A. (2008). Translational control of localized mRNAs: restricting protein synthesis in space and time. *Nat. Rev. Mol. Cell Biol.* 9, 971–980.
- Bezu, L., Sauvat, A., Humeau, J., Gomes-da-Silva, L.C., Iribarren, K., Forveille, S., Garcia, P., Zhao, L., Liu, P., Zitvogel, L., et al. (2018). eIF2 α phosphorylation is pathognomonic for immunogenic cell death. *Cell Death Differ.*
- Bhattacharyya, S.N., Habermacher, R., Martine, U., Closs, E.I., and Filipowicz, W. (2006). Relief of microRNA-mediated translational repression in human cells subjected to stress. *Cell* 125, 1111–1124.
- Böhl, F., Kruse, C., Frank, A., Ferring, D., and Jansen, R.-P. (2000). She2p, a novel RNA-binding protein tethers ASH1 mRNA to the Myo4p myosin motor via She3p. *EMBO J.* 19, 5514–5524.
- Boyce, M., Bryant, K.F., Jousse, C., Long, K., Harding, H.P., Scheuner, D., Kaufman, R.J., Ma, D., Coen, D.M., Ron, D., et al. (2005). A selective inhibitor of eIF2 α dephosphorylation protects cells from ER stress. *Science* 307, 935–939.
- Brar, G.A., Yassour, M., Friedman, N., Regev, A., Ingolia, N.T., and Weissman, J.S. (2012). High-resolution view of the yeast meiotic program revealed by ribosome profiling. *Science* 335, 552–557.
- Bregues, M., Teixeira, D., and Parker, R. (2005). Movement of eukaryotic mRNAs between polysomes and cytoplasmic processing bodies. *Science* 310, 486–489.
- Buchan, J.R. (2014). mRNP granules. Assembly, function, and connections with disease. *RNA Biol.* 11, 1019–1030.
- Buchan, J.R., and Parker, R. (2009). Eukaryotic stress granules: the ins and outs of translation. *Mol. Cell* 36, 932–941.
- Buchan, J.R., Muhrad, D., and Parker, R. (2008). P bodies promote stress granule assembly in *Saccharomyces cerevisiae*. *J. Cell Biol.* 183, 441–455.
- Buchan, J.R., Kolaitis, R.-M., Taylor, J.P., and Parker, R. (2013). Eukaryotic stress granules are cleared by autophagy and Cdc48/VCP function. *Cell* 153, 1461–1474.
- Burgess, H.M., Richardson, W.A., Anderson, R.C., Salaun, C., Graham, S.V., and Gray, N.K. (2011). Nuclear relocalisation of cytoplasmic poly(A)-binding proteins PABP1 and PABP4 in response to UV irradiation reveals mRNA-dependent export of metazoan PABPs. *J Cell Sci* 124, 3344–3355.
- Buttgereit, F., and Brand, M.D. (1995). A hierarchy of ATP-consuming processes in mammalian cells. *Biochem. J.* 312 (Pt 1), 163–167.
- Buxbaum, A.R., Haimovich, G., and Singer, R.H. (2015). In the right place at the right time: visualizing and understanding mRNA localization. *Nat. Rev. Mol. Cell Biol.* 16, 95–109.
- Carrara, M., Sigurdardottir, A., and Bertolotti, A. (2017). Decoding the selectivity of eIF2 α holophosphatases and PPP1R15A inhibitors. *Nat. Struct. Mol. Biol.* 24, 708–716.
- Chambers, J.E., Dalton, L.E., Clarke, H.J., Malzer, E., Dominicus, C.S., Patel, V., Moorhead, G., Ron, D., and Marciniak, S.J. (2015). Actin dynamics tune the integrated stress response by regulating eukaryotic initiation factor 2 α dephosphorylation. *ELife* 4, e04872.
- Chan, C.T.Y., Pang, Y.L.J., Deng, W., Babu, I.R., Dyavaiah, M., Begley, T.J., and Dedon, P.C. (2012). Reprogramming of tRNA modifications controls the oxidative stress response by codon-biased translation of proteins. *Nat. Commun.* 3, 937.

- Chao, J.A., Patskovsky, Y., Patel, V., Levy, M., Almo, S.C., and Singer, R.H. (2010). ZBP1 recognition of β -actin zipcode induces RNA looping. *Genes Dev.* 24, 148–158.
- Chartrand, P., Meng, X.H., Singer, R.H., and Long, R.M. (1999). Structural elements required for the localization of ASH1 mRNA and of a green fluorescent protein reporter particle in vivo. *Curr. Biol.* CB 9, 333–336.
- Chen, R., Rato, C., Yan, Y., Crespillo-Casado, A., Clarke, H.J., Harding, H.P., Marciniak, S.J., Read, R.J., and Ron, D. (2015). G-actin provides substrate-specificity to eukaryotic initiation factor 2 α holophosphatases. *ELife* 4, e04871.
- Chen, T., Ozel, D., Qiao, Y., Harbinski, F., Chen, L., Denoyelle, S., He, X., Zvereva, N., Supko, J.G., Chorev, M., et al. (2011). Chemical Genetics Identify eIF2 α Kinase Heme Regulated Inhibitor as Anti-Cancer Target. *Nat. Chem. Biol.* 7, 610–616.
- Chou, A., Krukowski, K., Jopson, T., Zhu, P.J., Costa-Mattioli, M., Walter, P., and Rosi, S. (2017). Inhibition of the integrated stress response reverses cognitive deficits after traumatic brain injury. *Proc. Natl. Acad. Sci.* 201707661.
- Cleary, J.D., and Ranum, L.P. (2017). New developments in RAN translation: insights from multiple diseases. *Curr. Opin. Genet. Dev.* 44, 125–134.
- Craig, C.L., and Weber, R.S. (1998). Selection costs of amino acid substitutions in ColE1 and Colla gene clusters harbored by *Escherichia coli*. *Mol. Biol. Evol.* 15, 774–776.
- Crespillo-Casado, A., Chambers, J.E., Fischer, P.M., Marciniak, S.J., and Ron, D. (2017). PPP1R15A-mediated dephosphorylation of eIF2 α is unaffected by Sephin1 or Guanabenz. *ELife* 6, e26109.
- Crespillo-Casado, A., Claes, Z., Choy, M.S., Peti, W., Bollen, M., and Ron, D. (2018). A Sephin1-insensitive tripartite holophosphatase dephosphorylates translation initiation factor 2 α . *J. Biol. Chem.* jbc.RA118.002325.
- Damgaard, C.K., and Lykke-Andersen, J. (2011). Translational coregulation of 5'TOP mRNAs by TIA-1 and TIAR. *Genes Dev.* 25, 2057–2068.
- Das, I., Krzyzosiak, A., Schneider, K., Wrabetz, L., D'Antonio, M., Barry, N., Sigurdardottir, A., and Bertolotti, A. (2015). Preventing proteostasis diseases by selective inhibition of a phosphatase regulatory subunit. *Science* 348, 239–242.
- Decker, C.J., and Parker, R. (2012). P-bodies and stress granules: possible roles in the control of translation and mRNA degradation. *Cold Spring Harb. Perspect. Biol.* 4, a012286.
- DeJesus-Hernandez, M., Mackenzie, I.R., Boeve, B.F., Boxer, A.L., Baker, M., Rutherford, N.J., Nicholson, A.M., Finch, N.A., Flynn, H., Adamson, J., et al. (2011). Expanded GGGGCC hexanucleotide repeat in noncoding region of C9ORF72 causes chromosome 9p-linked FTD and ALS. *Neuron* 72, 245–256.
- Dever, T.E., and Green, R. (2012). The elongation, termination, and recycling phases of translation in eukaryotes. *Cold Spring Harb. Perspect. Biol.* 4, a013706.
- D'Lima, N.G., Ma, J., Winkler, L., Chu, Q., Loh, K.H., Corpuz, E.O., Budnik, B.A., Lykke-Andersen, J., Saghatelian, A., and Slavoff, S.A. (2017). A human microprotein that interacts with the mRNA decapping complex. *Nat. Chem. Biol.* 13, 174–180.
- Dmitriev, S.E., Terenin, I.M., Andreev, D.E., Ivanov, P.A., Dunaevsky, J.E., Merrick, W.C., and Shatsky, I.N. (2010). GTP-independent tRNA Delivery to the Ribosomal P-site by a Novel Eukaryotic Translation Factor. *J. Biol. Chem.* 285, 26779–26787.
- Elfakess, R., and Dikstein, R. (2008). A Translation Initiation Element Specific to mRNAs with Very Short 5'UTR that Also Regulates Transcription. *PLOS ONE* 3, e3094.

Elfakess, R., Sinvani, H., Haimov, O., Svitkin, Y., Sonenberg, N., and Dikstein, R. (2011). Unique translation initiation of mRNAs-containing TISU element. *Nucleic Acids Res.* 39, 7598–7609.

Fonseca, B.D., Zakaria, C., Jia, J.-J., Graber, T.E., Svitkin, Y., Tahmasebi, S., Healy, D., Hoang, H.-D., Jensen, J.M., Diao, I.T., et al. (2015). La-related protein 1 (LARP1) represses terminal oligopyrimidine (TOP) mRNA translation downstream of mTOR complex 1 (mTORC1). *J. Biol. Chem.* jbc.M114.621730.

Franks, T.M., and Lykke-Andersen, J. (2008). The control of mRNA decapping and P-body formation. *Mol. Cell* 32, 605–615.

Fribourg, S., Braun, I.C., Izaurrealde, E., and Conti, E. (2001). Structural Basis for the Recognition of a Nucleoporin FG Repeat by the NTF2-like Domain of the TAP/p15 mRNA Nuclear Export Factor. *Mol. Cell* 8, 645–656.

Fujimura, K., Katahira, J., Kano, F., Yoneda, Y., and Murata, M. (2009). Microscopic dissection of the process of stress granule assembly. *Biochim. Biophys. Acta BBA - Mol. Cell Res.* 1793, 1728–1737.

Gamble, C.E., Brule, C.E., Dean, K.M., Fields, S., and Grayhack, E.J. (2016). Adjacent Codons Act in Concert to Modulate Translation Efficiency in Yeast. *Cell* 166, 679–690.

Gao, X., Wan, J., Liu, B., Ma, M., Shen, B., and Qian, S.-B. (2015). Quantitative profiling of initiating ribosomes in vivo. *Nat. Methods* 12, 147–153.

Gardner, B.M., and Walter, P. (2011). Unfolded proteins are Ire1-activating ligands that directly induce the unfolded protein response. *Science* 333, 1891–1894.

Gentilella, A., Morón-Duran, F.D., Fuentes, P., Zweig-Rocha, G., Riaño-Canalias, F., Pelletier, J., Ruiz, M., Turón, G., Castaño, J., Tauler, A., et al. (2017). Autogenous Control of 5'TOP mRNA Stability by 40S Ribosomes. *Mol. Cell* 67, 55-70.e4.

Gerashchenko, M.V., and Gladyshev, V.N. (2014). Translation inhibitors cause abnormalities in ribosome profiling experiments. *Nucleic Acids Res.* 42, e134.

Gijssels, I., Van Mossevelde, S., van der Zee, J., Sieben, A., Engelborghs, S., De Bleecker, J., Ivanoiu, A., Deryck, O., Edbauer, D., Zhang, M., et al. (2016). The C9orf72 repeat size correlates with onset age of disease, DNA methylation and transcriptional downregulation of the promoter. *Mol. Psychiatry* 21, 1112–1124.

Gilks, N., Kedersha, N., Ayodele, M., Shen, L., Stoecklin, G., Dember, L.M., and Anderson, P. (2004). Stress granule assembly is mediated by prion-like aggregation of TIA-1. *Mol. Biol. Cell* 15, 5383–5398.

Goodman, D.B., Church, G.M., and Kosuri, S. (2013). Causes and effects of N-terminal codon bias in bacterial genes. *Science* 342, 475–479.

Grabocka, E., and Bar-Sagi, D. (2016). Mutant KRAS Enhances Tumor Cell Fitness by Upregulating Stress Granules. *Cell* 167, 1803-1813.e12.

Grant, R.P., Hurt, E., Neuhaus, D., and Stewart, M. (2002). Structure of the C-terminal FG-nucleoporin binding domain of Tap/NXF1. *Nat. Struct. Biol.* 9, 247–251.

Grill Sonja, Gualerzi Claudio O., Londei Paola, and Bläsi Udo (2000). Selective stimulation of translation of leaderless mRNA by initiation factor 2: evolutionary implications for translation. *EMBO J.* 19, 4101–4110.

Grün, D., Kirchner, M., Thierfelder, N., Stoeckius, M., Selbach, M., and Rajewsky, N. (2014). Conservation of mRNA and Protein Expression during Development of *C. elegans*. *Cell Rep.* 6, 565–577.

Grünwald, D., and Singer, R.H. (2010). In vivo imaging of labelled endogenous β -actin mRNA during nucleocytoplasmic transport. *Nature* 467, 604–607.

- Gu, W., Deng, Y., Zenklusen, D., and Singer, R.H. (2004). A new yeast PUF family protein, Puf6p, represses ASH1 mRNA translation and is required for its localization. *Genes Dev.* 18, 1452–1465.
- Gygi, S.P., Rochon, Y., Franza, B.R., and Aebersold, R. (1999). Correlation between Protein and mRNA Abundance in Yeast. *Mol. Cell. Biol.* 19, 1720–1730.
- Haeusler, A.R., Donnelly, C.J., and Rothstein, J.D. (2016). The expanding biology of the C9orf72 nucleotide repeat expansion in neurodegenerative disease. *Nat. Rev. Neurosci.* 17, 383–395.
- Haimov, O., Sinvani, H., Martin, F., Ulitsky, I., Emmanuel, R., Tamarkin-Ben-Harush, A., Vardy, A., and Dikstein, R. (2017). Efficient and Accurate Translation Initiation Directed by TISU Involves RPS3 and RPS10e Binding and Differential Eukaryotic Initiation Factor 1A Regulation. *Mol. Cell. Biol.* 37, e00150-17.
- Halliday, M., Radford, H., Sekine, Y., Moreno, J., Verity, N., Quesne, J. le, Ortori, C.A., Barrett, D.A., Fromont, C., Fischer, P.M., et al. (2015). Partial restoration of protein synthesis rates by the small molecule ISRIB prevents neurodegeneration without pancreatic toxicity. *Cell Death Dis.* 6, e1672.
- Halstead, J.M., Lionnet, T., Wilbertz, J.H., Wippich, F., Ephrussi, A., Singer, R.H., and Chao, J.A. (2015). Translation. An RNA biosensor for imaging the first round of translation from single cells to living animals. *Science* 347, 1367–1671.
- Halstead, J.M., Wilbertz, J.H., Wippich, F., Lionnet, T., Ephrussi, A., and Chao, J.A. (2016). TRICK: A Single-Molecule Method for Imaging the First Round of Translation in Living Cells and Animals. *Methods Enzymol.* 572, 123–157.
- Hamanaka, R.B., Bennett, B.S., Cullinan, S.B., and Diehl, J.A. (2005). PERK and GCN2 contribute to eIF2alpha phosphorylation and cell cycle arrest after activation of the unfolded protein response pathway. *Mol. Biol. Cell* 16, 5493–5501.
- Han, D., Lerner, A.G., Vande Walle, L., Upton, J.-P., Xu, W., Hagen, A., Backes, B.J., Oakes, S.A., and Papa, F.R. (2009). IRE1alpha kinase activation modes control alternate endoribonuclease outputs to determine divergent cell fates. *Cell* 138, 562–575.
- Han, J., Back, S.H., Hur, J., Lin, Y.-H., Gildersleeve, R., Shan, J., Yuan, C.L., Krokowski, D., Wang, S., Hatzoglou, M., et al. (2013). ER-stress-induced transcriptional regulation increases protein synthesis leading to cell death. *Nat. Cell Biol.* 15, 481–490.
- Hanson, G., and Collier, J. (2018). Codon optimality, bias and usage in translation and mRNA decay. *Nat. Rev. Mol. Cell Biol.* 19, 20–30.
- Harb, M., Becker, M.M., Vitour, D., Baron, C.H., Vende, P., Brown, S.C., Bolte, S., Arold, S.T., and Poncet, D. (2008). Nuclear Localization of Cytoplasmic Poly(A)-Binding Protein upon Rotavirus Infection Involves the Interaction of NSP3 with eIF4G and RoXaN. *J. Virol.* 82, 11283–11293.
- Harding, H.P., Zhang, Y., and Ron, D. (1999). Protein translation and folding are coupled by an endoplasmic-reticulum-resident kinase. *Nature* 397, 271–274.
- Heberle, A.M., Prentzell, M.T., Eunen, K. van, Bakker, B.M., Grellscheid, S.N., and Thedieck, K. (2015). Molecular mechanisms of mTOR regulation by stress. *Mol. Cell. Oncol.* 2, e970489.
- Henis-Korenblit, S., Strumpf, N.L., Goldstaub, D., and Kimchi, A. (2000). A novel form of DAP5 protein accumulates in apoptotic cells as a result of caspase cleavage and internal ribosome entry site-mediated translation. *Mol. Cell. Biol.* 20, 496–506.

- Heuer, A., Gerovac, M., Schmidt, C., Trowitzsch, S., Preis, A., Kötter, P., Berninghausen, O., Becker, T., Beckmann, R., and Tampé, R. (2017). Structure of the 40S-ABCE1 post-splitting complex in ribosome recycling and translation initiation. *Nat. Struct. Mol. Biol.* 24, 453–460.
- Hinnebusch, A.G. (2005). Translational regulation of GCN4 and the general amino acid control of yeast. *Annu. Rev. Microbiol.* 59, 407–450.
- Hinnebusch, A.G. (2014). The scanning mechanism of eukaryotic translation initiation. *Annu. Rev. Biochem.* 83, 779–812.
- Hinnebusch, A.G. (2017). Structural Insights into the Mechanism of Scanning and Start Codon Recognition in Eukaryotic Translation Initiation. *Trends Biochem. Sci.* 42, 589–611.
- Hinnebusch, A.G., Ivanov, I.P., and Sonenberg, N. (2016). Translational control by 5'-untranslated regions of eukaryotic mRNAs. *Science* 352, 1413–1416.
- Hofmann, S., Cherkasova, V., Bankhead, P., Bukau, B., and Stoecklin, G. (2012). Translation suppression promotes stress granule formation and cell survival in response to cold shock. *Mol. Biol. Cell* 23, 3786–3800.
- Hollien, J., Lin, J.H., Li, H., Stevens, N., Walter, P., and Weissman, J.S. (2009). Regulated Ire1-dependent decay of messenger RNAs in mammalian cells. *J. Cell Biol.* 186, 323–331.
- Hong, S., Freeberg, M.A., Han, T., Kamath, A., Yao, Y., Fukuda, T., Suzuki, T., Kim, J.K., and Inoki, K. (2017). LARP1 functions as a molecular switch for mTORC1-mediated translation of an essential class of mRNAs. *ELife* 6, e25237.
- Hornstein, E., Tang, H., and Meyuhas, O. (2001). Mitogenic and nutritional signals are transduced into translational efficiency of TOP mRNAs. *Cold Spring Harb. Symp. Quant. Biol.* 66, 477–484.
- Horvathova, I., Voigt, F., Kotrys, A.V., Zhan, Y., Artus-Revel, C.G., Eglinger, J., Stadler, M.B., Giorgetti, L., and Chao, J.A. (2017). The Dynamics of mRNA Turnover Revealed by Single-Molecule Imaging in Single Cells. *Mol. Cell* 68, 615-625.e9.
- Hsieh, A.C., Liu, Y., Edlind, M.P., Ingolia, N.T., Janes, M.R., Sher, A., Shi, E.Y., Stumpf, C.R., Christensen, C., Bonham, M.J., et al. (2012). The translational landscape of mTOR signalling steers cancer initiation and metastasis. *Nature* 485, 55–61.
- Hubstenberger, A., Courel, M., Bénard, M., Souquere, S., Ernoult-Lange, M., Chouaib, R., Yi, Z., Morlot, J.-B., Munier, A., Fradet, M., et al. (2017). P-Body Purification Reveals the Condensation of Repressed mRNA Regulons. *Mol. Cell* 68, 144-157.e5.
- Hussmann, J.A., Patchett, S., Johnson, A., Sawyer, S., and Press, W.H. (2015). Understanding Biases in Ribosome Profiling Experiments Reveals Signatures of Translation Dynamics in Yeast. *PLOS Genet.* 11, e1005732.
- Hüttelmaier, S., Zenklusen, D., Lederer, M., Dichtenberg, J., Lorenz, M., Meng, X., Bassell, G.J., Condeelis, J., and Singer, R.H. (2005). Spatial regulation of beta-actin translation by Src-dependent phosphorylation of ZBP1. *Nature* 438, 512–515.
- Iadevaia, V., Caldarola, S., Tino, E., Amaldi, F., and Loreni, F. (2008). All translation elongation factors and the e, f, and h subunits of translation initiation factor 3 are encoded by 5'-terminal oligopyrimidine (TOP) mRNAs. *RNA* 14, 1730–1736.
- Ingolia, N.T., Ghaemmaghami, S., Newman, J.R.S., and Weissman, J.S. (2009). Genome-wide analysis in vivo of translation with nucleotide resolution using ribosome profiling. *Science* 324, 218–223.
- Ingolia, N.T., Lareau, L.F., and Weissman, J.S. (2011). Ribosome profiling of mouse embryonic stem cells reveals the complexity and dynamics of mammalian proteomes. *Cell* 147, 789–802.

- Jackson, R.J. (2013). The current status of vertebrate cellular mRNA IRESs. *Cold Spring Harb. Perspect. Biol.* 5.
- Jain, S., Wheeler, J.R., Walters, R.W., Agrawal, A., Barsic, A., and Parker, R. (2016). ATPase-Modulated Stress Granules Contain a Diverse Proteome and Substructure. *Cell* 164, 487–498.
- Jefferies, H.B., Reinhard, C., Kozma, S.C., and Thomas, G. (1994). Rapamycin selectively represses translation of the “polypyrimidine tract” mRNA family. *Proc. Natl. Acad. Sci.* 91, 4441–4445.
- Jefferies, H.B., Fumagalli, S., Dennis, P.B., Reinhard, C., Pearson, R.B., and Thomas, G. (1997). Rapamycin suppresses 5'TOP mRNA translation through inhibition of p70s6k. *EMBO J.* 16, 3693–3704.
- Johnstone, T.G., Bazzini, A.A., and Giraldez, A.J. (2016). Upstream ORFs are prevalent translational repressors in vertebrates. *EMBO J.* 35, 706–723.
- Jousse, C., Bruhat, A., Carraro, V., Urano, F., Ferrara, M., Ron, D., and Fafournoux, P. (2001). Inhibition of CHOP translation by a peptide encoded by an open reading frame localized in the chop 5'UTR. *Nucleic Acids Res.* 29, 4341–4351.
- Jung, H., Yoon, B.C., and Holt, C.E. (2012). Axonal mRNA localization and local protein synthesis in nervous system assembly, maintenance and repair. *Nat. Rev. Neurosci.* 13, 308–324.
- Kearse, M.G., and Wilusz, J.E. (2017). Non-AUG translation: a new start for protein synthesis in eukaryotes. *Genes Dev.* 31, 1717–1731.
- Kearse, M.G., Green, K.M., Krans, A., Rodriguez, C.M., Linsalata, A.E., Goldstrohm, A.C., and Todd, P.K. (2016). CGG Repeat-Associated Non-AUG Translation Utilizes a Cap-Dependent Scanning Mechanism of Initiation to Produce Toxic Proteins. *Mol. Cell* 62, 314–322.
- Kedersha, N., Cho, M.R., Li, W., Yacono, P.W., Chen, S., Gilks, N., Golan, D.E., and Anderson, P. (2000). Dynamic shuttling of TIA-1 accompanies the recruitment of mRNA to mammalian stress granules. *J. Cell Biol.* 151, 1257–1268.
- Kedersha, N., Chen, S., Gilks, N., Li, W., Miller, I.J., Stahl, J., and Anderson, P. (2002). Evidence that ternary complex (eIF2-GTP-tRNA(i)(Met))-deficient preinitiation complexes are core constituents of mammalian stress granules. *Mol. Biol. Cell* 13, 195–210.
- Kedersha, N., Stoecklin, G., Ayodele, M., Yacono, P., Lykke-Andersen, J., Fritzler, M.J., Scheuner, D., Kaufman, R.J., Golan, D.E., and Anderson, P. (2005). Stress granules and processing bodies are dynamically linked sites of mRNP remodeling. *J. Cell Biol.* 169, 871–884.
- Kedersha, N., Ivanov, P., and Anderson, P. (2013). Stress granules and cell signaling: more than just a passing phase? *Trends Biochem. Sci.* 38, 494–506.
- Kedersha, N., Panas, M.D., Achorn, C.A., Lyons, S., Tisdale, S., Hickman, T., Thomas, M., Lieberman, J., McInerney, G.M., Ivanov, P., et al. (2016). G3BP–Caprin1–USP10 complexes mediate stress granule condensation and associate with 40S subunits. *J Cell Biol* 212, 845–860.
- Kedersha, N.L., Gupta, M., Li, W., Miller, I., and Anderson, P. (1999). RNA-binding proteins TIA-1 and TIAR link the phosphorylation of eIF-2 alpha to the assembly of mammalian stress granules. *J. Cell Biol.* 147, 1431–1442.
- Khong, A., Matheny, T., Jain, S., Mitchell, S.F., Wheeler, J.R., and Parker, R. (2017). The Stress Granule Transcriptome Reveals Principles of mRNA Accumulation in Stress Granules. *Mol. Cell* 68, 808–820.e5.
- Kim Woo Jae, Kim Joon Hyun, and Jang Sung Key (2007). Anti-inflammatory lipid mediator 15d-PGJ2 inhibits translation through inactivation of eIF4A. *EMBO J.* 26, 5020–5032.

Kimball, S.R., Horetsky, R.L., Ron, D., Jefferson, L.S., and Harding, H.P. (2003). Mammalian stress granules represent sites of accumulation of stalled translation initiation complexes. *Am. J. Physiol. Cell Physiol.* *284*, C273-284.

Kislauskis, E.H., Zhu, X., and Singer, R.H. (1994). Sequences responsible for intracellular localization of beta-actin messenger RNA also affect cell phenotype. *J. Cell Biol.* *127*, 441–451.

Komar, A.A., and Hatzoglou, M. (2011). Cellular IRES-mediated translation: the war of ITAFs in pathophysiological states. *Cell Cycle Georget. Tex* *10*, 229–240.

Kozak, M. (1991). A short leader sequence impairs the fidelity of initiation by eukaryotic ribosomes. *Gene Expr.* *1*, 111–115.

Kumar, G.R., and Glaunsinger, B.A. (2010). Nuclear Import of Cytoplasmic Poly(A) Binding Protein Restricts Gene Expression via Hyperadenylation and Nuclear Retention of mRNA. *Mol. Cell. Biol.* *30*, 4996–5008.

Lahr, R.M., Mack, S.M., Héroux, A., Blagden, S.P., Bousquet-Antonelli, C., Deragon, J.-M., and Berman, A.J. (2015). The La-related protein 1-specific domain repurposes HEAT-like repeats to directly bind a 5' TOP sequence. *Nucleic Acids Res.* *43*, 8077–8088.

Lahr, R.M., Fonseca, B.D., Ciotti, G.E., Al-Ashtal, H.A., Jia, J.-J., Niklaus, M.R., Blagden, S.P., Alain, T., and Berman, A.J. (2017). La-related protein 1 (LARP1) binds the mRNA cap, blocking eIF4F assembly on TOP mRNAs. *ELife* *6*.

Lang, K.J.D., Kappel, A., and Goodall, G.J. (2002). Hypoxia-inducible factor-1 alpha mRNA contains an internal ribosome entry site that allows efficient translation during normoxia and hypoxia. *Mol. Biol. Cell* *13*, 1792–1801.

Lécuyer, E., Yoshida, H., Parthasarathy, N., Alm, C., Babak, T., Cerovina, T., Hughes, T.R., Tomancak, P., and Krause, H.M. (2007). Global analysis of mRNA localization reveals a prominent role in organizing cellular architecture and function. *Cell* *131*, 174–187.

Lee, Y.-Y., Cevallos, R.C., and Jan, E. (2009). An Upstream Open Reading Frame Regulates Translation of GADD34 during Cellular Stresses That Induce eIF2 α Phosphorylation. *J. Biol. Chem.* *284*, 6661–6673.

Lehman, S.L., Ryeom, S., and Koumenis, C. (2015). Signaling through alternative Integrated Stress Response pathways compensates for GCN2 loss in a mouse model of soft tissue sarcoma. *Sci. Rep.* *5*, 11781.

Leibovitch, M., and Topisirovic, I. (2018). Dysregulation of mRNA translation and energy metabolism in cancer. *Adv. Biol. Regul.* *67*, 30–39.

Lemaire, P.A., Anderson, E., Lary, J., and Cole, J.L. (2008). Mechanism of PKR Activation by dsRNA. *J. Mol. Biol.* *381*, 351–360.

Lewis, S.M., Cerquozzi, S., Graber, T.E., Ungureanu, N.H., Andrews, M., and Holcik, M. (2008). The eIF4G homolog DAP5/p97 supports the translation of select mRNAs during endoplasmic reticulum stress. *Nucleic Acids Res.* *36*, 168–178.

Liberman, N., Gandin, V., Svitkin, Y.V., David, M., Virgili, G., Jaramillo, M., Holcik, M., Nagar, B., Kimchi, A., and Sonenberg, N. (2015). DAP5 associates with eIF2 β and eIF4A1 to promote Internal Ribosome Entry Site driven translation. *Nucleic Acids Res.* *43*, 3764–3775.

Long, R.M., Singer, R.H., Meng, X., Gonzalez, I., Nasmyth, K., and Jansen, R.P. (1997). Mating type switching in yeast controlled by asymmetric localization of ASH1 mRNA. *Science* *277*, 383–387.

Lu, P.D., Harding, H.P., and Ron, D. (2004). Translation reinitiation at alternative open reading frames regulates gene expression in an integrated stress response. *J. Cell Biol.* *167*, 27–33.

- Ma, S., Bhattacharjee, R.B., and Bag, J. (2009). Expression of poly(A)-binding protein is upregulated during recovery from heat shock in HeLa cells. *FEBS J.* 276, 552–570.
- Markmiller, S., Soltanieh, S., Server, K.L., Mak, R., Jin, W., Fang, M.Y., Luo, E.-C., Krach, F., Yang, D., Sen, A., et al. (2018). Context-Dependent and Disease-Specific Diversity in Protein Interactions within Stress Granules. *Cell* 172, 590-604.e13.
- McCormick, C., and Khapersky, D.A. (2017). Translation inhibition and stress granules in the antiviral immune response. *Nat. Rev. Immunol.* 17, 647–660.
- McEwen, E., Kedersha, N., Song, B., Scheuner, D., Gilks, N., Han, A., Chen, J.-J., Anderson, P., and Kaufman, R.J. (2005). Heme-regulated inhibitor (HRI) kinase-mediated phosphorylation of eukaryotic translation initiation factor 2 (eIF2) inhibits translation, induces stress granule formation, and mediates survival upon arsenite exposure. *J. Biol. Chem.*
- Medioni, C., Mowry, K., and Besse, F. (2012). Principles and roles of mRNA localization in animal development. *Dev. Camb. Engl.* 139, 3263–3276.
- Merkulova Tatyana I., Frolova Lyudmila Y., Lazar Monique, Camonis Jacques, and Kisselev Lev L. (1999). C-terminal domains of human translation termination factors eRF1 and eRF3 mediate their in vivo interaction. *FEBS Lett.* 443, 41–47.
- Merrick, W.C. (2015). eIF4F: A Retrospective. *J. Biol. Chem.* 290, 24091–24099.
- Meyuhas, O., and Kahan, T. (2014). The race to decipher the top secrets of TOP mRNAs. *Biochim. Biophys. Acta.*
- Mokas, S., Mills, J.R., Garreau, C., Fournier, M.-J., Robert, F., Arya, P., Kaufman, R.J., Pelletier, J., and Mazroui, R. (2009). Uncoupling stress granule assembly and translation initiation inhibition. *Mol. Biol. Cell* 20, 2673–2683.
- Mollet, S., Cougot, N., Wilczynska, A., Dautry, F., Kress, M., Bertrand, E., and Weil, D. (2008). Translationally repressed mRNA transiently cycles through stress granules during stress. *Mol. Biol. Cell* 19, 4469–4479.
- Mor, A., Suliman, S., Ben-Yishay, R., Yunger, S., Brody, Y., and Shav-Tal, Y. (2010). Dynamics of single mRNP nucleocytoplasmic transport and export through the nuclear pore in living cells. *Nat. Cell Biol.* 12, 543–552.
- Mori, K., Weng, S.-M., Arzberger, T., May, S., Rentzsch, K., Kremmer, E., Schmid, B., Kretzschmar, H.A., Cruts, M., Van Broeckhoven, C., et al. (2013). The C9orf72 GGGGCC repeat is translated into aggregating dipeptide-repeat proteins in FTL/ALS. *Science* 339, 1335–1338.
- Namkoong, S., Ho, A., Woo, Y.M., Kwak, H., and Lee, J.H. (2018). Systematic Characterization of Stress-Induced RNA Granulation. *Mol. Cell* 70, 175-187.e8.
- Nicastro, G., Candel, A.M., Uhl, M., Oregioni, A., Hollingworth, D., Backofen, R., Martin, S.R., and Ramos, A. (2017). Mechanism of β -actin mRNA Recognition by ZBP1. *Cell Rep.* 18, 1187–1199.
- Niedner, A., Edelmann, F.T., and Niessing, D. (2014). Of social molecules: The interactive assembly of ASH1 mRNA-transport complexes in yeast. *RNA Biol.* 11, 998–1009.
- Nielsen, J., Christiansen, J., Lykke-Andersen, J., Johnsen, A.H., Wewer, U.M., and Nielsen, F.C. (1999). A family of insulin-like growth factor II mRNA-binding proteins represses translation in late development. *Mol. Cell. Biol.* 19, 1262–1270.
- Niewidok, B., Igaev, M., Graca, A.P. da, Strassner, A., Lenzen, C., Richter, C.P., Piehler, J., Kurre, R., and Brandt, R. (2018). Single-molecule imaging reveals dynamic biphasic partition of RNA-binding proteins in stress granules. *J Cell Biol* jcb.201709007.

- Novoa, E.M., and Ribas de Pouplana, L. (2012). Speeding with control: codon usage, tRNAs, and ribosomes. *Trends Genet.* *TIG* 28, 574–581.
- Nunomura, A., Lee, H., Zhu, X., and Perry, G. (2017). Consequences of RNA oxidation on protein synthesis rate and fidelity: implications for the pathophysiology of neuropsychiatric disorders. *Biochem. Soc. Trans.* BST20160433.
- Ohn, T., Kedersha, N., Hickman, T., Tisdale, S., and Anderson, P. (2008). A functional RNAi screen links O-GlcNAc modification of ribosomal proteins to stress granule and processing body assembly. *Nat. Cell Biol.* *10*, 1224–1231.
- Olivier, C., Poirier, G., Gendron, P., Boisgontier, A., Major, F., and Chartrand, P. (2005). Identification of a Conserved RNA Motif Essential for She2p Recognition and mRNA Localization to the Yeast Bud. *Mol. Cell. Biol.* *25*, 4752–4766.
- Pakos-Zebrucka, K., Koryga, I., Mnich, K., Lujic, M., Samali, A., and Gorman, A.M. (2016). The integrated stress response. *EMBO Rep.* *17*, 1374–1395.
- Palam, L.R., Baird, T.D., and Wek, R.C. (2011). Phosphorylation of eIF2 Facilitates Ribosomal Bypass of an Inhibitory Upstream ORF to Enhance CHOP Translation. *J. Biol. Chem.* *286*, 10939–10949.
- Panas, M.D., Ivanov, P., and Anderson, P. (2016). Mechanistic insights into mammalian stress granule dynamics. *J. Cell Biol.* *215*, 313–323.
- Pelechano, V., Wei, W., and Steinmetz, L.M. (2015). Widespread co-translational RNA decay reveals ribosome dynamics. *Cell* *161*, 1400–1412.
- Perego, J., Mendes, A., Bourbon, C., Camosseto, V., Combes, A., Liu, H., Manh, T.-P.V., Dalet, A., Chasson, L., Spinelli, L., et al. (2018). Guanabenz inhibits TLR9 signaling through a pathway that is independent of eIF2 α dephosphorylation by the GADD34/PP1c complex. *Sci Signal* *11*, eaam8104.
- Philippe, L., Vasseur, J.-J., Debart, F., and Thoreen, C.C. (2018). La-related protein 1 (LARP1) repression of TOP mRNA translation is mediated through its cap-binding domain and controlled by an adjacent regulatory region. *Nucleic Acids Res.* *46*, 1457–1469.
- Pisarev, A.V., Hellen, C.U.T., and Pestova, T.V. (2007). Recycling of eukaryotic posttermination ribosomal complexes. *Cell* *131*, 286–299.
- Pisarev, A.V., Skabkin, M.A., Pisareva, V.P., Skabkina, O.V., Rakotondrafara, A.M., Hentze, M.W., Hellen, C.U.T., and Pestova, T.V. (2010). The role of ABCE1 in eukaryotic posttermination ribosomal recycling. *Mol. Cell* *37*, 196–210.
- Placzek, A.N., Prisco, G.V.D., Khatiwada, S., Sgritta, M., Huang, W., Krnjević, K., Kaufman, R.J., Dani, J.A., Walter, P., and Costa-Mattioli, M. (2016). eIF2 α -mediated translational control regulates the persistence of cocaine-induced LTP in midbrain dopamine neurons. *ELife* *5*, e17517.
- Powrie, E.A., Zenklusen, D., and Singer, R.H. (2011). A nucleoporin, Nup60p, affects the nuclear and cytoplasmic localization of ASH1 mRNA in *S. cerevisiae*. *RNA* *17*, 134–144.
- Protter, D.S.W., and Parker, R. (2016). Principles and Properties of Stress Granules. *Trends Cell Biol.* *26*, 668–679.
- Quax, T.E.F., Claassens, N.J., Söll, D., and van der Oost, J. (2015). Codon Bias as a Means to Fine-Tune Gene Expression. *Mol. Cell* *59*, 149–161.
- Reid, D.W., Tay, A.S.L., Sundaram, J.R., Lee, I.C.J., Chen, Q., George, S.E., Nicchitta, C.V., and Shenolikar, S. (2016). Complementary Roles of GADD34- and CREP-Containing Eukaryotic Initiation Factor 2 α Phosphatases during the Unfolded Protein Response. *Mol. Cell. Biol.* *36*, 1868–1880.

Reineke, L.C., Tsai, W.-C., Jain, A., Kaelber, J.T., Jung, S.Y., and Lloyd, R.E. (2017). Casein Kinase 2 Is Linked to Stress Granule Dynamics through Phosphorylation of the Stress Granule Nucleating Protein G3BP1. *Mol. Cell. Biol.* 37, e00596-16.

Renton, A.E., Majounie, E., Waite, A., Simón-Sánchez, J., Rollinson, S., Gibbs, J.R., Schymick, J.C., Laaksovirta, H., van Swieten, J.C., Myllykangas, L., et al. (2011). A hexanucleotide repeat expansion in C9ORF72 is the cause of chromosome 9p21-linked ALS-FTD. *Neuron* 72, 257–268.

Rozelle, D.K., Filone, C.M., Kedersha, N., and Connor, J.H. (2014). Activation of stress response pathways promotes formation of antiviral granules and restricts virus replication. *Mol. Cell. Biol.* 34, 2003–2016.

Ruggieri, A., Dazert, E., Metz, P., Hofmann, S., Bergeest, J.-P., Mazur, J., Bankhead, P., Hiet, M.-S., Kallis, S., Alvisi, G., et al. (2012). Dynamic oscillation of translation and stress granule formation mark the cellular response to virus infection. *Cell Host Microbe* 12, 71–85.

Russell, J.B., and Cook, G.M. (1995). Energetics of bacterial growth: balance of anabolic and catabolic reactions. *Microbiol. Rev.* 59, 48–62.

Saavedra, C., Tung, K.S., Amberg, D.C., Hopper, A.K., and Cole, C.N. (1996). Regulation of mRNA export in response to stress in *Saccharomyces cerevisiae*. *Genes Dev.* 10, 1608–1620.

Saikia, M., Wang, X., Mao, Y., Wan, J., Pan, T., and Qian, S.-B. (2016). Codon optimality controls differential mRNA translation during amino acid starvation. *RNA N. Y. N* 22, 1719–1727.

Samandi, S., Roy, A.V., Delcourt, V., Lucier, J.-F., Gagnon, J., Beaudoin, M.C., Vanderperre, B., Breton, M.-A., Motard, J., Jacques, J.-F., et al. (2017). Deep transcriptome annotation enables the discovery and functional characterization of cryptic small proteins. *ELife* 6, e27860.

Schaechter, M., Maaløe, O., and Kjeldgaard, N.O. (1958). Dependency on Medium and Temperature of Cell Size and Chemical Composition during Balanced Growth of *Salmonella typhimurium*. *Microbiology* 19, 592–606.

Schepens, B., Tinton, S.A., Bruynooghe, Y., Beyaert, R., and Cornelis, S. (2005). The polypyrimidine tract-binding protein stimulates HIF-1 α IRES-mediated translation during hypoxia. *Nucleic Acids Res.* 33, 6884–6894.

Schibler, U., Kelley, D.E., and Perry, R.P. (1977). Comparison of methylated sequences in messenger RNA and heterogeneous nuclear RNA from mouse L cells. *J. Mol. Biol.* 115, 695–714.

Schmidt, C., Kowalinski, E., Shanmuganathan, V., Defenouillère, Q., Braunger, K., Heuer, A., Pech, M., Namane, A., Berninghausen, O., Fromont-Racine, M., et al. (2016). The cryo-EM structure of a ribosome-Ski2-Ski3-Ski8 helicase complex. *Science* 354, 1431–1433.

Schütz, S., Nöldeke, E.R., and Sprangers, R. (2017). A synergistic network of interactions promotes the formation of in vitro processing bodies and protects mRNA against decapping. *Nucleic Acids Res.* 45, 6911–6922.

Schwanhäusser, B., Busse, D., Li, N., Dittmar, G., Schuchhardt, J., Wolf, J., Chen, W., and Selbach, M. (2011). Global quantification of mammalian gene expression control. *Nature* 473, 337–342.

Sekine, Y., Zyryanova, A., Crespillo-Casado, A., Fischer, P.M., Harding, H.P., and Ron, D. (2015). Stress responses. Mutations in a translation initiation factor identify the target of a memory-enhancing compound. *Science* 348, 1027–1030.

Sfakianos, A.P., Mellor, L.E., Pang, Y.F., Kritsiligkou, P., Needs, H., Abou-Hamdan, H., Désaubry, L., Poulin, G.B., Ashe, M.P., and Whitmarsh, A.J. (2018). The mTOR-S6 kinase pathway promotes stress granule assembly. *Cell Death Differ.* 1.

Shahbajian, K., Jeronimo, C., Forget, A., Robert, F., and Chartrand, P. (2014). Co-transcriptional recruitment of Puf6 by She2 couples translational repression to mRNA localization. *Nucleic Acids Res.* *42*, 8692–8704.

Shama, S., Avni, D., Frederickson, R.M., Sonenberg, N., and Meyuhas, O. (1995). Overexpression of initiation factor eIF-4E does not relieve the translational repression of ribosomal protein mRNAs in quiescent cells. *Gene Expr.* *4*, 241–252.

Shan, P., Fan, G., Sun, L., Liu, J., Wang, W., Hu, C., Zhang, X., Zhai, Q., Song, X., Cao, L., et al. (2017). SIRT1 Functions as a Negative Regulator of Eukaryotic Poly(A)RNA Transport. *Curr. Biol.* *27*, 2271–2284.e5.

Shatsky, I.N., Dmitriev, S.E., Andreev, D.E., and Terenin, I.M. (2014). Transcriptome-wide studies uncover the diversity of modes of mRNA recruitment to eukaryotic ribosomes. *Crit. Rev. Biochem. Mol. Biol.* *49*, 164–177.

Sheinberger, J., and Shav-Tal, Y. (2017). mRNPs meet stress granules. *FEBS Lett.* *591*, 2534–2542.

Sheth, U., and Parker, R. (2006). Targeting of aberrant mRNAs to cytoplasmic processing bodies. *Cell* *125*, 1095–1109.

Shih, J.-W., Wang, W.-T., Tsai, T.-Y., Kuo, C.-Y., Li, H.-K., and Wu Lee, Y.-H. (2012). Critical roles of RNA helicase DDX3 and its interactions with eIF4E/PABP1 in stress granule assembly and stress response. *Biochem. J.* *441*, 119–129.

Sidrauski, C., and Walter, P. (1997). The transmembrane kinase Ire1p is a site-specific endonuclease that initiates mRNA splicing in the unfolded protein response. *Cell* *90*, 1031–1039.

Sidrauski, C., Acosta-Alvear, D., Khoutorsky, A., Vedantham, P., Hearn, B.R., Li, H., Gamache, K., Gallagher, C.M., Ang, K.K.-H., Wilson, C., et al. (2013). Pharmacological brake-release of mRNA translation enhances cognitive memory. *ELife* *2*, e00498.

Sidrauski, C., McGeachy, A.M., Ingolia, N.T., and Walter, P. (2015a). The small molecule ISRIB reverses the effects of eIF2 α phosphorylation on translation and stress granule assembly. *ELife* *4*, e05033.

Sidrauski, C., Tsai, J.C., Kampmann, M., Hearn, B.R., Vedantham, P., Jaishankar, P., Sokabe, M., Mendez, A.S., Newton, B.W., Tang, E.L., et al. (2015b). Pharmacological dimerization and activation of the exchange factor eIF2B antagonizes the integrated stress response. *ELife* *4*, e07314.

Siebrasse, J.P., Kaminski, T., and Kubitscheck, U. (2012). Nuclear export of single native mRNA molecules observed by light sheet fluorescence microscopy. *Proc. Natl. Acad. Sci.* *109*, 9426–9431.

Simms, C.L., Hudson, B.H., Mosior, J.W., Rangwala, A.S., and Zaher, H.S. (2014). An Active Role for the Ribosome in Determining the Fate of Oxidized mRNA. *Cell Rep.* *9*, 1256–1264.

Simonetti, A., Brito Querido, J., Myasnikov, A.G., Mancera-Martinez, E., Renaud, A., Kuhn, L., and Hashem, Y. (2016). eIF3 Peripheral Subunits Rearrangement after mRNA Binding and Start-Codon Recognition. *Mol. Cell* *63*, 206–217.

Singh, G., Kucukural, A., Cenik, C., Leszyk, J.D., Shaffer, S.A., Weng, Z., and Moore, M.J. (2012). The Cellular EJC Interactome Reveals Higher Order mRNP Structure and an EJC-SR Protein Nexus. *Cell* *151*, 750–764.

Sinvani, H., Haimov, O., Svitkin, Y., Sonenberg, N., Tamarkin-Ben-Harush, A., Viollet, B., and Dikstein, R. (2015). Translational Tolerance of Mitochondrial Genes to Metabolic Energy Stress Involves TISU and eIF1-eIF4G1 Cooperation in Start Codon Selection. *Cell Metab.* *21*, 479–492.

Slavoff, S.A., Mitchell, A.J., Schwaid, A.G., Cabili, M.N., Ma, J., Levin, J.Z., Karger, A.D., Budnik, B.A., Rinn, J.L., and Saghatelian, A. (2013). Peptidomic discovery of short open reading frame-encoded peptides in human cells. *Nat. Chem. Biol.* *9*, 59–64.

- Solomon, S., Xu, Y., Wang, B., David, M.D., Schubert, P., Kennedy, D., and Schrader, J.W. (2007). Distinct Structural Features of Caprin-1 Mediate Its Interaction with G3BP-1 and Its Induction of Phosphorylation of Eukaryotic Translation Initiation Factor 2 α , Entry to Cytoplasmic Stress Granules, and Selective Interaction with a Subset of mRNAs. *Mol. Cell. Biol.* 27, 2324–2342.
- Song, H., Mugnier, P., Das, A.K., Webb, H.M., Evans, D.R., Tuite, M.F., Hemmings, B.A., and Barford, D. (2000). The crystal structure of human eukaryotic release factor eRF1--mechanism of stop codon recognition and peptidyl-tRNA hydrolysis. *Cell* 100, 311–321.
- Song, T., Zheng, Y., Wang, Y., Katz, Z., Liu, X., Chen, S., Singer, R.H., and Gu, W. (2015). Specific interaction of KIF11 with ZBP1 regulates the transport of β -actin mRNA and cell motility. *J Cell Sci* 128, 1001–1010.
- Sørensen, M.A., and Pedersen, S. (1991). Absolute in vivo translation rates of individual codons in *Escherichia coli*. The two glutamic acid codons GAA and GAG are translated with a threefold difference in rate. *J. Mol. Biol.* 222, 265–280.
- Souquere, S., Mollet, S., Kress, M., Dautry, F., Pierron, G., and Weil, D. (2009). Unravelling the ultrastructure of stress granules and associated P-bodies in human cells. *J. Cell Sci.* 122, 3619–3626.
- Spriggs, K.A., Bushell, M., and Willis, A.E. (2010). Translational regulation of gene expression during conditions of cell stress. *Mol. Cell* 40, 228–237.
- Stadler, M., and Fire, A. (2013). Conserved Translatome Remodeling in Nematode Species Executing a Shared Developmental Transition. *PLOS Genet.* 9, e1003739.
- Starck, S.R., Jiang, V., Pavon-Eternod, M., Prasad, S., McCarthy, B., Pan, T., and Shastri, N. (2012). Leucine-tRNA Initiates at CUG Start Codons for Protein Synthesis and Presentation by MHC Class I. *Science* 336, 1719–1723.
- Starck, S.R., Tsai, J.C., Chen, K., Shodiya, M., Wang, L., Yahiro, K., Martins-Green, M., Shastri, N., and Walter, P. (2016). Translation from the 5' untranslated region shapes the integrated stress response. *Science* 351, aad3867.
- Stoecklin, G., and Kedersha, N. (2013). Relationship of GW/P-bodies with stress granules. *Adv. Exp. Med. Biol.* 768, 197–211.
- Stoecklin, G., Stubbs, T., Kedersha, N., Wax, S., Rigby, W.F.C., Blackwell, T.K., and Anderson, P. (2004). MK2-induced tristetraprolin:14-3-3 complexes prevent stress granule association and ARE-mRNA decay. *EMBO J.* 23, 1313–1324.
- Stöhr, N., Lederer, M., Reinke, C., Meyer, S., Hatzfeld, M., Singer, R.H., and Hüttelmaier, S. (2006). ZBP1 regulates mRNA stability during cellular stress. *J Cell Biol* 175, 527–534.
- Suragani, R.N.V.S., Zachariah, R.S., Velazquez, J.G., Liu, S., Sun, C.-W., Townes, T.M., and Chen, J.-J. (2012). Heme-regulated eIF2 α kinase activated Atf4 signaling pathway in oxidative stress and erythropoiesis. *Blood* 119, 5276–5284.
- Takahashi, K., Maruyama, M., Tokuzawa, Y., Murakami, M., Oda, Y., Yoshikane, N., Makabe, K.W., Ichisaka, T., and Yamanaka, S. (2005). Evolutionarily conserved non-AUG translation initiation in NAT1/p97/DAP5 (EIF4G2). *Genomics* 85, 360–371.
- Takizawa, P.A., Sil, A., Swedlow, J.R., Herskowitz, I., and Vale, R.D. (1997). Actin-dependent localization of an RNA encoding a cell-fate determinant in yeast. *Nature* 389, 90–93.
- Tamarkin-Ben-Harush, A., Vasseur, J.-J., Debart, F., Ulitsky, I., and Dikstein, R. (2017). Cap-proximal nucleotides via differential eIF4E binding and alternative promoter usage mediate translational response to energy stress. *ELife* 6, e21907.

- Tang, H., Hornstein, E., Stolovich, M., Levy, G., Livingstone, M., Templeton, D., Avruch, J., and Meyuhos, O. (2001). Amino Acid-Induced Translation of TOP mRNAs Is Fully Dependent on Phosphatidylinositol 3-Kinase-Mediated Signaling, Is Partially Inhibited by Rapamycin, and Is Independent of S6K1 and rpS6 Phosphorylation. *Mol. Cell Biol.* *21*, 8671–8683.
- Tang, L., Morris, J., Wan, J., Moore, C., Fujita, Y., Gillaspie, S., Aube, E., Nanda, J., Marques, M., Jangal, M., et al. (2017). Competition between translation initiation factor eIF5 and its mimic protein 5MP determines non-AUG initiation rate genome-wide. *Nucleic Acids Res.* *45*, 11941–11953.
- Taniuchi, S., Miyake, M., Tsugawa, K., Oyadomari, M., and Oyadomari, S. (2016). Integrated stress response of vertebrates is regulated by four eIF2 α kinases. *Sci. Rep.* *6*, 32886.
- Tcherkezian, J., Cargnello, M., Romeo, Y., Huttlin, E.L., Lavoie, G., Gygi, S.P., and Roux, P.P. (2014). Proteomic analysis of cap-dependent translation identifies LARP1 as a key regulator of 5'TOP mRNA translation. *Genes Dev.* *28*, 357–371.
- Thoreen, C.C., Chantranupong, L., Keys, H.R., Wang, T., Gray, N.S., and Sabatini, D.M. (2012). A unifying model for mTORC1-mediated regulation of mRNA translation. *Nature* *485*, 109–113.
- Tourrière, H., Chebli, K., Zekri, L., Courselaud, B., Blanchard, J.M., Bertrand, E., and Tazi, J. (2003). The RasGAP-associated endoribonuclease G3BP assembles stress granules. *J. Cell Biol.* *160*, 823–831.
- Tsai, J.C., Miller-Vedam, L.E., Anand, A.A., Jaishankar, P., Nguyen, H.C., Renslo, A.R., Frost, A., and Walter, P. (2018). Structure of the nucleotide exchange factor eIF2B reveals mechanism of memory-enhancing molecule. *Science* *359*, eaaq0939.
- Tsaytler, P., Harding, H.P., Ron, D., and Bertolotti, A. (2011). Selective inhibition of a regulatory subunit of protein phosphatase 1 restores proteostasis. *Science* *332*, 91–94.
- Valiente-Echeverría, F., Melnychuk, L., Vyboh, K., Ajamian, L., Gallouzi, I.E., Bernard, N., and Mouland, A.J. (2014). eEF2 and Ras-GAP SH3 domain-binding protein (G3BP1) modulate stress granule assembly during HIV-1 infection. *Nat. Commun.* *5*, 4819.
- Vattem, K.M., and Wek, R.C. (2004). Reinitiation involving upstream ORFs regulates ATF4 mRNA translation in mammalian cells. *Proc. Natl. Acad. Sci.* *101*, 11269–11274.
- Vikesaa, J., Hansen, T.V.O., Jønson, L., Borup, R., Wewer, U.M., Christiansen, J., and Nielsen, F.C. (2006). RNA-binding IMPs promote cell adhesion and invadopodia formation. *EMBO J.* *25*, 1456–1468.
- Voigt, F., Zhang, H., Cui, X.A., Triebold, D., Liu, A.X., Eglinger, J., Lee, E.S., Chao, J.A., and Palazzo, A.F. (2017). Single-Molecule Quantification of Translation-Dependent Association of mRNAs with the Endoplasmic Reticulum. *Cell Rep.* *21*, 3740–3753.
- Wagner, A. (2005). Energy Constraints on the Evolution of Gene Expression. *Mol. Biol. Evol.* *22*, 1365–1374.
- Wang, L., Miao, Y.-L., Zheng, X., Lackford, B., Zhou, B., Han, L., Yao, C., Ward, J.M., Burkholder, A., Lipchina, I., et al. (2013). The THO complex regulates pluripotency gene mRNA export and controls embryonic stem cell self-renewal and somatic cell reprogramming. *Cell Stem Cell* *13*, 676–690.
- Warner, J.R. (1999). The economics of ribosome biosynthesis in yeast. *Trends Biochem. Sci.* *24*, 437–440.
- Waxham, M.N. (2007). CHAPTER 1 - Molecular Mobility in Cells Examined with Optical Methods. In *Protein Trafficking in Neurons*, A.J. Bean, ed. (Burlington: Academic Press), pp. 3–27.

- Weinberg, D.E., Shah, P., Eichhorn, S.W., Hussmann, J.A., Plotkin, J.B., and Bartel, D.P. (2016). Improved Ribosome-Footprint and mRNA Measurements Provide Insights into Dynamics and Regulation of Yeast Translation. *Cell Rep.* *14*, 1787–1799.
- Weingarten-Gabbay, S., Elias-Kirma, S., Nir, R., Gritsenko, A.A., Stern-Ginossar, N., Yakhini, Z., Weinberger, A., and Segal, E. (2016). Systematic discovery of cap-independent translation sequences in human and viral genomes. *Science* *351*, aad4939.
- Wheeler, J.R., Matheny, T., Jain, S., Abrisch, R., and Parker, R. (2016). Distinct stages in stress granule assembly and disassembly. *ELife* *5*, e18413.
- Wickramasinghe, V.O., and Laskey, R.A. (2015). Control of mammalian gene expression by selective mRNA export. *Nat. Rev. Mol. Cell Biol.* *16*, 431–442.
- Wickramasinghe, V.O., Savill, J.M., Chavali, S., Jonsdottir, A.B., Rajendra, E., Grüner, T., Laskey, R.A., Babu, M.M., and Venkitaraman, A.R. (2013). Human inositol polyphosphate multikinase regulates transcript-selective nuclear mRNA export to preserve genome integrity. *Mol. Cell* *51*, 737–750.
- Wilczynska, A., Aigueperse, C., Kress, M., Dautry, F., and Weil, D. (2005). The translational regulator CPEB1 provides a link between dcp1 bodies and stress granules. *J. Cell Sci.* *118*, 981–992.
- Wippich, F., Bodenmiller, B., Trajkovska, M.G., Wanka, S., Aebersold, R., and Pelkmans, L. (2013). Dual specificity kinase DYRK3 couples stress granule condensation/dissolution to mTORC1 signaling. *Cell* *152*, 791–805.
- Wu, B., Buxbaum, A.R., Katz, Z.B., Yoon, Y.J., and Singer, R.H. (2015). Quantifying Protein-mRNA Interactions in Single Live Cells. *Cell* *162*, 211–220.
- Xu, Z., Poidevin, M., Li, X., Li, Y., Shu, L., Nelson, D.L., Li, H., Hales, C.M., Gearing, M., Wingo, T.S., et al. (2013). Expanded GGGGCC repeat RNA associated with amyotrophic lateral sclerosis and frontotemporal dementia causes neurodegeneration. *Proc. Natl. Acad. Sci.* *110*, 7778–7783.
- Yamamoto, H., Unbehaun, A., and Spahn, C.M.T. (2017). Ribosomal Chamber Music: Toward an Understanding of IRES Mechanisms. *Trends Biochem. Sci.* *42*, 655–668.
- Yan, X., Hoek, T.A., Vale, R.D., and Tanenbaum, M.E. (2016). Dynamics of Translation of Single mRNA Molecules In Vivo. *Cell* *165*, 976–989.
- Yang, X., Hu, Z., Fan, S., Zhang, Q., Zhong, Y., Guo, D., Qin, Y., and Chen, M. (2018). Picornavirus 2A protease regulates stress granule formation to facilitate viral translation. *PLOS Pathog.* *14*, e1006901.
- Young, D.J., Guydosh, N.R., Zhang, F., Hinnebusch, A.G., and Green, R. (2015). Rli1/ABCE1 Recycles Terminating Ribosomes and Controls Translation Reinitiation in 3'UTRs In Vivo. *Cell* *162*, 872–884.
- Young, R.M., Wang, S.-J., Gordan, J.D., Ji, X., Liebhaber, S.A., and Simon, M.C. (2008). Hypoxia-mediated selective mRNA translation by an internal ribosome entry site-independent mechanism. *J. Biol. Chem.* *283*, 16309–16319.
- Yu, C.-H., Dang, Y., Zhou, Z., Wu, C., Zhao, F., Sachs, M.S., and Liu, Y. (2015). Codon Usage Influences the Local Rate of Translation Elongation to Regulate Co-translational Protein Folding. *Mol. Cell* *59*, 744–754.
- Zhang, K., Daigle, J.G., Cunningham, K.M., Coyne, A.N., Ruan, K., Grima, J.C., Bowen, K.E., Wadhwa, H., Yang, P., Rigo, F., et al. (2018). Stress Granule Assembly Disrupts Nucleocytoplasmic Transport. *Cell* *0*.
- Zitomer, R.S., Walthall, D.A., Rymond, B.C., and Hollenberg, C.P. (1984). *Saccharomyces cerevisiae* ribosomes recognize non-AUG initiation codons. *Mol. Cell. Biol.* *4*, 1191–1197.

Zyryanova, A.F., Weis, F., Faille, A., Alard, A.A., Crespillo-Casado, A., Sekine, Y., Harding, H.P., Allen, F., Parts, L., Fromont, C., et al. (2018). Binding of ISRIB reveals a regulatory site in the nucleotide exchange factor eIF2B. *Science* 359, 1533–1536.

Chapter 2: Single-molecule RNA imaging in living cells reveals the function of stress granule and processing bodies during the integrated stress response

Wilbertz JH^{1,2}, Voigt F¹, Horvathova I^{1,2}, Chao JA¹

¹ Friedrich Miescher Institute for Biomedical Research, Basel, Switzerland

² University of Basel, Basel, Switzerland

Manuscript in preparation, deposited online on the bioRxiv pre-print server (doi: <https://doi.org/10.1101/332502>)

Upon stress, eukaryotic cells down regulate mRNA translation and form RNA and proteins containing cytoplasmic structures such as stress granules (SGs) and processing bodies (P-bodies, PBs). Direct high-resolution and spatio-temporal evidence for RNA biological functions of SGs and PBs is lacking. This chapter describes several dynamical and functional observations, obtained with various RNA single molecule imaging techniques during oxidative stress in human cells. We find that *cis* sequence determinants govern mRNA localization to SGs and PBs. Different mRNA species interact with these granules in different patterns and throughout the stress response. We identify LARP1 as a *trans*-acting factor which maintains mRNA presence in SGs and PBs. Further, the quantification of mRNA localization relative to SGs and PBs allowed us to assess the contribution of these granules on mRNA decay and translation. The majority of mRNA molecules remains stable and undergoes normal translation during the cellular recovery from stress. Although mRNAs interact frequently and dynamically with SGs and PBs, most of the direct cytosolic mRNA expression regulation can occur in a decentralized manner during stress and recovery.

2. 1 Introduction

Cells frequently face different kinds of stresses inflicted by their environment. To maintain homeostasis eukaryotic cells alter their gene expression especially on the translational level. Nutrient starvation and oxidative stresses can inhibit mammalian target of rapamycin (mTOR) which prevents the formation of the eukaryotic translation initiation factor (eIF) 4F complex (Panas et al., 2016; Sfakianos et al., 2018). Protein-folding stress, viral double stranded RNA, amino acid deprivation, heme levels and oxidative stress are sensed by PKR-like endoplasmic reticulum kinase (PERK), protein kinase R (PKR), general control non-depressible 2 (GCN2) or heme-regulated inhibitor (HRI), respectively. All four kinases phosphorylate eIF2 α (Ser51) which reduces the availability eIF2-GTP-tRNA^{Met} ternary complex (Pakos-Zebrucka et al., 2016). Stress-induced decreased canonical translation initiation often coincides with a reorganization of cytosolic RNAs and proteins into microscopically visible and non-membrane delimited messenger ribonucleoprotein (mRNP) complexes. The two most prominent stress-induced mRNP complexes are stress granules (SGs) and processing bodies (P-bodies, PBs).

SGs contain RNA, several eIFs and the small ribosomal 40S subunit. RNA binding proteins (RBPs) with low complexity domains (LCDs) such as TIAR and G3BP1 are also present in SGs. Presumably, these proteins aggregate on translationally stalled mRNAs to form early SG cores by phase separation, followed by the assembly of a more dynamic and liquid-like shell structure (Jain et al., 2016; Niewidok et al., 2018; Wheeler et al., 2016). While almost all expressed mRNAs can be detected inside of purified SG cores, the extent to which transcripts are present in SGs differs per gene. In total, 10% of all expressed mRNAs is present in SGs (Khong et al., 2017). Due to the striking correlation between the assembly of SG with general translation initiation repression and the presence of initiation factors eIF2, 3, 4A/E/G/B inside of SGs, it has been proposed that SGs act as local hubs for translation repression (Decker and Parker, 2012; Stoecklin and Kedersha, 2013). In addition, the presence of inhibitory proteins, miRNAs or the steric block of ribosomal assembly have been implicated in repressing mRNA translation locally inside of SGs (Buchan, 2014). PBs are present in unstressed cells and increase in number during stress. PBs contain RNAs and several RNA decay factors such as the decapping, exonuclease or helicase enzymes DCP1a, XRN1, and DDX6. This pointed towards a PB function for localized RNA decay (Decker and Parker, 2012). Others proposed that PBs function as sites for mRNA storage or protection from which mRNAs can return to polysomes (Bhattacharyya et al., 2006; Brengues et al., 2005) or where mRNAs are subject to an extra layer of translational repression during recovery from stress (Halstead et al., 2015). In

addition, a dual role for mRNA storage and decay has been proposed (Aizer et al., 2014), while another recent study did not detect any direct degradation events inside of PBs (Horvathova et al., 2017). Recently, the purification of PBs under unstressed conditions led to first insights into the PB transcriptome, which seems to include predominantly intact and coding mRNAs (Hubstenberger et al., 2017).

PBs and SGs have a varying composition depending on cellular context (Markmiller et al., 2018), fast formation and disassembly kinetics (Jain et al., 2016; Protter and Parker, 2016), and show frequent physical interactions with each other (Kedersha et al., 2005; Stoecklin and Kedersha, 2013).

Despite this, little is known about the dynamics of individual protein or RNAs with the surrounding cytosol. The exchange kinetics of RBPs have been mostly studied by bulk fluorescence recovery after photobleaching (FRAP) (Buchan and Parker, 2009; Kedersha et al., 2005; Mollet et al., 2008). The majority of examined proteins possessed recovery rates in the order of minutes (Buchan and Parker, 2009). Using single-molecule localization microscopy a recent study addressed the spatio-temporal dynamics of two SG proteins in more detail and found that exchange kinetics depend on whether a protein is localized within the stable core or the more dynamic shell of a SG (Niewidok et al., 2018). Less is known about the RNA dynamics of PBs and SGs. Previous studies often used transcriptome wide RNA labelling with oligo(dT) probes (Kedersha et al., 2000) or MS2-MCP mRNA labelling, but in combination with bulk FRAP approaches lacking single molecule sensitivity (Aizer et al., 2014; Mollet et al., 2008). Although potentially obscured by these technical limitations, residence times of mRNAs in PBs and SGs were generally found to be in the order of minutes.

Detailed and direct insights into mRNA dynamics and mRNA regulation relative to PBs and SGs are currently lacking. In particular, open questions are how dynamically mRNAs rather than proteins interact with granules during different stages of the stress response and whether mRNAs can exchange between different mRNP complexes. It is also unknown to what extent PB- and SG-attributed functions occur exclusively inside of these structures or also in the surrounding cytosol. Here, we applied live cell MS2-MCP single molecule mRNA imaging and tracking in combination with stably expressed fluorescent markers for PBs and SGs in human cells. We find that enrichment of mRNAs in granules occurs throughout the stress response and that a 5' terminal oligo pyrimidine (5'TOP) *cis*-acting element enhances mRNA recruitment into PBs and SGs. We quantified the high and low variability of mRNA interactions with SGs and PBs, respectively, and identified low-frequency movement of mRNAs from SGs to PBs. Further, we show that La-related protein 1 (LARP1) plays a role as *trans*-acting factor in

stabilizing 5'TOP mRNA presence inside of granules. Using single molecule degradation (Horvathova et al., 2017) and translation imaging (Yan et al., 2016) we demonstrate that mRNAs outside of granules are not specifically degraded and translate equally well during stress recovery as they did before stress onset. In summary, we present direct evidence by single molecule imaging that the presence of mRNAs inside of PBs and SGs is uncoupled from their biological regulation.

2.2 Results

In order to characterize the spatial and temporal localization of mRNAs in RNA-protein granules during stress, we engineered a HeLa cell line expressing fluorescent mRNAs, PB, and SG markers in three spectrally distinct colors to allow their simultaneous detection in living cells (Fig. 1A). First, G3BP1-GFP and DDX6-TagRFP-T were stably integrated into HeLa cells and served as SG and PB markers, respectively. Cells were then sorted for low GFP and TagRFP-T levels by fluorescence activated cell sorting (FACS) to prevent SG or excess PB formation in the absence of stress (Tourrière et al., 2003). After generation of this cell line, the cells were treated with 100 μ M sodium arsenite (SA) to confirm that eIF2 α was phosphorylated on Ser51 (Fig. S1A) and that translation was inhibited (Fig. S1B) indicating the activation of the integrated stress response. The number of G3BP1-GFP and DDX6-TagRFP-T granules was similar to the levels observed for endogenous G3BP1 in the absence and presence of SA (Fig. S1C). Next, we confirmed that the size, number, and formation kinetics of both G3BP1-GFP and DDX6-TagRFP-T granules were comparable with previous reports (Fig. S1D,E) (Ohshima et al., 2015; Wheeler et al., 2016).

To detect mRNAs in living cells we cloned 24 MS2 stem-loops into the 3'UTR of three different types of transcripts that we anticipated could have potentially different localization behaviors during the stress response (Fig. 1A). The first reporter mRNA contained Renilla luciferase in the coding sequence and was generated to represent a standard mRNA encoding a cytosolic protein. The second mRNA reporter was identical except for the addition the first 50 nts of the RPL32 5'UTR which contains a 5'TOP motif. The 5'TOP motif is found in all ribosomal proteins and many translation factors and 5'TOP mRNAs are thought to constitute ~20% of all transcripts present in cells (Hornstein et al., 2001; Iadevaia et al., 2008). Based on previous observations by us and others (Damgaard and Lykke-Andersen, 2011; Halstead et al., 2015) we expected the 5'TOP Renilla reporter to accumulate more in SGs and PBs compared to the Renilla reporter. The third reporter contained Gaussia luciferase in the coding sequence, a secreted protein, instead of Renilla luciferase and was generated to represent an mRNA that is translated on the endoplasmic reticulum (ER) (Voigt et al., 2017). Earlier reports suggested that ER localization protects mRNAs from entering SGs (Backlund et al., 2016; Unsworth et al., 2010). Accurate detection and tracking of single mRNA molecules is facilitated by physiological expression levels. We therefore utilized doxycycline-inducible HeLa cells and stably integrated single-copies of the reporters (Weidenfeld et al., 2009). To visualize mRNAs, we stably co-expressed nuclear localization signal (NLS)

containing Halo-tagged MS2 bacteriophage coat protein (NLS-MCP-Halo) that binds with high affinity to MS2 stem-loops (Bertrand et al., 1998; Grimm et al., 2015; Wu et al., 2015). Together, this allowed us to image single mRNA molecules in live unstressed and stressed human cells.

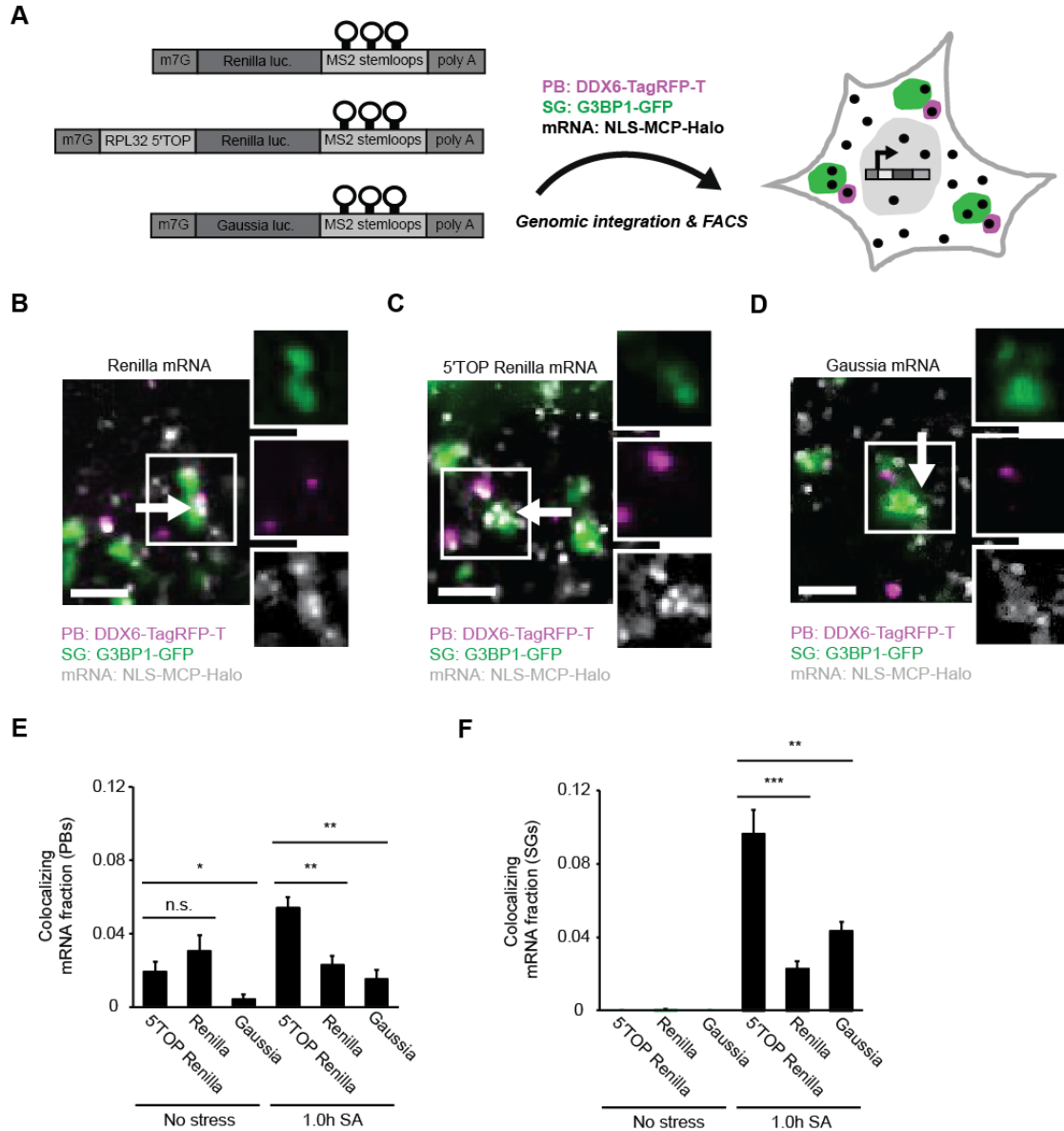


Fig 1: Triple-color live cell imaging identifies stress- and 5'TOP element-dependent mRNA localization to PBs and SGs

(A) Scheme depicting the used mRNA reporters and HeLa cell line expressing DDX6-TagRFP-T as PB markers and G3BP1-GFP as SG markers. mRNAs were expressed from a doxycycline inducible single locus and were labelled with NLS-MCP-Halo. (B-D) All cell lines expressing one of the reporters, respectively, formed PBs and SGs after treatment with 100µM SA for 1h. mRNAs localization to PBs and SGs was reporter-dependent. (B) Cells expressing Renilla reporter mRNAs showed modest mRNAs localization to PBs and SGs. Larger mRNA clusters were absent. (C) Cells expressing 5'TOP Renilla mRNA reporters showed the most mRNA colocalization with PBs and SGs. (D) Most mRNAs in cells expressing Gaussia reporter mRNAs diffused freely

through the cytoplasm, but a fraction was localized to PBs and SGs. (E) Colocalization analysis and quantification of the data presented in (B-D). All tested mRNA reporters were able to localize to PBs and SGs during SA stress, but 5'TOP Renilla reporter mRNAs were significantly more enriched than Renilla or Gaussia mRNA reporters (arrows indicate mRNA colocalization with SGs; scale bars = 2 μ m; mean \pm SEM; two-tailed, unpaired Student's t-test; * = $p < 0.05$, ** = $p < 0.01$, *** = $p < 0.001$; >20 fields of view per time point and experiment, 3 biological replicates).

After doxycycline induction, we imaged all three cell lines in the absence and presence of SA. In the absence of stress, Renilla reporter mRNAs rapidly moved throughout the cytoplasm, SGs were absent and PB numbers were low. After 1 hour of SA treatment, the majority of Renilla mRNAs still diffused freely in the cytosol, but a fraction of molecules localized to SGs and PBs, which reduced their mobility (Fig. 1B). In unstressed cells, the 5'TOP Renilla reporter mRNAs behaved similar to the Renilla reporter, however, a larger fraction of 5'TOP Renilla reporter mRNAs was localized to SGs and PBs during stress (Fig. 1C). Gaussia mRNA reporters moved less in the cytoplasm and were mostly static, which is consistent with a previous study that demonstrated their translation-dependent association with the ER (Voigt et al., 2017). Upon addition of SA, when translation initiation is inhibited, the majority of Gaussia reporters became mobile (Fig. 1D). Interestingly, a small fraction of Gaussia mRNAs did localize to SGs and PBs indicating that ER-association prior to stress does not prevent their entry into granules. Single molecule tracking and colocalization quantification of mRNA reporter localization to PBs (Fig. 1E) and SGs (Fig. 1F) demonstrated that the 5'TOP Renilla reporter mRNAs localized significantly more to both granules than Renilla or Gaussia mRNA reporters.

In order confirm the localization patterns observed in living cells, we performed single molecule mRNA fluorescence *in situ* hybridization (smFISH) in HeLa cells with probes against the endogenous GAPDH and RPL32 transcripts, combined with IF against endogenous G3BP1 and DDX6 (Fig. S2A,B). Upon addition of SA, only a small fraction of GAPDH transcripts colocalized with PBs and SGs (Fig. S2A,C), which is similar to previous reports (Khong et al., 2017). Endogenous RPL32 transcripts accumulated in PBs and SGs similar to the levels we observed for the 5'TOP Renilla reporter (Fig. S2B,C). Taken as whole, our results demonstrate that *cis*-acting elements within transcripts can promote their association with granules during stress.

After having observed the differential localization of Renilla and 5'TOP Renilla mRNA reporters to SGs and PBs, we next sought to understand how this pattern was established. In principle, the differential recruitment of mRNAs to stress-induced mRNPs could either occur during the formation of granules or only after mature granules had formed. To address this question, we quantified the colocalization of Renilla and 5'TOP Renilla transcripts with SGs and PBs over time (Fig. 2A). For PBs we

observed that 5'TOP Renilla reporters entered these structures mainly during the first 30 minutes, after which the colocalizing mRNA fraction stayed constant until the end of the time course (Fig. 2B). In contrast, the Renilla reporter showed a significantly smaller time-dependent colocalization increase with PBs compared to 5'TOP Renilla reporters (Fig. 2B). mRNA recruitment kinetics to SGs were similar to the results obtained for PBs. 5'TOP Renilla reporters entered SGs faster and in higher numbers than the Renilla transcripts (Fig. 2C). Most mRNAs were recruited during the first 30 minute of SA stress, reaching a plateau phase afterwards. Renilla reporters showed only a modest increase in SG colocalization over time which was significantly smaller than the increase observed for 5'TOP Renilla mRNAs (Fig. 2C). Based on these results we show that 5'TOP element-dependent mRNA localization to PBs and SGs correlates with PB and SG formation during stress onset. Interestingly, the granule localization difference between 5'TOP Renilla and Renilla reporters arises already early during their formation and not after they have fully matured indicating that *cis*-acting elements within mRNAs can contribute to the rate at which different mRNAs localize to stress-induced mRNP complexes.

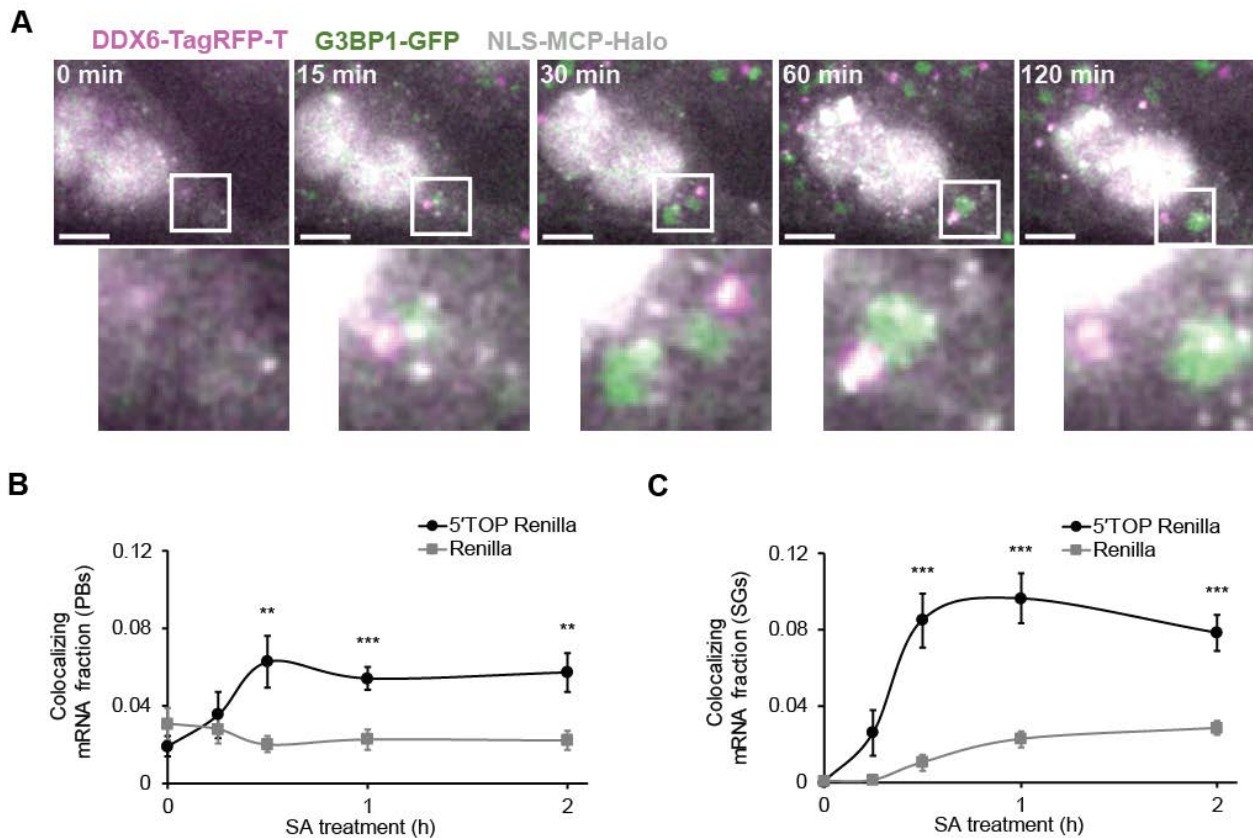


Fig. 2: 5'TOP element-dependent mRNA localization correlates with PB and SG formation during stress onset. (A) HeLa cells stably expressing G3BP1-GFP, DDX6-TagRFP-T, NLS-MCP-Halo and inducible 5'TOP Renilla reporter mRNAs were treated with 100 μ M SA for 2h and single cells were imaged at the indicated intervals. Cytoplasmic mRNAs dynamically bound to PBs

and SGs during and after their formation. (B) and (C) HeLa cell lines stably expressing G3BP1-GFP, DDX6-TagRFP-T, NLS-MCP-Halo and either inducible Renilla or 5'TOP Renilla reporter mRNAs were treated with 100 μ M of SA for 2h and different cells were imaged over time and mRNA colocalization with PBs (B) and SG (C) was assessed. 5'TOP Renilla reporter mRNAs were rapidly recruited to PBs and SGs. Renilla reporter mRNAs localized significantly less to PBs and SGs (scale bars = 10 μ m; mean \pm SEM; two-tailed, unpaired Student's t-test; ** = $p < 0.01$, *** = $p < 0.001$; >20 fields of view per time point and experiment, 3 biological replicates).

In order to characterize the dynamics of granule localization during stress, we extracted directionality information from mRNA tracks relative to PBs and SGs (Fig. 3A). mRNA molecules that were overlapping with a PB or SG received a localization index value of 1 and mRNAs outside of granules received a value of 0. A change of localization index value within one mRNA track therefore indicated a change of direction relative to the granule. This analysis allowed us to distinguish four different categories of mRNA movement relative to PBs and SGs (Fig. 3A). mRNAs could either be classified as static during the observation period, they could show multiple transient interactions, or simply move inside or outside of a granule. Renilla reporters had lower levels for all interactions with PBs (Fig. 3B) and SGs (Fig. 3C) than 5'TOP Renilla reporters. In addition, no single movement class was significantly more prominent than the others. For the 5'TOP Renilla reporter, it was interesting to see that mRNAs behaved differently when interacting with either PBs (Fig. 3D) or SGs (Fig. 3E). Up to half of 5'TOP Renilla reporter localization behavior to SGs was explained by static mRNA interaction with the SG, while the other half was composed of mainly multiple transient interaction and, to smaller extent, unidirectional movements (Fig. 3E). The 5'TOP Renilla reporter interaction patterns with PBs were less dynamic. Here, between 70-85% of localization behavior to PBs was explained by static mRNA interaction with the PB. The remaining fraction was composed of similar amounts of transient and unidirectional movement (Fig. 3D). It is important to note that the distribution of movement patterns was similar at all time points indicating that interactions between granules and RNAs was constant throughout granule formation and maturation.

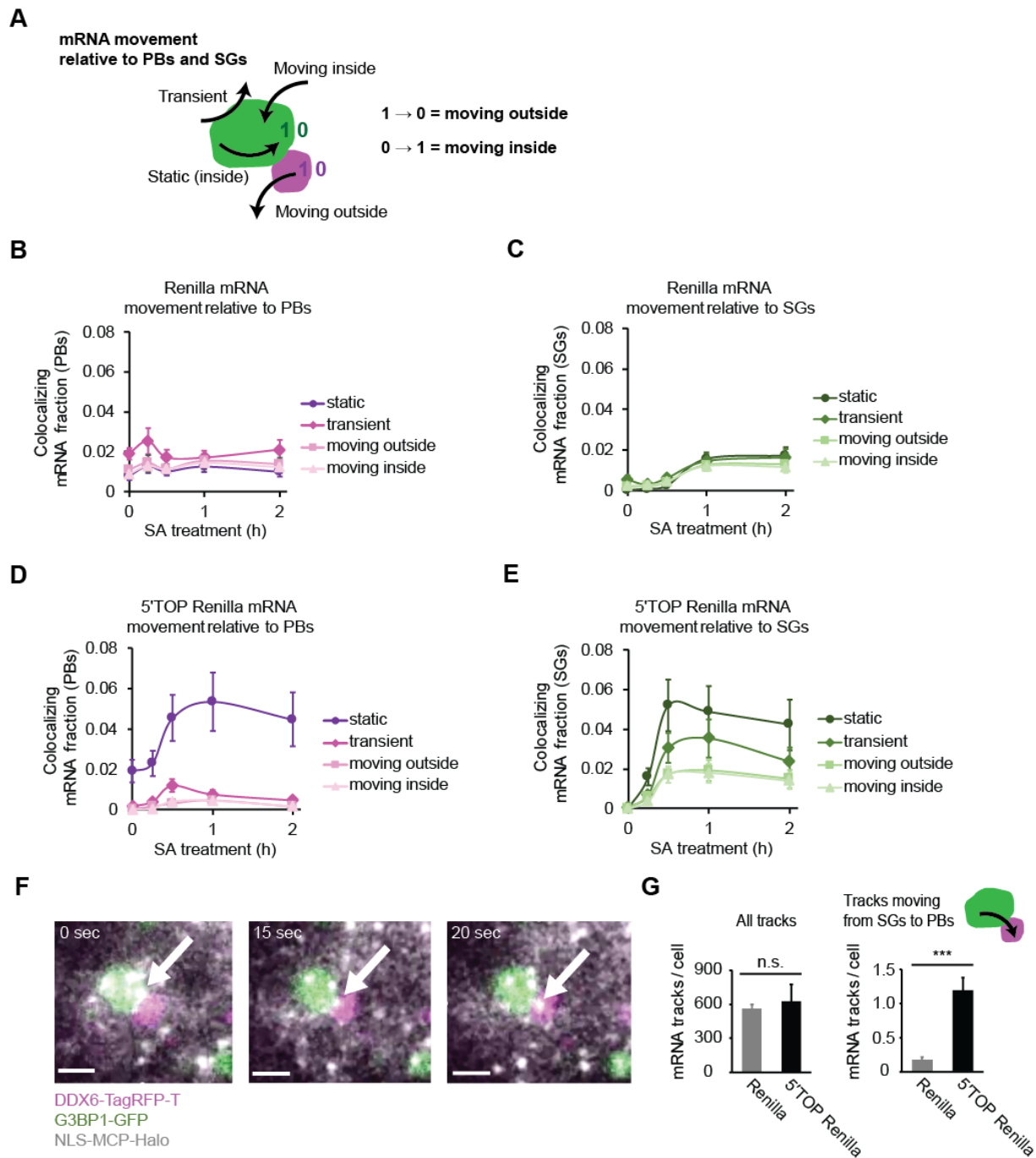


Fig. 3: mRNA tracking reveals recruitment dynamics into SGs and PBs. (A) Data analysis workflow to quantify the movement of mRNAs relative to PBs and SGs. A localization index change from 1 to 0 represented an outward movement, a change from 0 to 1 represented an inward movement relative to a PB or SG. mRNA tracks with localization indices of exclusively 1, were considered to be static. Tracks with more than one entry and exit event were categorized as transient interactions. (B) and (C) HeLa cells stably expressing G3BP1-GFP, DDX6-TagRFP-T, NLS-MCP-Halo coat proteins and inducible Renilla reporter mRNAs were treated with 100 μ M SA for 2h and different cells were imaged over time and their mRNA movement patterns were analyzed. Renilla mRNAs had no predominant movement pattern relative to PBs (B) or SGs (C) during the stress time-

course (>20 fields of view per time point and experiment, 3 biological replicates). (D) and (E) HeLa cells stably expressing G3BP1-GFP, DDX6-TagRFP-T, NLS-MCP-Halo coat proteins and inducible 5'TOP Renilla reporter mRNAs were treated with 100 μ M SA for 2h and different cells were imaged over time and their mRNA movement patterns were analyzed. (D) PB-associated mRNAs were mostly static. (E) SG-associated mRNAs were mostly static or showed transient interactions. (F) 5'TOP Renilla reporter mRNAs can move from a SG to a PB during SA stress (scale bars = 3 μ m). (E) Analysis of all mRNA movement patterns for shuttling events from SGs to PBs indicated that only a minor fraction of cytoplasmic 5'TOP Renilla reporter mRNAs move between both granules (mean \pm SEM; two-tailed, unpaired Student's t-test; *** = $p < 0.001$; >20 fields of view per time point and experiment, 3 biological replicates).

The time course experiments indicated that mRNA recruitment to granules correlates with granule size and number (Fig. 2 & Fig S1), but that there is a significant amount of mRNA exchange between granules and the cytoplasm during earlier and later phases of stress (Fig. 3B-E). Since SGs and PBs have been found to interact very frequently and dynamically with each other (Kedersha et al., 2005), it has also been proposed that mRNAs can be sorted from SGs to PBs in a process referred to as "mRNA triage" (Anderson and Kedersha, 2008; Kedersha and Anderson, 2002). Since to our knowledge there is no direct mRNA-based evidence for the mRNA triage model, we specifically searched for mRNA tracks within our stress time course data set that moved from SGs to PBs. We were able to detect a small number of such events (Fig. 3F). Despite this, the frequency of these events across the entire duration of the 120-minute time course was extremely low. For, on average, ~600 detected mRNA tracks per cell we could only identify 1 event using the 5'TOP Renilla reporter (Fig. 3G). We also searched for mRNA movement events in the inverse direction from PBs to SGs, but were not able to detect such events. Presumably, this is due to the high static mRNA localization and low outside mRNA movement rates of PBs (Fig. 3B, right panel).

Since we observed that the 5'TOP sequence promoted mRNA localization to granules during the stress response, we then asked if there was a *trans*-acting factor that also contributed to this effect. Recently, the RNA binding protein La-related protein 1 (LARP1) has been shown to bind the m⁷G-cap and 5'TOP-element of mRNAs and to regulate their translation (Fonseca et al., 2015; Hong et al., 2017; Lahr et al., 2015, 2017; Philippe et al., 2018; Tcherkezian et al., 2014). In addition, LARP1 is present in SGs and PBs (Fig. S3A and (Hopkins et al., 2016; Merret et al., 2013; Nykamp et al., 2008). We decreased levels of LARP1 in HeLa cells by 48h siRNA-mediated knock-down (KD) (Fig. 4A, Fig. S3A) and performed a 120-minute time-course experiment identical to the one described previously. Importantly, LARP1 KD did not affect mRNA numbers as detected by single molecule imaging (Fig. 4B). Furthermore, LARP1 KD also did not alter the size or numbers of SGs, while PBs were slightly reduced in size (Fig. S3B,C). Interestingly, the association of 5'TOP Renilla mRNAs into PBs (Fig. 4C) and SGs (Fig. 4D) during the first

30 minutes of SA stress was unperturbed. At later time points, however, the fraction of 5'TOP Renilla mRNA in both granules was reduced indicating that LARP1 was necessary for anchoring 5'TOP Renilla within granules. In order to confirm that LARP1 also affected the localization of endogenous transcripts during stress, we performed IF against G3BP1 and DDX6 in combination with smFISH against either RPL32 mRNA or GAPDH mRNA (Fig. S4A). RPL32 mRNA localization to SGs, but not PBs, was reduced during LARP1 KD while GAPDH localization to granules was unaffected (Fig. S4A,B). These experiments indicate that RNA-binding proteins can control the localization of specific transcripts to SGs and PBs during stress and that this regulation can occur even after transcripts have already entered mRNP granules.

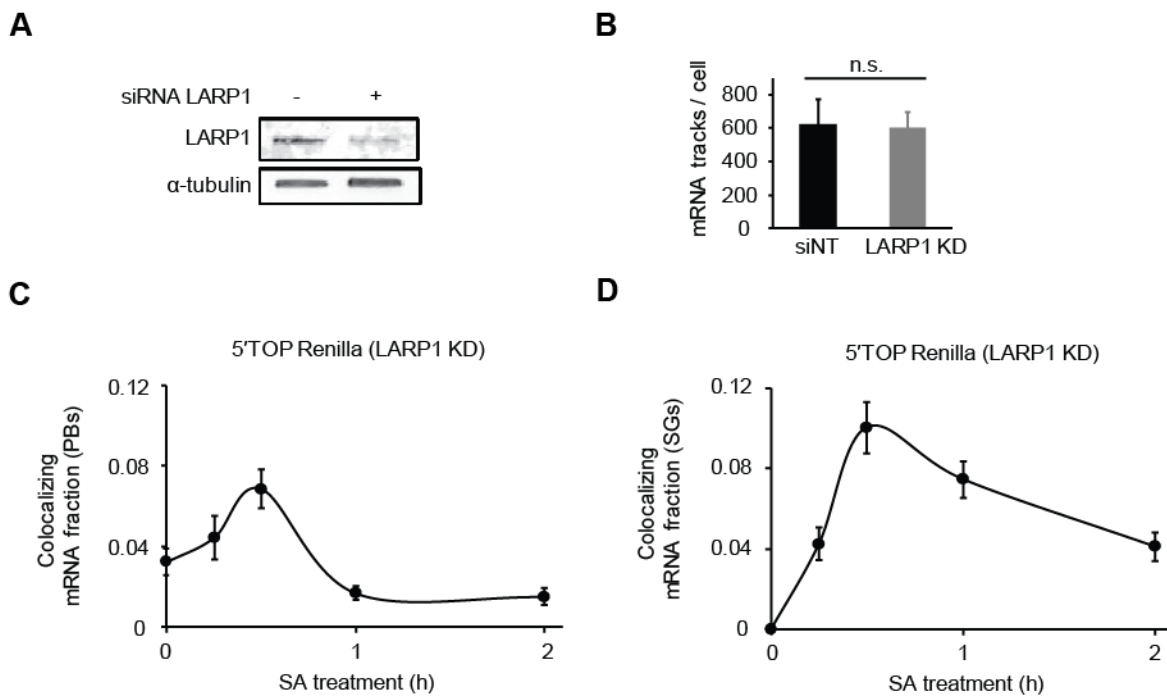


Fig. 4: LARP1 knock-down decreases 5'TOP mRNA accumulation in SGs during the progressed stressed response. (A) Transfection of HeLa cells with siRNAs against LARP1 for 48h decreased LARP1 expression. (B) LARP1 knock-down did not decrease the number of tracked mRNAs across all time points. (C) and (D) HeLa cell lines stably expressing G3BP1-GFP, DDX6-TagRFP-T, MCP-Halo coat proteins and inducible 5'TOP Renilla reporter mRNAs were transfected with siRNAs against LARP1 for 48h and treated with 100 μ M SA for 2h. Different cells were imaged over time and the mRNA fraction colocalizing with PBs (C) and SGs (D) was analyzed (mean \pm SEM; >20 fields of view per time point and experiment, 3 biological replicates).

To what extent the sequestration mRNAs into granules has an effect on their decay and translation is currently unclear. Previously, we have found that translation and degradation of Renilla and 5'TOP Renilla mRNAs is inhibited throughout the cytoplasm, regardless of granule localization, during the stress response (Halstead et al., 2015; Horvathova et al., 2017). It has, however, been

suggested that stress-induced PBs (Bhattacharyya et al., 2006; Brengues et al., 2005) and SGs (Kedersha and Anderson, 2002) could serve as sites for storage where mRNA molecules could be protected from the harmful effects of stress. Additionally, during the stress response the oxidation of mRNAs can also potentially lead to decreased mRNA half-lives through no-go decay (Nunomura et al., 2017; Simms et al., 2014). While only ~15% of 5'TOP Renilla mRNA reporters were found to be inside of PBs and SGs during stress (Fig. 2), this provided an entry point for exploring the effect of this localization on the fate of transcripts after stress has been relieved.

To assess the potential protective effect of granule localization on mRNA decay we used 3(Three)'-RNA End Accumulation during Turnover (TREAT) to quantify mRNA degradation with single-molecule resolution (Horvathova et al., 2017). After doxycycline induction for 45 minutes, cells were stressed for 45 minutes with SA and then washed to remove both doxycycline and SA. Doxycycline removal stopped transcription of the mRNA reporter, so that only transcripts that experienced stress were monitored during the recovery phase. Cells were then fixed at different time points during an 8-hour stress recovery time course and intact and stabilized 3'-end fragments were quantified by smFISH (Preliminary Fig. 5). These experiments are still on going, but preliminary analysis of the ratio between intact and stabilized 3'-end fragments across all time points showed two interesting findings. First, mRNA degradation remains inhibited during the first two hours of recovery from stress even though eIF2 α has been dephosphorylated (Fig. S1A) and SGs have completely dissolved during the first hour of stress recovery (Fig. S5). The single-molecule sensitivity of TREAT allows to exclude the possibilities of either rapid mRNA decay of cytosolic or granule-localized transcripts during the first two hours of stress recovery. Based on the TREAT data, however, we cannot exclude the possibility that the small fraction of mRNAs within PBs (~5%) are rapidly degraded during stress relief, however, we previously detected 5'TOP transcripts within PBs during stress relief suggesting that they are not actively degraded there (Halstead et al., 2015). The second observation is that once mRNA decay resumes after two hours of recovery, the half-life of 5'TOP Renilla transcripts is similar to the stability measured in unstressed cells. These experiments, however, are ongoing experiments and they will clarify the effect of granule

localization

on

mRNA

decay.

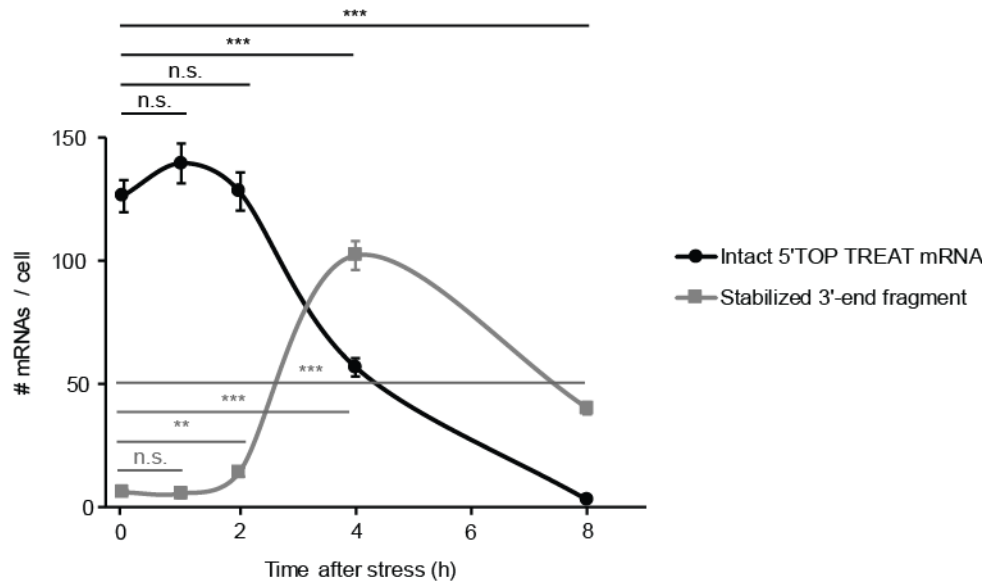


Fig. 5: 5'TOP TREAT mRNAs do not rapidly degrade during the recovery from stress. (A) In HeLa cells the expression of 5'TOP Renilla TREAT mRNAs was induced for 45 minutes followed by treatment with 100 μ m SA for 45 minutes and a washing step. Cells were then fixed at different time points during the recovery phase and RNA smFISH was performed. Intact 5'TOP TREAT mRNAs were detected as dual colored spots, while viral pseudoknot-protected stabilized 3'-end fragments were detected as single colored spots (mean \pm SEM; two-tailed, unpaired Student's t-test; ** = $p < 0.01$, *** = $p < 0.001$; > 200 cells / time point).

Since we did not observe a granule-localization effect on mRNA decay, we wanted to further test whether PBs and SGs might have a protective role during stress for translation after the stress is over. We utilized a recently developed nascent polypeptide-based translation imaging system, since it offers the possibility to quantify the fraction of translating mRNAs per cell, as well their individual translational activity (Morisaki et al., 2016; Pichon et al., 2016; Wang et al., 2016; Wu et al., 2016; Yan et al., 2016). This technique relies on the binding of the scFv-GFP to the nascent SunTag epitopes that emerge from the ribosome as a fluorescent measurement of translation per mRNA molecule. We fused a 24x SunTag repeat cassette to the N-terminus of the Renilla luciferase coding sequence of our reporter, giving rise to a 5'TOP SunTag Renilla reporter (Fig. 6A). We then genomically integrated a single copy of this reporter into the previously used doxycycline-inducible HeLa cells. In addition, single-chain antibodies fused to GFP (scFv-GFP) were stably integrated into the cells. Individual mRNAs were visualized by the binding of NLS-MCP-Halo to the MS2 stem loops in the 3'UTR of the reporter.

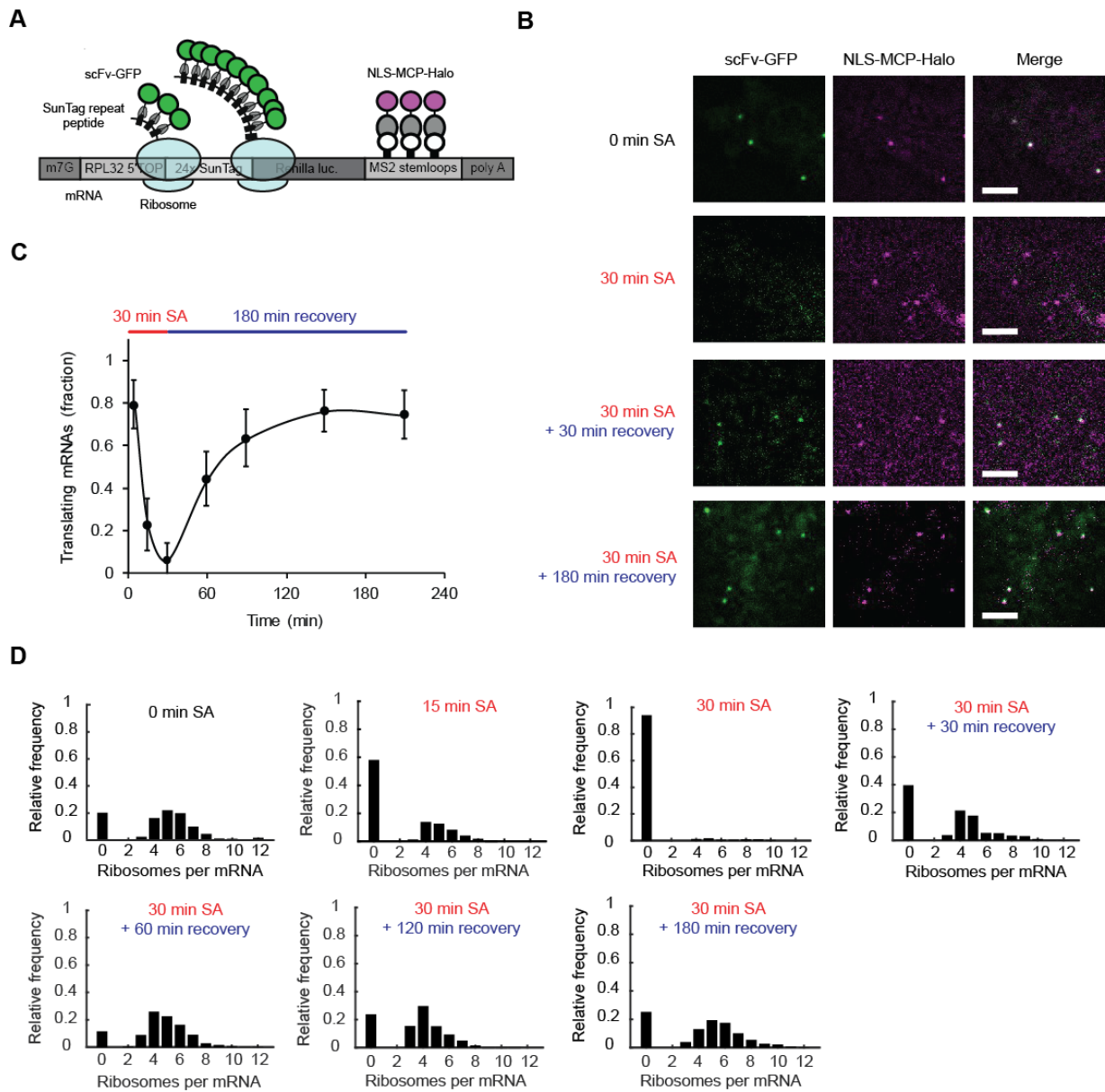


Fig. 6: 5'TOP SunTag mRNAs can undergo normal and mRNP granule-independent translation during recovery from stress. (A) Schematic depiction of the 5'TOP SunTag Renilla mRNA reporter. Single-chain antibodies fused to GFP (scFv-GFP) label the ribosome emerging SunTag peptide chain in a length-dependent manner. (B) Representative images for SunTag translation imaging in cells stably expressing scFv-GFP, NLS-MCP-Halo, and inducible 5'TOP SunTag Renilla mRNA reporters. Under non-stress conditions most mRNAs (NLS-MCP-Halo) colocalized with a translation site (scFv-GFP). 30min of 100 μ m SA treatment blocked translation. During recovery from stress translation sites colocalizing with mRNAs reappeared (scale bar = 2 μ m). (C) Quantification of the fraction of 5'TOP SunTag Renilla mRNAs colocalizing with translation sites showed that mRNA translation fully resumed to pre-stress levels during the recovery from stress (mean \pm SEM; 2 biological replicates). (D) The ribosomal occupancy distribution on mRNAs decreased during 30min of SA treatment and reached a pre-stress distribution after 180min of recovery from stress. For details on ribosome occupancy quantification, see Material and Methods.

We then used these cells to quantify the translation of individual mRNA molecules before, during and after stress. In the absence of stress, the majority of 5'TOP SunTag Renilla reporters (~80%) were undergoing active translation as detected by the colocalization of the SunTag GFP signal with the NLS-MCP-Halo signal (Fig. 6B,C). After 30 minutes of SA-induced stress, almost all mRNAs (> 95%) were translationally inhibited, indicated by the absence of scFv-GFP labelled translation sites on mRNAs (Fig. 6B,C). Next, we used the colocalization frequency of scFv-GFP with NLS-MCP-Halo to quantify the fraction of mRNAs undergoing active translation for all time points during the stress and recovery time course (Fig. 6C). If only the 15% of 5'TOP SunTag Renilla mRNAs bound to stress-induced mRNPs would be protected from stress, we expected that during translational recovery we should not observe more than 15% of mRNAs undergoing translation. Our experiment, however, indicates that 44% of all cytoplasmic mRNAs had already resumed translation after only 30 minutes of translational recovery. Translation then gradually recovered over the next 2.5 hours to levels comparable to the pre-stress time point (Fig. 6C).

Due to the binary readout of using colocalization for the determination of translation, it remained a possibility that oxidative stress-inflicted chemical modifications to non-sequestered mRNPs might decrease their translational efficiency, although not fully abrogating translation initiation. These potential defects in translation should be manifested in the number of ribosomes per mRNAs. SunTag-based translation imaging allowed quantifying the ribosomal occupancy per mRNA. In brief, ribosomal occupancy was calculated by dividing the fluorescent intensity of the translation site by the fluorescent intensity of a mature SunTag Renilla protein. We analyzed the distribution of all translation site intensities for all stress and recovery time points and calculated the ribosome occupancy per mRNA (Fig. 6D). In unstressed cells, each mRNA was bound by 4-5 ribosomes. After 30 minutes of stress, most mRNAs had no detectable translation sites. After 30 minute of recovery the fraction of translating mRNAs increased again and the average ribosome occupancy increased to 3 ribosomes per mRNAs. After 3 hours of recovery, most mRNAs had regained their full ribosome occupancy and were bound by 4 ribosomes per mRNA. The ribosomal distribution per mRNA therefore showed that there was only a minor difference between pre-stress translation activity levels and recovery translation activity levels (Fig. 6D).

2.3 Summary and discussion

How single mRNAs interact with stress-induced mRNP complexes and whether this has functional consequences is unknown. Here, we used single molecule mRNA imaging in SA-stressed living human cells to quantify the spatio-temporal as well as decay and translation dynamics of transcripts inside and outside of PBs and SGs. We find that 5'TOP Renilla reporter mRNAs are more enriched in stress-induced mRNP complexes than Renilla and Gaussia luciferase reporters lacking a TOP element in their 5'UTRs (Fig. 1). We demonstrate that mRNA recruitment to PBs and SGs occurs throughout the stress response. After 30 minutes of SA stress, the number of mRNA molecules in PBs and SGs stays constant (Fig. 2), while mRNA movement remains dynamic (Fig. 3). 5'TOP Renilla reporter mRNAs interact more dynamically with SGs than PBs, where the majority of interacting mRNAs is statically bound. mRNAs are able to move from SGs to PBs, but the frequency of such events is very low (Fig. 3). We further show that the known 5'TOP-element binding and SG-resident protein LARP1 is a *trans*-acting factor able to stabilize 5'TOP Renilla reporter mRNA presence in SGs during extended periods of stress (Fig. 4). Using mRNA reporters to detect localized decay and translation, we find that the majority of mRNAs, which have not been inside of PBs or SGs, have unchanged half-lives and translation rates during the recovery from stress (Fig. 5 and 6).

The recently developed purification approaches for SG cores and tagged PB components, allowed the sequencing of the transcriptome of both granules and helped to determine which mRNA might preferentially enter PBs and SGs. Broader defined transcript features such as long coding sequences (CDS), long untranslated regions (UTR) or poor translation efficiency were identified next to *cis*-acting sequences such as AU-rich elements (ARE) or 3'UTR sequences (Hubstenberger et al., 2017; Khong et al., 2017; Namkoong et al., 2018). Based on these results, the educated testing of specific high and low abundant candidates by RNA smFISH showed a range of localization efficiencies (Khong et al., 2017). In addition, reporter mRNAs bearing a 5'TOP element have been observed in SGs by RNA FISH (Damgaard and Lykke-Andersen, 2011). Here, we observed up to 15% of 5'TOP Renilla MS2 and 4% of Renilla MS2 reporters in PBs and SGs after 1h of SA treatment, while the majority of transcripts were unbound and diffused through the cytosol (Fig. 1). RNA smFISH against endogenous TOP element harboring RPL32 mRNAs and GAPDH mRNAs showed similar colocalization levels (Fig. S2). Mollet *et al.* used β -Gal-MS2 bound by MCP-GFP to study mRNAs in SGs. Although lacking single molecule resolution, they found that 7% of MCP-GFP signal was overlapping with SG marker fluorescence (Mollet et al., 2008). Using transfected RNA-binding probes and MS2-MCP labelling, two other studies found

that ca. 4% of β -actin mRNAs localized to SGs in living human cells (Aizer et al., 2014; Zurla et al., 2011). Taken together, the mRNA recruitment levels observed in our study are similar to previously observed levels. The 5'TOP Renilla reporter is at least 2-fold more enriched than other previously tested non-TOP mRNAs, although mRNA species exist with even higher levels in SGs (Khong et al., 2017). Taken together, the 5'TOP element-dependent mRNA colocalization to stress-induced mRNP complexes is in line with a previous TOP RNA study (Damgaard and Lykke-Andersen, 2011) and complements recent findings that sequence elements determine RNA abundance in PBs and SGs (Hubstenberger et al., 2017; Khong et al., 2017; Namkoong et al., 2018).

The recently proposed two-stage assembly model describes that dense SG cores form first, followed by the phase separation of a more liquid-like shell surrounding the core. Core-shell structures can then fuse with each other forming mature and full-sized SGs (Jain et al., 2016; Wheeler et al., 2016). In Fig. 2 we show that mRNAs with different *cis*-acting elements bind to granules at different rates. This observation could explain the varying single time point enrichment levels of different mRNAs that have been observed by others (Hubstenberger et al., 2017; Khong et al., 2017; Namkoong et al., 2018). . It will be interesting to see if single mRNAs can already bind the early forming SG core, or whether mRNAs can only bind to the fully assembled core-shell structure. We also show that mRNAs can enter and leave PBs and SGs after their maturation (> 30 minutes of SA stress) and identify subpopulations of mRNAs that interact differently with granules (Fig. 3). Approximately 50% of SG-interacting mRNAs are dynamic. These findings are in accordance with earlier ensemble FRAP experiments that had identified a mean MCP-GFP residence time of ca. 1 minute which is significantly shorter than mRNA residence time in the cytosol (Mollet et al., 2008). Taken together, these findings point towards a dynamic equilibrium model in which mRNA in-rates are higher during granule formation and reach an equilibrium with out-rates during the later phases of the stress response. It has been proposed that stress-induced mRNP complexes might act as sites for mRNA triage, where mRNAs can become sorted to undergo translational repression or decay in SGs and PB, respectively (Anderson and Kedersha, 2008; Kedersha et al., 2005). Although lacking single molecule resolution, this model was challenged early on when the majority of RNAs were found to localize outside of SGs and to enter PBs independently of SGs (Mollet et al., 2008). Using single molecule tracking, we confirm that the majority of mRNAs enter PBs directly through the cytosol, but we also observe the direct movement of mRNAs from SGs to PBs (Fig. 3F). However, these events are rare and might not fulfill a significant biological function. We were not able to detect mRNAs moving in the opposite direction from PBs to SGs. Presumably, this is the case due to the high static mRNA localization and low outward movement rates of mRNA bound to PBs (Fig. 3E).

Knock-down of LARP1 decreases 5'TOP Renilla mRNA presence inside of PBs and SG (Fig. 4). Interestingly, the initial mRNA recruitment into both structures during the early phase of the stress response is not affected, while the mRNA content only decreases after 30 minutes of SA treatment. LARP1 might therefore fulfill an mRNA anchoring instead of recruitment function. LARP1 is mainly present in SGs during SA stress (Fig. S3A), but has also been found to localize to PBs in plants, *Caenorhabditis elegans*, and human cells (Hopkins et al., 2016; Merret et al., 2013; Nykamp et al., 2008). Whether the decreased mRNA content of PBs is due to lower total mRNA transfer from SGs or a different mechanism is unknown. A presumably granule-independent regulative effect of LARP1 on TOP mRNA gene expression is becoming increasingly clear. The mTORC1-mediated regulation of the direct binding of LARP1 to the mRNA cap structure and the 5'TOP element has been recently demonstrated (Hong et al., 2017; Lahr et al., 2017; Philippe et al., 2018). Despite this, there is currently no consensus on LARP1 being a translational repressor (Fonseca et al., 2015; Hong et al., 2017; Lahr et al., 2015; Philippe et al., 2018) or activator (Tcherkezian et al., 2014). Via binding to the poly(A) tail of 5'TOP element-containing mRNAs LARP1 also possesses an mRNA stabilizing function *in vitro* (Aoki et al., 2013). In another study, depletion of LARP1 in human adult CD34+ bone marrow precursor cells decreased 5'TOP mRNA stability (Gentilella et al., 2017). At least in HeLa cells and during our 120-minute stress time-course experiment we did not observe any effect on the stability of 5'TOP Renilla reporters (Fig. 4B). SA treatment might mask a decay effect due to the strong mRNA decay inhibition during translation repression (Horvathova et al., 2017).

To what extent the LARP1-mediated sequestration of approximately 15% of mRNAs has an effect on 5'TOP mRNA stability or translation is unclear. We show that during the recovery from stress no immediate mRNA degradation occurs (Preliminary Fig. 5). Further, we observe a 2-hour lag-time before degradation onset (Preliminary Fig. 5), while translation resumes immediately during the recovery from stress for all cytosolic mRNAs without a delay (Fig. 6). Independently of translation, SG require 2 hours to fully disassemble during the recovery from stress (Fig. S5A). We cannot fully exclude that the 15% of 5'TOP Renilla mRNAs residing inside of PBs and SGs are more protected from SA-induced stress and therefore might have longer half-lives or faster translation initiation rates (Arimoto-Matsuzaki et al., 2016; Simms et al., 2014). However, we can conclude that the 85% of mRNAs that have not been permanently bound to mRNP granules are not immediately degraded and have a similar half-life than mRNAs that have not been subject to SA stress (Horvathova et al., 2017). In addition, translation resumes for all cytosolic mRNAs to pre-stress levels and not just for a fraction of 15%. It is more likely that mRNAs are protected from the harmful effects of oxidative stress by chaperoning RBPs in a decentralized

manner in the cytosol (Nunomura et al., 2017), rather than being required to localize into visible aggregates of such chaperoning proteins. Taken together, our findings question a direct role of stress-induced mRNP complexes for a localized regulation of mRNA biology including protection, decay and translation during or after the stress response.

Decentralized (non-granular) roles for many SG/PB-related proteins in mRNA decay and translation are well established. Why these proteins accumulate into mRNP complexes and how they help cells to cope with stress remain open questions. The recruitment of catalytically active molecules into mRNP complexes results in a high local concentration. Consequently, reaction equilibria are driven towards bound states that can specifically enhance or block a reaction (Decker and Parker, 2012; Schütz et al., 2017). Secondly, mRNP complexes can reduce molecular interactions in the cytosol through sequestration and physical separation of two binding partners (Arimoto et al., 2008). It will therefore be interesting to develop experimental approaches to uncouple protein functions from their presence inside or outside of granule. Given the role that SGs seem to play in signaling (Grabocka and Bar-Sagi, 2016; Wippich et al., 2013), apoptosis regulation (Arimoto et al., 2008), viral replication (McCormick and Khapersky, 2017) and potentially neurological diseases (Zhang et al., 2018), perturbing and further understanding the link between mRNA regulation inside and outside of granules will be crucial for the development of novel therapies.

2.4 Material and methods

Generation of mRNA reporter cell line

5' TOP Renilla and Renilla only mRNA reporters were expressed from a stably integrated single, tetracycline inducible locus in HeLa cells. A similar cell line generation procedure has been described previously in (Halstead et al., 2015, 2016). In brief, the tetracycline-inducible promoter and 5' UTR of human RPL32 originating from rpl32- β -globin (Damgaard and Lykke-Andersen, 2011) were cloned 5' of a chimeric intron – Renilla luciferase – stop codon 24xMS2 stem-loop cassette SV40 polyA. The Renilla only reporter was cloned without the RPL32 5' UTR. Both reporters were flanked by FLP recombinase-mediated cassette exchange (RCME) sites. The reporters were then stably integrated into a HeLa cell line expressing a rtTA2-M2 tetracycline reverse transactivator for tetracycline inducible expression and a single FLP RCME site as described in (Weidenfeld et al., 2009). In brief, RMCE of the hygromycin-thymidine kinase (hyg^{tk}) positive-negative selection cassette in the target site for the desired reporter was achieved by co-transfecting 2 μ g of reporter plasmid together with 2 μ g of pCAGGS-FLPe-IRESpuro using Lipofectamine 2000 (Life Technologies) according to the manufacturer's protocol. 12 h post transfection, selection with 5 μ g/ml puromycin (Sigma-Aldrich) was performed for 36 h to enrich for transfected cells. Surviving cells were treated with 40 μ M ganciclovir (Sigma-Aldrich) for 10 days to select for cells having undergone RMCE. Surviving cells were pooled, single-cell sorted and expanded. Clones were tested by Renilla luciferase assays (Promega) for successful reporter expression. Unless noted otherwise, HeLa cells were cultured in DMEM supplemented with Tet-free FBS (Cloneteck) and 1%Pen Strep at 37°C and 5% CO₂.

As described previously (Halstead et al., 2015, 2016) NLS-MCP-Halo was stably integrated into reporter expressing clones by lentiviral transduction using standard protocols, followed by FACS to select for low expressing cells in order to reduce background fluorescence and allow single molecule RNA imaging.

Generation of SG and PB reporter cell line

In order to visualize SGs and PBs in living cells, G3BP1-2xGFP and DDX6-Tag-RFP-T fusion proteins were cloned into the pHAGE UbiC lentiviral vectors, respectively. Constructs were simultaneously and stably integrated by lentiviral transduction according to standard protocols. To prevent SG formation or excess PB formation in the absence of stress due to overexpression, FACS was utilized to identify only low expressing dual positive cells. Immunofluorescence against TIAR (1/100, cat. # 610352, BD Biosciences),

G3BP1 (1/200, cat. # ARP37713_T100, Aviva Systems Biology), DDX6 (1/300, cat. # A300-461A, Bethyl Labs) and DCP1a (1/300, cat. # 47998, Abcam) was performed to confirm physiological SG and PB numbers and behavior.

Immunofluorescence

HeLa cells were seeded two days prior to fixation at a concentration of 40×10^3 cells/ml on standard glass coverslips (18mm, Biosystems). Cells were then washed in PBS and fixed in 4% paraformaldehyde (PFA)/PBS (Electron Microscopy Science) for 15 minutes, washed again and permeabilized in 1% Triton-X1000 (v/v)/PBS for 5 minutes at room temperature. Next, cells were PBS-washed three times for 5 minutes each time. Blocking was performed with 1% BSA/PBS (Sigma-Aldrich) for 15 minutes. Primary antibodies were diluted in blocking solution and a drop of 50 μ L was pipetted into a Petri dish. Coverslips were removed from wells, placed cell-side down onto the primary antibody solution, incubated for two hours at room temperature and placed back into the well. Coverslips were placed back into a 12-well plate and washing was performed three times 5 minutes each in 0.2% BSA/PBS. Secondary antibodies (Alexa fluorophores, Life Technologies), were diluted in blocking buffer, added onto the coverslip for 30 minutes and washed out three times with PBS for 5 minutes each time. Next, cells were DAPI stained (0.5 mg/L) and coverslips were mounted (ProLong Gold, Life Technologies) on glass slides and imaged.

RNA smFISH combined with immunofluorescence

HeLa cells were cultured on coverslips and fixed as described above. PFA was subsequently quenched by a wash in 25mM glycine/PBS. Cells were then washed twice with PBS and permeabilized with 1% (v/v) Triton-X1000/PBS for 5 minutes at room temperature, followed by three washes with PBS and incubation with prehybridization solution (2xSSC, 10% (v/v) formamide (Sigma) in PBS) for five minutes at room temperature. Coverslips were then placed cell-side down into a drop of 50 μ L of hybridization solution (2xSSC, 10% (v/v) formamide (Sigma), 10% (w/v) dextran sulfate, 0.5% (w/v) BSA in PBS) containing 250nM Renilla mRNA FISH probes (Quasar570, Biosearch Technologies), DDX6 antibody (1/300, cat. # A300-461A, Bethyl Labs), and G3BP1 antibody (1/200, cat. # 611127, BD Biosciences) inside of a humidified Petri dish for four hours at 37°C. After hybridization, coverslips were placed back into a 12-well plate and washing was performed in prehybridization solution containing secondary antibodies (goat anti-rabbit Alexa647, donkey anti-mouse Alexa488, Life Technologies) for 30 minutes at 37°C. Next, cells were washed again in prehybridization solution without secondary antibodies for 30 minutes at room temperature. Prehybridization solution was washed out three times with PBS for 5

minutes each time. Cells were DAPI stained (0.5 mg/L) and coverslips were mounted (ProLong Gold, Life Technologies) on glass slides and imaged.

Fixed cell imaging and data analysis

Imaging

For combined smRNA FISH and SG and PB immunofluorescence experiments slides were prepared as described above and imaged on a Zeiss Axioimager Z1 widefield microscope using a Plan-APOCHROMAT 100x 1.4NA DIC oil immersion objective (Zeiss) and AxioCam MRc camera with pixel size 6.45 μ M x 6.45 μ M (Zeiss). An X-Cite 120 (EXFO) metal halide lamp was used as a light source together with filters for Cy5, Cy3 (AHF), GFP/Alexa488 and DAPI (Zeiss). Images were acquired as Z-stacks (3 μ M in 0.2 μ M steps) with Zen software (Zeiss).

Data analysis

The quantification of mRNA colocalization in fixed cells with SGs or PBs has been described previously (Halstead et al., 2015). In brief, unprocessed image stacks were maximum intensity projected in FIJI (Rueden et al., 2017; Schindelin et al., 2012), spot detection was performed by a custom-written Matlab (Mathworks) script (available on request) and binary masks for PBs and SGs were generated by intensity thresholding (FIJI). Next, spot images and binary masks were assigned to opposing binary values and multiplied with each other. The remaining spots were then counted (FIJI) to determine the quantity inside and outside of subcellular structures.

LARP1 knockdown

Cells were seeded one day prior to the experiment at a concentration of 150x10³ cells/ml in 6-well plates. A pool of human sequence LARP1 siRNAs (cat. # L-027187-00-0005, GE Dharmacon) was transfected with Lipofectamine RNAiMAX reagent (ThermoFisher) at a final concentration of 25 pmol per well according to the manufacturer's protocol.

#	siRNA (LARP1)
J-027187-05	GCAAGAAUACCU CGGCAAA
J-027187-06	GAGAAGGGAGUGAUAGUAA
J-027187-07	CACAACACGUCUACCAUAA
J-027187-08	ACACAAGUGGGUCCAUAUA

6h after transfection cells were re-seeded. The knockdown was validated after 48h by western blotting: Cells were lysed in RIPA buffer and sonicated, 5% BSA(w/v)/PBS was used for blocking and the PVDF membrane was subsequently probed using a polyclonal LARP1 antibody (cat. # A302-087A, Bethyl) and a near-infrared secondary antibody (LI-COR Biosciences) according to the manufacturers protocol.

mRNA colocalization imaging and data analysis in live cells

Imaging

HeLa cells expressing G3BP1-2xGFP, DDX6-Tag-RFP-T, NLS-MCP-Halo and either the 5' TOP Renilla or Renilla only mRNA reporters were seeded 2 days prior to the experiment at a concentration of 25×10^3 cells/ml on a glass bottom 35mm μ -Dish (Ibidi) and were cultured in DMEM, 10% (v/v) Tet-free FBS (Clontech) and 1% (v/v) Pen Strep at 37°C and 5% CO₂ in a humidified incubator. On the day of the experiment 100nM of Janelia Fluor 647 (Grimm et al., 2016) was added to the cells to fluorescently label the mRNA-binding NLS-MCP-Halo protein and incubated for 15 minutes at 37°C and 5% CO₂. Cells were then washed 3x with 37°C warm PBS, followed by 90 minutes incubation with 1 μ g/mL doxycycline in DMEM, 10% (v/v) FBS and 1% (v/v) Pen Strep at 37°C and 5% CO₂ to induce reporter mRNA expression and ensure sufficient amounts of mRNAs in the cytoplasm. Induction was stopped by 2x washes with warm PBS and addition of FluoroBrite™ DMEM (Life Technologies) + 10% (v/v) FBS for imaging. Stress experiments were performed by incubating the cells in 100 μ M sodium arsenite (SA) (Sigma).

Cells were imaged through a highly inclined and laminated optical sheet (HILO) setup (Tokunaga et al., 2008) on a Nikon Eclipse Ti-E inverted widefield microscope equipped with a Total Internal Reflection Microscopy iLAS² module (Roper Scientific), a Perfect Focus System (Nikon) and motorized Z-Piezo stage (ASI) using a CFI APO TIRF 100x 1.49NA oil immersion objective (Nikon). Images were collected on three precisely aligned back-illuminated Evolve 512 Delta EMCCD cameras with a pixel size of 16 μ m x 16 μ m (Photometrics). A laser bank with combiner including 488nm (200mW), 640nm (150mW) (Toptica iBEAM SMART) and 561nm (200mW) (Coherent Sapphire) lasers was used as excitation source. Cells were constantly kept at 37°C and 5% CO₂ during imaging through an enclosed microscope environmental control setup (The BOX (heating) and The CUBE2(CO₂) (Life Science Instruments)). Images were acquired from a single plane every 50ms with Visiview software (Visitron).

Spot detection & tracking

For each movie a cytoplasmic ROI was manually defined to exclude nuclear mRNAs. Detection of mRNA spots in all frames and their linking into trajectories was performed with the FIJI suite plugin Trackmate

(Tinevez et al., 2017). The Laplacian of Gaussian (LoG) filter was used to perform sub-pixel spot detection for spots of an estimated size of 0.38 μ m. To guarantee optimal spot detection, the detection threshold was manually chosen due to high cell-to-cell variability. The Simple LAP tracker was used to calculate trajectories from spot detection data. Maximum distances for spot-to-spot linking between frames and gap-closing were chosen to be 0.6 μ m. The maximum allowed gap size was set to 2 frames. Spots in tracks statistics including spot and trajectory IDs and time and space coordinates were saved and served as input for the colocalization analysis.

Colocalization of tracks with subcellular structures and mRNA track directionality analysis

Automated segmentation of PBs and SGs, colocalization of mRNA tracks with those structures and the determination of track directionality was performed with a custom-built pipeline in the open-source Konstanz Information Miner (KNIME) software (Berthold et al., 2009). In brief, data analysis in KNIME relies on freely available computation nodes each with a different functionality, which can be arranged in any order to achieve the desired task.

Here, the spot statistics files and the two unprocessed imaging channels containing SG and PB imaging data served as the three required inputs. Gaussian convolution was applied to smoothen images. Next, a Yen thresholder and a Mean Absolute Deviation (MAD) based spot detection algorithm was used to reliably detect PBs and SGs over multiple time points in different cells, respectively. The obtained binary masks were then transformed into a distance map, which contains the minimal distance of each foreground pixel to the nearest background pixel. Simultaneously, the spot statistics file was read as a third input and a binary image was created for every frame containing a single pixel representing the corresponding mRNA molecule. Next, the PB and SG distance maps were combined with the newly generated binary spot image and for each spot in each frame, the mean intensity in the distance map was measured. Whenever an mRNA spot would have positive value for >2 frames it was considered to be colocalized with the respective subcellular structure and for ease of calculation was given the value 1. On the contrary, a negative value indicated that this mRNA molecule was outside of the respective subcellular structure and was given the value 0. As a result, each spot now contained two localization indices (LI_{PB} and LI_{SG}) indicating whether at a given time it colocalized with a PB or SG.

Next, the Cummulative Localization Index (CLI) for each trajectory was calculated by summing up all values of the spots belonging to that trajectory across all frames i .

$$\sum_{i=Frame_0}^{Frame_N} LI_i = \text{Cummulative Localization Index (CLI)}$$

(1)

Since each spot contained information on its position relative to a PB or SGs (LI_{PB} and LI_{SG}), each trajectory also was assigned to two CLIs to describe its position (CLI_{PB} and CLI_{SG}). A $CLI_{PB} > 0$ or $CLI_{SG} > 0$ indicated that the whole track or parts of it were colocalizing with a PB or SG, respectively. This data was subsequently used to calculate the fraction of colocalizing trajectories per cell and for all cells across all time points.

In addition, directionality information could be obtained from this data. Movement of an mRNA particle between a SG and PB and was detected by identifying trajectories which had both a $CLI_{PB} > 0$ and $CLI_{SG} > 0$ at the same time. For all trajectories that did not fulfill this criterion and had either a $CLI_{PB} > 0$ or $CLI_{SG} > 0$ the entry or leaving direction into PBs or SGs was determined by looking at the LI of its respective spot components and its change from one frame to another.

(2) $LI_{t_0} = 0$ and $LI_{t_1} = 1$ (mRNA moved inwards)

(3) $LI_{t_0} = 1$ and $LI_{t_1} = 0$ (mRNA moved outwards)

In (2) a situation is shown in which an mRNA molecule had initially not been colocalizing while one frame later it did, meaning that it moved from the cytoplasm into the respective subcellular structure. In (3) the opposite scenario is shown.

Cell line generation for SunTag translation site imaging

The used reporter cassette is identical to the 24x SunTag Renilla luciferase reporter used by Voigt *et al.* (Voigt *et al.*, 2017), except for an exchanged promoter region with a tetracycline-inducible promoter and 5' UTR of human RPL32 originating from rpL32- β -globin (Damgaard and Lykke-Andersen, 2011). The reporter cassette was then stably integrated into HeLa cells containing a single FLP site constitutively expressed reverse tetracycline-controlled transactivator (rtTA2-M2) for inducible reporter expression as described above (Weidenfeld *et al.*, 2009). MS2 stem loop-binding NLS-MCP-Halo to visualize the mRNA reporter and scFv-GFP (Yan *et al.*, 2016) to visualize translation sites were stably integrated into the cells by lentiviral transduction as described above. To reduce fluorescent background, cells were FACS sorted and cultured under standard conditions as described above

SunTag translation site imaging and data analysis in live cells

Imaging

5'TOP SunTag Renilla reporter cell lines were prepared for imaging as described above, except for using Janelia Fluor 549 (Grimm et al., 2016) to fluorescently label the mRNA-binding NLS-MCP-Halo proteins. Cells were then imaged with the same HILO microscopy setup as described above. To detect translation sites (GFP) and mRNAs (NLS-MCP-Halo), images were acquired simultaneously with two cameras in a single plane for 100 consecutive frames with an exposure time of 46 ms. Reporter transcription was stopped before the stress/recovery time-course experiment by washing the cells 2x in PBS in the temperature controlled microscope chamber. Cells were stressed by incubation in FluoroBrite™ DMEM (Life Technologies) + 10% (v/v) FBS and 100µM sodium arsenite (Sigma). Stress recovery was achieved by 2x washes with PBS in the temperature controlled microscope chamber and incubation in FluoroBrite™ DMEM (Life Technologies) + 10% (v/v) FBS.

Fraction of translating mRNAs

Single particle detection and subsequent tracking was executed for both the GFP and NLS-MCP-Halo channels in the same manner as described above with the FIJI suite plugin Trackmate (Tinevez et al., 2017). To determine the fraction of translating mRNAs, the obtained x, y, t coordinates per GFP and NLS-MCP-Halo track were colocalized in a custom written script executed in KNIME (equation (4)). Details on the colocalization procedure can be found elsewhere (Voigt et al., 2018). In brief, only tracks with a minimum length of 5 frames were considered for the analysis. Tracks were called colocalized when they were within 3 pixels (321 nm) for at least two consecutive frames for both tracks.

$$(4) \quad \textit{Translating mRNAs} = \frac{\# \textit{Transl. sites coloc. with mRNAs}}{\# \textit{mRNAs}}$$

mRNA ribosome occupancy

The number of ribosomes per mRNA molecule was calculated based on the mean total fluorescence intensity of the first 5 frames of each detected GFP SunTag translation site colocalizing with an NLS-MCP-Halo mRNA. In addition, the mean fluorescence intensity of single released SunTag-Renilla peptides was determined. Since the length of the emerging scFv-GFP labelled polypeptide chain is different for ribosomes on the 5'- and 3'-ends of mRNAs, simply dividing the total intensity by the intensity of the single released peptide does not suffice. We used a simplified model to calculate ribosome occupancy which was described previously (Voigt et al., 2017; Yan et al., 2016). In brief, a single correction factor is used to account for the ribosome position within the open reading frame (ORF). The correction factor is determined based on two assumptions: The Renilla luciferase fraction of the ORF is invisible to detection since it does not bind scFv-GFP, still the ribosome translates this region. Peptide

chains with the maximum number of bound scFv-GFPs are therefore overrepresented when considering the length of the SunTag cassette alone. Secondly, we assume that the ribosome moves with a constant speed through the ORF and is therefore homogeneously distributed throughout the ORF. Based on the sequence length contributions of the SunTag element and the Renilla luciferase within the ORF the correction factor displayed in equation (5) is calculated.

$$(5) \quad \text{Ribosomes per mRNA} = \frac{\text{Total intensity single transl. site}}{\text{Total intensity single released peptide} \times 0.70425}$$

Using the correction factor, the total number of ribosomes on each mRNA molecule was then calculated using equation (5).

2.5 Supplementary figures

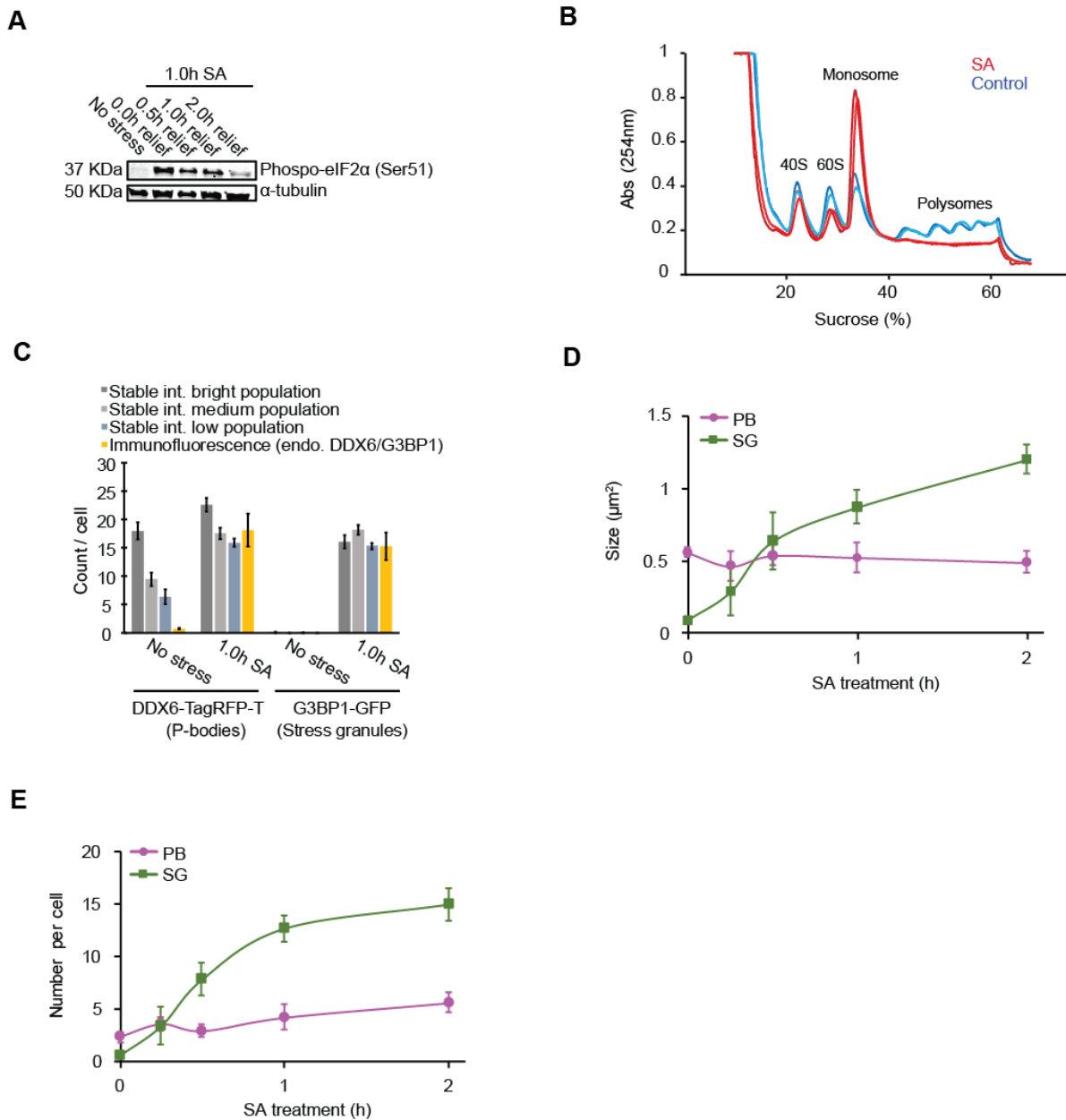


Fig. S1: Cells stably expressing G3BP1-GFP and DDX6-TagRFP-T form stress-induced SGs and PBs with typical numbers per cell, size, and formation kinetics. (A) eIF2α is reversibly phosphorylated upon treatment with 100μM SA for 1h in HeLa cells. (B) Polysome profiling of HeLa cells subject to 100μM SA for 1h showed that translation is generally off during SA treatment (two replicates shown per condition). (C) After FACS, HeLa cells stably expressing G3BP1-GFP and DDX6-TagRFP-T did not form atypical levels SGs and PBs in the presence or absence of 100μM SA when compared to endogenous SGs and PBs detected by IF. (D) and (E) HeLa cells stably expressing G3BP1-GFP and DDX6-TagRFP-T and treated with 100μM SA formed SG

and PB with similar sizes (D), numbers per cell (E) and formation kinetics as previously described by others (Ohshima et al., 2015; Wheeler et al., 2016).

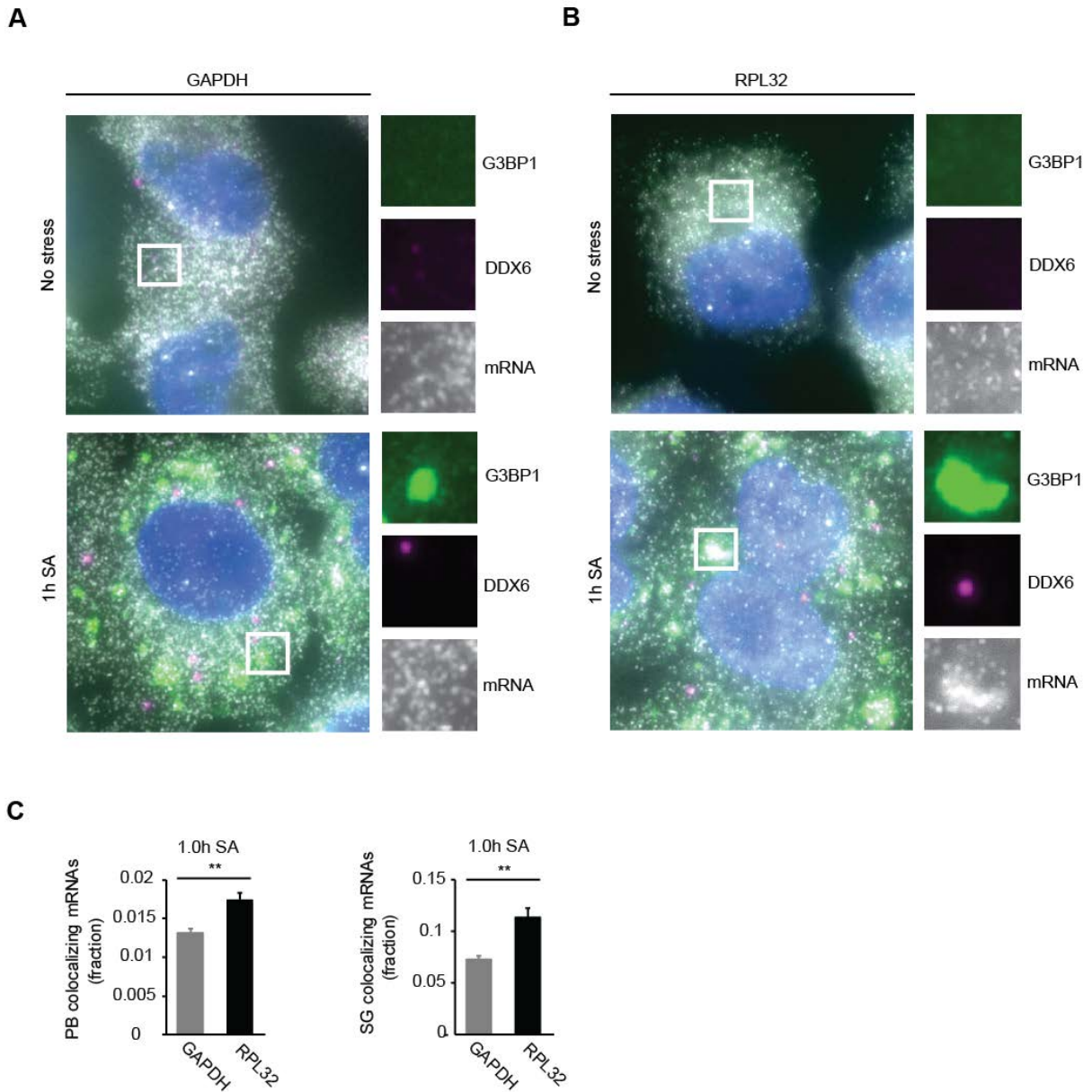


Fig. S2: RNA smFISH against endogenous RPL32 confirms 5'TOP-element dependent mRNA localization to SGs and PBs.

(A) HeLa cells were control treated or stressed with 100 μ M SA for 1 hour, fixed, stained for G3BP1 and DDX6, and RNA smFISH against endogenous GAPDH mRNA was performed. (B) HeLa cells were control treated or stressed with 100 μ M SA for 1 hour, fixed, stained for G3BP1 and DDX6, and RNA smFISH against endogenous 5'TOP element-containing RPL32 mRNA was performed. (C) Colocalization-based quantification of the data presented in (A) and (B) showed that RPL32 mRNAs localized significantly more to PBs and SGs (scale bars = 10 μ m; mean \pm SEM; two-tailed, unpaired Student's t-test; * = $p < 0.05$; >100 cells per time point and experiment, 3 biological replicates).

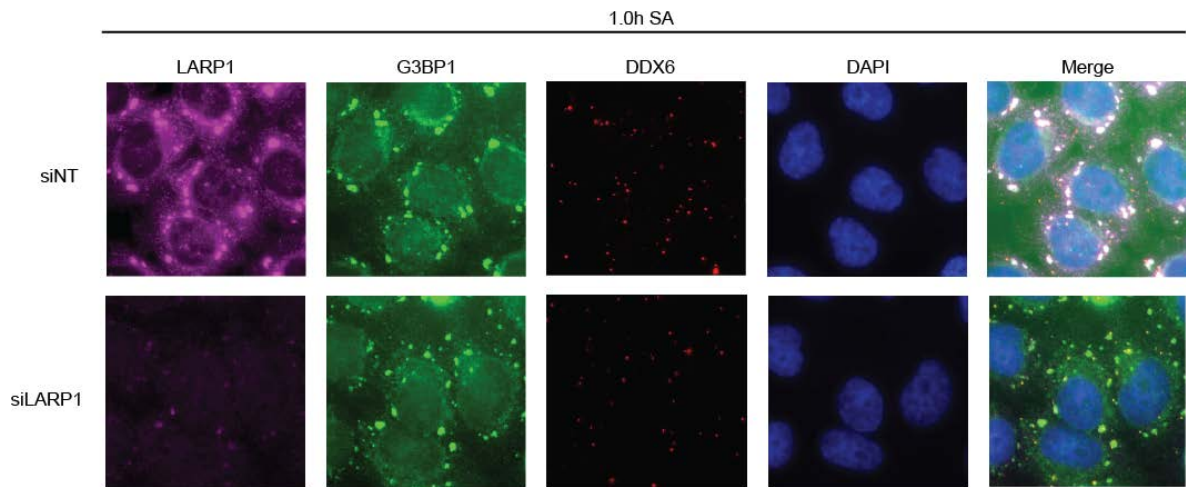
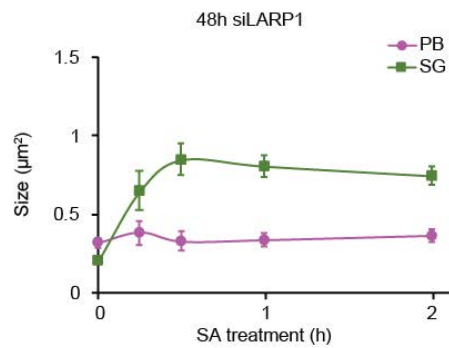
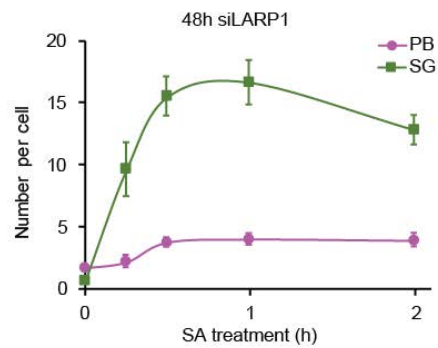
A**B****C**

Fig. S3: LARP1 KD decreases cytoplasmic LARP1 levels, but does not influence PBs and SG negatively. (A) HeLa cells were control transfected or transfected with siRNAs against LARP1 for 48 hours. Cells were then stressed with 100µM SA for 1 hour, fixed, and stained for LARP1, G3BP1 and DDX6. The reduction of LARP1 does not prevent the formation of endogenous PBs and SGs. (B) and (C) 48h LARP1 KD does not alter the size and number of PBs and SGs in HeLa cells stably expressing G3BP1-GFP and DDX6-TagRFP-T.

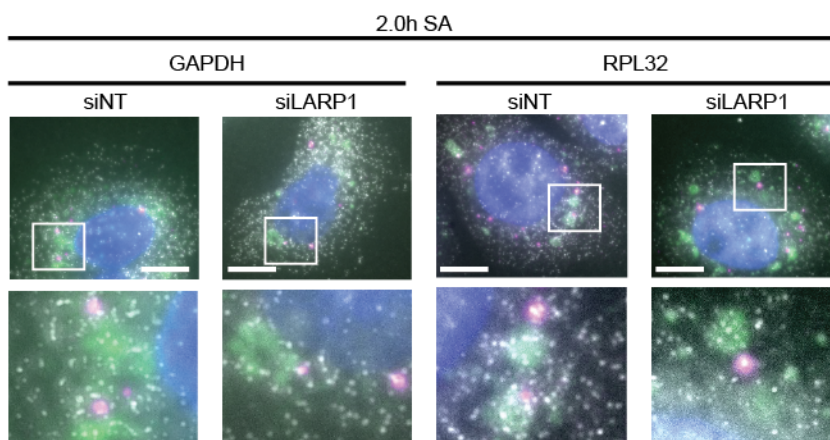
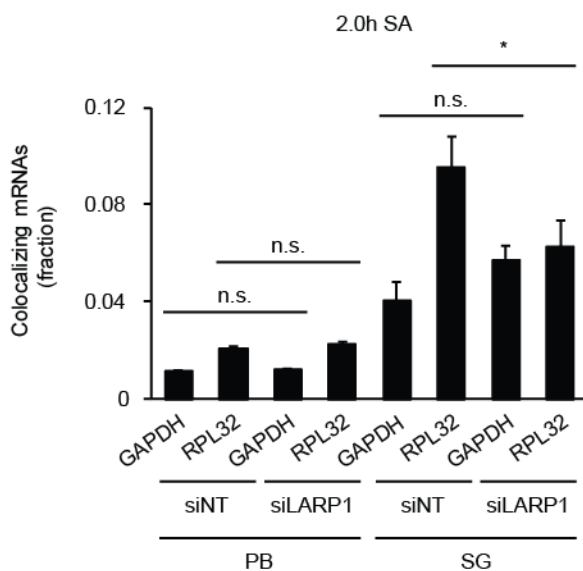
A**B**

Fig. S4: LARP1 KD reduces the number of endogenous 5'TOP element-containing RPL32 mRNAs in SGs after 2 hours of SA treatment. (A) RNA smFISH against endogenous GAPDH or RPL32 5'TOP mRNAs combined with IF against G3BP1 and DDX6 in LARP1-depleted HeLa cells treated with 100 μ M SA for 2h showed lower RPL32 5'TOP mRNAs localization to SGs, but unchanged levels for GAPDH. (B) Colocalization analysis and quantification of the data presented in (A). LARP1 depletion led to a decrease of RPL32 5'TOP mRNAs colocalizing with SGs after 2h of SA treatment (scale bars = 10 μ m; mean \pm SEM; two-tailed, unpaired Student's t-test; * = $p < 0.05$; >100 cells per time point and experiment, 2 biological replicates).

A

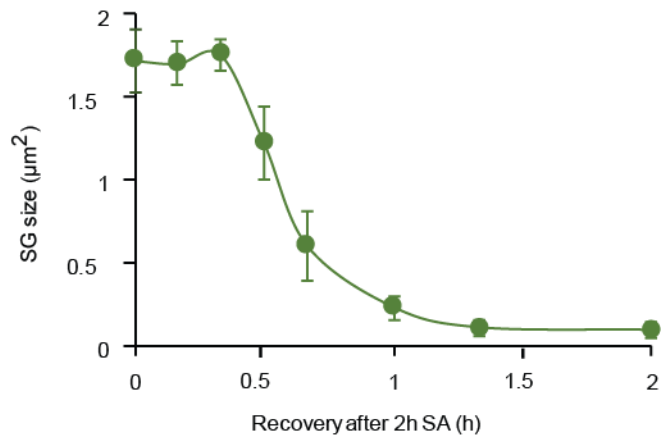


Fig. S5: G3BP1-GFP SGs fully disassemble during the recovery from stress. (A) HeLa cells expressing G3BP1-GFP were treated with 100µM SA for 1h, and washed with PBS. SG size was measured during a 2h time course. After a short lag-phase, SGs fully disassembled after 2h of recovery.

References

- Aizer, A., Kalo, A., Kafri, P., Shraga, A., Ben-Yishay, R., Jacob, A., Kinor, N., and Shav-Tal, Y. (2014). Quantifying mRNA targeting to P bodies in living human cells reveals a dual role in mRNA decay and storage. *J. Cell Sci.*
- Anderson, P., and Kedersha, N. (2008). Stress granules: the Tao of RNA triage. *Trends Biochem. Sci.* 33, 141–150.
- Aoki, K., Adachi, S., Homoto, M., Kusano, H., Koike, K., and Natsume, T. (2013). LARP1 specifically recognizes the 3' terminus of poly(A) mRNA. *FEBS Lett.* 587, 2173–2178.
- Arimoto, K., Fukuda, H., Imajoh-Ohmi, S., Saito, H., and Takekawa, M. (2008). Formation of stress granules inhibits apoptosis by suppressing stress-responsive MAPK pathways. *Nat. Cell Biol.* 10, 1324–1332.
- Arimoto-Matsuzaki, K., Saito, H., and Takekawa, M. (2016). TIA1 oxidation inhibits stress granule assembly and sensitizes cells to stress-induced apoptosis. *Nat. Commun.* 7, 10252.
- Backlund, M., Paukku, K., Kontula, K.K., and Lehtonen, J.Y.A. (2016). Endoplasmic reticulum stress increases AT1R mRNA expression via TIA-1-dependent mechanism. *Nucleic Acids Res.* 44, 3095–3104.
- Berthold, M.R., Cebron, N., Dill, F., Gabriel, T.R., Kötter, T., Meinel, T., Ohl, P., Thiel, K., and Wiswedel, B. (2009). KNIME - the Konstanz Information Miner: Version 2.0 and Beyond. *SIGKDD Explor Newsl* 11, 26–31.
- Bertrand, E., Chartrand, P., Schaefer, M., Shenoy, S.M., Singer, R.H., and Long, R.M. (1998). Localization of ASH1 mRNA particles in living yeast. *Mol. Cell* 2, 437–445.
- Bhattacharyya, S.N., Habermacher, R., Martine, U., Closs, E.I., and Filipowicz, W. (2006). Relief of microRNA-mediated translational repression in human cells subjected to stress. *Cell* 125, 1111–1124.
- Bregues, M., Teixeira, D., and Parker, R. (2005). Movement of eukaryotic mRNAs between polysomes and cytoplasmic processing bodies. *Science* 310, 486–489.
- Buchan, J.R. (2014). mRNP granules. Assembly, function, and connections with disease. *RNA Biol.* 11, 1019–1030.
- Buchan, J.R., and Parker, R. (2009). Eukaryotic stress granules: the ins and outs of translation. *Mol. Cell* 36, 932–941.
- Damgaard, C.K., and Lykke-Andersen, J. (2011). Translational coregulation of 5'TOP mRNAs by TIA-1 and TIAR. *Genes Dev.* 25, 2057–2068.
- Decker, C.J., and Parker, R. (2012). P-bodies and stress granules: possible roles in the control of translation and mRNA degradation. *Cold Spring Harb. Perspect. Biol.* 4, a012286.
- Fonseca, B.D., Zakaria, C., Jia, J.-J., Graber, T.E., Svitkin, Y., Tahmasebi, S., Healy, D., Hoang, H.-D., Jensen, J.M., Diao, I.T., et al. (2015). La-related protein 1 (LARP1) represses terminal oligopyrimidine (TOP) mRNA translation downstream of mTOR complex 1 (mTORC1). *J. Biol. Chem.* jbc.M114.621730.
- Gentilella, A., Morón-Duran, F.D., Fuentes, P., Zweig-Rocha, G., Riaño-Canalias, F., Pelletier, J., Ruiz, M., Turón, G., Castaño, J., Tauler, A., et al. (2017). Autogenous Control of 5'TOP mRNA Stability by 40S Ribosomes. *Mol. Cell* 67, 55-70.e4.
- Grabocka, E., and Bar-Sagi, D. (2016). Mutant KRAS Enhances Tumor Cell Fitness by Upregulating Stress Granules. *Cell* 167, 1803-1813.e12.

Grimm, J.B., English, B.P., Chen, J., Slaughter, J.P., Zhang, Z., Revyakin, A., Patel, R., Macklin, J.J., Normanno, D., Singer, R.H., et al. (2015). A general method to improve fluorophores for live-cell and single-molecule microscopy. *Nat. Methods* 12, 244–250, 3 p following 250.

Grimm, J.B., English, B.P., Choi, H., Muthusamy, A.K., Mehl, B.P., Dong, P., Brown, T.A., Lippincott-Schwartz, J., Liu, Z., Lionnet, T., et al. (2016). Bright photoactivatable fluorophores for single-molecule imaging. *Nat. Methods* 13, 985–988.

Halstead, J.M., Lionnet, T., Wilbertz, J.H., Wippich, F., Ephrussi, A., Singer, R.H., and Chao, J.A. (2015). Translation. An RNA biosensor for imaging the first round of translation from single cells to living animals. *Science* 347, 1367–1671.

Halstead, J.M., Wilbertz, J.H., Wippich, F., Lionnet, T., Ephrussi, A., and Chao, J.A. (2016). TRICK: A Single-Molecule Method for Imaging the First Round of Translation in Living Cells and Animals. *Methods Enzymol.* 572, 123–157.

Hong, S., Freeberg, M.A., Han, T., Kamath, A., Yao, Y., Fukuda, T., Suzuki, T., Kim, J.K., and Inoki, K. (2017). LARP1 functions as a molecular switch for mTORC1-mediated translation of an essential class of mRNAs. *ELife* 6, e25237.

Hopkins, T.G., Mura, M., Al-Ashtal, H.A., Lahr, R.M., Abd-Latip, N., Sweeney, K., Lu, H., Weir, J., El-Bahrawy, M., Steel, J.H., et al. (2016). The RNA-binding protein LARP1 is a post-transcriptional regulator of survival and tumorigenesis in ovarian cancer. *Nucleic Acids Res.* 44, 1227–1246.

Hornstein, E., Tang, H., and Meyuhas, O. (2001). Mitogenic and nutritional signals are transduced into translational efficiency of TOP mRNAs. *Cold Spring Harb. Symp. Quant. Biol.* 66, 477–484.

Horvathova, I., Voigt, F., Kotrys, A.V., Zhan, Y., Artus-Revel, C.G., Eglinger, J., Stadler, M.B., Giorgetti, L., and Chao, J.A. (2017). The Dynamics of mRNA Turnover Revealed by Single-Molecule Imaging in Single Cells. *Mol. Cell* 68, 615-625.e9.

Hubstenberger, A., Courel, M., Bénard, M., Souquere, S., Ernoult-Lange, M., Chouaib, R., Yi, Z., Morlot, J.-B., Munier, A., Fradet, M., et al. (2017). P-Body Purification Reveals the Condensation of Repressed mRNA Regulons. *Mol. Cell* 68, 144-157.e5.

Iadevaia, V., Caldarola, S., Tino, E., Amaldi, F., and Loreni, F. (2008). All translation elongation factors and the e, f, and h subunits of translation initiation factor 3 are encoded by 5'-terminal oligopyrimidine (TOP) mRNAs. *RNA* 14, 1730–1736.

Jain, S., Wheeler, J.R., Walters, R.W., Agrawal, A., Barsic, A., and Parker, R. (2016). ATPase-Modulated Stress Granules Contain a Diverse Proteome and Substructure. *Cell* 164, 487–498.

Kedersha, N., and Anderson, P. (2002). Stress granules: sites of mRNA triage that regulate mRNA stability and translatability. *Biochem. Soc. Trans.* 30, 963–969.

Kedersha, N., Cho, M.R., Li, W., Yacono, P.W., Chen, S., Gilks, N., Golan, D.E., and Anderson, P. (2000). Dynamic shuttling of TIA-1 accompanies the recruitment of mRNA to mammalian stress granules. *J. Cell Biol.* 151, 1257–1268.

Kedersha, N., Stoecklin, G., Ayodele, M., Yacono, P., Lykke-Andersen, J., Fritzler, M.J., Scheuner, D., Kaufman, R.J., Golan, D.E., and Anderson, P. (2005). Stress granules and processing bodies are dynamically linked sites of mRNP remodeling. *J. Cell Biol.* 169, 871–884.

Khong, A., Matheny, T., Jain, S., Mitchell, S.F., Wheeler, J.R., and Parker, R. (2017). The Stress Granule Transcriptome Reveals Principles of mRNA Accumulation in Stress Granules. *Mol. Cell* 68, 808-820.e5.

- Lahr, R.M., Mack, S.M., Héroux, A., Blagden, S.P., Bousquet-Antonelli, C., Deragon, J.-M., and Berman, A.J. (2015). The La-related protein 1-specific domain repurposes HEAT-like repeats to directly bind a 5'TOP sequence. *Nucleic Acids Res.* *43*, 8077–8088.
- Lahr, R.M., Fonseca, B.D., Ciotti, G.E., Al-Ashtal, H.A., Jia, J.-J., Niklaus, M.R., Blagden, S.P., Alain, T., and Berman, A.J. (2017). La-related protein 1 (LARP1) binds the mRNA cap, blocking eIF4F assembly on TOP mRNAs. *ELife* *6*.
- Markmiller, S., Soltanieh, S., Server, K.L., Mak, R., Jin, W., Fang, M.Y., Luo, E.-C., Krach, F., Yang, D., Sen, A., et al. (2018). Context-Dependent and Disease-Specific Diversity in Protein Interactions within Stress Granules. *Cell* *172*, 590-604.e13.
- McCormick, C., and Khapersky, D.A. (2017). Translation inhibition and stress granules in the antiviral immune response. *Nat. Rev. Immunol.* *17*, 647–660.
- Merret, R., Descombin, J., Juan, Y., Favory, J.-J., Carpentier, M.-C., Chaparro, C., Charng, Y., Deragon, J.-M., and Bousquet-Antonelli, C. (2013). XRN4 and LARP1 are required for a heat-triggered mRNA decay pathway involved in plant acclimation and survival during thermal stress. *Cell Rep.* *5*, 1279–1293.
- Mollet, S., Cougot, N., Wilczynska, A., Dautry, F., Kress, M., Bertrand, E., and Weil, D. (2008). Translationally repressed mRNA transiently cycles through stress granules during stress. *Mol. Biol. Cell* *19*, 4469–4479.
- Morisaki, T., Lyon, K., DeLuca, K.F., DeLuca, J.G., English, B.P., Zhang, Z., Lavis, L.D., Grimm, J.B., Viswanathan, S., Looger, L.L., et al. (2016). Real-time quantification of single RNA translation dynamics in living cells. *Science* *352*, 1425–1429.
- Namkoong, S., Ho, A., Woo, Y.M., Kwak, H., and Lee, J.H. (2018). Systematic Characterization of Stress-Induced RNA Granulation. *Mol. Cell* *70*, 175-187.e8.
- Niewidok, B., Igaev, M., Graca, A.P. da, Strassner, A., Lenzen, C., Richter, C.P., Piehler, J., Kurre, R., and Brandt, R. (2018). Single-molecule imaging reveals dynamic biphasic partition of RNA-binding proteins in stress granules. *J Cell Biol* jcb.201709007.
- Nunomura, A., Lee, H., Zhu, X., and Perry, G. (2017). Consequences of RNA oxidation on protein synthesis rate and fidelity: implications for the pathophysiology of neuropsychiatric disorders. *Biochem. Soc. Trans.* BST20160433.
- Nykamp, K., Lee, M.-H., and Kimble, J. (2008). *C. elegans* La-related protein, LARP-1, localizes to germline P bodies and attenuates Ras-MAPK signaling during oogenesis. *RNA N. Y. N* *14*, 1378–1389.
- Ohshima, D., Arimoto-Matsuzaki, K., Tomida, T., Takekawa, M., and Ichikawa, K. (2015). Spatio-temporal Dynamics and Mechanisms of Stress Granule Assembly. *PLOS Comput. Biol.* *11*, e1004326.
- Pakos-Zebrucka, K., Koryga, I., Mnich, K., Ljujic, M., Samali, A., and Gorman, A.M. (2016). The integrated stress response. *EMBO Rep.* *17*, 1374–1395.
- Panas, M.D., Ivanov, P., and Anderson, P. (2016). Mechanistic insights into mammalian stress granule dynamics. *J. Cell Biol.* *215*, 313–323.
- Philippe, L., Vasseur, J.-J., Debart, F., and Thoreen, C.C. (2018). La-related protein 1 (LARP1) repression of TOP mRNA translation is mediated through its cap-binding domain and controlled by an adjacent regulatory region. *Nucleic Acids Res.* *46*, 1457–1469.
- Pichon, X., Bastide, A., Safieddine, A., Chouaib, R., Samacoits, A., Basyuk, E., Peter, M., Mueller, F., and Bertrand, E. (2016). Visualization of single endogenous polysomes reveals the dynamics of translation in live human cells. *J Cell Biol* jcb.201605024.
- Protter, D.S.W., and Parker, R. (2016). Principles and Properties of Stress Granules. *Trends Cell Biol.* *26*, 668–679.

- Rueden, C.T., Schindelin, J., Hiner, M.C., DeZonia, B.E., Walter, A.E., Arena, E.T., and Eliceiri, K.W. (2017). ImageJ2: ImageJ for the next generation of scientific image data. *BMC Bioinformatics* 18.
- Schindelin, J., Arganda-Carreras, I., Frise, E., Kaynig, V., Longair, M., Pietzsch, T., Preibisch, S., Rueden, C., Saalfeld, S., Schmid, B., et al. (2012). Fiji: an open-source platform for biological-image analysis. *Nat. Methods* 9, 676–682.
- Schütz, S., Nöldeke, E.R., and Sprangers, R. (2017). A synergistic network of interactions promotes the formation of in vitro processing bodies and protects mRNA against decapping. *Nucleic Acids Res.* 45, 6911–6922.
- Sfakianos, A.P., Mellor, L.E., Pang, Y.F., Kritsiligkou, P., Needs, H., Abou-Hamdan, H., Désaubry, L., Poulin, G.B., Ashe, M.P., and Whitmarsh, A.J. (2018). The mTOR-S6 kinase pathway promotes stress granule assembly. *Cell Death Differ.* 1.
- Simms, C.L., Hudson, B.H., Mosior, J.W., Rangwala, A.S., and Zaher, H.S. (2014). An Active Role for the Ribosome in Determining the Fate of Oxidized mRNA. *Cell Rep.* 9, 1256–1264.
- Stoecklin, G., and Kedersha, N. (2013). Relationship of GW/P-bodies with stress granules. *Adv. Exp. Med. Biol.* 768, 197–211.
- Tcherkezian, J., Cargnello, M., Romeo, Y., Huttlin, E.L., Lavoie, G., Gygi, S.P., and Roux, P.P. (2014). Proteomic analysis of cap-dependent translation identifies LARP1 as a key regulator of 5'TOP mRNA translation. *Genes Dev.* 28, 357–371.
- Tinevez, J.-Y., Perry, N., Schindelin, J., Hoopes, G.M., Reynolds, G.D., Laplantine, E., Bednarek, S.Y., Shorte, S.L., and Eliceiri, K.W. (2017). TrackMate: An open and extensible platform for single-particle tracking. *Methods* 115, 80–90.
- Tokunaga, M., Imamoto, N., and Sakata-Sogawa, K. (2008). Highly inclined thin illumination enables clear single-molecule imaging in cells. *Nat. Methods* 5, 159–161.
- Tourrière, H., Chebli, K., Zekri, L., Courselaud, B., Blanchard, J.M., Bertrand, E., and Tazi, J. (2003). The RasGAP-associated endoribonuclease G3BP assembles stress granules. *J. Cell Biol.* 160, 823–831.
- Unsworth, H., Raguz, S., Edwards, H.J., Higgins, C.F., and Yagüe, E. (2010). mRNA escape from stress granule sequestration is dictated by localization to the endoplasmic reticulum. *FASEB J. Off. Publ. Fed. Am. Soc. Exp. Biol.* 24, 3370–3380.
- Voigt, F., Zhang, H., Cui, X.A., Triebold, D., Liu, A.X., Eglinger, J., Lee, E.S., Chao, J.A., and Palazzo, A.F. (2017). Single-Molecule Quantification of Translation-Dependent Association of mRNAs with the Endoplasmic Reticulum. *Cell Rep.* 21, 3740–3753.
- Voigt, F., Eglinger, J., and Chao, J.A. (2018). Detection of the First Round of Translation: The TRICK Assay. *Methods Mol. Biol. Clifton NJ* 1649, 373–384.
- Wang, C., Han, B., Zhou, R., and Zhuang, X. (2016). Real-Time Imaging of Translation on Single mRNA Transcripts in Live Cells. *Cell* 165, 990–1001.
- Weidenfeld, I., Gossen, M., Löw, R., Kentner, D., Berger, S., Görlich, D., Bartsch, D., Bujard, H., and Schönig, K. (2009). Inducible expression of coding and inhibitory RNAs from retargetable genomic loci. *Nucleic Acids Res.* 37, e50.
- Wheeler, J.R., Matheny, T., Jain, S., Abrisch, R., and Parker, R. (2016). Distinct stages in stress granule assembly and disassembly. *ELife* 5, e18413.
- Wippich, F., Bodenmiller, B., Trajkovska, M.G., Wanka, S., Aebersold, R., and Pelkmans, L. (2013). Dual specificity kinase DYRK3 couples stress granule condensation/dissolution to mTORC1 signaling. *Cell* 152, 791–805.

Wu, B., Miskolci, V., Sato, H., Tutucci, E., Kenworthy, C.A., Donnelly, S.K., Yoon, Y.J., Cox, D., Singer, R.H., and Hodgson, L. (2015). Synonymous modification results in high-fidelity gene expression of repetitive protein and nucleotide sequences. *Genes Dev.* 29, 876–886.

Wu, B., Eliscovich, C., Yoon, Y.J., and Singer, R.H. (2016). Translation dynamics of single mRNAs in live cells and neurons. *Science* 352, 1430–1435.

Yan, X., Hoek, T.A., Vale, R.D., and Tanenbaum, M.E. (2016). Dynamics of Translation of Single mRNA Molecules In Vivo. *Cell* 165, 976–989.

Zhang, K., Daigle, J.G., Cunningham, K.M., Coyne, A.N., Ruan, K., Grima, J.C., Bowen, K.E., Wadhwa, H., Yang, P., Rigo, F., et al. (2018). Stress Granule Assembly Disrupts Nucleocytoplasmic Transport. *Cell* 0.

Zurla, C., Lifland, A.W., and Santangelo, P.J. (2011). Characterizing mRNA Interactions with RNA Granules during Translation Initiation Inhibition. *PLOS ONE* 6, e19727.

Chapter 3: Several small molecules negatively modulate stress granules and decrease cell viability

Wilbertz JH^{1,2}, Miller HR³, Iesmantavicius V¹, Seebacher J¹, Ross NT³, Chao JA¹

¹ Friedrich Miescher Institute for Biomedical Research, Basel, Switzerland

² University of Basel, Basel, Switzerland

³ Novartis Institutes for Biomedical Research (NIBR), Cambridge, MA, USA

Manuscript in preparation

This chapter describes results obtained with a small molecule compound library with known mode-of-actions in order to identify molecules, which are able to negatively influence stress granule formation or stability. Work on this project is still in progress and the long-term goal is to expand the screening approach to gain detailed and unbiased insights into the mechanisms of SG formation and function.

3.1 Introduction

Cells prioritize their activities during various stresses in order to ensure survival, which occurs for example in solid tumors or neurological disorders involving protein aggregation. During the cellular stress response cap-dependent translation is downregulated and the cytoplasm is reorganized into microscopically visible stress granules (SGs) and processing bodies (PBs) (see also sections 1.2 and 1.3). Recently, the small molecule ISRIB (Integrated Stress Reponse InhiBitor) has been described to rapidly disassemble SGs and reactivate translation in mammalian cells in a eIF2 α -independent, but eIF2B dependent manner (Sidrauski et al., 2013), (Sidrauski et al., 2015), (Sekine et al., 2015). PB integrity in stressed cells does not seem to be affected. ISRIB hyperactivates the guanine nucleotide exchange factor (GEF) eIF2B by binding to the two δ -subunits of the homodimer. As a result, eIF2B is still able to fulfill its GEF function by converting inactive eIF2-GDP to the active eIF2-GTP even if eIF2 α is phosphorylated, which is one hallmark of the cellular stress response. eIF2-GTP can then contribute to an active ternary complex which allows the initiation of mRNA translation (Fig. 1). ISRIB presumably also has positive effects on cognition, dopamine-related learning processes and depression symptoms in mice (Sidrauski et al., 2013), (Placzek et al., 2016), (Kabir et al., 2017) and might be able to enhance memory formation after traumatic brain injury (Chou et al., 2017). Four scenarios are possible to explain the observed cell biological and brain physiological effects of ISRIB: The molecule might act due to (1) its disassembly effect on SGs, (2) its capability to reactivate translation, (3) a combination of both, or (4) an unknown non-eIF2B target.

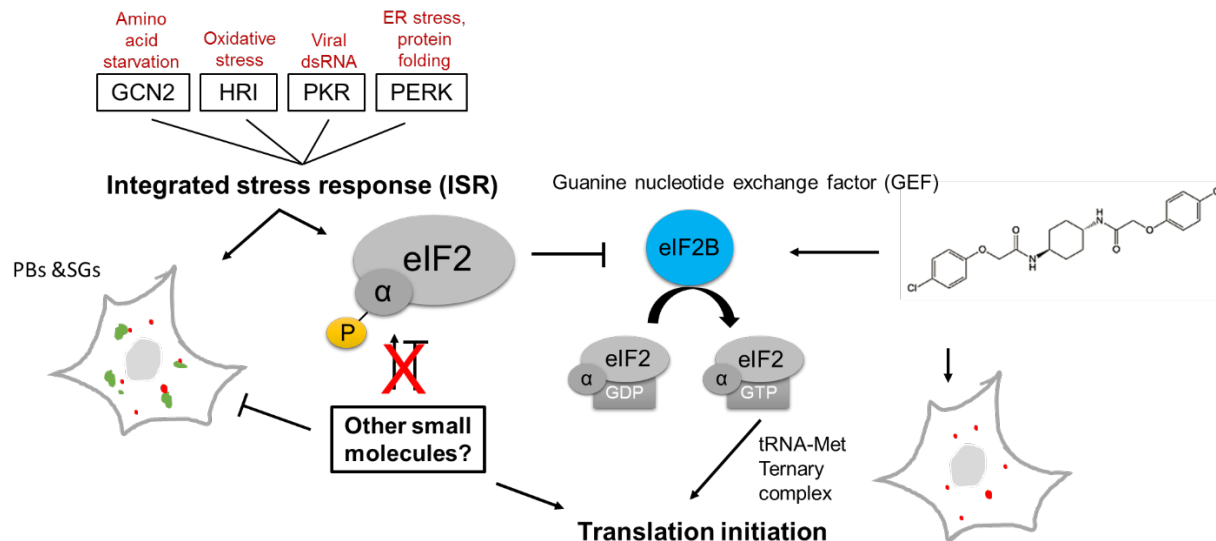


Fig. 1: Do other small molecules with ISRIB-like effects exist? During the ISR ISRIB lends cells resistant to eIF2 α -phosphorylation on Ser51, by hyperactivation of eIF2B, presumably through enhancing the dimerization of its two δ subunits. ISRIB treated cells can therefore still initiate translation and SG disassemble. Whether these two processes are linked and whether other molecules exist that can reduce the number of SGs and resume translation during stress in a PB- and eIF2 α -phosphorylation-independent manner is not known.

Currently, it is under debate whether SGs have a pro-survival or rather pro-apoptotic effect during the cellular stress response (see section 1.7). It proved to be difficult to untangle the effects of stress-induced translational regulation and the presence of SGs themselves on this process. There is increasing evidence that SG presence and translation inhibition might not always be as tightly linked as previously thought. One study for example found that inhibition of the last step of translation initiation by blocking the recruitment of 60S ribosome either with 2-(4-methyl-2,6-dinitroanilino)-N-methylpropionamide or through depletion of the large ribosomal subunits protein L28 does not induce SG assembly (Mokas et al., 2009). Later the inverse was found to be true as well. USP10, when overexpressed, was observed to inhibit SG assembly downstream of polysome disassembly, most likely due to preventing mRNP condensation which is required for SG formation (Kedersha et al., 2016). We observed a third case highlighting the complexity of the relationship between translation inhibition and SG formation. When adding ISRIB to thapsigargin (Tg)-induced ER-stressed HeLa cells, we observed SG disassembly and reinitiation of translation measured by Renilla luciferase (Fig. 2a) similarly to what had been described in the original ISRIB paper (Sidrauski et al., 2013). When performing the same experiment under sodium arsenite (SA)-induced oxidative stress, ISRIB still dissolved SGs, but could surprisingly not reactivate translation (Fig. 2a). Independently of the Renilla luciferase readout, we observed the failure to initiate translation also more generally by polysome profiling (Fig. 2b). Here, the

combination of SA and ISRIB does not lead to reappearing polysomes comparable to the unstressed control. ISRIB might therefore fulfill two independent functions. Under some conditions the molecule is able to reactivate translation and dissolve SGs, while under more severe stress conditions ISRIB fails to reactivate translation, but still dissolves SGs. ISRIB might therefore have at least one more molecular target next to eIF2B. The knockdown of candidate proteins to address the uncoupling of translation and SG formation is challenging. Such experiments often influence both translation and SG integrity at the same time, making it difficult to draw any causative conclusions. To understand the beneficial effects and potential side effects of ISRIB or other small molecules on fundamental biological processes, it is crucial to fill this knowledge gap. Here, we therefore performed two imaging based screens to detect known small molecules with an unknown function to dissolve SGs in a PB- and eIF2 α -phosphorylation-independent manner.

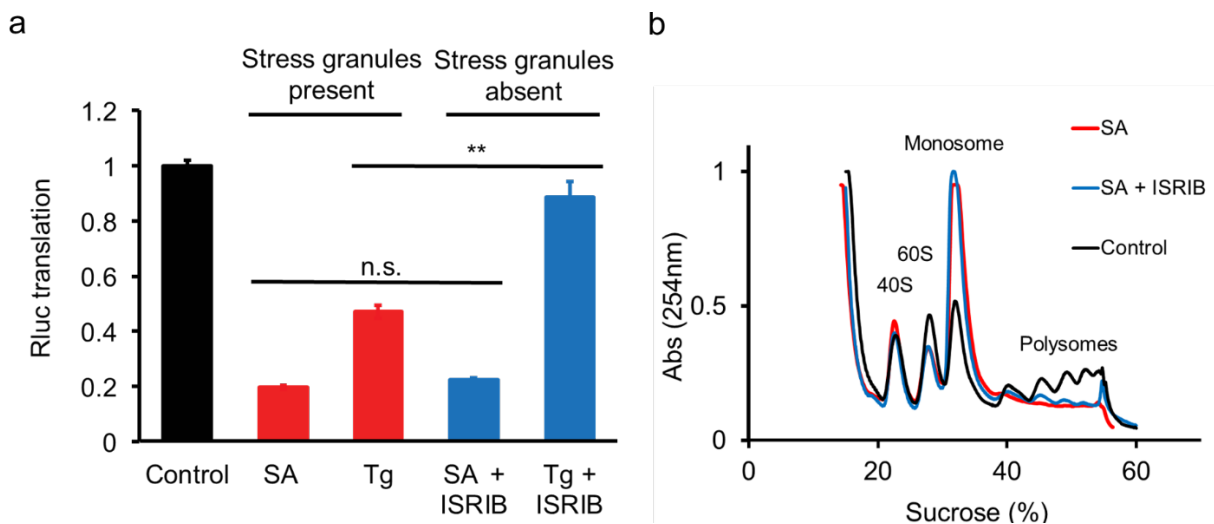


Fig. 2: ISRIB can uncouple translation repression from SG presence. (a) Renilla luciferase assays showed that ISRIB can reactivate translation and dissolve SGs when HeLa cells were stressed with 500 nM Tg for 2h and 100 nM ISRIB are added for another 1h. ISRIB failed to reactivate translation, but still dissolved SGs when cells were stressed with 100 μ M SA. (b) Polysome profiling also showed that the combination of SA and ISRIB failed to reactivate translation.

We identified a number of small molecules targeting a multitude of biochemical pathways, which all negatively modulate SGs. This allowed us to study SG effects on translation and cell survival from multiple targeting angles without the need to deplete SG-related proteins. We excluded compounds that broadly target all stress induced mRNPs complexes or the four already identified stress-activated kinases HRI, PKR, PERK, and GCN2. To achieve this, compounds were only selected when no or only minor negative effects on PB numbers or eIF2 α -phosphorylation were present (Fig. 1). Using a Novartis mode of action (MoA) box containing 3078 small molecules each with a described target in

an imaging-based screen, we identified 23 compounds functioning as SG disassembly enhancers and 4 compounds acting as SG formation blockers. Although all compounds compromised SG integrity, no rescue of cap- or uORF-dependent translation was observed. One GSK3 inhibitor (SB216763) resulted in a mild, but significant uORF-dependent translation up regulation. The majority of identified compounds decreased cell survival through apoptosis up regulation in the presence of ER stress, but not during its absence.

In summary, the identification and characterization of several small molecular compounds with known MoAs, allowed us to study the cellular stress response in the presence and absence of SGs without perturbing SG protein levels. We find that translation is regulated independently of SGs and that the absence of SGs correlates with increased apoptosis. These findings are consistent for a number of different biochemical targets and are in support of the notion that SGs fulfill a pro-survival function when unperturbed.

3.2 Results

To study the effects of SGs on cellular physiology in a protein level independent manner, we chose to perform an imaging-based screening utilizing the Novartis MoA box containing 3078 small molecules each with a described target. HeLa cells stably expressing G3BP1-GFP and DDX6-TagRFP-T as SG and PB markers, respectively, were fixed and stained for eIF2 α -phosphorylation (Ser51) and imaged after having been exposed to sodium arsenite (SA). SGs, increased numbers of PBs and increased levels of eIF2 α -phosphorylation were only detectable in the presence of sodium arsenite. (Fig. 3a). To perturb SG integrity we designed two different experiments. The first experiment was aimed to identify SG assembly blockers, while with the second experiment we intended to identify SG disassembly enhancers (Fig. 3b and 2c). In the screen for SG assembly blockers, cells were first treated with the compounds at concentrations ranging from 0.01-100 μ M for 6 hours, stressed with 125 μ M SA for 0.5 hours, fixed and immunostained for eIF2 α -phosphorylation. Next SGs and PBs were segmented and quantified and eIF2 α -phosphorylation stain intensity was determined (Fig. 3b). In the screen for SG disassembly enhancers, cells were pre-treated with 125 μ M SA for 1.0 hour and then exposed to the compounds at concentrations ranging from 0.01-100 μ M for 0.5 hours. Next, SGs, PBs, and eIF2 α -phosphorylation were quantified (Fig. 3c). In total 23 compounds were identified as PB- and eIF2 α -phosphorylation independent SG assembly blockers, while 4 compounds could be found acting as SG disassembly enhancers in two independent screening replicates.

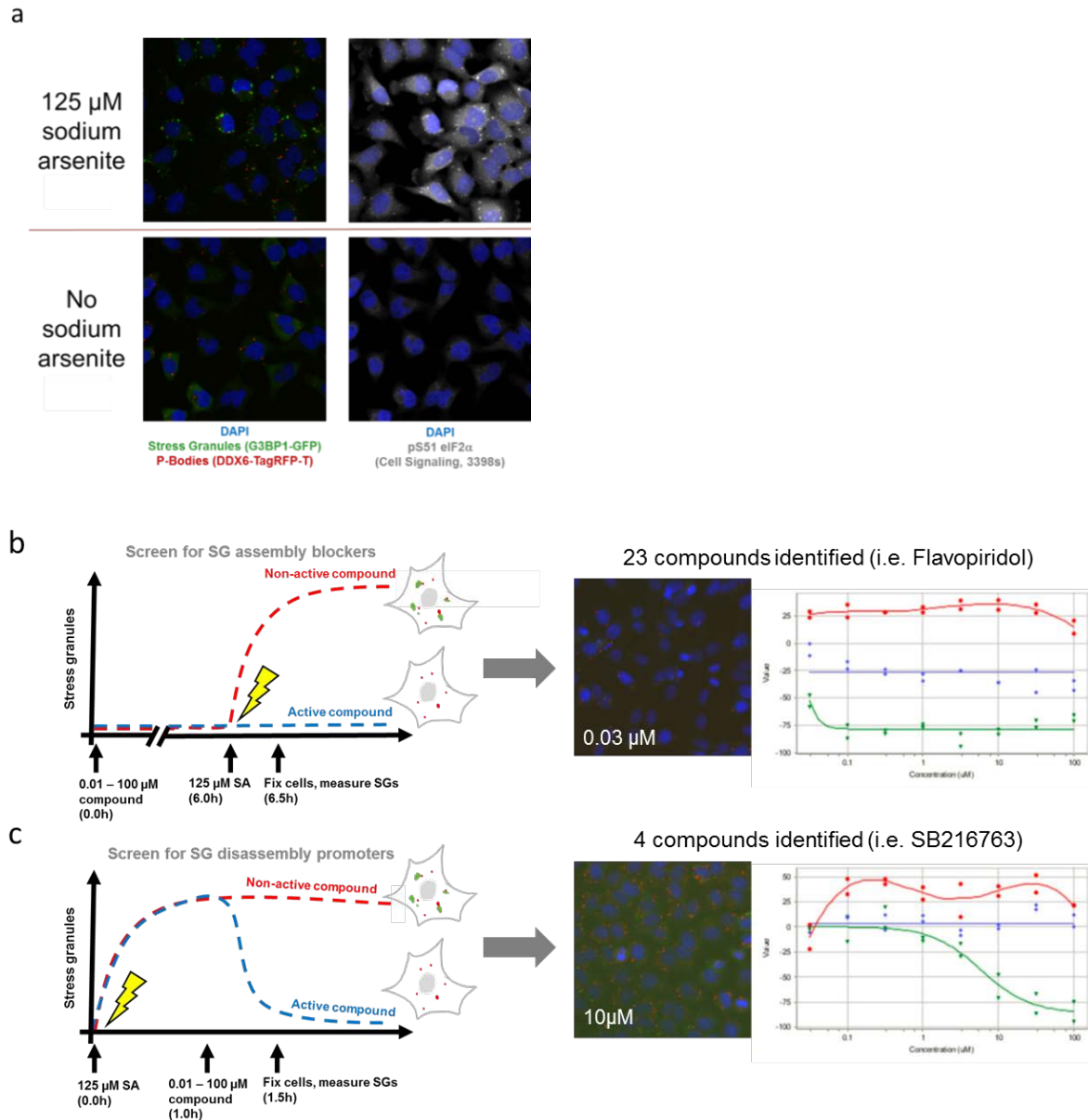


Fig. 3: Automated screening for processing body and eIF2 α -independent stress granule modulators in human cells. (a) HeLa cells expressing G3BP1-2xGFP and DDX6-Tag-RFP-T are treated for 1 hour with 125 μM sodium arsenite (SA), fixed and are positive for stress granules (SGs), P-bodies (PBs) and stress-induced eIF2 α (Ser51) phosphorylation. (b) In the screen for SG assembly blockers cells are first pre-treated for 6 hours with small molecules from the Novartis Mode of Action library at concentrations ranging from 0.01 – 100 μM , then treated with 125 μM SA for 30 minutes and subsequently fixed. The presence of SGs, PBs and eIF2 α (Ser51) phosphorylation is assessed for all compounds at all used concentrations by automated image analysis. 23 compounds fulfill the screening criteria. (c) In the screen for SG disassembly promoters cells are first treated with 125 μM SA for 1 hour, treated with small molecules from the Novartis Mode of Action library at concentrations ranging from 0.01 – 100 μM for 30 minutes and subsequently fixed. The presence of SGs, PBs and eIF2 α (Ser51) phosphorylation is assessed for all compounds at all used concentrations by automated image analysis. 4 compounds fulfill the screening criteria.

Each of the 23 identified compounds received a reference number, which is used throughout this chapter to refer to the compound (Tab. 1, column 1). The identified compounds target enzymes over a large mode of action spectrum, although CDK1, CDK2, and CDK4 inhibitors are most common (Tab. 1, column 4). 20 compounds acted exclusively as SG assembly inhibitors, 1 compound promoted exclusively the disassembly of pre-formed SGs, and 3 compounds had both effects (Tab. 1, column 5). Only compounds exerting their maximum effect in the low μM range were considered for follow up experiments and are represented in the unmarked top half of Tab. 1. Of those compounds, the concentration with the approximate half maximal effect on SGs without affecting PBs and eIF2 α -phosphorylation was used for all experiments with the respective compound described here (Tab. 1, column 6). Compound #13 was excluded from follow up experiments due to intellectual property limitations. All other identified compounds are freely available.

Tab. 1: Overview of the 12 selected inhibitors obtained during the screen. The indicated concentrations were used for all follow-up experiments reported here. Red: Remaining 12 compounds which have not been tested further.

#	Compound name	PubChem Identifier	Mode of Action	SG-related function	Concentration (μM)
1	2-aminothiazole 2	5329665	CDK2/Cyclin E Inhibitors	SG assembly inhibitor	1
2	Diacetoxyscirpenol	15571694	Apoptosis Inducers;SGLT-1 Inhibitors	SG disassembly enhancer, SG assembly inhibitor (?)	4
3	Digitoxigenin	4369270	?	SG assembly inhibitor	1
4	SB216763	176158	Glycogen Synthase Kinase 3 (GSK-3) Inhibitors	SG disassembly enhancer	4
5	SCHEMBL5732902	9861036	CDK1 Inhibitors	SG assembly inhibitor	1
6	UNII-09RR39UU4V	5282335	CDK2/Cyclin E Inhibitors;CDK1 Inhibitors;CDK4 Inhibitors	SG assembly inhibitor	1
7	SNS032	3025986	CDK7 Inhibitors;CDK2/Cyclin E Inhibitors;CDK9 Inhibitors	SG assembly inhibitor	1
8	CHEMBL368895	10209082	Inhibitors of Signal Transduction Pathways;Protein Kinase PKC beta Inhibitors;Angiogenesis Inhibitors	SG disassembly enhancer, SG assembly inhibitor	4
9	CGP60474	644215	Protein Kinase C (PKC) Inhibitors;CDK1 Inhibitors;CDK2 Inhibitors	SG assembly inhibitor	0.5
10	AT7519	11338033	Apoptosis Inducers;Inhibitors of Signal Transduction Pathways;CDK2/Cyclin A Inhibitors;CDK1/Cyclin B Inhibitors	SG assembly inhibitor	0.5
11	Flavopiridol	5287969	?	SG assembly inhibitor	2
12	Meriolin 1	11637090	?	SG assembly inhibitor	3
13	?	?	?	SG assembly inhibitor	not used
14	SCHEMBL6110484	21948241	CDK1 Inhibitors	SG assembly inhibitor, SG disassembly enhancer	not used
15	SCHEMBL5894047	9846976	Tyrosine Kinase Inhibitors;CDK1 Inhibitors;CDK2 Inhibitors	SG assembly inhibitor	not used
16	SCHEMBL3681671	11477833	Flt3 (FLK2/STK1) Inhibitors	SG assembly inhibitor	not used
17	?	?	?	SG assembly inhibitor	not used
18	SCHEMBL5742011	5329333	?	SG assembly inhibitor	not used
19	JNJ7706621	5330790	Antimitotic Drugs;Apoptosis Inducers;Aurora Kinase Inhibitors;CDK1/Cyclin B Inhibitors;CDK2/Cyclin A Inhibitors;Inhibitors of Signal Transduction Pathways	SG assembly inhibitor	not used
20	CHEMBL522328	44201333	ITK (EMT) Kinase Inhibitors;IL-4 Production Inhibitors;L-2 Production Inhibitors	SG assembly inhibitor	not used
21	SCHEMBL5726610	9867295	CDK4 Inhibitors	SG assembly inhibitor	not used
22	A-674563	11314340	cAMP-Dependent Protein Kinase (PKA) Inhibitors;Inhibitors of Signal Transduction Pathways;PKB alpha/Akt1 Inhibitors	SG assembly inhibitor	not used
23	SCHEMBL4711594	11427778	?	SG assembly inhibitor	not used
24	K03861	11260561	Flt3 (FLK2/STK1) Inhibitors	SG assembly inhibitor	not used

The 12 selected compounds mentioned in Tab. 1 were then validated for their effects on endogenous SGs stained for with a G3BP1 antibody (Fig. 4a). As identified in the screen, the majority of the compounds acted at least a SG assembly blocker reducing the size (Fig. 4a), the SG number per cell (Fig. 4b), or both when administered simultaneous with SA to HeLa cells. Compounds #6 and #7 led only to a modest decrease of endogenous SG size and have no significant effect on the SG number per cell. Treatments with 100 μM SA or DMSO served as positive and negative controls, respectively.

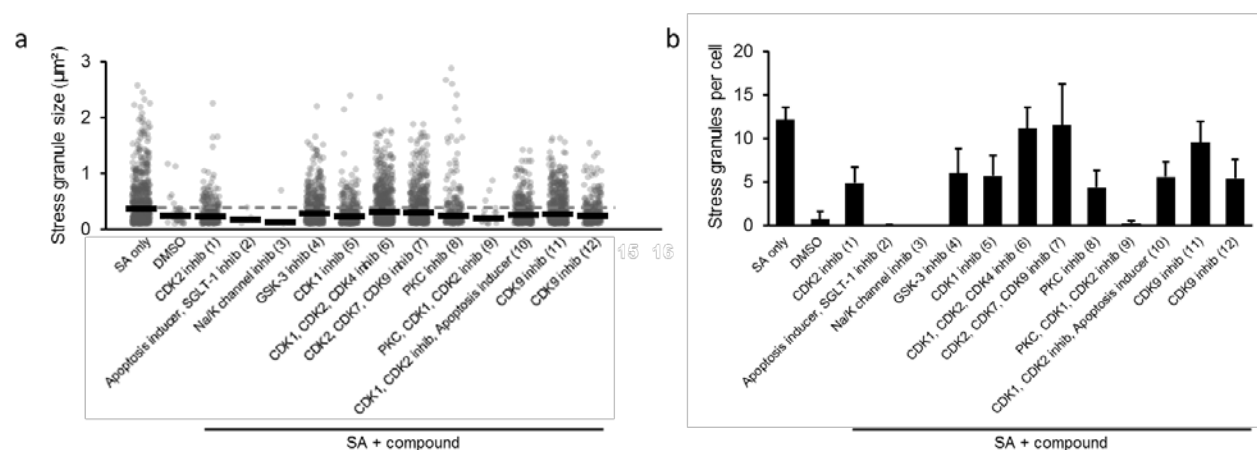


Fig. 4: Validation of screen hits by immunofluorescence. Multiple selected compounds negatively impact endogenous SG size and number. (a) All selected compounds reduce the size of SGs when treated over night, stressed for 1 hour with SA, fixed and stained for SGs with an G3BP1 antibody. Each dot represents one detected SG. Black horizontal bars represent medians. 30 cells were analyzed per treatment condition. (b) Most tested compounds reduce the average number of SGs per cell when treated over night, stressed for 1 hour with SA, fixed and stained for SGs with an G3BP1 antibody. Error bars represent standard error of the mean (SEM).

In order to test the effect of the 12 identified compounds on translation; we generated HeLa cell lines expressing stably integrated Renilla luciferase reporters from a single doxycycline inducible locus. Two different reporter systems were used. The first served the purpose to assess compound effects on canonical cap-dependent translation. This reporter contained a single start codon followed by the Renilla luciferase open reading frame (ORF) (Fig. 5a, top panel). The second reporter was designed to test compound effects on upstream ORF (uORF) mediated translation. uORF mediated translation is common for transcripts encoding for stress responsive proteins such as ATF4, CHOP or GADD34. For this reporter we utilized the ATF4 uORF structure and fused it to the main Renilla luciferase ORF (Fig. 5b, top panel). The reporter contains two uORFs of which the downstream one overlaps with the main Renilla luciferase ORF. Under stress conditions “leaky scanning” due to impaired translation reinitiation can occur resulting in the skipping of uORF2 and a higher chance for main ORF translation (see section 1.2.2). This second reporter would therefore be higher expressed during the stress response, while the first reporter would remain silent.

Control experiments of HeLa cells expressing the cap-dependent translation reporter treated with DMSO showed reduced Renilla luciferase expression when stressed for 1.5h with the ER-stressor Tg (Fig. 5a, bottom panel). Unstressed cells were treated with DMSO instead and showed ca. 40% higher

Renilla luciferase expression levels. Despite being able to block SG formation none of the 12 tested compounds was able to rescue translation to levels comparable to unstressed cells treated only with compound. Interestingly, compounds #2, #6 and #7 repressed translation even in the absence of stress. The three compounds are therefore functionally similar to the translation elongation blocker cycloheximide which is able to dissolve SGs and repress translation at the same time.

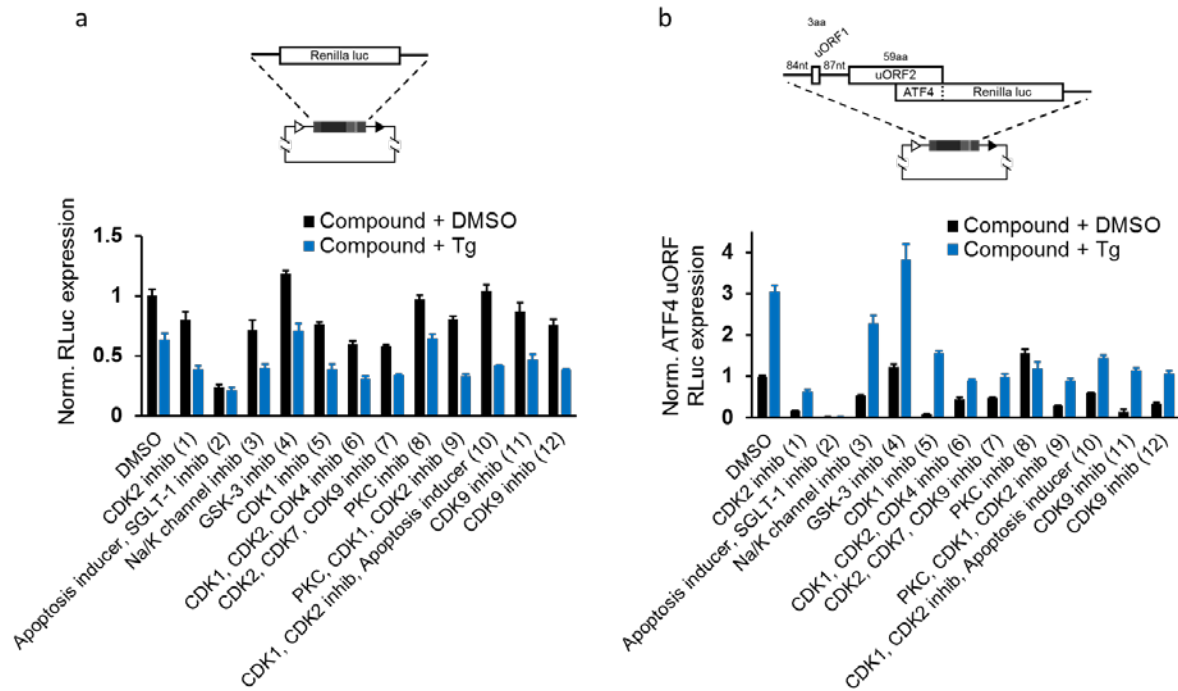


Fig. 5: The majority of the selected small molecule inhibitors does not rescue translation during stress, while one GSK3 inhibitor upregulates stress-induced uORF-mediated translation. (a) Cap-dependent translation was assessed by Doxycyclin induction of a Renilla luciferase encoding reporter for 1.5h, followed by a PBS wash and a 1.5h treatment with compound and 1 μ M thapsigargin (prevention of measuring transcriptional effects of compounds). (b) uORF-mediated translation was assessed by Doxycyclin induction of a reporter containing the ATF4 uORF structure fused to Renilla luciferase for 1.5h, followed by a PBS wash and a 1.5h treatment with compound and 1 μ M thapsigargin (prevention of measuring the transcriptional effects of compounds).

In contrast to cap-dependent translation, uORF-mediated translation was 3-fold up regulated in the Renilla luciferase reporter assay when cells were mock treated with DMSO and stressed with Tg (Fig. 5b, bottom panel). For compounds targeting translation initiation fidelity we expected a down regulation of translation when compound and stress were combined. In contrast to this hypothesis, we observed that the majority of the compounds seemed to block translation in the absence stress and did

not lead to a reduction of translation when compound and stress were combined. Compound #8 is an exception to this observation and behaves as expected. Furthermore, a GSK3 inhibitor (compound #4) shows an interesting expression pattern, since its uORF-mediated translation is mildly up regulated when stressed compared to equally stressed, but DMSO treated control cells.

Since the compounds identified in our screen target a wide range of biochemical pathways (Tab. 1), we reasoned that testing the compounds in a viability assay would lead to insights concerning the proposed pro-survival role of SGs independent of a specific single biochemical pathway. By assessing Caspase 3/7 activity for all tested 12 compounds in the presence and absence of ER stress we were able to test if compounds alone are apoptosis inducing. In addition this experimental setup allowed us to study whether a compound in combination with cell stress leads to increased apoptosis.

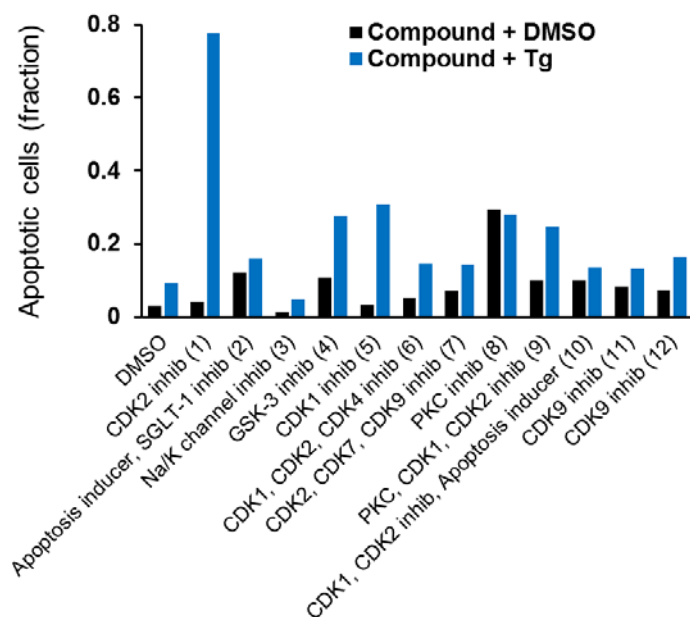


Fig. 6: The majority of negative SG modulators with differing targets upregulate apoptosis during stress. HeLa cells were seeded one day prior to experiment and then treated with small molecule inhibitors (Tab. 1) and 0.5µM thapsigargin for 48h. Cells were then stained with Hoechst and Caspase3/7 activity was assessed by imaging. The total cell count and the fraction of apoptotic cells was then quantified by automated-image analysis (FIJI macro).

When we co-treated HeLa cells with each of the identified compounds in the absence of stress only compounds #2, #4, #8 seemed to be toxic for cells (Fig. 6, black bars). When each compound was

combined with the ER stress inducer thapsigargin an increase in Caspase 3/7 activity was observed for all compounds, except compound #8 (Fig. 6, blue bars). Especially compounds #1 and #5 are interesting in this context since they both show very low baseline toxicity and a dramatic apoptosis activation increase when combined with thapsigargin. Both compounds target cyclin dependent kinases (CDKs).

The uORF-controlled and stress-induced transcription factor ATF4 is linked to the cellular stress response and its overexpression might induce apoptosis through the suppression of stress adaptation. Since compound #4 led to an increase in uORF reporter expression during ER stress (Fig. 5b), we decided to investigate its effects in more detail. Compound #4 is a GSK3 inhibitor and will be referred to as SB216763 from now on. To test whether GSK3 inhibition is responsible for the observed uORF-controlled reporter upregulation we performed a luciferase assay with another GSK3 inhibitor called CHIR99021. HeLa cells expressing ATF uORF-controlled renilla luciferase were treated overnight for 16 hours with either DMSO, SB216763 or CHIR99021 and then treated either with DMSO or with thapsigargin for 2 hours to induce renilla luciferase expression. During the absence of stress, neither SB216763 nor CHIR99021 led to an increase of uORF-mediated translation (Fig. 7a). When cells were treated with thapsigargin and SB216763 or CHIR99021, uORF-mediated translation increased mildly, but significantly for both compounds (Fig. 7a).

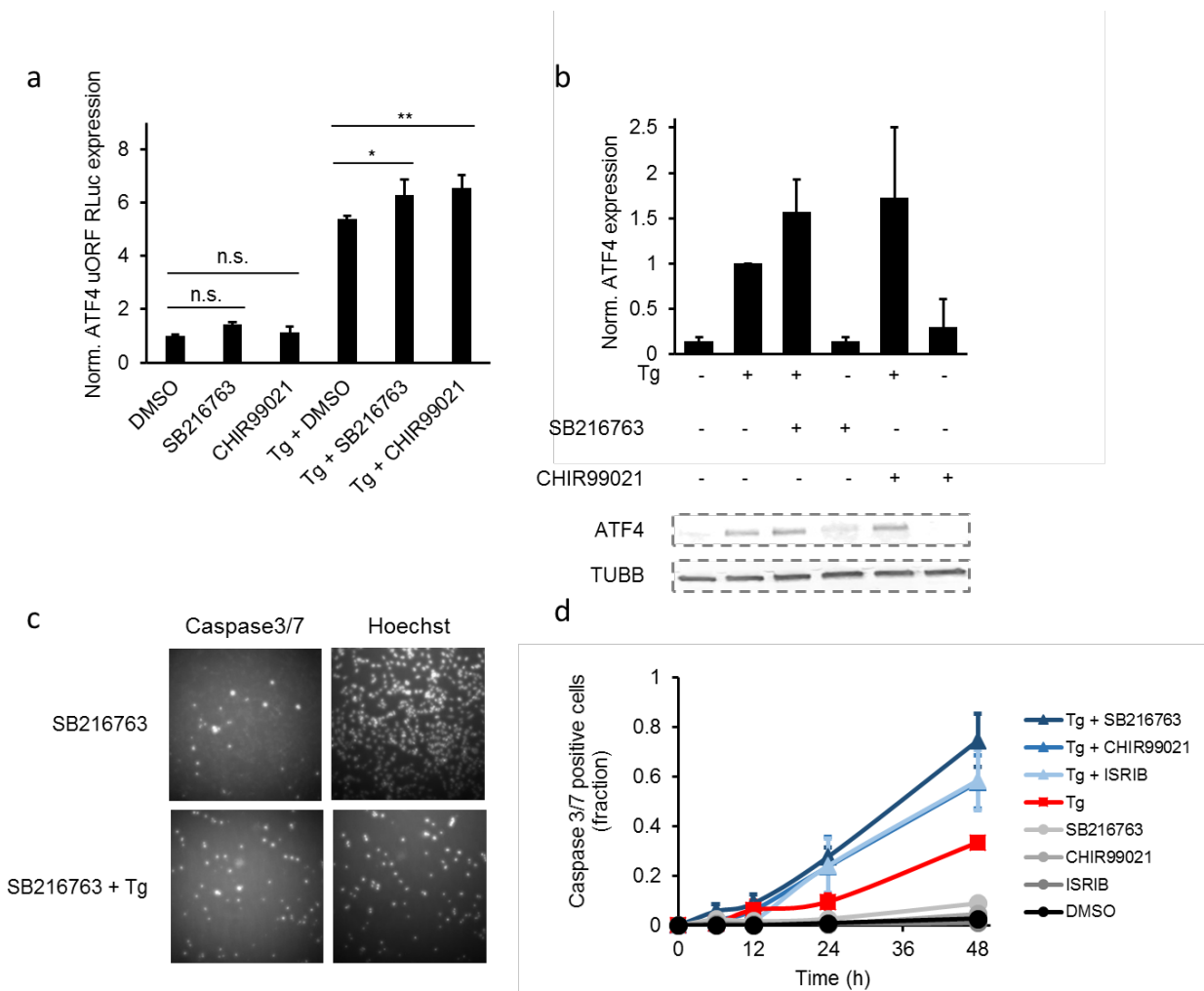


Fig. 7: Two GSK3 inhibitors upregulate uORF-mediated ATF4 expression, inhibit cell growth and induce apoptosis. Important to note: Only SB216763 (identified in screen) negatively impacts SGs. CHIR99021 has no visible effect on SGs (see also Fig. 8). (a) HeLa cells treated with the indicated compounds for 16h followed by 2h of 0.5 μ M thapsigargin induced stress show hyperactivated uORF-mediated translation. (b) Endogenous uORF-translation-mediated ATF4 protein is also upregulated in compound treated and stressed HeLa cells. (c) 48h treatment with SB216763 + Tg reduces cell growth (Hoechst) and induces apoptosis (Caspase3/7). SB216763 alone does not lead to these effects. (d) The three stress-response modulators SB216763, CHIR99021 and ISRIB induce apoptosis only in the presence of 0.5 μ M thapsigargin. Cells were then stained with Hoechst and Caspase3/7 activity was assessed by imaging as in (c). The total cell count and the fraction of apoptotic cells was then quantified by automated-image analysis (FIJI macro). Three biological replicates were performed.

Next, we tested whether SB216763 and CHIR99021 were able to upregulate endogenous uORF-mediated ATF4 expression. Western blotting showed an increase of endogenous ATF4 expression when HeLa cells were co-treated with thapsigargin and either SB216763 or CHIR99021 (Fig. 7b). Each compound alone did not induce ATF4 expression in the absence of ER stress. It is important to note that only SB216763 was able to decrease the number of SGs, while CHIR99021 was not (Fig. 8). Since

increased levels of ATF4 might compromise a cells ability to survive stress, we next tested the effects of both GSK3 inhibitors on cell viability. As shown in Fig. 7c, after 48 hours of treatment with thapsigargin and SB216763 cell numbers where drastically reduced (Hoechst) and almost all remaining cells were positive for active Caspase 3/7. Although SB216763 treatment alone led to some Caspase 3/7 activation, cell proliferation was not affected. In a time course experiment these effects where confirmed further (Fig. 7d). In the absence of stress SB216763, CHIR99021 and the ATF4 repressor and SG dissolver ISRIB had no effect on the fraction of apoptotic cells (< 10%) (Fig. 7c, gray traces). Thapsigargin alone resulted in 33% Caspase 3/7 positive cells (Fig. 7c, red trace). The combination of either SB216763, CHIR99021, and ISRIB with thapsigargin caused higher apoptosis rates after 48 hours (Fig. 7c, blue traces). The screen-identified compound SB216763 resulted in the highest fraction of Caspase 3/7 positive cells (74%).

As described in Fig. 7 both SB216763 and CHIR99021 treatment led to increased ATF4 expression and decreased cell viability. Despite this, both compounds have opposing effects on SGs. While SB216763 decreases the number and size of SGs in the presence of SA stress (Fig. 3c, Fig. 4, Fig. 8) the other GSK3 inhibitor CHIR99021 fails to do so (Fig. 8). To investigate the discrepancy between shared ATF4 and apoptosis upregulation, but differing effects on SGs we decided to perform phosphoproteomics to identify shared and differing targets of both compounds.

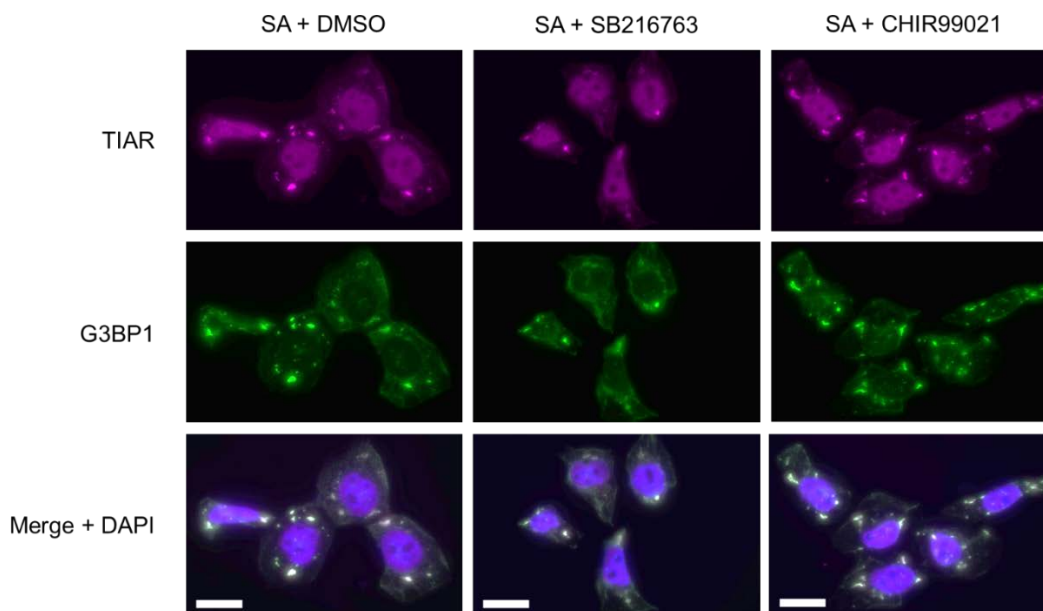


Fig. 8: Two GSK3 inhibitors have differing effects on SG integrity. HeLa cells were treated with 100 μ M SA for 1h, followed by 2h of SA combined with either DMSO, SB216763, or CHIR99021. Then immunofluorescence was performed against the two SG markers proteins TIAR and G3BP1. Scale bar = 10 μ M.

HeLa cells were treated overnight for 16 hours with either SB216763, CHIR99021 or DMSO. The next day the cells were stressed with thapsigargin for 2 hours and processed for phosphoproteomics. Fig. 9 shows significant phosphopeptide abundance changes when DMSO + thapsigargin experiments were compared to compound + thapsigargin experiments. Changes are expected to be due to direct inhibition effects of GSK3, other unknown direct targets or due to indirect network effects. These significant abundance changes were then plotted for both compounds in the same graph. Phosphopeptides changing during SB216763 treatment are depicted on the x-axis and phosphopeptides changing during CHIR99021 treatment are depicted on the y-axis of Fig. 9. Peptide changes on an imaginary diagonal spanning from the lower left to the top right part of the graph correlate between treatments. Since both compounds are GSK3 inhibitors, several GSK3 downstream targets are identified (GYS1, APC, AXIN1, DPYSL2, MACF1). In addition, the GSK3-targetted consensus sequence pSXXXpS is enriched in our dataset. Off-diagonal phosphopeptides are differentially regulated between both compound treatments. Among the interesting hits are for example ATXN2L (Ataxin-2-like), which has been implicated in SG regulation (Kaehler et al., 2012), or the two kinases MTK1 and ZAK. Both are implicated in the suppression of apoptosis through MAPK pathways, potentially through sequestration within SGs (Arimoto et al., 2008).

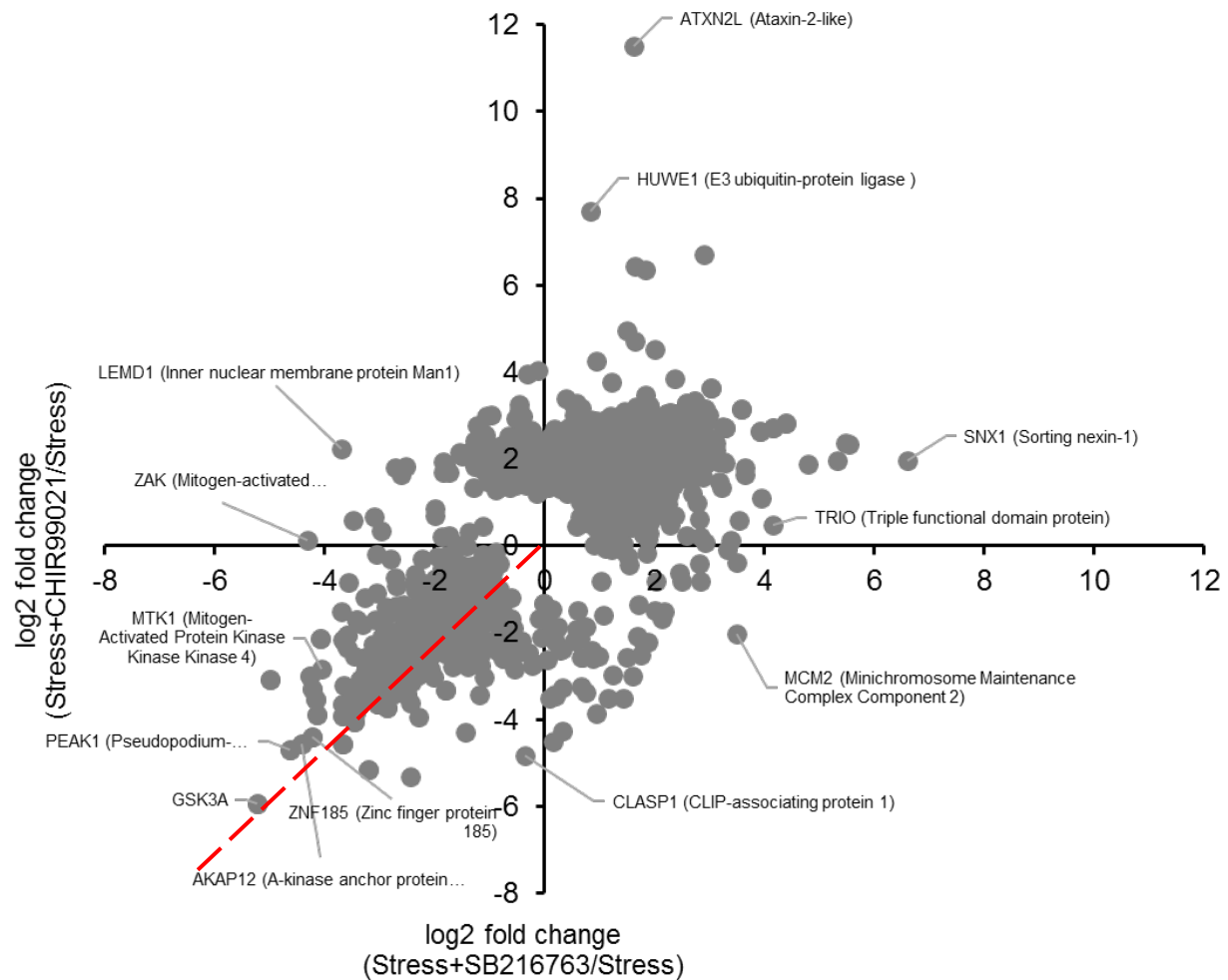


Fig. 9: Phosphoproteome comparison between the two GSK3 inhibitors SB216763 (promotes SG disassembly) and CHIR99021 (no effect on SG integrity). The plot shows significantly changing peptides of thapsigargin stressed HeLa cells treated with the respective compound versus HeLa cells that were only subject to thapsigargin stress and not treated with the compound. The cells were treated for 16 hours with the respective compound, then stressed with 1 μ M thapsigargin for 2h, lysed, protease treated, enriched for phosphopeptides and analyzed by mass spectrometry. The broken red line serves as guide for the eye for peptides that co-downregulated for both inhibitors. Three independent replicates were performed and only significantly changing peptides are shown.

3.3 Summary and discussion

Here we describe several small molecule inhibitors which are able to negatively influence SGs in a PB and eIF2 α -phosphorylation (Ser51) independent manner (Fig. 3 & Tab. 1). At a single tested concentration, all of the selected compounds also negatively influenced endogenous SGs, although to a varying extent (Fig. 4). Contrary to our initial expectation, the selected small molecule inhibitors did not rescue cap-dependent translation during stress. Interestingly, one GSK3 inhibitor upregulated stress-induced uORF-mediated translation, which plays a role for many stress-induced genes i.e. ATF4. Importantly, the disassembly or prevention of SGs through a variety of pathways does not necessarily result in translation re-initiation (Fig. 5). 11 out of the 12 tested compounds have a negative impact on cell viability in stressful conditions when compared to cell stress alone (Fig. 6). This finding supports the notion that SGs might fulfill a pro-survival function in cells facing stress. In this context, compound #1, a CDK2 inhibitor, could be a valuable tool to study the effect of SG dissolution on apoptosis due to its strong cellular responses both in the SG and apoptosis assays.

When we focused on the GSK3 inhibitor SB216763 due to its capability to upregulate uORF-mediated translation we were able to confirm this effect also for another GSK3 inhibitor called CHIR99021, which was not part of the screen. Interestingly, CHIR99021 does not fully dissolve SGs in contrast to SB216763 (Fig. 8). In a 48h time course experiment, both compounds resulted in increased apoptosis in stressed cells. ATF4 upregulation, disassembly of SGs or the combination of both might be useful to control cell viability during stress (Fig. 7). Due to their similar effect on ATF4 expression, but differing effect on SGs we performed phosphoproteomics for the two GSK3 inhibitors SB216763 and CHIR99021. Interestingly, we identify GSK3A as the strongest co-downregulated phosphopeptide in our dataset, suggesting an autoregulatory mechanism. Although in the absence of stress, previous work has shown that lithium, another GSK3 inhibitor, causes a GSK3 phosphorylation increase (Zhang et al., 2003). This presumably occurs through inhibiting the GSK-3-mediated activation of protein phosphatase PP1 subunit I2. Blocking PP1 in turn upregulates GSK3 phosphorylation. Why we see the opposite effect on GSK3A phosphorylation levels during thapsigargin-induced ER stress is currently not clear. One possibility is that the observed ATF4 overexpression induces the transcription factor CHOP, which in turn induces the PP1 subunit GADD34 (Novoa et al., 2003), (Wortel et al., 2017). Whether PP1-GADD34 can dephosphorylate GSK3 remains an open question. In addition, prolonged upregulation of the ATF4-CHOP-GADD34 axis has been implicated in increased apoptosis, which is in line with our findings. This

occurs presumably due to dephosphorylation of eIF2 α allowing the unwanted re-initiation of canonical translation under stress conditions (Kang et al., 2011), (Dennis et al., 2013), (Han et al., 2013), (Guan et al., 2014). However, it is also a possibility that the observed inhibitor effects are unrelated to GSK3 due to off-target effects. Off-target effects become more likely at high concentrations and/or prolonged incubation times. Interesting non-GSK3 related hits include the two MAPKKK kinases ZAK (also known as MAP3K20, MLT or MLTK) and MTK1 (also known as MAP3K4 or MEKK4).

ZAK has been implicated in apoptosis upregulation in several cancers (Vin et al., 2013), (Markowitz et al., 2016). Since ZAK phosphorylation is specifically downregulated during SB216763 treatment and not during CHIR99021 treatment, it will be interesting to see whether ZAK is localized to SGs and to what extent it changes its subcellular distribution during SB216763 treatment. MTK1 is another interesting hit and also a MAPKKK kinase. MTK1 is able to bind RACK1 which activates apoptosis through p38 and JNK. Interestingly, RACK1 is also able to prevent apoptotic responses by associating with SGs. Sequestration of RACK1 inside of SGs significantly reduces its ability to associate with MTK1 and therefore inhibits the MTK1-dependent apoptosis activation (Arimoto et al., 2008). Liberating RACK1 from SGs through SB216763 could potentially explain the observed higher levels of apoptosis. Whether CHIR99021 is able to increase the free RACK1 pool is unclear. Further, it will be interesting to see if dephosphorylated MTK1, as observed by mass spectrometry, has elevated RACK1 binding capacity when treated with either SB216763 or CHIR99021.

In summary, here we identify several small molecules with SG destabilizing and apoptosis inducing properties. These compounds might be a valuable resource to study the biological role of SGs without the need to perturb protein levels.

3.4 Material and methods

Generation of SG and PB marker cell line

In order to visualize stress granules and P-bodies in living cells, G3BP1-2xGFP and DDX6-Tag-RFP-T fusion proteins were cloned into the phage UbiC lentiviral vectors, respectively. Constructs were simultaneously and stably integrated by lentiviral transduction according to standard protocols. To prevent stress granule formation or excess P-body formation in the absence of stress due to overexpression, FACS was utilized to identify only low expressing dual positive cells. Immunofluorescence against TIAR (1/100, cat. # 610352, BD Biosciences), G3BP1 (1/200, cat. # ARP37713_T100, Aviva Systems Biology), DDX6 (1/300, cat. # A300-461A, Bethyl Labs) and DCP1a (1/300, cat. # 47998, Abcam) was performed to confirm physiological stress granule and P-body numbers and behavior.

Screen setup & analysis

For both screens G3BP1-2xGFP and DDX6-Tag-RFP-T expressing HeLa cells were seeded in DMEM + 10% FBS in 1536-well plates one day prior to the experiment and incubated at 37°C and 5% CO₂. In the screen for blockers of SG assembly each of the 3,078 Novartis Mode of Action library compounds was administered to the cells 6h prior to fixation at concentrations ranging from 0.01 – 100 µM. Cells were then treated with 125 µM SA (Sigma) diluted in water for 30 minutes, followed by fixation in 4% paraformaldehyde (PFA). DMSO treated cells exposed to water and DMSO or SA and DMSO served as negative and positive controls, respectively (see also Fig. 3b for a schematic representation). After fixation cells were imaged.

In the screen for enhancers of SG disassembly cells were first stressed with 125 µM SA (Sigma) for 1h, followed by the addition of each of the 3,078 Novartis Mode of Action library compounds at concentrations ranging from 0.01 – 100 µM. Negative control cells were treated with DMSO instead. Positive control cells were subject to two PBS washes, followed by the addition of fresh DMEM + 10% FBS. After 30 minutes of treatment cells were fixed in 4% paraformaldehyde (PFA) and imaged (see also Fig. 3c for a schematic representation).

Image acquisition and liquid-handling during the initial high-content screen and the follow-up experiment was performed on a IN Cell 6000 (GE Healthcare Life Sciences) laser-based confocal imaging platform. High-content screening image analysis was performed with CellProfiler. Feature selection and

IC50 calculations were performed by a custom-built multi-parametric data analysis (MPDA) workflow (details available upon request). Image rendering, data visualization and analysis was performed in Spotfire (Tibco).

Compounds capable of dissolving SGs or block their formation accounted for a total of 70 hits in both screening approaches. In a validation experiment the 70 hits were reassessed and their effect on eIF2 α -phosphorylation during SA treatment was measured. Of those 70 compounds, 24 compounds were validated and in addition were found to have no significant effect on eIF2 α -phosphorylation during SA treatment. Stress-induced eIF2 α -phosphorylation on Ser51 was assessed by immunofluorescence (1/200, cat. # 3398, Cell Signaling), preceded by 20 minutes of 4% PFA fixation. Of those 24 compounds 12 compounds were selected for follow-up experiments (Tab. 1) based on low IC50 scores.

Immunofluorescence & SG quantification

HeLa cells were seeded two days prior to fixation at a concentration of 40×10^3 cells/ml on standard glass coverslips (18mm, Biosystems). Cells were then washed in PBS and fixed in 4% paraformaldehyde (PFA)/PBS (Electron Microscopy Science) for 15 minutes, washed again and permeabilized in 1% Triton-X1000 (v/v)/PBS for 5 minutes at room temperature. Next, cells were PBS-washed three times for 5 minutes each time. Blocking was performed with 1% BSA/PBS (Sigma-Aldrich) for 15 minutes. Primary antibodies were diluted in blocking solution and a drop of 50 μ L was pipetted into a Petri dish. Coverslips were removed from wells, placed cell-side down onto the primary antibody solution, incubated for two hours at room temperature and placed back into the well. Coverslips were placed back into a 12-well plate and washing was performed three times 5 minutes each in 0.2% BSA/PBS. Secondary antibodies (Alexa fluorophores, Life Technologies), were diluted in blocking buffer, added onto the coverslip for 30 minutes and washed out three times with PBS for 5 minutes each time. Next, cells were DAPI stained (0.5 mg/L) and coverslips were mounted (ProLong Gold, Life Technologies) on glass slides and imaged.

Luciferase assays

Cell lines containing either Renilla luciferase reporters to assess cap- or uORF-dependent translation were seeded two days prior to the experiment at a concentration of 100×10^3 cells/ml in 12-well plates in DMEM + 10% FBS at incubated at 37°C and 5% CO₂. Cell were induced with doxycycline (1 μ g/ml) for 1.5h, followed by a PBS wash. Next, cells were treated for 1.5h with compound and 1 μ M

thapsigargin (Life Technologies). Used compound concentrations are indicated in Tab. 1. Cells were then washed in ice-cold PBS, lysed, and processed according to the manufacturer's protocol (Promega).

Viability assay

In a 96-well plate 5×10^3 cells/well were seeded one day prior to the experiment. Cells were then either treated with DMSO, 500 μ M thapsigargin (Life Technologies), compound only, or compound + 500 μ M thapsigargin for 48h. Staining was performed with CellEvent™ Caspase3/7 reagent (ThermoFisher Scientific) and Hoechst 33342 (ThermoFisher Scientific) shortly before analysis on a Nikon widefield microscope. Images were analyzed in FIJI (Schindelin et al., 2012) by utilizing the *Batch* → *Macro* function and the following script:

```
run("Subtract Background...", "rolling=10 stack");
run("Z Project...", "projection=[Max Intensity]");
setThreshold(0, 10000);
setOption("BlackBackground", false);
run("Convert to Mask");
run("Invert");
run("Analyze Particles...", "size=7-Infinity pixel show=Outlines display summarize");
```

Phosphoproteomics

3×10^6 HeLa cells were seeded on Day 0 per 15cm plate and treated on Day 1 with 10 μ M SB216763, 3 μ M CHIR99021 or DMSO for 16 hours over night. On Day 2 cells were either stressed with 1 μ M thapsigargin or treated with DMSO for 2h. The plates were then washed in ice-cold PBS, kept on ice at all times and cells were scraped off in PBS. The scraped cells were then lysed in lysis buffer (2% sodium deoxycholate (NaDOC), 10mM Tris, 50mM NaCl, 1% NP40), sonicated, heated for 5 minutes heated at 95°C, and the protein concentration was measured by Bradford assay. Next cysteines were alkylated with CSA and TCEP in HEPES pH8.5. Samples were then diluted 2-fold and Lys-C digested for 2h at room temperature. Next, Trypsin was then added at 1/300 of total protein per tube and samples were incubated over night at 37°C. On Day 3 samples were diluted 2-fold in HEPES pH8.5 and Trypsin was readded at 37°C for 3 hours. Sample preparation for mass spectrometry including acidification, phosphopeptide TiO₂ enrichment (Thermo Scientific) and mass spectrometry measurements were

performed according to standard protocols. Phosphopeptide changes were normalized to corresponding proteomic changes.

References

- Arimoto, K., Fukuda, H., Imajoh-Ohmi, S., Saito, H., and Takekawa, M. (2008). Formation of stress granules inhibits apoptosis by suppressing stress-responsive MAPK pathways. *Nat. Cell Biol.* *10*, 1324–1332.
- Chou, A., Krukowski, K., Jopson, T., Zhu, P.J., Costa-Mattioli, M., Walter, P., and Rosi, S. (2017). Inhibition of the integrated stress response reverses cognitive deficits after traumatic brain injury. *Proc. Natl. Acad. Sci.* 201707661.
- Dennis, M.D., McGhee, N.K., Jefferson, L.S., and Kimball, S.R. (2013). Regulated in DNA damage and development 1 (REDD1) promotes cell survival during serum deprivation by sustaining repression of signaling through the mechanistic target of rapamycin in complex 1 (mTORC1). *Cell. Signal.* *25*, 2709–2716.
- Guan, B.-J., Krokowski, D., Majumder, M., Schmotzer, C.L., Kimball, S.R., Merrick, W.C., Koromilas, A.E., and Hatzoglou, M. (2014). Translational Control during Endoplasmic Reticulum Stress beyond Phosphorylation of the Translation Initiation Factor eIF2 α . *J. Biol. Chem.* *289*, 12593–12611.
- Han, J., Back, S.H., Hur, J., Lin, Y.-H., Gildersleeve, R., Shan, J., Yuan, C.L., Krokowski, D., Wang, S., Hatzoglou, M., et al. (2013). ER-stress-induced transcriptional regulation increases protein synthesis leading to cell death. *Nat. Cell Biol.* *15*, 481–490.
- Kabir, Z.D., Che, A., Fischer, D.K., Rice, R.C., Rizzo, B.K., Byrne, M., Glass, M.J., De Marco Garcia, N.V., and Rajadhyaksha, A.M. (2017). Rescue of impaired sociability and anxiety-like behavior in adult *cacna1c*-deficient mice by pharmacologically targeting eIF2 α . *Mol. Psychiatry* *22*, 1096–1109.
- Kaehler, C., Isensee, J., Nonhoff, U., Terrey, M., Hucho, T., Lehrach, H., and Krobitsch, S. (2012). Ataxin-2-Like Is a Regulator of Stress Granules and Processing Bodies. *PLOS ONE* *7*, e50134.
- Kang, R., Zeh, H.J., Lotze, M.T., and Tang, D. (2011). The Beclin 1 network regulates autophagy and apoptosis. *Cell Death Differ.* *18*, 571–580.
- Kedersha, N., Panas, M.D., Achorn, C.A., Lyons, S., Tisdale, S., Hickman, T., Thomas, M., Lieberman, J., McInerney, G.M., Ivanov, P., et al. (2016). G3BP–Caprin1–USP10 complexes mediate stress granule condensation and associate with 40S subunits. *J Cell Biol* *212*, 845–860.
- Markowitz, D., Powell, C., Tran, N.L., Berens, M.E., Ryken, T.C., Vanan, M., Rosen, L., He, M., Sun, S., Symons, M., et al. (2016). Pharmacological Inhibition of the Protein Kinase MRK/ZAK Radiosensitizes Medulloblastoma. *Mol. Cancer Ther.* *15*, 1799–1808.
- Mokas, S., Mills, J.R., Garreau, C., Fournier, M.-J., Robert, F., Arya, P., Kaufman, R.J., Pelletier, J., and Mazroui, R. (2009). Uncoupling stress granule assembly and translation initiation inhibition. *Mol. Biol. Cell* *20*, 2673–2683.
- Novoa, I., Zhang, Y., Zeng, H., Jungreis, R., Harding, H.P., and Ron, D. (2003). Stress-induced gene expression requires programmed recovery from translational repression. *EMBO J.* *22*, 1180–1187.
- Placzek, A.N., Prisco, G.V.D., Khatiwada, S., Sgritta, M., Huang, W., Krnjević, K., Kaufman, R.J., Dani, J.A., Walter, P., and Costa-Mattioli, M. (2016). eIF2 α -mediated translational control regulates the persistence of cocaine-induced LTP in midbrain dopamine neurons. *ELife* *5*, e17517.
- Schindelin, J., Arganda-Carreras, I., Frise, E., Kaynig, V., Longair, M., Pietzsch, T., Preibisch, S., Rueden, C., Saalfeld, S., Schmid, B., et al. (2012). Fiji: an open-source platform for biological-image analysis. *Nat. Methods* *9*, 676–682.

Sekine, Y., Zyryanova, A., Crespillo-Casado, A., Fischer, P.M., Harding, H.P., and Ron, D. (2015). Stress responses. Mutations in a translation initiation factor identify the target of a memory-enhancing compound. *Science* 348, 1027–1030.

Sidrauski, C., Acosta-Alvear, D., Khoutorsky, A., Vedantham, P., Hearn, B.R., Li, H., Gamache, K., Gallagher, C.M., Ang, K.K.-H., Wilson, C., et al. (2013). Pharmacological brake-release of mRNA translation enhances cognitive memory. *ELife* 2, e00498.

Sidrauski, C., McGeachy, A.M., Ingolia, N.T., and Walter, P. (2015). The small molecule ISRIB reverses the effects of eIF2 α phosphorylation on translation and stress granule assembly. *ELife* 4, e05033.

Vin, H., Ojeda, S.S., Ching, G., Leung, M.L., Chitsazzadeh, V., Dwyer, D.W., Adelman, C.H., Restrepo, M., Richards, K.N., Stewart, L.R., et al. (2013). BRAF inhibitors suppress apoptosis through off-target inhibition of JNK signaling. *ELife* 2, e00969.

Wortel, I.M.N., Meer, L.T. van der, Kilberg, M.S., and Leeuwen, F.N. van (2017). Surviving Stress: Modulation of ATF4-Mediated Stress Responses in Normal and Malignant Cells. *Trends Endocrinol. Metab.* 28, 794–806.

Zhang, F., Phiel, C.J., Spece, L., Gurvich, N., and Klein, P.S. (2003). Inhibitory Phosphorylation of Glycogen Synthase Kinase-3 (GSK-3) in Response to Lithium EVIDENCE FOR AUTOREGULATION OF GSK-3. *J. Biol. Chem.* 278, 33067–33077.

Chapter 4: mRNAs are translationally repressed inside of processing bodies during stress relief

Halstead JM^{1,*}, Lionnet T^{2,*}, Wilbertz JH^{1,3,*}, Wippich F^{4*}, Ephrussi A⁴, Singer RH⁵, Chao JA¹

* shared first author

¹ Friedrich Miescher Institute for Biomedical Research, Basel, Switzerland

² Transcription Imaging Consortium, HHMI Janelia Research Campus, Ashburn, VA, USA

³ University of Basel, Basel, Switzerland

⁴ European Molecular Biology Laboratory, Heidelberg, Germany

⁵ Department of Anatomy and Structural Biology, Albert Einstein College of Medicine, Bronx, NY, USA.

Gruss-Lipper Biophotonics Center, Albert Einstein College of Medicine, Bronx, NY, USA. Transcription Imaging Consortium, Howard Hughes Medical Institute Janelia Farm Research Campus, Ashburn, VA, USA

Published in **Science**, 2015; 347(6228):1367-671

The chapter describes the development and experimental application of an RNA-based biosensor to study the first round of translation of a single mRNA molecule inside of living cells (TRICK reporter) in different biological contexts. Relevant for this thesis is the result that it is possible to study translation on the single molecule level in different cell types and that mRNAs specifically localize to processing bodies (PBs) during the cellular stress response. The mRNAs remain translationally repressed inside of PBs, even if translation in the surrounding cytoplasm reinitiates during stress relief. This work serves as a specific example for RNA-protein granule-modulated sub-cellular translation regulation.

4. G. R. Tanner, A. Lutas, J. R. Martinez-Francois, G. Yellen, *J. Neurosci.* **31**, 8689–8696 (2011).
5. A. Giménez-Cassina et al., *Neuron* **74**, 719–730 (2012).
6. N. Juge et al., *Neuron* **68**, 99–112 (2010).
7. S. A. Masino et al., *J. Clin. Invest.* **121**, 2679–2683 (2011).
8. A. Lutas, G. Yellen, *Trends Neurosci.* **36**, 32–40 (2013).
9. B. S. Meldrum, M. A. Rogawski, *Neurotherapeutics* **4**, 18–61 (2007).
10. K. J. Bough et al., *Ann. Neurol.* **60**, 223–235 (2006).
11. Materials and methods are available as supplementary materials on Science Online.
12. D. Dybdal, K. Gale, *J. Neurosci.* **20**, 6728–6733 (2000).
13. M. J. Iadarola, K. Gale, *Science* **218**, 1237–1240 (1982).
14. I. A. Silver, M. Erecińska, *J. Neurosci.* **14**, 5068–5076 (1994).
15. Z. Song, B. E. Levin, J. J. McArdle, N. Bakhos, V. H. Routh, *Diabetes* **50**, 2673–2681 (2001).
16. M. O. Cunningham et al., *Proc. Natl. Acad. Sci. U.S.A.* **103**, 5597–5601 (2006).
17. M. Bélanger, I. Allaman, P. J. Magistretti, *Cell Metab.* **14**, 724–738 (2011).
18. N. Rouach, A. Koulakoff, V. Abudara, K. Willecke, C. Giaume, *Science* **322**, 1551–1555 (2008).
19. M. P. Parsons, M. Hirasawa, *J. Neurosci.* **30**, 8061–8070 (2010).
20. A. Suzuki et al., *Cell* **144**, 810–823 (2011).
21. H. Shimizu et al., *Neuron* **54**, 59–72 (2007).
22. T. K. Lam, R. Gutierrez-Juarez, A. Pocai, L. Rossetti, *Science* **309**, 943–947 (2005).
23. R. D'Ambrosio, J. Wenzel, P. A. Schwartzkroin, G. M. McKhann 2nd, D. Janigro, *J. Neurosci.* **18**, 4425–4438 (1998).
24. V. Riban et al., *Neuroscience* **112**, 101–111 (2002).
25. R. Samala, J. Klein, K. Borges, *Neurochem. Int.* **58**, 5–8 (2011).
26. C. Chiron et al., *Lancet* **356**, 1638–1642 (2000).
27. R. H. Carballo et al., *Epilepsia* **46**, 1539–1544 (2005).
28. L. M. Deck et al., *J. Med. Chem.* **41**, 3879–3887 (1998).
29. C. Granchi et al., *J. Med. Chem.* **54**, 1599–1612 (2011).
30. M. K. Trojnar, K. Wojtal, M. P. Trojnar, S. J. Czuczwar, *Pharmacol. Rep.* **57**, 154–160 (2005).
31. P. P. Quilichini, C. Chiron, Y. Ben-Ari, H. Gozlan, *Epilepsia* **47**, 704–716 (2006).

ACKNOWLEDGMENTS

We thank K. Imoto for comments on this manuscript, D. Kase for technical advice on in vivo recordings at the initial stage, and

A. Wakasa and K. Urakawa for their technical support on the intrahippocampal kainate model. N.S., S.L., T.O., and T.I. are inventors on a patent (World Intellectual Property Organization WO2014/115764) related to clinical use of stiripentol as LDH inhibitors, and N.S. and T.I. are also inventors on a patent (Japan JP2015-023572) related to isosafrole as antiepileptic compounds. These patent applications have been filed by Okayama University. All data described in the paper are presented in this report and supplementary materials. This work was supported by grants from the Japan Society for the Promotion of Science (24590114) and by research grants from Takeda Science Foundation and Ryobi-Teien Memory Foundation.

SUPPLEMENTARY MATERIALS

www.sciencemag.org/content/347/6228/1362/suppl/DC1
Materials and Methods
Supplementary Text
Figs. S1 to S26
References (32–59)

21 October 2014; accepted 9 February 2015
10.1126/science.aaa1299

TRANSLATION

An RNA biosensor for imaging the first round of translation from single cells to living animals

James M. Halstead,^{1*} Timothée Lionnet,^{2,3,4*} Johannes H. Wilbertz,^{1,5*} Frank Wippich,^{6*} Anne Ephrussi,^{6†} Robert H. Singer,^{2,3,4†} Jeffrey A. Chao^{1,2‡}

Analysis of single molecules in living cells has provided quantitative insights into the kinetics of fundamental biological processes; however, the dynamics of messenger RNA (mRNA) translation have yet to be addressed. We have developed a fluorescence microscopy technique that reports on the first translation events of individual mRNA molecules. This allowed us to examine the spatiotemporal regulation of translation during normal growth and stress and during *Drosophila* oocyte development. We have shown that mRNAs are not translated in the nucleus but translate within minutes after export, that sequestration within P-bodies regulates translation, and that *oskar* mRNA is not translated until it reaches the posterior pole of the oocyte. This methodology provides a framework for studying initiation of protein synthesis on single mRNAs in living cells.

During translation, mRNAs are bound by the ribosome. Measurements of ribosome occupancy of mRNAs and protein abundance provide a genome-wide view of translation regulation (1, 2). Fluorescence microscopy complements these global approaches because it allows analysis of gene expression with single-molecule resolution in living cells and provides mechanistic insights obscured by ensemble mea-

surements (3, 4). Imaging methods have been developed that allow newly synthesized proteins to be discerned from the preexisting population or enable actively translating ribosomes to be identified within the cell; however, these approaches are limited by low signal-to-noise ratio and lack the resolution to correlate these events with specific mRNA molecules (5). Here, we describe a single-molecule assay that allows untranslated mRNAs to be distinguished unequivocally from previously translated ones and provides a foundation for investigating the spatiotemporal regulation of translation in living cells.

Because the ribosome or its associated factors must displace endogenous RNA-binding proteins during the first round of translation, we reasoned that it would be possible to construct an RNA biosensor whose fluorescent signal would depend on this process. The orthogonal bacteriophage PP7 and MS2 stem-loops were used to label a transcript within both the coding sequence (PP7) and

the 3' untranslated region (UTR) (MS2) with spectrally distinct fluorescent proteins (6). Simultaneous expression of the PP7 coat protein fused to a nuclear localization sequence (NLS) and green fluorescent protein (NLS-PCP-GFP) and the MS2 coat protein fused to an NLS and red fluorescent protein (NLS-MCP-RFP) resulted in nuclear transcripts labeled with both fluorescent proteins (Fig. 1A). Upon export of the reporter mRNA, the first round of translation displaces NLS-PCP-GFP from the transcript, as the ribosome traverses the coding region that contains the PP7 stem-loops. The NLS limits the concentration of free NLS-PCP-GFP in the cytoplasm, yielding translated mRNAs that are labeled with only NLS-MCP-RFP bound to the stem-loops in the 3' UTR (Fig. 1, A and B). We refer to this technique as translating RNA imaging by coat protein knock-off (TRICK).

Efficient translation of a 6xPP7 stem-loop cassette required optimization of the distance between adjacent stem-loops, stem-loop folding, and codon usage so that they would not block or stall elongation of the ribosome, which might elicit decay of the transcript (7) (Fig. 1C). The polypeptide encoded by the PP7 stem-loops has a molecular mass of ~14 kD and is not homologous to any known protein. Binding of NLS-MCP-RFP to the 3' UTR had no effect on translation, and binding of NLS-PCP-GFP to the PP7 stem-loop cassette in the coding region also did not result in reduced translation of the reporter mRNA (Fig. 1C and fig. S1). Similarly, binding of the fluorescent proteins to the reporter mRNA also did not alter the stability of the transcript (fig. S2).

The TRICK reporter mRNA was expressed in a U-2 OS human osteosarcoma cell line stably expressing NLS-PCP-GFP and NLS-MCP-RFP. Fluorescence-activated cell sorting isolated cells with small amounts of both fluorescent proteins, allowing detection of all reporter mRNAs (figs. S3 and S4). The cells were imaged on a fluorescence microscope equipped with two registered cameras, allowing simultaneous visualization of single mRNA molecules in both channels. In the nucleus, single mRNAs were fluorescently labeled with both red

¹Friedrich Miescher Institute for Biomedical Research, CH-4058 Basel, Switzerland. ²Department of Anatomy and Structural Biology, Albert Einstein College of Medicine, Bronx, NY 10461, USA. ³Gruss-Lipper Biophotonics Center, Albert Einstein College of Medicine, Bronx, NY 10461, USA. ⁴Transcription Imaging Consortium, Howard Hughes Medical Institute Janelia Farm Research Campus, Ashburn, VA 20147, USA. ⁵University of Basel, CH-4003 Basel, Switzerland. ⁶Developmental Biology Unit, European Molecular Biology Laboratory, 69117 Heidelberg, Germany. *These authors contributed equally to this work. †Corresponding author. E-mail: ephrussi@embl.de (A.E.); robert.singer@einstein.yu.edu (R.H.S.); jeffrey.chao@fmi.ch (J.A.C.)

and green proteins and thus appeared yellow (Fig. 1D). In contrast, almost all of the mRNAs appeared as red particles in the cytoplasm, indicating that only NLS-MCP-RFP was bound (Fig. 1, D and E). Quantification of the steady-state number of yellow mRNAs in the cytoplasm revealed that ~94% of TRICK reporter mRNAs had been translated at least once (Fig. 1, E and H). To confirm that loss of NLS-PCP-GFP from cytoplasmic transcripts was translation-dependent, we induced transcription of the TRICK reporter by ponasterone A (ponA) in the presence of translational inhibitors (8). Adding either cycloheximide, which inhibits elongation, or puromycin, which causes premature termination, for 30 min before induction of TRICK reporter mRNA expression resulted in an increase in the number of untranslated mRNAs in the cytoplasm (Fig. 1, F to H, and movies S1 to S3). Consistent with the imaging, polysome analysis indicated that NLS-PCP-GFP was absent from actively translating mRNAs, whereas NLS-MCP-RFP could be detected within polysomes (fig. S5). This demonstrated that translation of the PP7 stem-loops by the ribosome was required for displacement of the green signal from the mRNA.

Although translation is thought to occur exclusively in the cytoplasm, recent studies suggest that protein synthesis can occur in the nucleus (9, 10). Because the TRICK assay can distinguish between untranslated and translated mRNAs, we imaged TRICK reporter mRNAs in the nucleus 30 min after ponA induction. Single-particle tracking (SPT) of nuclear mRNAs determined that they undergo both corralled ($D = 0.02 \mu\text{m}^2 \text{s}^{-1}$) and random diffusion ($D = 0.09 \mu\text{m}^2 \text{s}^{-1}$), similar to the movements observed for other nuclear mRNAs (11, 12). We found $91.3 \pm 0.9\%$ of mRNAs labeled with both colors, which is not significantly different from the fraction of double-labeled mRNAs in the cytoplasm of cells treated with translational inhibitors ($P = 0.75$, unpaired t test) (fig. S6, A and B, and movie S4). We cannot, however, exclude the possibility that the fusion protein rebound the PP7 stem-loops immediately after translation. If translation were occurring in the nucleus, addition of small amounts of cycloheximide would increase polysome formation, causing occlusion of the PP7 stem-loops and thereby preventing NLS-PCP-GFP from rebinding (13) (fig. S7A). Similar to experiments in the absence of cycloheximide, $90.7 \pm 0.6\%$ of nuclear mRNAs were labeled with

both colors when cells were treated with $1 \mu\text{g ml}^{-1}$ cycloheximide ($P = 0.44$, unpaired t test) (fig. S7, B and C, and movie S5). Although it is possible that nuclear translation could occur for specific mRNAs, this was not observed for the TRICK reporter. These findings are consistent with the previous observation that mRNAs containing premature stop codons are exported before undergoing decay in the cytoplasm (14).

The rapid diffusion of mRNAs in the cytoplasm and photobleaching prevented us from imaging a single mRNA from the time it entered the cytoplasm until it was translated (figs. S8 and S9). Untranslated mRNAs, however, could be detected after export from the nucleus and were observed throughout the cytoplasm (fig. S8). To verify these live-cell observations, we measured the spatial distribution of untranslated reporter mRNAs in fixed cells, using a combined immunofluorescence-fluorescence in situ hybridization (IF-FISH) approach. FISH probes targeted to the MS2 stem-loops allowed detection of all reporter mRNAs, whereas a GFP nanobody was used to identify the untranslated ones (fig. S10, A and B). In agreement with live-cell results, we observed a large percentage of cytoplasmic translated mRNAs (93.7%). As mRNAs

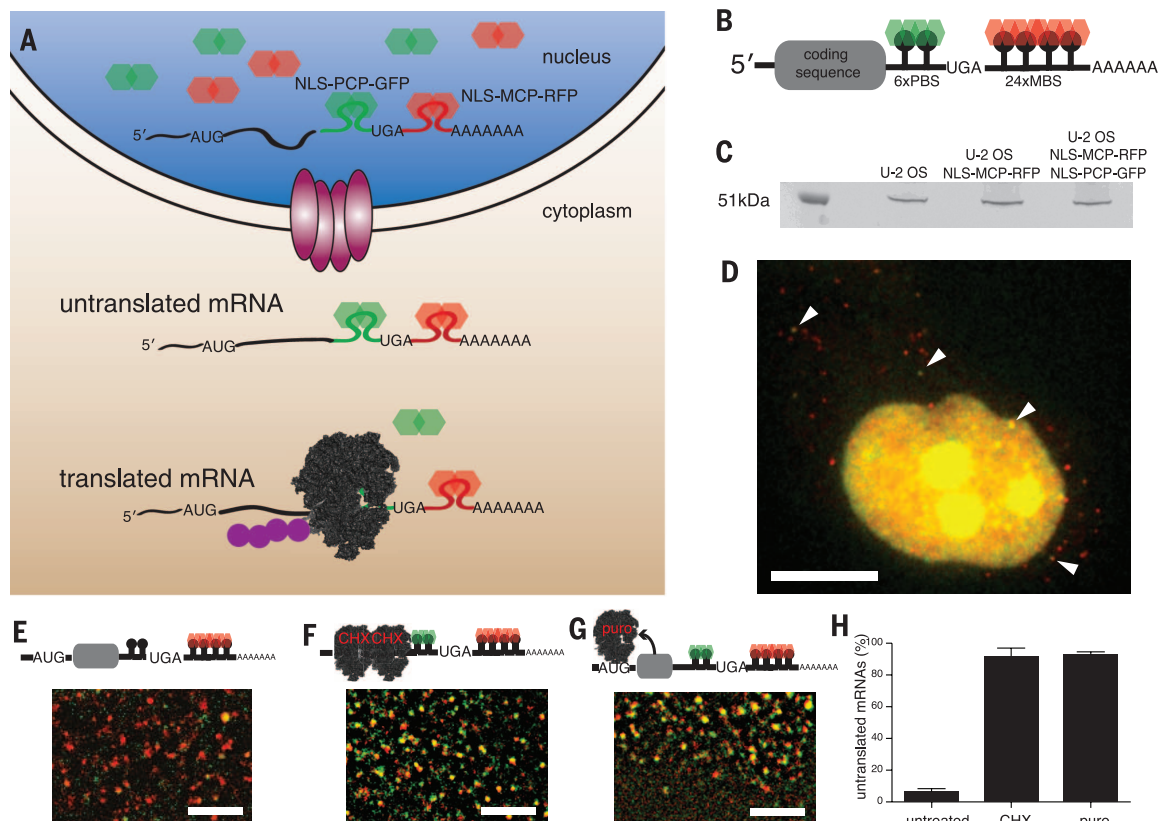


Fig. 1. Imaging translation of mRNAs in living cells. (A) Schematic of TRICK assay. (B) Schematic of TRICK reporter transcript. 6xPP7 stem-loops (PBS) inserted in-frame with the C terminus of a protein-coding sequence and 24xMS2 stem-loops (MBS) in the 3' UTR. (C) Expression of TRICK reporter mRNA in U-2 OS cells. The protein encoded by the TRICK reporter (51.4 kDa) is translated in U-2 OS cells, and expression is not affected by NLS-MCP-RFP and NLS-PCP-GFP. (D) U-2 OS cell expressing TRICK reporter. Arrows indicate untranslated nuclear mRNA and three untranslated mRNAs

detected in the cytoplasm. Scale bar, 10 μm . (E) Cytoplasmic region of untreated U-2 OS cells. (F) Addition of cycloheximide ($100 \mu\text{g ml}^{-1}$) and (G) addition of puromycin ($100 \mu\text{g ml}^{-1}$) during ponA induction of TRICK reporter mRNAs. Scale bar (E to G), 2 μm . (H) Percentage of untranslated TRICK mRNAs in U-2 OS cells. In untreated cells, $5.8 \pm 1.4\%$ of mRNAs colocalize with both NLS-PCP-GFP and NLS-MCP-RFP compared to $91.0 \pm 3.0\%$ for cycloheximide-treated and $92.6 \pm 1.0\%$ for puromycin-treated cells. $n = 5$ cells for each condition.

diffuse away from the nucleus, their chances to collide with the 43S preinitiation complex and become translated increase over time. Indeed, we observed that the fraction of untranslated mRNAs decreased gradually as the distance from the nucleus increased (fig. S10C). Spatial profiles of untranslated mRNAs demonstrated that some mRNAs diffused micrometers away from the nucleus before undergoing translation, indicating that translation does not occur immediately upon export, but occurs minutes after the mRNA has entered the cytoplasm (the time before an mRNA translates should scale as L^2/D , where $L \sim 5 \mu\text{m}$ is the radial extent of the untranslated mRNA profile and $D = 0.02$ to $0.13 \mu\text{m}^2 \text{s}^{-1}$ is the range of diffusion coefficients; fig. S9). Furthermore, we find no evidence for enrichment or depletion at specific cytosolic locations, suggesting that translation can occur homogeneously throughout the cytoplasm.

We next investigated how stress conditions affect translation. Upon a variety of cellular stresses, signaling pathways inhibit translation through phosphorylation of eukaryotic translation initiation factor 2 α (eIF2 α), resulting in disassembly of polysomes and formation of cytoplasmic stress granules and processing bodies (P-bodies), cyto-

plasmic organelles whose role in RNA metabolism is not well understood (15, 16). The mRNAs and proteins that constitute these organelles are dynamic and rapidly exchange with the cytosol (17, 18). However, mRNAs containing 5' terminal oligopyrimidine (TOP) motifs accumulate in stress granules upon amino acid starvation, suggesting that certain mRNA classes may be differentially regulated within these compartments (19). To characterize the spatiotemporal regulation of 5' TOP mRNA translation during stress, a tetracycline-inducible HeLa cell line expressing a 5' TOP TRICK reporter mRNA with green (NLS-PCP-GFP) and red (NLS-MCP-Halo; JF₅₄₉) fluorescent proteins required for single-molecule RNA imaging were stressed with arsenite. 5' TOP TRICK mRNAs were detected as single molecules distributed throughout the cytosol or located within stress granules and P-bodies. Only mRNAs sequestered within P-bodies formed large clusters. This association with P-bodies was specific for the 5' TOP TRICK mRNAs because a reporter that lacked the 5' TOP motif did not form multimeric assemblies within these cytoplasmic foci (Fig. 2, A to C).

To address the translational regulation of cytosolic mRNAs and those clustered in P-bodies,

we induced transcription of the 5' TOP TRICK reporter mRNA for a short period before addition of arsenite. This resulted in an increase in the number of untranslated mRNAs in the cytoplasm to be detected compared to unstressed cells, consistent with an inhibition of eIF2.GTP.Met-tRNA^{Met} formation (Fig. 2, D and F). The untranslated 5' TOP TRICK reporter mRNAs in the cytoplasm were detected as either single mobile mRNAs or static clusters within P-bodies. Photobleaching of the clustered mRNAs indicated that they were stably associated with P-bodies (fig. S11). Upon removal of arsenite, 5' TOP TRICK mRNAs in the cytosol underwent translation; however, the clustered transcripts retained in P-bodies remained untranslated, indicating that these cellular structures can provide a distinct level of regulation (Fig. 2, E and F, and movies S6 to S7).

Messenger ribonucleoprotein (mRNP) granules form not only during cellular stress, but also as part of normal regulatory pathways. In *Drosophila*, localized expression of Oskar protein at the posterior pole of the oocyte is essential for correct body patterning and germ cell formation (20). Precise spatiotemporal translational regulation is crucial during long-range transport of *oskar* mRNA (*osk*) from the nurse cells, where the mRNA

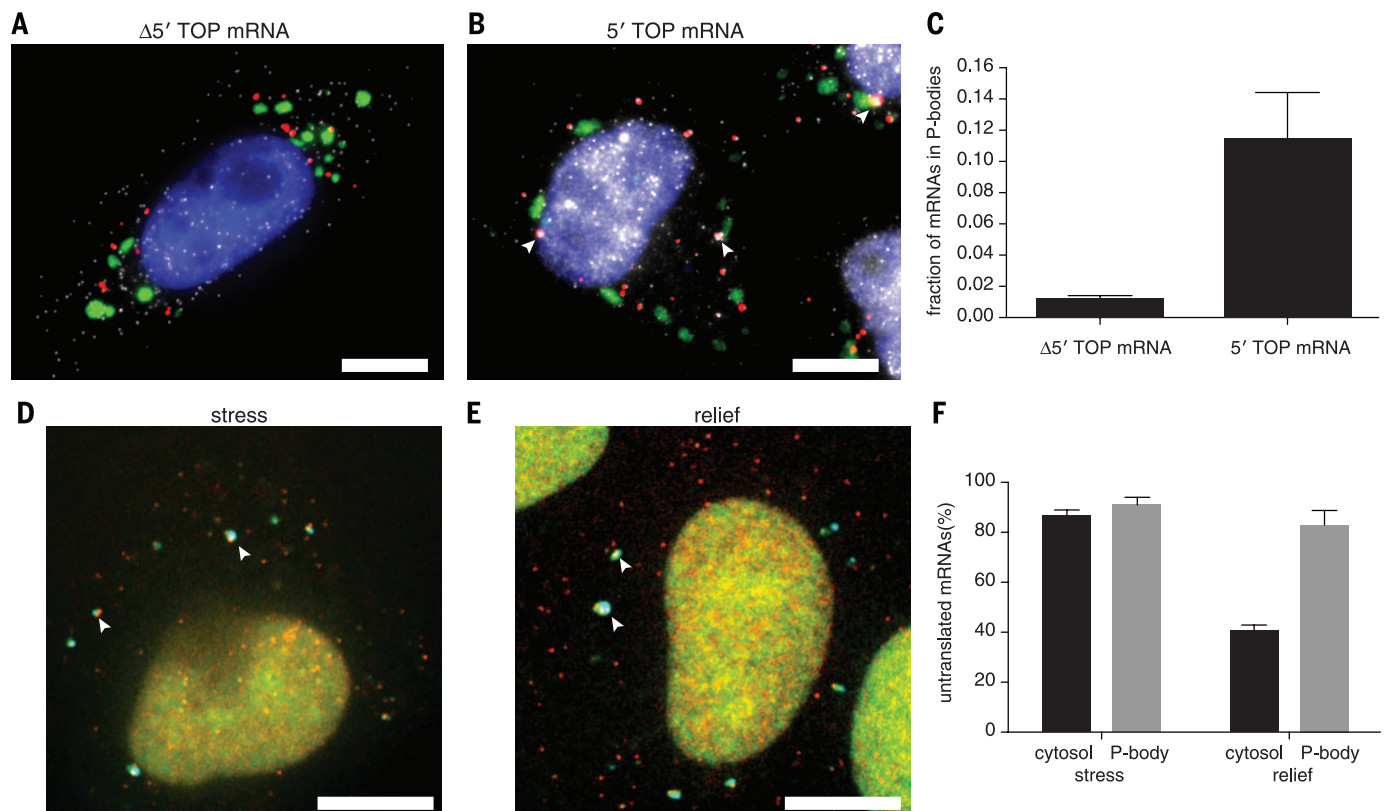


Fig. 2. P-bodies are sites of translation regulation during stress in HeLa cells. (A and B) IF-FISH of cells expressing $\Delta 5'$ TOP TRICK reporter mRNA [(A), gray] or 5' TOP TRICK reporter mRNA [(B), gray] during arsenite stress (0.5 mM) contain stress granules (TIAR, green) and P-bodies (DDX6, red). Arrows: mRNA clusters in P-bodies. (C) Fraction of cytoplasmic $\Delta 5'$ TOP ($n = 19$ cells) and 5' TOP ($n = 17$ cells) mRNAs located within P-bodies after 60 min of arsenite (0.5 mM) stress ($P = 0.0009$, unpaired t test). (D and E) Live-cell image of 5' TOP TRICK reporter mRNA during arsenite stress (D) and relief of

stress (E). In stressed cells, mRNAs (red, green) in cytosol and P-bodies (cyan) are untranslated. In relieved cells, many mRNAs (red, green) in cytosol have been translated whereas mRNAs retained in P-bodies (cyan) remain untranslated. Arrow: clustered mRNAs. Scale bar (A, B, D, E), 10 μm . (F) Percentage of untranslated mRNAs (cytosol and P-bodies) during stress ($n = 9$ cells) and relief of stress ($n = 10$ cells). Upon relief of stress, 5' TOP mRNAs in P-bodies are not translated ($P = 0.31$, unpaired t test); mRNAs in the cytosol have undergone translation ($P < 0.0001$, unpaired t test).

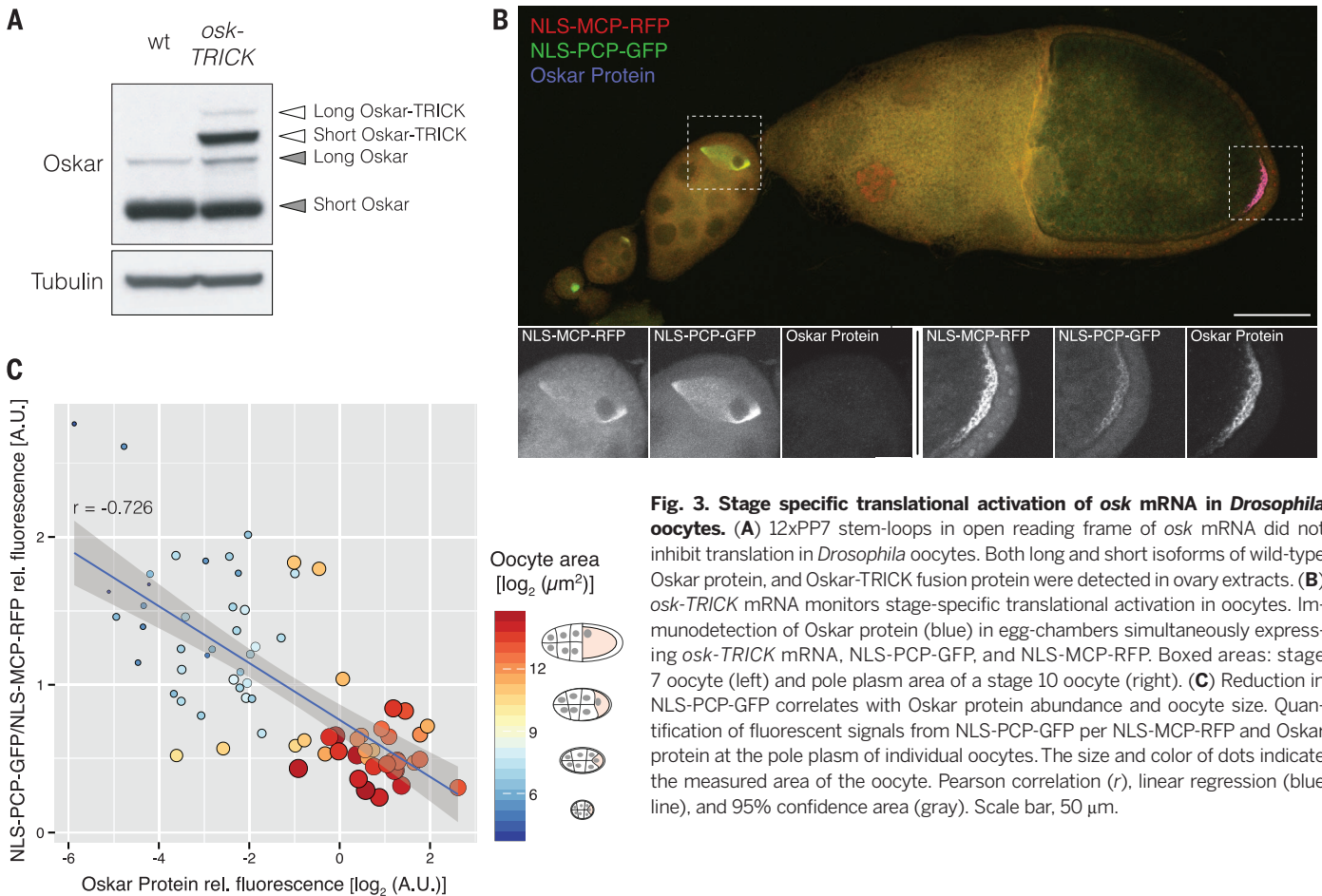


Fig. 3. Stage specific translational activation of *osk* mRNA in *Drosophila* oocytes. (A) 12xPP7 stem-loops in open reading frame of *osk* mRNA did not inhibit translation in *Drosophila* oocytes. Both long and short isoforms of wild-type Oskar protein, and Oskar-TRICK fusion protein were detected in ovary extracts. (B) *osk-TRICK* mRNA monitors stage-specific translational activation in oocytes. Immunodetection of Oskar protein (blue) in egg-chambers simultaneously expressing *osk-TRICK* mRNA, NLS-PCP-GFP, and NLS-MCP-RFP. Boxed areas: stage 7 oocyte (left) and pole plasm area of a stage 10 oocyte (right). (C) Reduction in NLS-PCP-GFP correlates with Oskar protein abundance and oocyte size. Quantification of fluorescent signals from NLS-PCP-GFP per NLS-MCP-RFP and Oskar protein at the pole plasm of individual oocytes. The size and color of dots indicate the measured area of the oocyte. Pearson correlation (r), linear regression (blue line), and 95% confidence area (gray). Scale bar, 50 μm .

is transcribed, to the posterior pole of the oocyte, where Oskar protein first appears during mid-oogenesis (stage 9) (21, 22). Additional mechanisms ensure degradation of ectopically expressed Oskar protein; hence, absence of the protein does not indicate lack of translation of its mRNA (23).

To monitor translation, we generated an *osk-TRICK* reporter mRNA by placing 12xPP7 stem-loops within the coding region of a construct that contained 6xMS2 stem-loops in the 3' UTR (fig. S12) (24). Introducing 12xPP7 stem-loops into the open reading frame of *osk* mRNA did not inhibit translation of the reporter transcript, and the fusion protein was expressed at levels comparable to that of the wild-type protein (Fig. 3A). In early-stage oocytes of flies coexpressing *osk-TRICK* mRNA, NLS-MCP-RFP, and NLS-PCP-GFP, *osk-TRICK* mRNA was labeled by both NLS-PCP-GFP and NLS-MCP-RFP, indicating translational repression consistent with the absence of Oskar protein (Fig. 3B). In later stages, the NLS-PCP-GFP fluorescent signal was reduced at the posterior pole and Oskar protein was detected by immunofluorescence, consistent with translation of a portion of the transcripts (Fig. 3, B and C). This methodology provides a framework for analyzing the cascade of regulatory mechanisms required for local translation during *Drosophila* development. It will also be informative in neurons where regulation of the first round of translation has been

shown to be important for local protein synthesis in axons and dendrites (25, 26).

This methodology pinpoints the precise time and place of the first translation event of single mRNA molecules. It reveals the translation control of mRNAs sequestered within cytoplasmic organelles or when and where the translation of a key cell fate determinant occurs in an organism undergoing development. The kinetics of translational regulation can now be coupled with single-molecule imaging of proteins to provide insights into mechanisms of regulation that were previously unapproachable by ensemble biochemical or genetic approaches (27). Observing regulation of mRNA translation in single living cells will lead to a better understanding of disease mechanisms.

REFERENCES AND NOTES

- N. T. Ingolia, S. Ghaemmaghami, J. R. Newman, J. S. Weissman, *Science* **324**, 218–223 (2009).
- B. Schwahnhauser *et al.*, *Nature* **473**, 337–342 (2011).
- D. R. Larson, D. Zenklusen, B. Wu, J. A. Chao, R. H. Singer, *Science* **332**, 475–478 (2011).
- A. Raj, A. van Oudenaarden, *Annu. Rev. Biophys.* **38**, 255–270 (2009).
- J. A. Chao, Y. J. Yoon, R. H. Singer, *Cold Spring Harb. Perspect. Biol.* **4**, a012310 (2012).
- S. Hocine, P. Raymond, D. Zenklusen, J. A. Chao, R. H. Singer, *Nat. Methods* **10**, 119–121 (2013).
- M. K. Doma, R. Parker, *Nature* **440**, 561–564 (2006).
- D. No, T. P. Yao, R. M. Evans, *Proc. Natl. Acad. Sci. U.S.A.* **93**, 3346–3351 (1996).
- K. Al-Jubran *et al.*, *RNA* **19**, 1669–1683 (2013).

- A. David *et al.*, *J. Cell Biol.* **197**, 45–57 (2012).
- Y. Shav-Tal *et al.*, *Science* **304**, 1797–1800 (2004).
- A. Mor *et al.*, *Nat. Cell Biol.* **12**, 543–552 (2010).
- C. P. Stanners, *Biochem. Biophys. Res. Commun.* **24**, 758–764 (1966).
- T. Trcek, H. Sato, R. H. Singer, L. E. Maquat, *Genes Dev.* **27**, 541–551 (2013).
- J. R. Buchan, R. Parker, *Mol. Cell* **36**, 932–941 (2009).
- N. Kedersha, P. Ivanov, P. Anderson, *Trends Biochem. Sci.* **38**, 494–506 (2013).
- N. Kedersha *et al.*, *J. Cell Biol.* **169**, 871–884 (2005).
- S. Mollet *et al.*, *Mol. Biol. Cell* **19**, 4469–4479 (2008).
- C. K. Damgaard, J. Lykke-Andersen, *Genes Dev.* **25**, 2057–2068 (2011).
- A. Ephrussi, R. Lehmann, *Nature* **358**, 387–392 (1992).
- J. Kim-Ha, K. Kerr, P. M. Macdonald, *Cell* **81**, 403–412 (1995).
- F. H. Markussen, A. M. Michon, W. Breitwieser, A. Ephrussi, *Development* **121**, 3723–3732 (1995).
- E. Morais-de-Sá, A. Vega-Rioja, V. Trovisco, D. St Johnston, *Dev. Cell* **26**, 303–314 (2013).
- M. D. Lin *et al.*, *Dev. Biol.* **322**, 276–288 (2008).
- D. Colak, S. J. Ji, B. T. Porse, S. R. Jaffrey, *Cell* **153**, 1252–1265 (2013).
- C. Giorgi *et al.*, *Cell* **130**, 179–191 (2007).
- M. E. Tanenbaum, L. A. Gilbert, L. S. Qi, J. S. Weissman, R. D. Vale, *Cell* **159**, 635–646 (2014).

ACKNOWLEDGMENTS

This work supported by the Novartis Research Foundation (J.A.C.); NIH grants NS83085, EB013571, and GM57071 (R.H.S.); Howard Hughes Medical Institute (R.H.S. and T.L.); European Molecular Biology Laboratory (EMBL) (A.E.); and a postdoctoral fellowship from the EMBL Interdisciplinary Postdoc Program (EIPOD) under Marie Curie COFUND actions (F.W.). We thank C. Damgaard (University of Aarhus) for providing the rpl32-

β -globin plasmid; S. Shenoy (Albert Einstein College of Medicine), L. Gelman and S. Bource (Friedrich Miescher Institute), and EMBL Advanced Light Microscopy Facility for microscopy support; D. Cieplewski (Nikon) for providing access to NIS tracking software; C. Eliscovich (Albert Einstein College of Medicine) for advice on IF-FISH; L. Lavis (Janelia Farm) for providing JF₅₄₉ dye; M. Beal (Biosearch Technologies) for Stellaris FISH probes;

A. Arnold (FMI) for assistance with polysome analysis; I. Gáspár (EMBL) for pHsp83 vector; and S. Chao, U. Meier, and J. Warner for helpful discussions.

SUPPLEMENTARY MATERIALS

www.sciencemag.org/content/347/6228/1367/suppl/DC1
Materials and Methods

Figs. S1 to S12
Movies S1 to S7
References (28–37)

20 November 2014; accepted 6 February 2015
10.1126/science.aaa3380

RNA BIOCHEMISTRY

Determination of in vivo target search kinetics of regulatory noncoding RNA

Jingyi Fei,¹ Digvijay Singh,² Qiucen Zhang,¹ Seongjin Park,¹ Divya Balasubramanian,³ Ido Golding,^{1,4} Carin K. Vanderpool,^{3*} Taekjip Ha^{1,2,5,6*}

Base-pairing interactions between nucleic acids mediate target recognition in many biological processes. We developed a super-resolution imaging and modeling platform that enabled the in vivo determination of base pairing–mediated target recognition kinetics. We examined a stress-induced bacterial small RNA, SgrS, which induces the degradation of target messenger RNAs (mRNAs). SgrS binds to a primary target mRNA in a reversible and dynamic fashion, and formation of SgrS-mRNA complexes is rate-limiting, dictating the overall regulation efficiency in vivo. Examination of a secondary target indicated that differences in the target search kinetics contribute to setting the regulation priority among different target mRNAs. This super-resolution imaging and analysis approach provides a conceptual framework that can be generalized to other small RNA systems and other target search processes.

Base-pairing interactions between nucleic acids constitute a large category of target recognition processes such as noncoding RNA-based gene regulation [e.g., microRNAs (1) and long noncoding RNAs (2) in eukaryotes and small RNAs (sRNAs) in bacteria (3)], bacterial adaptive immunity [e.g., the clustered regularly interspaced short palindromic repeat (CRISPR) system (4)], and homologous recombination (5). Although target search kinetics by transcription factors has been studied in vivo (6), the rate constants for target identification via base-pairing interactions in vivo are not known for any system. Here, we developed a super-resolution imaging and analysis platform to assess the kinetics of base-pairing interaction-mediated target recognition for a bacterial sRNA, SgrS. SgrS is produced upon sugar-phosphate stress, and its function is dependent on an RNA chaperone protein Hfq. SgrS regulates several target mRNAs posttranscriptionally through base-pairing interactions that affect mRNA translation and stability (7). We combined single-molecule fluorescence in situ hybridization (smFISH) (8) with single-molecule localization-based super-resolution microscopy (9) to count RNAs and obtain infor-

mation on subcellular localization. High spatial resolution is required for accurate quantification of the high-copy-number RNAs and sRNA-mRNA complexes. Here, simultaneous measurements of sRNA, mRNA, and sRNA-mRNA complexes together with mathematical modeling allow determination of key parameters describing sRNA target search and downstream codegradation of sRNA-mRNA complexes.

We first studied the kinetic properties of SgrS regulation of *ptsG* mRNA, encoding a primary glucose transporter. SgrS binds within the 5' untranslated region (UTR) of *ptsG* mRNA, blocks its translation, and induces its degradation (10). We induced stress and SgrS production in *Escherichia coli* strains derived from wild-type MG1655 (table S1) using a nonmetabolizable sugar analog, α -methyl glucoside (α MG) (10, 11). Fractions of cell culture were taken at different time points after induction and fixed (12). Oligonucleotide probes (table S2) labeled with photo-switchable dyes, Alexa 647 and Alexa 568, were used to detect SgrS (9 probes) and *ptsG* mRNA (28 probes), respectively, using smFISH (8). We then imaged the cells using two-color three-dimensional (3D) super-resolution microscopy (9, 12) (Fig. 1A; compare to diffraction limited images in Fig. 1B).

In the wild-type strain (table S1), we observed production of SgrS and corresponding reduction of *ptsG* mRNA over a few minutes (Fig. 1A), consistent with SgrS-mediated degradation of *ptsG* mRNA (10). In a strain producing an SgrS that does not base pair with *ptsG* mRNA due to mutations in the seed region (13, 14) and in an Hfq deletion (Δ Hfq) strain (table S1), *ptsG* mRNA re-

duction was not observed (figs. S1 and S2). To quantify the copy number of RNAs in each cell, we employed a density-based clustering algorithm to map single-molecule localization signal to individual clusters corresponding to individual RNAs (12, 15, 16) (Fig. 1C and movies S1 and S2). The absolute copy number quantification was validated by quantitative polymerase chain reaction (qPCR) (12) (Fig. 1D).

We next built a kinetic model containing the following kinetic steps: transcription of SgrS (with rate constant α_s) and *ptsG* (α_p), endogenous degradation of *ptsG* mRNA (with rate constant β_p), degradation of SgrS in the absence of codegradation with *ptsG* mRNA ($\beta_{s,p}$), binding of SgrS to *ptsG* mRNA (with rate constant k_{on}), dissociation of SgrS from *ptsG* mRNA (k_{off}), and ribonuclease E (RNase E)-mediated codegradation of SgrS-*ptsG* mRNA complex (k_{cat}) (Fig. 1E). We independently measured β_p and the total SgrS degradation rate, including endogenous and mRNA-coupled degradation [table S4, fig. S3, and supplementary materials section 1.9 (SM 1.9)]. Because *ptsG* mRNA levels remained constant in the absence of SgrS-mediated degradation, as observed in the base-pairing mutant strain (fig. S1), we determined α_p as the product of β_p and *ptsG* mRNA concentration before SgrS induction (table S4 and SM 1.10).

To determine k_{on} and k_{off} , it is necessary to count the SgrS-*ptsG* mRNA complexes. Colocalization of *ptsG* mRNA and SgrS at the 40-nm resolution was rarely observed in the wild-type strain (up to ~5%, similar to ~3% colocalization by chance, estimated using the base-pairing mutant as a negative control) (Fig. 2). This is possibly because SgrS regulates several other target mRNAs (7) and/or the SgrS-*ptsG* mRNA complex may be unstable due to rapid codegradation or disassembly. In an RNase E mutant strain, in which codegradation is blocked (17, 18) (table S1), *ptsG* mRNA levels stayed the same as SgrS levels increased (fig. S4) (17, 18), and a fraction of *ptsG* mRNA colocalized with SgrS, increasing over time to reach ~15% (Fig. 2 and fig. S5). A positive control using *ptsG* mRNA simultaneously labeled with two colors (Fig. 2 and SM 1.8) showed a high degree of colocalization (~70%), similar to the reported detection efficiency of colocalization by super-resolution imaging (19).

We then applied these measured parameters (α_p and β_p), used total SgrS degradation rate as a constraint for $\beta_{s,p}$, and determined the remaining parameters (α_s , $\beta_{s,p}$, k_{on} , k_{off} , and k_{cat}) by fitting equations (Fig. 1E) to the six time-course changes of SgrS, *ptsG* mRNA, and SgrS-*ptsG* mRNA complex in both the wild-type and the RNase E mutant strains (Fig. 3A, table S4, and SM 1.10). We further validated the model by changing

¹Center for the Physics of Living Cells, Department of Physics, University of Illinois, Urbana, IL, USA. ²Center for Biophysics and Computational Biology, University of Illinois, Urbana, IL, USA.

³Department of Microbiology, University of Illinois, Urbana, IL, USA. ⁴Verna and Marrs McLean Department of Biochemistry and Molecular Biology, Baylor College of Medicine, Houston, TX, USA. ⁵Carl R. Woese Institute for Genomic Biology, Howard Hughes Medical Institute, Urbana, IL, USA. ⁶Howard Hughes Medical Institute, Urbana, IL, USA.

*Corresponding author. E-mail: tjha@illinois.edu (T.H.); cvanderp@life.uiuc.edu (C.K.V.)

Chapter 5: Protocol for single-molecule imaging with the TRICK translation biosensor

Halstead JM^{1,}, Wilbertz JH^{1,2,*}, Wippich F³, Lionnet T⁴, Ephrussi A³, Chao JA¹*

** shared first author*

¹ *Friedrich Miescher Institute for Biomedical Research, Basel, Switzerland*

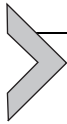
² *University of Basel, Basel, Switzerland*

³ *European Molecular Biology Laboratory, Heidelberg, Germany*

⁴ *Transcription Imaging Consortium, HHMI Janelia Research Campus, Ashburn, VA, USA*

*Published in **Methods Enzymology**, 2016; 572:123-5*

This chapter describes the design and application of a TRICK reporter to detect the first round of translation of single RNA molecules. This methodological protocol describes how to generate TRICK reporters and expressing cell lines, which fulfill all requirements to perform RNA imaging. In addition, technical requirements, necessary controls and data analysis approaches are presented.



TRICK: A Single-Molecule Method for Imaging the First Round of Translation in Living Cells and Animals

J.M. Halstead^{*,1}, J.H. Wilbertz^{*,†,1}, F. Wippich[‡], T. Lionnet[§],
A. Ephrussi[‡], J.A. Chao^{*,2}

^{*}Friedrich Miescher Institute for Biomedical Research, Basel, Switzerland

[†]University of Basel, Basel, Switzerland

[‡]European Molecular Biology Laboratory, Heidelberg, Germany

[§]Transcription Imaging Consortium, HHMI Janelia Research Campus, Ashburn, VA, United States

²Corresponding author: e-mail address: jeffrey.chao@fmi.ch

Contents

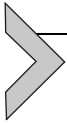
1. Introduction	124
2. Design of TRICK Reporter mRNAs	125
3. TRICK Experiment in Mammalian Cells	128
3.1 Expression of TRICK Reporter Transcripts	128
3.2 Expression of Coat Proteins Fused to Fluorescent Proteins	129
3.3 Considerations and Challenges of TRICK in Primary Cells	131
3.4 Controls	132
4. Microscopy	132
4.1 Imaging Modality	132
4.2 Light Source	135
4.3 Signal Detection	136
4.4 Temperature and CO ₂ Control	137
5. Data Collection	138
5.1 Considerations for Single-Molecule Detection and Tracking	138
5.2 Considerations for Long Time-Lapse Experiments	139
6. Analysis	140
6.1 Single-Molecule Detection and Tracking	141
6.2 Determining Colocalization of Tracked Two-Colored mRNA Particles	143
6.3 Controls	145
7. TRICK Experiment in HeLa Cells to Determine Fraction of Untranslated mRNAs	145
7.1 Preparation of Cells for Live-Cell Imaging	145
7.2 Image Acquisition	146
7.3 Image Analysis	147

¹ These authors contributed equally to this work.

8. TRICK Experiment in <i>Drosophila</i>	148
8.1 Imaging and Analysis	149
8.2 Controls	151
9. Outlook	152
Acknowledgments	153
References	153

Abstract

The life of an mRNA is dynamic within a cell. The development of quantitative fluorescent microscopy techniques to image single molecules of RNA has allowed many aspects of the mRNA lifecycle to be directly observed in living cells. Recent advances in live-cell multicolor RNA imaging, however, have now made it possible to investigate RNA metabolism in greater detail. In this chapter, we present an overview of the design and implementation of the translating RNA imaging by coat protein knockoff RNA biosensor, which allows untranslated mRNAs to be distinguished from ones that have undergone a round of translation. The methods required for establishing this system in mammalian cell lines and *Drosophila melanogaster* oocytes are described here, but the principles may be applied to any experimental system.



1. INTRODUCTION

Messenger RNA (mRNA) translation is tightly regulated to produce protein at the correct time and place with appropriate abundance. While many of the principles of translation regulation have been elucidated from ensemble biochemical measurements, understanding the mechanisms controlling where and when an mRNA is translated within a single cell is an emerging research goal. Indeed, considerable evidence now suggests that regulation of translation is devolved to specific cytoplasmic compartments, and that well-timed mRNA translation at a defined location is critical to several physiological processes, ranging from synaptic plasticity (Holt & Schuman, 2013), axis specification (Kumano, 2012), and cell motility (Liao, Mingle, Van De Water, & Liu, 2015). Understanding the mechanistic basis of localized translation regulation therefore requires spatial and temporal information to be extracted from single translation events in single living cells.

While technical advances have expanded the toolbox available to measure translation, spatial and temporal information are rarely simultaneously acquired. Ribosome profiling maps transcriptome-wide ribosome occupancy to subcodon resolution, providing a powerful readout of translation

on the timescale of minutes (Ingolia, Ghaemmaghami, Newman, & Weissman, 2009). Spatial information, however, is either restricted to particular organelles (Jan, Williams, & Weissman, 2014) or lost altogether. Imaging assays for translation provide broad spatial information by labeling components of the translational machinery (Pan, Kirillov, & Cooperman, 2007), or the nascent polypeptide itself (David et al., 2012; Dieterich et al., 2010; Terskikh et al., 2000). While these approaches have elegantly demonstrated that protein production is locally regulated within subcellular domains, they do not measure single translation events in real time. Recently, the fluorescence of single protein molecules has been used to detect local translation events; however, maturation of fluorescent proteins (FPs) occurs several minutes after translation (Ifrim, Williams, & Bassell, 2015; Tatavirt et al., 2012; Yu, Xiao, Ren, Lao, & Xie, 2006).

To detect single translation events with high temporal and spatial resolution in living cells, we developed an RNA biosensor that enables identification of untranslated mRNAs from ones that have undergone at least one round of translation (Halstead et al., 2015). This technique relies on the ribosome removing a unique fluorescent signal from the coding sequence of a transcript during the first round of translation. We refer to this methodology as translating RNA imaging by coat protein knockoff (TRICK).

In this chapter, we describe the steps to design, express, acquire, and analyze data from the TRICK system. Particular attention is given to expressing TRICK transgenes at levels appropriate for single-molecule RNA imaging and to acquiring and analyzing two-color imaging data. Though emphasis is given to establishing the TRICK system in mammalian cell lines and *Drosophila melanogaster*, many of the principles described here are applicable to other experimental systems.



2. DESIGN OF TRICK REPORTER mRNAs

Considering translation from the perspective of a transcript has the advantage that robust methods have been developed that allow detection of single molecules of mRNA in living cells using fluorescent microscopy. The highly specific interaction between the MS2 bacteriophage coat protein (MCP) and its cognate RNA stem-loop has been extensively used to image RNAs in many experimental systems ranging from bacteria to mouse neurons (Urbanek, Galka-Marciniak, Olejniczak, & Krzyzosiak, 2014). This strategy relies on insertion of multiple copies of the MS2 stem-loop (usually 24) within the 3'-untranslated region (UTR) of a transcript of interest and

the binding of a chimeric fusion of MCP with a FP to these sequences. Since the transcripts are bound by many fluorescent MCP-FPs, the mRNAs appear as bright diffraction-limited spots that can be detected above the background of the unbound MCP-FP. The inclusion of a nuclear localization sequence (NLS) to MCP-FP increases imaging sensitivity, because the unbound NLS-MCP-FP is concentrated in the nucleus, which enables rapid labeling of MS2 transcripts during transcription and reduces background in the cytoplasm (Fusco et al., 2003).

In order to take advantage of the spectrum of FPs that have been created, a number of other RNA-protein complexes have been engineered to visualize mRNAs (Chen et al., 2009; Daigle & Ellenberg, 2007; Takizawa & Vale, 2000). Given the success of the MS2 system, we developed the PP7 bacteriophage coat protein (PCP) that binds to a unique RNA stem-loop as an orthogonal RNA-labeling system (Chao, Patskovsky, Almo, & Singer, 2008; Larson, Zenklusen, Wu, Chao, & Singer, 2011). Using the MS2 and PP7 systems together allows simultaneous single-molecule RNA imaging of two distinct species of transcripts within a living cell and also enables the possibility of labeling a single mRNA within two different regions of the transcript (Coulon et al., 2014; Hocine, Raymond, Zenklusen, Chao, & Singer, 2013; Martin, Rino, Carvalho, Kirchhausen, & Carmo-Fonseca, 2013).

The act of translation requires that a ribosome traverses the coding sequence of an mRNA thereby decoding the information contained within a transcript in order to synthesize polypeptides. Consequently, any RNA-binding proteins that are bound to the transcript within the coding sequence must be removed by the ribosome. In particular, the exon junction complex, a multiprotein complex deposited upstream of exon-exon boundaries during splicing, is displaced by the ribosome during the first round of translation and therefore identifies transcripts that have never been translated (Ishigaki, Li, Serin, & Maquat, 2001). We reasoned that it should be possible to engineer a fluorescent RNA biosensor based upon this principle that would enable untranslated mRNAs to be distinguished from ones that had undergone at least one round of translation.

In order to construct an RNA biosensor to image the first round of translation, we designed PP7 stem-loops that could be translated by the ribosome that permitted the labeling of a transcript within the coding sequence (PP7) and the 3'-UTR (MS2) (Fig. 1A). When this transcript is untranslated, it will be bound by the two coat proteins fused to distinct FPs (eg, NLS-PCP-GFP and NLS-MCP-RFP) and will appear yellow when imaged because it will be labeled by both green and red FPs (Fig. 1B). During the first round of

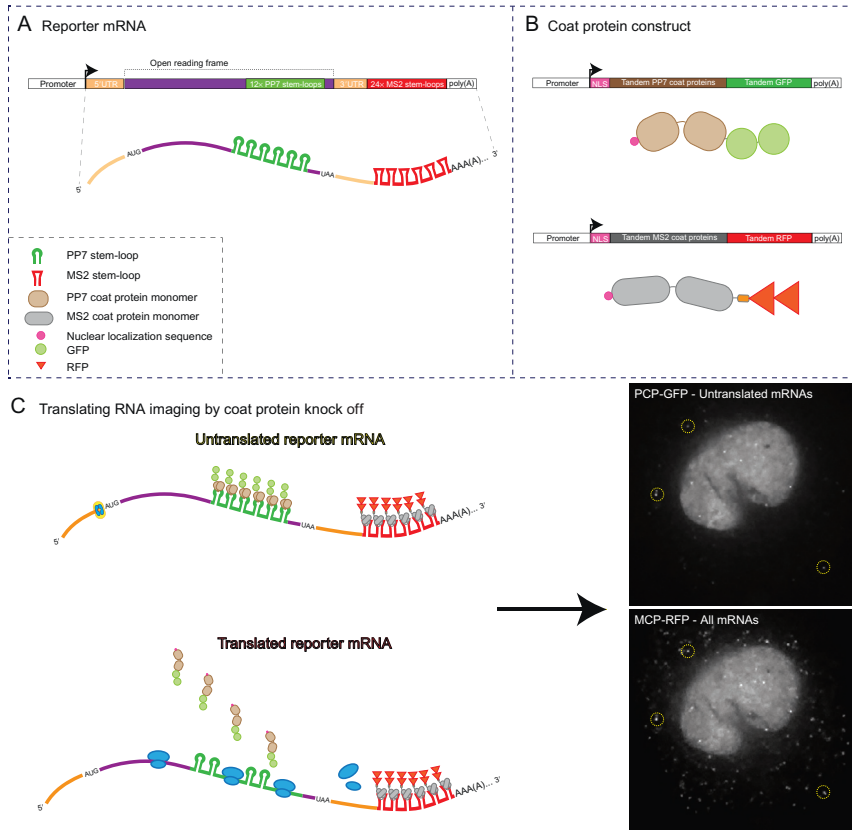
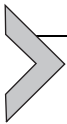


Fig. 1 Translating RNA imaging by coat protein knockoff. (A) TRICK reporter transcript contains translatable PP7 stem-loops in the open reading frame and MS2 stem-loops in the 3'-UTR. (B) PP7 and MS2 bacteriophage coat proteins are fused to spectrally distinct fluorescent proteins (eg, NLS-PCP-GFP and NLS-MCP-RFP). The addition of nuclear localization sequences (NLS) results in accumulation of unbound fluorescent proteins in the nucleus. (C) Untranslated mRNAs are bound by both fluorescent fusion proteins while translated mRNAs are labeled with only NLS-MCP-RFP. Dual-color RNA imaging can distinguish single molecules of untranslated mRNAs that are fluorescent in both *green* and *red* channels (yellow circles) from those that have been translated and are detected in the *red* channel alone.

translation, however, the ribosome will strip the NLS-PCP-GFP signal from the transcript resulting in the appearance of a red mRNA that is labeled with only NLS-MCP-RFP. Since the concentration of NLS-PCP-GFP is low in the cytoplasm, rebinding of NLS-PCP-GFP is not favorable and the displaced FP returns to the nucleus (Fig. 1C).

Since it is possible to design translatable RNA sequences for any of the RNA–protein complexes used to image RNAs, we have outlined the principles we used to design the PP7 stem-loops. The first MS2 stem-loops used to image RNAs were constructed by PCR by making two copies of the stem-loops that could then be multimerized by ligation with DNA fragments digested using restriction enzymes that generate compatible cohesive ends (eg, *Bam*HI and *Bgl*II) (Bertrand et al., 1998). Consequently, adjacent MS2 stem-loops were spaced by 20 nucleotides due to limitations, at the time, on the synthesis of large DNA oligonucleotides. A translating ribosome, however, produces a footprint of ~30 nts on a transcript, and we found that tight spacing of stem-loops results in a significant block of translation (Ingolia et al., 2009; Steitz, 1969). By spacing PP7 stem-loops farther apart (40 nts), we found that the ribosome could efficiently translate through them. Since the PP7 stem-loops will encode a polypeptide, we removed stop codons from the open reading frame and optimized codon usage for expression in mammalian cells by considering both codon frequency and coding potential. RNA folding was assessed using the *mfold* software to confirm that all PP7 stem-loops were predicted to fold correctly (Zuker, 2003).

Initially, a cassette containing six copies of the PP7 stem-loops was synthesized and tested for its translatability when fused to the C-terminus of a reporter gene. While western blot analysis revealed that the PP7 stem-loops were efficiently translated, imaging of this construct was difficult due to the low signal-to-noise ratio resulting from the small number of stem-loops. A 12×PP7 cassette was then generated which improved imaging of single mRNA molecules without inducing adverse effects on translation. In instances when addition of the polypeptide encoded by the PP7 stem-loops is not desirable (eg, labeling of endogenous genes), the addition of self-cleaving 2A sequences between the C-terminus of the protein of interest and the stem-loops may be advantageous (Kim et al., 2011). We have also found that it is possible to place the PP7 stem-loops within the N-terminus of a reporter gene, which may facilitate experiments designed to measure translation initiation rates by reducing the effect of ribosome elongation.



3. TRICK EXPERIMENT IN MAMMALIAN CELLS

3.1 Expression of TRICK Reporter Transcripts

The TRICK system provides a fluorescent readout from three transgenes, a reporter mRNA and two coat proteins, each of which must be expressed at appropriate levels in the same cell. Selecting the appropriate promoter to drive expression of the reporter mRNA is therefore key to designing a

TRICK experiment. As the TRICK system reports on the first round of translation only, there are advantages to controlling precisely when the reporter mRNA is expressed. While constitutive expression produces a mixed population of reporter transcripts that have been transcribed at different time points, including those transcribed and translated before imaging began, an inducible promoter can provide a population of nascent mRNAs whose pioneer round of translation is restricted to the experimental window. As a result, inducible expression of reporter mRNA is better suited to many experiments, particularly those examining the temporal regulation of translation. We found that both the tetracycline- and ponasterone A-inducible systems are well suited for performing TRICK experiments (Gossen et al., 1995; No, Yao, & Evans, 1996).

TRICK reporter mRNAs can be expressed from plasmids that are transiently transfected or stably integrated into the genome. Transient transfection is relatively fast and simple, with constitutive reporter mRNA expression peaking 24–48 h after transfection by lipid-based reagents, and can allow different TRICK reporters to be rapidly tested. Delivery of DNA plasmids by transient methods, however, can result in significant cell-to-cell variation in expression levels that can complicate image analysis. As it is possible to determine the translational status of every single TRICK reporter mRNA within a cell, the most meaningful quantitative comparisons are between cells expressing similar numbers of transcripts and at levels comparable to endogenous transcripts. It is possible to transiently transfect and identify cells within a heterogeneous population that meet this criteria, however, this limits data acquisition to a relatively small number of cells per experiment. Instead, reproducible and more uniform expression is best achieved by stably integrating the TRICK reporter into the cell genome by either random or site-specific integration. We have found that site-specific integration of an inducible TRICK reporter by recombinase-mediated cassette exchange to be an efficient method for generating TRICK cell lines. In this system, reporter mRNA expression is consistent across cells thereby limiting experimental variability. We use a HeLa cell line that contains both the rtTA2-M2 tetracycline reverse transactivator required for doxycycline-inducible expression and a single RCME site that allows stable integration of TRICK reporter mRNAs (Weidenfeld et al., 2009).

3.2 Expression of Coat Proteins Fused to Fluorescent Proteins

The crux of the TRICK experiment is to spectrally distinguish translated and untranslated mRNAs. Consequently, the appropriate selection and

expression of the coat protein (CP; PCP and MCP)–FP pairs is critical to the success of the experiment. The CP–FPs used in the TRICK experiment must be fused to spectrally distinct fluorophores that are suitable for single-molecule RNA imaging. Both CP–FPs must also be expressed at cellular levels that allow robust labeling of all reporter mRNAs and, importantly for the TRICK experiment, do not favor rebinding of PCP–FP to the transcript once it has been displaced by the ribosome in the cytoplasm.

Single-molecule two-color imaging of mRNAs requires that the coat proteins are fused to fluorophores that satisfy a number of criteria. Foremost, as TRICK requires unambiguous separation of two fluorescent signals, spectrally distinct fluorophores must be selected to label each coat protein. Overlap of emission spectra and cross-excitation of overlapping absorption bands can be avoided by judicious choice of fluorophores. As a result, optimal imaging requires that distinct fluorophores are also matched to the light source and filters that will be used to acquire data.

Within these criteria, brightness, the product of quantum yield and extinction coefficient, and photostability, the decrease in emission over sequential excitation events, are the leading properties for fluorophore selection. This is particularly important for single-particle tracking (SPT) experiments because single mRNAs must be imaged multiple times and photobleaching of one channel can bias analysis. Genetically encoded FPs, such as GFP, exist in a range of spectra (Shaner, Steinbach, & Tsien, 2005) and have been successfully used in a number of single-molecule RNA imaging studies. We have found that NLS-PCP-EGFP and NLS-MCP-TagRFP-T are compatible with two-color RNA imaging with short (≤ 50 ms) exposure times. Other FPs can be used to suit other imaging modalities, however, the properties must fit the experiment parameters. For example, while tdTomato (extinction coefficient = $138,000 M^{-1} \text{ cm}^{-1}$, quantum yield = 0.69) is brighter than TagRFP-T (extinction coefficient = $81,000 M^{-1} \text{ cm}^{-1}$, quantum yield = 0.41), tdTomato is significantly less photostable and less suitable for time-lapse imaging (Shaner et al., 2008). The recent development of alternative intracellular fluorescent labeling technologies, including the Halo-Tag, Snap-Tag, and Clip-Tag, can also be used to conjugate chimeric coat proteins to inorganic dyes (Gautier et al., 2008; Juillerat et al., 2003; Los et al., 2008). This approach allows the coat proteins to be specifically covalently bonded to inorganic dyes such as tetramethylrhodamine-based dyes, which are bright (extinction coefficient = $101,000 M^{-1} \text{ cm}^{-1}$, quantum yield = 0.88) and significantly more photostable than FPs (Grimm et al., 2015).

While inducible promoters are useful for controlling acute and robust reporter mRNA transcription, CP-FPs are best expressed constitutively at low levels. A number of constitutive promoters are commonly used, including SV40, CMV, UbiC, EF1a, PGK, and CAGG variants, of which PGK and UbiC have been found to reproducibly give lower expression levels (Qin et al., 2010). We have found that lentiviral transduction is an efficient means to stably express CP-FPs (Lionnet et al., 2011). Cells can be coinfecting with two viruses each encoding a different CP-FP and cells that are double positive can be isolated by fluorescence-activated cell sorting (FACS). Successive rounds of FACS followed by fluorescent microscopy can be used to generate cell lines that express both CP-FPs at levels suitable for two-color single-molecule RNA imaging. The use of tandem single-chain dimers of the MS2 and PP7 coat proteins enables cells to be sorted for very low levels of the FPs without disrupting the RNA-binding function of the coat proteins (Wu, Chao, & Singer, 2012; Wu et al., 2015).

3.3 Considerations and Challenges of TRICK in Primary Cells

Balancing CP-FPs and TRICK reporter mRNA expression is particularly challenging in primary cells. Unless the cells are derived from an animal stably expressing the TRICK transgenes, both the reporter mRNA and CP-FPs must be introduced. While stable transgene integration followed by FACS of positive cells is optimal in cell lines, many primary cells can only be passaged a limited number of times and growing a sufficient number cells from a sorted population may not be possible.

In particular, primary neurons present a number of challenges for establishing single-molecule two-color RNA imaging. First, neurons are postmitotic and transient transfection rates are low. While other means of delivering transgenes (eg, infection using lentiviruses or electroporation) are more efficacious, a small percentage of cells will express the transgenes at appropriate levels that must be individually identified by fluorescence microscopy during each experiment. To increase the number of positive cells in a primary culture, the both CP-FP constructs can be expressed in a single bicistronic plasmid separated by an internal ribosome entry site (IRES), or a 2A peptide sequence. It is necessary to ensure that the CP-FPs are expressed properly because IRES-driven expression is typically lower than cap-dependent translation (Mizuguchi, Xu, Ishii-Watabe, Uchida, & Hayakawa, 2000) and 2A peptide sequences can produce chimeric fusion proteins that will undermine TRICK analysis (Kim et al., 2011).

3.4 Controls

To confirm that any TRICK construct gives a precise readout of translation, it is necessary to test if the insertion of either of the stem-loops or the binding of the CP-FPs perturbs reporter mRNA metabolism. The stability of the TRICK reporter mRNA can be assessed by real-time PCR following inhibition of transcription, either by small-molecules (eg, actinomycin D) or washing away activators of inducible promoters. The translation of the TRICK reporter construct should also be confirmed by western blotting to demonstrate that a protein of appropriate molecular weight is produced. It is also advantageous for the TRICK reporter to encode a protein with a functional readout (eg, fluorescence, bioluminescence, or enzymatic activity). We have found it useful for TRICK reporters to encode Renilla or Firefly luciferase because translation can be measured using a common luciferase assay that can be correlated with imaging data. Control experiments should be performed both with and without stem-loops and with and without coexpression of CP-FPs (Table 1). This approach will identify any element of the TRICK construct that affects reporter stability or translation and provides a starting point for troubleshooting.



4. MICROSCOPY

The success of a TRICK experiment largely depends on its accurate imaging readout. The field of live-cell single-molecule imaging has utilized different light microscopy variants, broadly characterized into epifluorescence wide-field, confocal, and total internal reflection fluorescence (TIRF) microscopy. Each of these microscopy setups offers certain advantages and drawbacks when dual-color single mRNAs, as in TRICK, are to be imaged in live cells.

4.1 Imaging Modality

A straightforward and cost-effective way of imaging single RNA molecules in live cells is conventional wide-field or epifluorescence microscopy. Here, a collimated/parallelized beam of light illuminates the entire thickness of the sample, resulting in a large field-of-view and a high number of molecules that can potentially be tracked. This advantage however comes at the price of a large fraction of out-of-focus light, resulting in high background levels and reduced single-molecule detection. Wide-field microscopy is therefore especially suited for specimens with a low number of fluorescent molecules

Table 1 Controls for TRICK Reporter mRNA Expression

Control Experiment	Reporter mRNA Expression	CP-FP Expression	Method
Is reporter mRNA stability affected by stem-loops?	1. TRICK reporter lacking stem-loops 2. TRICK reporter with stem-loops in the coding region and 3'-UTR	None	Measurement of mRNA half-life by real-time PCR. Northern blotting of mRNA
Is reporter mRNA stability affected by CP-FP binding?	TRICK reporter with stem-loops in the coding region and 3'-UTR	1. CP-FP bound to the coding region 2. CP-FP bound to the 3'-UTR 3. CP-FPs bound to both the coding region and 3'-UTR	Measurement of mRNA half-life by real-time PCR. Northern blotting of mRNA
Is reporter mRNA translation affected by stem-loops?	TRICK reporter with stem-loops in the coding region and 3'-UTR	None	Measurement of protein MW and levels by Western blot
Is reporter mRNA translation affected by CP-FP binding?	TRICK reporter with stem-loops in the coding region and 3'-UTR	1. CP-FP bound only to the coding region 2. CP-FP bound only to the 3'-UTR 3. CP-FPs bound to both the coding region and 3'-UTR	Measurement of protein MW and levels by Western blot
Is the translated reporter protein functional?	TRICK reporter with stem-loops in the coding region and 3'-UTR	CP-FPs bound to both the coding region and 3'-UTR	Functional readout of protein activity (eg, fluorescence, bioluminescence, enzymatic activity)

and a thin imaging volume (a few microns or less), causing low background fluorescence. Consequently, cells with a small thickness such as yeast, bacterial, and epithelial cells or certain cellular extensions such as axons are well suited to be imaged by wide-field microscopy.

As opposed to wide-field microscopy, a confocal illumination scheme effectively reduces out-of-focus light and thereby enables the recording of high-contrast images in all spatial dimensions. Focusing the laser beam

to the size of a diffraction-limited spot and using a pinhole aperture that rejects all light emitted outside of the focal volume are the two key elements to the spatial filtering of out-of-focus light. However, the confocal illumination scheme suffers from two major drawbacks. Since only a single diffraction-limited spot is illuminated at a time, the focal plane needs to be scanned point-by-point by either moving the sample or the laser beam, as in traditional laser scanning confocal microscopy (LSCM). Secondly, the pinhole aperture filters out a large fraction of the total light used for sample excitation. In combination, loss of emitted light and point-by-point scanning lead to long pixel dwell times to collect enough photons and long scanning times because relevant field-of-views typically require 10^5 – 10^6 pixels, resulting in a low frame rate that can become limiting when imaging rapidly moving mRNA molecules. Spinning-disk confocal microscopy has been developed as a faster alternative, and we have successfully used it for TRICK experiments. In spinning-disk microscopy, a first disk with a large number of spirally oriented microlenses is rotating at high speed and essentially focuses thousands of split laser beams on the sample. A second spinning disk, with a spiral array of pinholes, is aligned to the first and blocks all out-of-focus light. As a result, the fast, synchronized disk rotation and spiral orientation of microlenses and pinholes enables the near-simultaneous scanning of a single imaging plane. While allowing the high temporal resolution (subsecond frame intervals) required for TRICK experiments, a spinning-disk confocal microscope suffers from reduced fluorescence intensity detection due to beam splitting and the use of pinholes. Rapid photobleaching due to out-of-focus fluorescence excitation is another major limitation of all confocal microscopy approaches.

Reducing photobleaching is imperative during TRICK experiments. The pair of fluorophores that fluorescently label reporter mRNAs usually have different sensitivities to photobleaching. If one fluorophore bleaches faster than the other, the detection efficiency of the corresponding fluorophore will vary over the time of one experiment and might result in a bias toward incorrect identification of translational state. One way to reduce photobleaching (as well background fluorescence due to out-of-focus excitation) is to use an optical sectioning method called TIRF microscopy. TIRF is based on the observation that a collimated laser beam propagating through one medium when reaching a second medium is reflected at the interface, if a large enough angle and appropriately different refractive indices of the two media are chosen. The reflection creates an exponentially decaying evanescent wave in the z -direction within the sample, allowing

only the excitation of molecules within a few hundred nanometers within the sample and leading to an excellent reduction of bleaching and high contrast. While TIRF can be a good option for live-cell imaging, it allows only the imaging of molecules close to the sample-glass interface, making it impossible to image and detect TRICK transcripts deep inside of the cell. Furthermore, the rapidly decreasing intensity of the evanescent wave with increasing distance from the coverslip leads to a wide distribution of fluorescent particle brightnesses—a substantial challenge for quantitative analysis. Another optical sectioning method is more widely applicable to imaging TRICK reporter mRNAs and allows for the detection of translation in all cellular compartments. Here, an inclined laser beam just below the critical angle for TIRF is used. Instead of creating an evanescent wave, the laser beam now passes directly into the sample, but in the form of a highly inclined laminated optical sheet (HILO) with a thickness in the low micrometer range (Tokunaga, Imamoto, & Sakata-Sogawa, 2008). A rotating mirror ensures that the sample is illuminated from all angles. Because any form of point scanning is not necessary, high frame rates can be achieved. We have successfully applied HILO to perform TRICK experiments in live cells. HILO offers low amounts of out-of-focus light, low bleaching, and fast image acquisition rates.

4.2 Light Source

Since a large number of fluorophores with excitation–emission spectra ranging from near-ultraviolet, visible, to near-infrared regions are currently available (Kremers, Gilbert, Cranfill, Davidson, & Piston, 2011; Xia, Li, & Fang, 2013), it is often most appropriate to match the required fluorophores to the already existing illumination setup.

Two spectrally distinct lasers constitute the illumination source of choice (especially for confocal imaging) since they provide a narrowly defined excitation wavelength range, low divergence when passing through the optical setup, and high excitation power. Gas lasers such as argon or krypton ion lasers or solid-state lasers such as diode lasers are most commonly used. For dual-color imaging, the most important criterion when choosing a light source is to maximize the fluorophores excitation efficiency while minimizing excitation cross talk. For dual-color mRNA imaging with the described MS2 and PP7 system, 488 and 561-nm emitting lasers have been found to be appropriate to excite the commonly used FPs such as GFP or RFP-variants while providing sufficiently separated emission spectra. More information

on how to optimize the laser excitation of various fluorophores for live-cell imaging has been described elsewhere (Xia et al., 2013).

For wide-field microscopy, cost-effective alternatives to laser excitation can be used, eg, arc-discharge lamps such as mercury or xenon arc lamps, or more recently light-emitting diodes (LEDs) (Cho et al., 2013; Gerhardt, Mai, Lamas-Linares, & Kurtsiefer, 2011; Higashida et al., 2008). The commonly used mercury-based arc lamps typically display intensity peaks at certain wavelengths and therefore do not provide an even intensity across the full light spectrum. These considerations are important when deciding on a light source for simultaneous dual-color imaging. Xenon-based arc lamps display a more even intensity profile, but lack the shorter wavelength range typically employed for fluorescent microscopy. A third form of arc-discharge-based light sources is metal-halide lamps. This type of lamp combines the properties of xenon and mercury, resulting in an even, high intensity emission across the entire light spectrum from ultraviolet to infrared. The use of LEDs for dual-color RNA imaging is currently limited since the detection of single molecules has so far only been demonstrated in the close blue and green spectra (Gerhardt et al., 2011; Kuo, Kuyper, Allen, Fiorini, & Chiu, 2004). Recently, white LEDs have been used for super-resolution microscopy in live cells (Cho et al., 2013) and might represent an attractive alternative to laser light sources for dual-color single-molecule imaging in the future.

4.3 Signal Detection

For TRICK experiments, it is key to detect both fluorescence channels unambiguously to avoid a systematic analysis bias toward one of the channels and incorrect conclusions about the translation state. Signal bleed-through due to overlapping fluorophore emission spectra can be effectively minimized by appropriate design of the bandpass excitation and emission barrier filters and should be controlled for. mRNA particles can travel relatively fast with diffusion coefficients up to $3.42 \mu\text{m}^2 \text{s}^{-1}$ (Ma et al., 2013) and transport rates of $\approx 1.3 \mu\text{m} \text{s}^{-1}$ (Park et al., 2014). The mRNA's image on the camera chip can therefore move by one pixel or more between frames, even when imaging at subsecond intervals. Consequently, it is crucial to image the two-color channels simultaneously in order to unambiguously identify dual-labeled particles. As a consequence, filter cube switching is not an option for TRICK imaging. Instead, the best setup for the microscope emission path is to first separate the emission light from the excitation source with

a multiline dichroic mirror, followed by a second dichroic mirror that will split the collected fluorescence in two beams (eg, GFP vs RFP fluorescence). The two beams can then be imaged by two separate cameras or recombined on the two halves of the same camera chip.

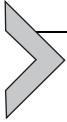
The two most used camera types include scientific complementary metal oxide semiconductor (sCMOS) and electron multiplying charge coupled device (EMCCD) cameras. Due to the coupling of photon detection and voltage conversion at the physical pixel level on the chip, sCMOS cameras allow for high-speed imaging of more than 100 frames s^{-1} . The consequence is a relatively high internally generated background (dark noise) and readout noise, limiting the photon sensitivity under low light conditions, as is the case for single-molecule RNA imaging. In contrast, EMCCD cameras achieve single-photon sensitivity. Despite having a lower chip readout speed, which is generally still permissive for single mRNA tracking, EMCCD cameras currently offer significant advantages over other types of camera sensors, especially when applied under low emitted light conditions.

TRICK experiments require the acquisition of both fluorescent channels simultaneously in order to guarantee signal colocalization. The solution of choice to image relatively large biological structures (eg, an entire mammalian cell, typically tens of microns across) is to separately collect the fluorescence from the two channels on two well-aligned cameras. At a magnification that permits the detection of single molecules, the use of two cameras provides a large enough field-of-view in each fluorescent channel to fully capture the sample. A practical alternative to the costly dual-camera approach is the use of a split chip on a single camera. Here, the image is divided into two spatially equivalent, but separate halves on the camera chip. Postimaging registration of both halves of the chip into a single image can be performed.

4.4 Temperature and CO₂ Control

Translation is very sensitive to changes in the extracellular environment. TRICK live-cell experiments therefore require strictly physiological conditions during imaging. Mammalian cells generally require an incubation temperature of 37°C and a CO₂ atmosphere of 5–7% to maintain an appropriate pH, depending on the growth medium. The humidity level should also be controlled in order to prevent excessive evaporation and drying. Several commercial systems are available to keep the biological sample under these

physiological conditions during imaging. A simple and inexpensive method is to use heating elements directly adjacent to the objective and sample dish. Repeated cycles of heating and cooling, however, lead to thermal movements of the objective and the sample itself leading to a loss of focus over time. While less economical, a Plexiglas incubation box, which fully encloses the microscope body, is more suitable for live-cell imaging. A second cover that seals with the stage can then be placed on top of the specimen to regulate CO₂ and humidity within this restricted volume.



5. DATA COLLECTION

The quantification of data obtained from TRICK experiments involves two major steps. First, all mRNA particles per imaging frame need to be detected in each of the two respective channels. Then the detected particle positions in consecutive frames are combined to give individual mRNA trajectories in a computational process termed SPT. To avoid detection biases toward one channel based on the different fluorophore properties, the acquired imaging data needs to be of high quality by fulfilling the two following major criteria: first, the signal-to-noise ratio (SNR) needs to be as high as possible, while, second, the imaging frame rate needs to be sufficiently high to connect the positions of individual mRNAs over time (Park, Buxbaum, & Singer, 2010).

5.1 Considerations for Single-Molecule Detection and Tracking

A major limitation of live-cell imaging experiments is that a high SNR and frame rate will lead to rapid photobleaching and phototoxicity caused by an excessive amount of photons hitting the specimen. Finding a balance between frame rate, exposure time, and excitation power is therefore key to being able to image and subsequently track single mRNAs in two colors (Magidson & Khodjakov, 2013).

Because of the diffraction of light, individual fluorescent particles appear as spots of a few 100 nm in size when imaged through a microscope. The shape of the spot depends on the microscope and the fluorophore and is called the point spread function (PSF). The spatial profile of the PSF on the camera is nearly Gaussian, which makes it possible through fitting to measure the position of each particle center with high accuracy (typically ≈ 40 nm). If the PSF is spread onto a large number of camera pixels, each spot becomes hard to separate from the background and readout noise. Conversely, if the spot on the image is concentrated onto a single pixel, it is hard

to achieve a high localization precision through fitting. A high SNR is therefore typically obtained by combining a high numerical aperture objective (which means a high light collection power), and a magnification optimized for single-molecule imaging. In practice, magnifications that yield 100–200 nm per pixel tend to give optimal localization precision for single-molecule tracking (Thompson, Larson, & Webb, 2002). As images of mRNA labeled in separate colors need to be registered, chromatic aberrations pose a significant challenge. They are minimized by using apochromatic objectives and can be corrected postacquisition using adequate calibration techniques, eg, using multicolor beads or fiducial markers within the sample (Grunwald & Singer, 2010).

Diffusion coefficients of mRNAs have been shown to range from 0.009 to $3.42 \mu\text{m}^2 \text{s}^{-1}$ depending on the type of transcript and subcellular localization (Fusco et al., 2003; Ma et al., 2013; Mor et al., 2010; Shav-Tal et al., 2004). Therefore, exposure times need to be long enough for a good SNR while being short enough to prevent blurring of fast moving mRNA particles. In addition, the frame rate needs to be short enough to reliably track an mRNA's position from frame-to-frame. Exposure times and frame rates should therefore be optimized based on each system's dynamic range, ensuring unbiased detection while minimizing oversampling and photobleaching. In cases where very fast frame rates and short exposure times are crucial, but the chip readout speed is limiting, it is possible to readout only a subarray of the chip, thereby decreasing the total required readout time per frame at the expense of a reduced field-of-view.

Besides optimizing the frame rate, other means to increase the SNR can be used, such as pixel binning. During pixel binning a group of pixels on the camera chip (eg, 2×2 pixels) are binned together and assigned to a single pixel value during the readout of the chip. A 2×2 binning for example increases the signal fourfold (four times more photons per pixel) at the cost of a twofold lower resolution (pixel information is lost). Finally, optimizing the camera gain and the chip readout speed can also improve the SNR and dynamic range. Slower chip readout speeds result in lower readout noise and can be compensated for by utilizing only a subarray of the chip, as described earlier.

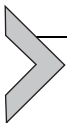
5.2 Considerations for Long Time-Lapse Experiments

The TRICK technique can be used to study translation regulation with subcellular resolution over a wide range of time scales: from fast, single-molecule dynamics movies (subsecond frame rates covering a few seconds

to minutes) to longer, time-lapsed acquisitions matching the dynamics of cellular responses (minutes to hours). Minimizing photobleaching by the previously described imaging optimizations is key for successful longer time-lapse experiments. Although the detailed mechanism of photobleaching is not entirely known, photo-oxidation of the fluorophores is thought to be caused by reactive oxygen species (ROS). The addition of chemical compounds such as ascorbic acid (vitamin C) (Vigers, Coue, & McIntosh, 1988), trolox (a vitamin E derivative) (Rasnik, McKinney, & Ha, 2006), mercaptoethylamine (Widengren, Chmyrov, Eggeling, Lofdahl, & Seidel, 2007), or enzymatic deoxygenation systems (Aitken, Marshall, & Puglisi, 2008) has been shown to delay photobleaching. Since oxygen plays an important role in cell physiology, the use of ROS scavengers can have unwanted effects that need to be taken into account.

Stage stability over long time periods in all three spatial dimensions is crucial for long-term live-cell experiments. Especially when heated incubation chambers are used, it is important to thermally equilibrate the whole microscope body, including the stage, prior to the experiment in order to prevent thermal drift and to avoid permanent refocusing. Motorized Piezo stages that are equipped with reflection-based rather than image-based auto-focus systems minimize manual interventions during an experiment.

Some adherent cell types growing on coverslips can move extensively in the x, y dimension even on the order of minutes and might require the use of cell motion tracking (Rabut & Ellenberg, 2004). Several software packages that can be coupled to the appropriate microscope hardware are currently available by commercial suppliers.



6. ANALYSIS

Dual-color single-molecule mRNA imaging during a TRICK experiment allows direct observation of two distinct translational states depending on the presence of one or both fluorophores. In order to reconstruct the trajectories of individual mRNA particles and determine their translation state, multiple computational steps must be performed (Fig. 2). First one needs to identify and localize discrete particles on each acquired image (Fig. 2A); this step outputs a list of particle positions for each time point and color channel (Fig. 2B). The second step consists of tracking the particles, which means connecting together the spot positions that correspond to the same particle at different times, yielding a list of trajectories for each color channel (Fig. 2C). Finally, one sorts the trajectories present in both channels

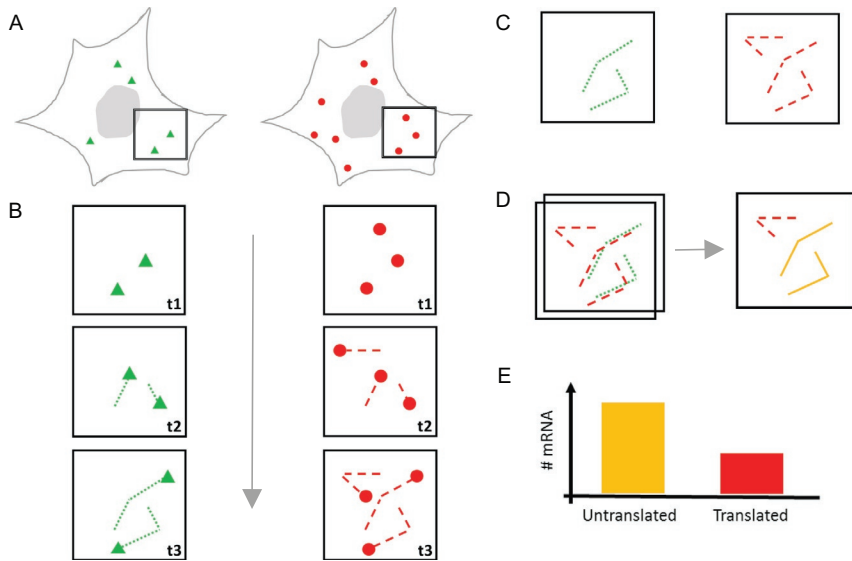


Fig. 2 Schematic depiction of the analysis workflow for a TRICK experiment in living cells. (A) Each cell is imaged simultaneously in two colors, resulting in two fluorescent channels. Here, the mRNAs labeled with NLS-PCP-GFP and NLS-MCP-RFP are depicted by *triangles* and *circles*, respectively. (B) After image acquisition all mRNA diffraction-limited spots in each imaging frame are detected. Spot detection is best performed individually for each fluorescent channel. (C) Next, spot tracking is performed. Here, the spot positions in each frame are taken into account and tracks for each mRNA molecule are calculated. (D) The resulting tracks from both fluorescent channels originating from the same cell are then assessed for colocalization. *Red* (*dark gray* in the print version) and *green* (*light gray* in the print version) mRNA tracks represent the same dual-colored molecule when a significant overlap exists. (E) mRNAs that have been determined to be dual-colored are considered to be untranslated, while single *red* (*dark gray* in the print version) colored mRNAs have been translated at least once.

(corresponding to dual-labeled untranslated mRNA) from those present in a single channel only (single-labeled translated mRNAs) (Fig. 2D and E). Measuring the spatiotemporal evolution of single- vs dual-color-labeled molecules then gives an indication about the localization and translational status of the mRNAs.

6.1 Single-Molecule Detection and Tracking

Detection and tracking of single particles should be performed for each fluorescent channel individually (Fig. 2A and B). A number of commercially and freely available software packages exist that combine detection and tracking

of all single particles in each frame within a given image sequence in two consecutive steps in a semiautomated manner. Different particle tracking approaches have recently been extensively tested and reviewed by [Chenouard et al. \(2014\)](#). In general particle detection and tracking should be performed on unprocessed data that have been recorded according to the earlier described principles in order to maximize the SNR and to fulfill the Nyquist criterion on temporal sampling so that individual particles can be tracked over time ([Park et al., 2010](#)). The precise particle detection and tracking methodology needs to be chosen based on the data quality, particle density, and intended tracking time frame. For the detection of single particles several approaches exist. Maxima-based detection relies on the identification of the highest local pixel values, which are then defined as spots. Thresholding utilizes the principle of a particle's higher intensity over the surrounding background based on an appropriate intensity threshold. More accurate (and computationally intensive) approaches involve PSF fitting and centroid estimation. Fitting often relies on the PSF-based fitting of a Gaussian intensity distribution to each spot candidate or uses other linear or nonlinear models. Centroid estimation detects diffraction-limited spots by determination of the radial spot center, which often does not coincide with the local maximum and is a reliable method to distinguish neighboring spots ([Parthasarathy, 2012](#)).

Once spots have been detected and their positions evaluated, one needs to connect the spots in order to generate trajectories ([Fig. 2C](#)). The simplest method to achieve this connects each spot with its nearest neighbor in the next frame, allowing for only a limited displacement range (based on knowledge of the typical transport properties of the biological species), and a given number of gaps—false negatives are common in single-molecule tracking because fluorescence of a particle might be intermittently obscured by noise or background, resulting in a missed detection. Multiframe or multitrack and motion model-based tracking approaches are more sophisticated techniques that go beyond frame-to-frame nearest-neighbor linking and are suitable for live-cell mRNA imaging. They are robust against partial detection failures and crossing trajectories. Multiframe or multitrack approaches take the history of a tracked particle into account in order to match it to a future estimated trajectory. Motion-based models fit the trajectories to typical single-particle movement patterns such as Brownian motion, corralled diffusion, or directed motion ([Park et al., 2010](#)). The most robust particle tracking methods rely on a combination of several of the aforementioned detection and tracking approaches ([Chenouard et al., 2014](#)). Because it is technically difficult using wide-field epifluorescence or confocal microscopy

to acquire 3D volumes at frame rates compatible with single-molecule tracking with sufficient SNR, single mRNA tracking has mostly been performed in 2D planes where particle movement in and out-of-focus limits the observation time to a few seconds in ideal cases. However, innovative microscopy approaches have recently been developed to overcome this issue and collect 3D trajectories of mRNA particles (Smith et al., 2015; Spille et al., 2015). These imaging modalities circumvent the problem of particles moving out-of-focus and are able to generate longer trajectories; the tracking analysis techniques are conceptually identical to those used for 2D tracking.

Although long trajectories are ideal to investigate the fate of individual mRNA molecules, short observations times are not necessarily limiting to determine the translation state of a two-color-labeled mRNAs (Fig. 2). Short trajectories of a few 100 ms are often sufficient to reliably determine the degree of colocalization of an mRNA population within a cell.

6.2 Determining Colocalization of Tracked Two-Colored mRNA Particles

The determination of colocalization between both fluorescent channels is key to determine translation, as in the case of TRICK or other dynamic properties probed by a two-color mRNA imaging experiment. Since every field-of-view typically contains a large number of tracked mRNAs, colocalization between the two trajectory data sets is best performed in an automated fashion (Deschout et al., 2013; Dupont, Stirnagel, Lindemann, & Lamb, 2013; Koyama-Honda et al., 2005).

One important first step in colocalization is to ensure one can accurately register the two-color channels. This calibration is usually performed by imaging small (≈ 100 nm) fluorescent beads or gold nanorods that emit a broad spectrum of light spanning the two channels used in the experiment. Each bead produces one diffraction-limited spot in each channel. By using detection algorithms to measure the position of each bead image in the separate channels, one can calculate the spatial transformation needed to precisely map the position of the red beads onto the green ones. This process corrects for systematic chromatic aberrations (specific to one microscope because of the properties of its lenses, but invariant over time) and misalignments. As microscopes can substantially drift over time, it is important to perform these calibration routines frequently, ideally on a daily basis if one desires to achieve high registration accuracies. Typical registration errors can be as small as 5–10 nm. The spatial transformation generated during the calibration is then applied to the measured spots after the experiment, before matching them to the second channel.

Algorithms carrying out this kind of colocalization have been described in more detail before (Espenel et al., 2008; Halstead et al., 2015). Although in principle one could assess colocalization at each time point by matching positions of green and red spots, this strategy is very sensitive to missed or spurious detections, which are not uncommon when tracking individual molecules in the low SNR regime. We found that a more effective approach consists of matching trajectories rather than individual spot positions (Fig. 2D). The reason is that tracking algorithms are designed to accommodate both false negatives (short gaps are usually allowed in trajectories) and false positives (only trajectories longer than a few frames are considered, which cleans up spurious detections). As a result, matching trajectories rather than spots is a robust way to assess colocalization at the single-molecule level.

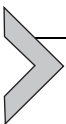
The algorithm to match trajectories consists of measuring the spatiotemporal overlap between all green and red trajectories. If two trajectories are found to be within a certain distance threshold of one another (typical value in our experiments is 100 nm) for a certain number of frames (typical value in our experiments is three frames), then they are scored as colocalized. Even though the number of frames used as our colocalization criterion might seem small, longer colocalized trajectories are usually visibly moving together for their entire duration. Perfect trajectory overlap is often not achievable, because of the uncertainty in measuring the position of each spot (in our conditions, around 40 nm in x,y), and the error in registering the two channels together (≈ 15 nm). This algorithm works best when the particles are bright and well separated in space, but is robust in a wide range of SNR and concentrations typical of single-molecule tracking. One advantage of TRICK is that out of three potential trajectory combinations (red only, green only, and colocalized red + green), one only expects to observe two: red only (3'-UTR label only for translated mRNAs) and colocalized green + red (both ORF and 3'-UTR label for untranslated mRNAs) because the 3'-UTR red label always remains bound to its target. Therefore, the measurement carries an internal control: the number of colocalized trajectories over the total number of green trajectories (green only and colocalized) is a direct metric of the experimental sensitivity (typical values in our experiments 80–90%). The results can be expressed as colocalization percentages per cell (Fig. 2E), indicating for example the amount of translated mRNA at different time points after reporter induction. Trajectories can then be analyzed separately to investigate the relative importance of location, transport, and dynamic properties of various mRNA translation states.

6.3 Controls

It is important to bracket imaging experiments with positive and negative controls. Imaging and performing particle detection on cells lacking CF-FPs should not reveal fluorescent signal. Similarly, imaging cells expressing CF-FPs, but not the reporter mRNA, should show diffuse CP-FP signal in the nucleus only, and no bright single particles. To determine if every mRNA is detectable via live-cell imaging, TRICK can be combined with single-molecule fluorescence in situ hybridization (mRNA FISH). In fixed cells, multiple singly labeled fluorescent FISH probes robustly detect single reporter mRNAs, which should correspond to the same number of mRNAs detected in live cells by CP-FPs. Imaging the entire cell volume in a 3D stack can confirm that every reporter mRNA is fluorescently labeled by coat proteins.

Under steady state conditions in mammalian cells $\approx 6\%$ of our standard reporter mRNAs are untranslated and so fluoresce in both red and green channels, while $\approx 94\%$ of mRNAs are translated and appear in the red channel only. Imaging cells expressing only one CP-FP in both channels should yield no colocalization and controls for fluorophore cross talk. As a positive control for detection of colocalization, both stem-loop cassettes can be inserted into the reporter 3'-UTR, which should result in 100% of mRNAs that fluoresce in both channels independent of translation. This is a particularly useful control for optimizing the colocalization of two-color trajectories from SPT data.

Inhibitors of translation can demonstrate that the TRICK signal (loss of fluorescence from the coding sequence) is translation-dependent and serve as a powerful control. Small-molecule inhibitors affecting different steps of translation can be used as complementary controls (eg, puromycin causes premature termination and cycloheximide halts elongation).



7. TRICK EXPERIMENT IN HeLa CELLS TO DETERMINE FRACTION OF UNTRANSLATED mRNAs

7.1 Preparation of Cells for Live-Cell Imaging

Materials

- Tetracycline-inducible HeLa cells stably expressing NLS-PCP-GFP, NLS-MCP-Halo, and a TRICK reporter mRNA containing PP7 (coding region) and MS2 (noncoding region) stem-loops

- Dulbecco's Modified Eagle Medium (DMEM; Life Technologies, 10566-016) supplemented with 10% (v/v) Tet-free FBS (Clontech, 631106) and 1% (v/v) penicillin and streptomycin (pen/strep)
- 35 mm μ -Dish (Ibidi, 81158)
- Automated cell counter and counting slides (Biorad, D9891-1G)
- Doxycycline (Sigma, D9891-1G)
- JF₅₄₉ (HHMI Janelia Research Campus)

Day 1

1. HeLa cells are grown using standard cell culture techniques as adherent monolayers in DMEM + 10% FBS + 1% Pen/Strep.
2. Prepare a cell suspension of HeLa cells at a density of 20,000 cells mL⁻¹ and ensure dissociation into single cells.
3. Seed 2 mL of cell solution per 35 mm imaging dish. Care should be taken in order to obtain a homogenous distribution of cells within the dish.
4. Incubate 2 days at 37°C and 5% CO₂. Shorter incubation periods are also possible depending on the time it takes for cells to attach and spread on the surface of the imaging dish.

Day 3

1. Prewarm PBS and DMEM + 10% FBS to 37°C.
2. Halo-label cells by addition of 1 mL 100 nM JF₅₄₉ in DMEM + 10% FBS.
3. Return cells to incubator (37°C, 5% CO₂) for 15 min.
4. Remove medium and wash cells 3 × with PBS.
5. Replace medium with 37°C warm DMEM + 10% FBS containing 1 μ g mL⁻¹ doxycycline to induce TRICK reporter expression.

7.2 Image Acquisition

Materials

- Olympus IX81 inverted microscope (Olympus) equipped with a Yokogawa CSU-X1 scanhead (Yokogawa) and Borealis modification (Andor)
- Dichroic beam-splitter in scanhead (Semrock Di01-T488/568-13x15x0.5)
- 100 × 1.45NA PlanApo TIRFM oil immersion objective (Olympus)
- Two back-illuminated EvolveDelta EMCCD cameras (Photometrics)
- Emission filters for GFP (Semrock, FF01-617/73-25) and JF₅₄₉ (Semrock, FF02-525/40-25) fluorescence

- Beam-splitter between cameras (Chroma, 565DCXR)
- Solid-state lasers (100 mW 491 nm and 100 mW 561 nm; Cobolt)
- Motorized X,Y,Z-Piezo controlled stage (ASI)
- Incubation box around microscope providing heating and CO₂ regulation (Life Imaging Services)

Day 3

1. Equilibrate microscope imaging chamber to 37°C and 5% CO₂.
2. Select cells for imaging using MCP-Halo channel by identifying cells that contain well-resolved diffraction-limited particles (spot width ~2 pixels). Image using low laser power to limit photobleaching before acquisition of TRICK data.
3. Simultaneously image cells in both channels using laser powers, camera gain, and exposure times compatible for SPT. Exposure times should be 40–50 ms or less, in order to ensure that fast moving mRNPs can still be unambiguously tracked between subsequent frames. Laser power optimization is a tradeoff: high laser powers result in bright, well-resolved particles that are easier to track, but induce rapid photobleaching. Once adequate exposure and laser power settings have been set, the camera gain should be optimized to provide the largest possible intensity dynamic range without saturating the detector.

7.3 Image Analysis

Materials

- Broad-emitting beads, Tetraspeck microspheres mounted on a slide (ThermoFisher Scientific T-14792)
- ImageJ with TrackMate plugin
- Matlab (Mathworks) software and scripts

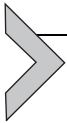
Day 4 (Tracking)

1. Ensure that both channels are precisely registered. Cameras should be aligned prior to image acquisition using multicolor beads mounted on a standard slide. Any residual systematic offset between channels can be corrected using the translate function within ImageJ.
2. Particle tracking can be performed on a small number of frames (typically 3–5) to prevent biasing the analysis toward immobile particles.
3. Define a region of interest for analysis (eg, a single cell, nucleus, or cytoplasm).
4. Filter out randomly distributed noise using the FFT bandpass filter within ImageJ. Filter small objects below 3 pixels to reduce noise.

5. Detect spots using the Laplacian of Gaussian (LoG) detector in TrackMate (ImageJ). Spot size and thresholds should be optimized for detection of single mRNA particles.
6. Detected spots can be joined into trajectories in TrackMate using the linear assignment problem (LAP) tracker. The parameters linking max distance, gap-closing distance, and gap-closing max frame gap should be optimized as necessary to increase or reduce tracking stringency.
7. Use the visual inspector to ensure that particles are appropriately tracked.
8. Export tracking data as a spreadsheet.

Day 4 (Colocalization)

9. Colocalization analysis of trajectories is performed in Matlab (Mathworks) with custom written scripts.
10. Two tracks are considered to be colocalized if at least two spots of the green trajectory are within a pixel in x,y of a red trajectory.
11. Colocalization is then evaluated for accuracy by assessing individual colocalized trajectories.
12. Orphan red channel trajectories are identified as the translated mRNA fraction while the colocalized trajectories represent the mRNA fraction that has remained untranslated.



8. TRICK EXPERIMENT IN *DROSOPHILA*

Maternally deposited mRNAs of *D. melanogaster* encoding embryonic axis determinants such as *oskar*, *bicoid*, *gurken*, and *nanos* are frequently used as model systems to study mRNA transport and translational regulation. In the past, transport of these mRNAs has been successfully studied using transgenic animals expressing MS2-tagged reporter mRNAs (Forrest & Gavis, 2003; Jaramillo, Weil, Goodhouse, Gavis, & Schupbach, 2008; Weil, Forrest, & Gavis, 2006; Zimyanin et al., 2008). However, the insertion of MS2-binding sites has to be planned carefully in order to not destroy important *cis*-regulatory elements that are often located in the 3'-UTR and essential for proper transport and translational control (eg, oocyte entry signal (Jambor, Mueller, Bullock, & Ephrussi, 2014); translational control element (Gavis, Lunsford, Bergsten, & Lehmann, 1996)). Notably, some mRNAs such as *oskar* require splicing for transport and translational control (Ghosh, Marchand, Gaspar, & Ephrussi, 2012; Hachet & Ephrussi, 2004). We therefore always modify genomic DNA fragments.

To show the feasibility of imaging the first round of translation in *Drosophila*, we chose the *oskar* mRNA, which is produced in the nurse cells and transported over a long distance in order to localize to the posterior pole of

the developing oocyte, where it is finally translated. We used a genomic rescuing construct of 6.45 kb (Ephrussi & Lehmann, 1992) in which 6×MS2 loops were inserted into the 3'-UTR (Fig. 3A). This insertion has been previously used to study transport and has been shown to give rise to functional Oskar protein (Lin et al., 2008). Using the endogenous *oskar* promoter ensures that expression of the TRICK reporter is comparable to wild-type levels. In order to generate the functional *osk-TRICK* reporter, we inserted 12×PP7-binding sites in frame into the coding region (Fig. 3A). To generate transgenic animals, the full genomic region was subjected to P element-mediated germline transformation.

In order to provide the coat proteins necessary for labeling of the TRICK mRNA in the nurse cell nuclei, we express NLS-MCP-RFP and NLS-PCP-GFP fusion proteins under the control of a weak maternally active promoter, such as the *hsp83* promoter (Forrest & Gavis, 2003). Importantly, only this moderate expression of the coat proteins ensures no labeling artifacts, as seen by UAS-Gal4 driven constructs that produce nonspecific motile particles even in the absence of MS2-labeled mRNA (Xu, Brechbiel, & Gavis, 2013).

8.1 Imaging and Analysis

Materials

- 1 × PBS
- 16% paraformaldehyde solution (Electron Microscopy Sciences, #15710)
- Tween20 (Sigma, T9284)
- Triton X-100 (Sigma, P1379)
- BSA (bovine serum albumin, Sigma, A2153)
- Glass slides and coverslips
- Mounting solution (eg, Shandon Immu-Mount, Fisher Scientific, 9990402)

Protocol for *Drosophila* Oocytes

1. Dissect ovaries from well-fed female flies expressing *TRICK* mRNA, NLS-MCP-RFP, and NLS-PCP-GFP in 1 × PBS.
2. Replace PBS with fixative (1 × PBS supplemented with 4% paraformaldehyde) and incubate for 20 min.
3. Wash twice with PBST (1 × PBS, 0.1% Tween20).
4. Permeabilize ovaries for 1 h in 1 × PBS with 1% Triton X-100.
5. Wash twice with PBST (1 × PBS, 0.1% Tween20).
6. Block with blocking buffer (1 × PBST with 0.5% BSA) for 30 min.
7. Remove blocking buffer and add primary antibody (eg, anti-Oskar) in blocking buffer for 2 h.

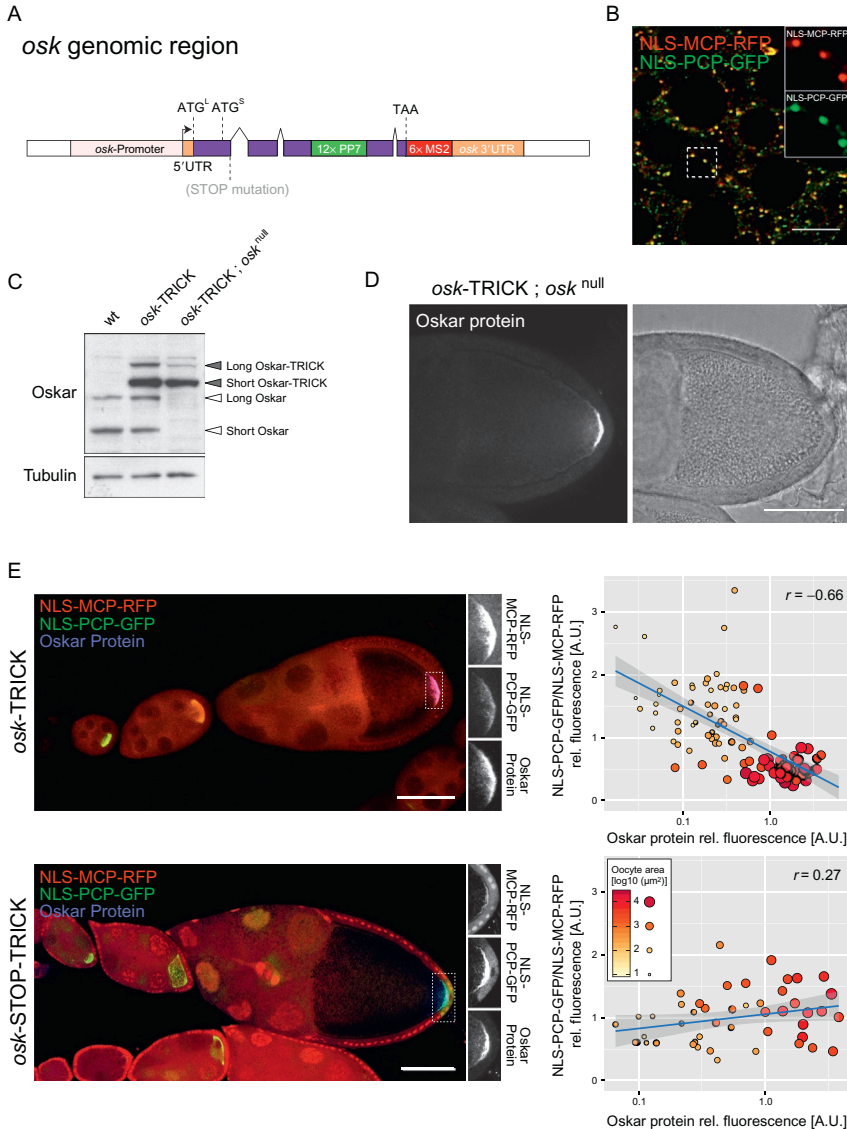


Fig. 3 TRICK in *Drosophila* oocytes. (A) Schematic of a genomic *osk*-TRICK reporter construct. The alternative translational start sites producing the long and short Oskar isoforms (ATG^L and ATG^S), the insertion site of 12×PP7 in the coding region, 6×MS2-binding sites right after the stop codon (TAA), and the position of the stop codon mutation used for control experiments are indicated. (B) Imaging of individual mRNPs in the ooplasm of an egg-chamber expressing *osk*-TRICK mRNA, NLS-MCP-RFP and NLS-PCP-GFP using FP-booster, scale bar 5 μm. (C) Insertion of 12×PP7-binding sites does not disturb translation of *oskar* mRNA. Western blot analysis of ovarian samples

8. Wash three times with PBST.
9. Incubate ovaries with secondary antibody conjugated to fluorophores spectrally distinct from EGFP and TagRFP-T (eg, Cy5, Alexa 647) in blocking buffer for 1 h.
10. Wash three times with PBST.
11. Separate individual egg-chambers, mount them on a glass slide using mounting solution and cover with a coverslip.
12. Acquire images on a standard wide-field or confocal microscope.
13. Images are further processed and the fluorescent signals and oocyte size of individual egg-chambers are measured using ImageJ (<http://rsb.info.nih.gov/ij/>). The ratio of NLS-PCP-GFP per NLS-MCP-RFP is calculated and plotted against the protein signal intensity and oocyte size.

Optional: *Drosophila* egg-chambers are relatively thick (from ~ 50 to $>100 \mu\text{m}$), which can present challenges for imaging. In order to obtain a good SNR, immunostaining with direct-coupled antibodies (eg, Anti-GFP-CF488A (Sigma, SAB4600051), RFP-booster (ChromoTek, rba594-100)) against FPs of the coat proteins can help to overcome this issue in fixed egg-chambers. This allows higher resolution imaging of individual RNA-protein particles containing *osk*-TRICK mRNA by confocal microscopy followed by deconvolution (Fig. 3B). Single-particle analysis can be carried out as described earlier.

8.2 Controls

As a first test for any defects in translation of the TRICK reporter transgenes, we recommend to use western blot analysis to identify the fusion protein derived from the *osk*-TRICK reporter, which appears with an increase in molecular weight of approximately 30 kDa caused by the extra polypeptide sequence derived from the $12\times\text{PP7}$ -binding sites insertion (see Fig. 3C, middle lane). The use of mutant alleles to deplete any wild-type protein

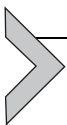
from wild-type flies, flies expressing *osk*-TRICK and *osk*-TRICK in an *osk*^{null} background. (D) Immunostaining against Oskar protein in an egg-chamber expressing *osk*-TRICK in an *osk*^{null} background shows exclusive synthesis of Oskar protein at the posterior pole of the oocyte. (E) Quantification of fluorescent signals from NLS-PCP-GFP/NLS-MCP-RFP, Oskar protein immunostaining and oocyte area (color- and size-coded) of individual oocytes. The correlation of the TRICK reporter readout with Oskar protein and oocyte area observed in *osk*-TRICK expressing egg-chambers (*upper* plot) is abolished by the introduction of the STOP mutation prior the PP7-binding sites (*lower* plot). Pearson correlation coefficient (*r*), scale bars 50 μm .

allows standard immuno-fluorescence techniques and the use of well-established antibodies to detect protein derived exclusively from the TRICK reporter (Fig. 3C, right lane). This is important when considering the use of constructs in which the coding region and the PP7 loops are separated by a self-cleaving 2A peptide, making reporter and wild-type protein difficult to distinguish by mass.

Only at the posterior pole of the oocyte is translational repression of *oskar* mRNA relieved and Oskar protein produced. This process requires a precise orchestration of the transport machinery and translational regulators. Therefore, correct localization of Oskar protein exclusively at the posterior pole is a significant indicator of undisturbed regulation of the localized translation of the TRICK reporter construct. The use of mutant alleles (eg, *osk^{hull}*) and standard immuno-fluorescence allows detection of Oskar protein solely derived from the *oskar*-TRICK reporter mRNA and confirms the correct localization of the protein independent of wild-type transcript and protein (Fig. 3D). This demonstrates that the introduction of PP7- and MS2-binding sites has no impact on the transport, translational repression, and translational activation of *osk*-TRICK mRNA.

Oskar protein first appears during mid-oogenesis (Kim-Ha, Kerr, & Macdonald, 1995), allowing a precise readout of the TRICK reporter performance to report on the translational status of *osk*-TRICK mRNA of individual egg-chambers during different developmental stages. A comparison of oocyte area, fluorescent intensities of Oskar protein immunostaining, and the NLS-PCP-GFP to NLS-MCP-RFP ratio shows the correlation of loss of NLS-PCP-GFP signal with oocyte size and Oskar protein appearance (Fig. 3E). In order to demonstrate that the observed loss of the NLS-PCP-GFP signal in later stage oocytes depends on active translation, introduction of a STOP codon by site-directed mutagenesis upstream of the PP7-binding sites of the *osk*-TRICK mRNA (*osk*-STOP-TRICK) should be used (Fig. 3E). Similar to TRICK experiments in cultured mammalian cells, small-molecule inhibitors of translation can also be used.

TRICK reporter mRNAs can be used to monitor the first round of translation with single mRNP resolution in the animal model system *Drosophila*, a powerful resource with established genetic toolboxes and well-studied examples of localized translation.



9. OUTLOOK

The development of multiple orthogonal fluorescent labeling methodologies for imaging single molecules of RNA in living cells has made it

possible to perform more detailed analyses of RNA metabolism. RNA biosensors, which go beyond simply being able to observe mRNAs, enable direct measurement of specific events in an mRNA's life. We have engineered the TRICK system that reports on the first round of translation, but we envision that conceptually similar approaches may also be applied to mRNA turnover and other aspects of RNA metabolism. These advances coupled to the revolution in genome engineering tools will allow the complete lives of endogenous mRNAs to be imaged in living cells.

ACKNOWLEDGMENTS

This work was supported by the Novartis Research Foundation and the Swiss National Science Foundation (J.A.C); the European Molecular Biology Lab (A.E.); and postdoctoral fellowships from the Peter and Traudl Engelhorn Foundation (J.M.H) and the EMBL Interdisciplinary Postdoc Program (EIPOD) under Marie Curie COFUND actions (F.W.).

REFERENCES

- Aitken, C. E., Marshall, R. A., & Puglisi, J. D. (2008). An oxygen scavenging system for improvement of dye stability in single-molecule fluorescence experiments. *Biophysical Journal*, *94*(5), 1826–1835.
- Bertrand, E., Chartrand, P., Schaefer, M., Shenoy, S. M., Singer, R. H., & Long, R. M. (1998). Localization of ASH1 mRNA particles in living yeast. *Molecular Cell*, *2*(4), 437–445.
- Chao, J. A., Patskovsky, Y., Almo, S. C., & Singer, R. H. (2008). Structural basis for the coevolution of a viral RNA-protein complex. *Nature Structural & Molecular Biology*, *15*(1), 103–105.
- Chen, J., Nikolaitchik, O., Singh, J., Wright, A., Bencsics, C. E., Coffin, J. M., ... Hu, W. S. (2009). High efficiency of HIV-1 genomic RNA packaging and heterozygote formation revealed by single virion analysis. *Proceedings of the National Academy of Sciences of the United States of America*, *106*(32), 13535–13540.
- Chenouard, N., Smal, I., de Chaumont, F., Maska, M., Sbalzarini, I. F., Gong, Y., ... Meijering, E. (2014). Objective comparison of particle tracking methods. *Nature Methods*, *11*(3), 281–289.
- Cho, S., Jang, J., Song, C., Lee, H., Ganesan, P., Yoon, T. Y., ... Park, Y. (2013). Simple super-resolution live-cell imaging based on diffusion-assisted Forster resonance energy transfer. *Scientific Reports*, *3*, 1208.
- Coulon, A., Ferguson, M. L., de Turrís, V., Palangat, M., Chow, C. C., & Larson, D. R. (2014). Kinetic competition during the transcription cycle results in stochastic RNA processing. *Elife*, *3*, e03939.
- Daigle, N., & Ellenberg, J. (2007). LambdaN-GFP: An RNA reporter system for live-cell imaging. *Nature Methods*, *4*(8), 633–636.
- David, A., Dolan, B. P., Hickman, H. D., Knowlton, J. J., Clavarino, G., Pierre, P., ... Yewdell, J. W. (2012). Nuclear translation visualized by ribosome-bound nascent chain puromycylation. *The Journal of Cell Biology*, *197*(1), 45–57.
- Deschout, H., Martens, T., Vercauteren, D., Remaut, K., Demeester, J., De Smedt, S. C., ... Braeckmans, K. (2013). Correlation of dual colour single particle trajectories for improved detection and analysis of interactions in living cells. *International Journal of Molecular Sciences*, *14*(8), 16485–16514.

- Dieterich, D. C., Hodas, J. J., Gouzer, G., Shadrin, I. Y., Ngo, J. T., Triller, A., ... Schuman, E. M. (2010). In situ visualization and dynamics of newly synthesized proteins in rat hippocampal neurons. *Nature Neuroscience*, *13*(7), 897–905.
- Dupont, A., Stirnagel, K., Lindemann, D., & Lamb, D. C. (2013). Tracking image correlation: Combining single-particle tracking and image correlation. *Biophysical Journal*, *104*(11), 2373–2382.
- Ephrussi, A., & Lehmann, R. (1992). Induction of germ cell formation by oskar. *Nature*, *358*(6385), 387–392.
- Espenel, C., Margeat, E., Dosset, P., Arduise, C., Le Grimellec, C., Royer, C. A., ... Milhiet, P. E. (2008). Single-molecule analysis of CD9 dynamics and partitioning reveals multiple modes of interaction in the tetraspanin web. *The Journal of Cell Biology*, *182*(4), 765–776.
- Forrest, K. M., & Gavis, E. R. (2003). Live imaging of endogenous RNA reveals a diffusion and entrapment mechanism for nanos mRNA localization in *Drosophila*. *Current Biology*, *13*(14), 1159–1168.
- Fusco, D., Accornero, N., Lavoie, B., Shenoy, S. M., Blanchard, J. M., Singer, R. H., & Bertrand, E. (2003). Single mRNA molecules demonstrate probabilistic movement in living mammalian cells. *Current Biology*, *13*(2), 161–167.
- Gautier, A., Juillerat, A., Heinis, C., Correa, I. R., Kindermann, M., Beaufils, F., & Johnsson, K. (2008). An engineered protein tag for multiprotein labeling in living cells. *Chemistry & Biology*, *15*(2), 128–136.
- Gavis, E. R., Lunsford, L., Bergsten, S. E., & Lehmann, R. (1996). A conserved 90 nucleotide element mediates translational repression of nanos RNA. *Development*, *122*(9), 2791–2800.
- Gerhardt, I., Mai, L., Lamas-Linares, A., & Kurtsiefer, C. (2011). Detection of single molecules illuminated by a light-emitting diode. *Sensors (Basel)*, *11*(1), 905–916.
- Ghosh, S., Marchand, V., Gaspar, I., & Ephrussi, A. (2012). Control of RNP motility and localization by a splicing-dependent structure in oskar mRNA. *Nature Structural & Molecular Biology*, *19*(4), 441–449.
- Gossen, M., Freundlieb, S., Bender, G., Muller, G., Hillen, W., & Bujard, H. (1995). Transcriptional activation by tetracyclines in mammalian cells. *Science*, *268*(5218), 1766–1769.
- Grimm, J. B., English, B. P., Chen, J., Slaughter, J. P., Zhang, Z., Revyakin, A., & Lavis, L. D. (2015). A general method to improve fluorophores for live-cell and single-molecule microscopy. *Nature Methods*, *12*(3), 244–250. 243 pp. following 250 pp.
- Grunwald, D., & Singer, R. H. (2010). In vivo imaging of labelled endogenous beta-actin mRNA during nucleocytoplasmic transport. *Nature*, *467*(7315), 604–607.
- Hachet, O., & Ephrussi, A. (2004). Splicing of oskar RNA in the nucleus is coupled to its cytoplasmic localization. *Nature*, *428*(6986), 959–963.
- Halstead, J. M., Lionnet, T., Wilbertz, J. H., Wippich, F., Ephrussi, A., Singer, R. H., & Chao, J. A. (2015). Translation. An RNA biosensor for imaging the first round of translation from single cells to living animals. *Science*, *347*(6228), 1367–1671.
- Higashida, C., Suetsugu, S., Tsuji, T., Monypenny, J., Narumiya, S., & Watanabe, N. (2008). G-actin regulates rapid induction of actin nucleation by mDia1 to restore cellular actin polymers. *Journal of Cell Science*, *121*(Pt. 20), 3403–3412.
- Hocine, S., Raymond, P., Zenklusen, D., Chao, J. A., & Singer, R. H. (2013). Single-molecule analysis of gene expression using two-color RNA labeling in live yeast. *Nature Methods*, *10*(2), 119–121.
- Holt, C. E., & Schuman, E. M. (2013). The central dogma decentralized: New perspectives on RNA function and local translation in neurons. *Neuron*, *80*(3), 648–657.
- Ifrim, M. F., Williams, K. R., & Bassell, G. J. (2015). Single-molecule imaging of PSD-95 mRNA translation in dendrites and its dysregulation in a mouse model of fragile

- X syndrome. *The Journal of Neuroscience*, 35(18), 7116–7130. <http://dx.doi.org/10.1523/JNEUROSCI.2802-14.2015>.
- Ingolia, N. T., Ghaemmaghani, S., Newman, J. R., & Weissman, J. S. (2009). Genome-wide analysis in vivo of translation with nucleotide resolution using ribosome profiling. *Science*, 324(5924), 218–223.
- Ishigaki, Y., Li, X., Serin, G., & Maquat, L. E. (2001). Evidence for a pioneer round of mRNA translation: mRNAs subject to nonsense-mediated decay in mammalian cells are bound by CBP80 and CBP20. *Cell*, 106(5), 607–617.
- Jambor, H., Mueller, S., Bullock, S. L., & Ephrussi, A. (2014). A stem-loop structure directs oskar mRNA to microtubule minus ends. *RNA*, 20(4), 429–439.
- Jan, C. H., Williams, C. C., & Weissman, J. S. (2014). Principles of ER cotranslational translocation revealed by proximity-specific ribosome profiling. *Science*, 346(6210), 1257521.
- Jaramillo, A. M., Weil, T. T., Goodhouse, J., Gavis, E. R., & Schupbach, T. (2008). The dynamics of fluorescently labeled endogenous gurken mRNA in *Drosophila*. *Journal of Cell Science*, 121(Pt. 6), 887–894.
- Juillerat, A., Gronemeyer, T., Keppler, A., Gendreizig, S., Pick, H., Vogel, H., & Johnson, K. (2003). Directed evolution of O-6-alkylguanine-DNA alkyltransferase for efficient labeling of fusion proteins with small molecules in vivo. *Chemistry & Biology*, 10(4), 313–317.
- Kim, J. H., Lee, S. R., Li, L. H., Park, H. J., Park, J. H., Lee, K. Y., ... Choi, S. Y. (2011). High cleavage efficiency of a 2A peptide derived from porcine teschovirus-1 in human cell lines, zebrafish and mice. *PloS One*, 6(4), e18556.
- Kim-Ha, J., Kerr, K., & Macdonald, P. M. (1995). Translational regulation of oskar mRNA by bruno, an ovarian RNA-binding protein, is essential. *Cell*, 81(3), 403–412.
- Koyama-Honda, I., Ritchie, K., Fujiwara, T., Iino, R., Murakoshi, H., Kasai, R. S., & Kusumi, A. (2005). Fluorescence imaging for monitoring the colocalization of two single molecules in living cells. *Biophysical Journal*, 88(3), 2126–2136.
- Kremers, G. J., Gilbert, S. G., Cranfill, P. J., Davidson, M. W., & Piston, D. W. (2011). Fluorescent proteins at a glance. *Journal of Cell Science*, 124(Pt. 2), 157–160.
- Kumano, G. (2012). Polarizing animal cells via mRNA localization in oogenesis and early development. *Development, Growth & Differentiation*, 54(1), 1–18.
- Kuo, J. S., Kuyper, C. L., Allen, P. B., Fiorini, G. S., & Chiu, D. T. (2004). High-power blue/UV light-emitting diodes as excitation sources for sensitive detection. *Electrophoresis*, 25(21–22), 3796–3804.
- Larson, D. R., Zenklusen, D., Wu, B., Chao, J. A., & Singer, R. H. (2011). Real-time observation of transcription initiation and elongation on an endogenous yeast gene. *Science*, 332(6028), 475–478.
- Liao, G., Mingle, L., Van De Water, L., & Liu, G. (2015). Control of cell migration through mRNA localization and local translation. *Wiley Interdisciplinary Reviews. RNA*, 6(1), 1–15.
- Lin, M. D., Jiao, X., Grima, D., Newbury, S. F., Kiledjian, M., & Chou, T. B. (2008). *Drosophila* processing bodies in oogenesis. *Developmental Biology*, 322(2), 276–288.
- Lionnet, T., Czaplinski, K., Darzacq, X., Shav-Tal, Y., Wells, A. L., Chao, J. A., ... Singer, R. H. (2011). A transgenic mouse for in vivo detection of endogenous labeled mRNA. *Nature Methods*, 8(2), 165–170.
- Los, G. V., Encell, L. P., McDougall, M. G., Hartzell, D. D., Karassina, N., Zimprich, C., ... Wood, K. V. (2008). HatoTag: A novel protein labeling technology for cell imaging and protein analysis. *ACS Chemical Biology*, 3(6), 373–382.
- Ma, J., Liu, Z., Michelotti, N., Pitchiaya, S., Veerapaneni, R., Androsavich, J. R., ... Yang, W. (2013). High-resolution three-dimensional mapping of mRNA export through the nuclear pore. *Nature Communications*, 4, 2414.

- Magidson, V., & Khodjakov, A. (2013). Circumventing photodamage in live-cell microscopy. *Methods in Cell Biology*, *114*, 545–560.
- Martin, R. M., Rino, J., Carvalho, C., Kirchhausen, T., & Carmo-Fonseca, M. (2013). Live-cell visualization of pre-mRNA splicing with single-molecule sensitivity. *Cell Reports*, *4*(6), 1144–1155.
- Mizuguchi, H., Xu, Z., Ishii-Watabe, A., Uchida, E., & Hayakawa, T. (2000). IRES-dependent second gene expression is significantly lower than cap-dependent first gene expression in a bicistronic vector. *Molecular Therapy*, *1*(4), 376–382.
- Mor, A., Suliman, S., Ben-Yishay, R., Yunger, S., Brody, Y., & Shav-Tal, Y. (2010). Dynamics of single mRNP nucleocytoplasmic transport and export through the nuclear pore in living cells. *Nature Cell Biology*, *12*(6), 543–552.
- No, D., Yao, T. P., & Evans, R. M. (1996). Ecdysone-inducible gene expression in mammalian cells and transgenic mice. *Proceedings of the National Academy of Sciences of the United States of America*, *93*(8), 3346–3351.
- Pan, D., Kirillov, S. V., & Cooperman, B. S. (2007). Kinetically competent intermediates in the translocation step of protein synthesis. *Molecular Cell*, *25*(4), 519–529.
- Park, H. Y., Buxbaum, A. R., & Singer, R. H. (2010). Single mRNA tracking in live cells. *Methods in Enzymology*, *472*, 387–406.
- Park, H. Y., Lim, H., Yoon, Y. J., Follenzi, A., Nwokafor, C., Lopez-Jones, M., ... Singer, R. H. (2014). Visualization of dynamics of single endogenous mRNA labeled in live mouse. *Science*, *343*(6169), 422–424.
- Parthasarathy, R. (2012). Rapid, accurate particle tracking by calculation of radial symmetry centers. *Nature Methods*, *9*(7), 724–726.
- Qin, J. Y., Zhang, L., Clift, K. L., Hular, I., Xiang, A. P., Ren, B. Z., & Lahn, B. T. (2010). Systematic comparison of constitutive promoters and the doxycycline-inducible promoter. *PLoS One*, *5*(5), e10611.
- Rabut, G., & Ellenberg, J. (2004). Automatic real-time three-dimensional cell tracking by fluorescence microscopy. *Journal of Microscopy*, *216*(Pt. 2), 131–137.
- Rasnik, I., McKinney, S. A., & Ha, T. (2006). Nonblinking and long-lasting single-molecule fluorescence imaging. *Nature Methods*, *3*(11), 891–893.
- Shaner, N. C., Lin, M. Z., McKeown, M. R., Steinbach, P. A., Hazelwood, K. L., Davidson, M. W., & Tsien, R. Y. (2008). Improving the photostability of bright monomeric orange and red fluorescent proteins. *Nature Methods*, *5*(6), 545–551.
- Shaner, N. C., Steinbach, P. A., & Tsien, R. Y. (2005). A guide to choosing fluorescent proteins. *Nature Methods*, *2*(12), 905–909.
- Shav-Tal, Y., Darzacq, X., Shenoy, S. M., Fusco, D., Janicki, S. M., Spector, D. L., & Singer, R. H. (2004). Dynamics of single mRNPs in nuclei of living cells. *Science*, *304*(5678), 1797–1800.
- Smith, C. S., Preibisch, S., Joseph, A., Abrahamsson, S., Rieger, B., Myers, E., ... Grunwald, D. (2015). Nuclear accessibility of beta-actin mRNA is measured by 3D single-molecule real-time tracking. *The Journal of Cell Biology*, *209*(4), 609–619.
- Spille, J. H., Kaminski, T. P., Scherer, K., Rinne, J. S., Heckel, A., & Kubitscheck, U. (2015). Direct observation of mobility state transitions in RNA trajectories by sensitive single molecule feedback tracking. *Nucleic Acids Research*, *43*(2), e14.
- Steitz, J. A. (1969). Nucleotide sequences of the ribosomal binding sites of bacteriophage R17 RNA. *Cold Spring Harbor Symposia on Quantitative Biology*, *34*, 621–630.
- Takizawa, P. A., & Vale, R. D. (2000). The myosin motor, Myo4p, binds Ash1 mRNA via the adapter protein, She3p. *Proceedings of the National Academy of Sciences of the United States of America*, *97*(10), 5273–5278.
- Tatavarty, V., Ifrim, M. F., Levin, M., Korza, G., Barbarese, E., Yu, J., & Carson, J. H. (2012). Single-molecule imaging of translational output from individual RNA granules in neurons. *Molecular Biology of the Cell*, *23*(5), 918–929.

- Terskikh, A., Fradkov, A., Ermakova, G., Zaraisky, A., Tan, P., Kajava, A. V., ... Siebert, P. (2000). "Fluorescent timer": Protein that changes color with time. *Science*, 290(5496), 1585–1588.
- Thompson, R. E., Larson, D. R., & Webb, W. W. (2002). Precise nanometer localization analysis for individual fluorescent probes. *Biophysical Journal*, 82(5), 2775–2783.
- Tokunaga, M., Imamoto, N., & Sakata-Sogawa, K. (2008). Highly inclined thin illumination enables clear single-molecule imaging in cells. *Nature Methods*, 5(2), 159–161.
- Urbanek, M. O., Galka-Marciniak, P., Olejniczak, M., & Krzyzosiak, W. J. (2014). RNA imaging in living cells—Methods and applications. *RNA Biology*, 11(8), 1083–1095.
- Vigers, G. P., Coue, M., & McIntosh, J. R. (1988). Fluorescent microtubules break up under illumination. *The Journal of Cell Biology*, 107(3), 1011–1024.
- Weidenfeld, I., Gossen, M., Low, R., Kentner, D., Berger, S., Gorlich, D., ... Schonig, K. (2009). Inducible expression of coding and inhibitory RNAs from retargetable genomic loci. *Nucleic Acids Research*, 37(7), e50.
- Weil, T. T., Forrest, K. M., & Gavis, E. R. (2006). Localization of bicoid mRNA in late oocytes is maintained by continual active transport. *Developmental Cell*, 11(2), 251–262.
- Widengren, J., Chmyrov, A., Eggeling, C., Lofdahl, P. A., & Seidel, C. A. (2007). Strategies to improve photostabilities in ultrasensitive fluorescence spectroscopy. *The Journal of Physical Chemistry. A*, 111(3), 429–440.
- Wu, B., Chao, J. A., & Singer, R. H. (2012). Fluorescence fluctuation spectroscopy enables quantitative imaging of single mRNAs in living cells. *Biophysical Journal*, 102(12), 2936–2944.
- Wu, B., Miskolci, V., Sato, H., Tutucci, E., Kenworthy, C. A., Donnelly, S. K., ... Hodgson, L. (2015). Synonymous modification results in high-fidelity gene expression of repetitive protein and nucleotide sequences. *Genes & Development*, 29(8), 876–886.
- Xia, T., Li, N., & Fang, X. (2013). Single-molecule fluorescence imaging in living cells. *Annual Review of Physical Chemistry*, 64, 459–480.
- Xu, X., Brechbiel, J. L., & Gavis, E. R. (2013). Dynein-dependent transport of nanos RNA in *Drosophila* sensory neurons requires Rumpelstiltskin and the germ plasm organizer Oskar. *The Journal of Neuroscience*, 33(37), 14791–14800.
- Yu, J., Xiao, J., Ren, X., Lao, K., & Xie, X. S. (2006). Probing gene expression in live cells, one protein molecule at a time. *Science*, 311(5767), 1600–1603.
- Zimyanin, V. L., Belaya, K., Pecreaux, J., Gilchrist, M. J., Clark, A., Davis, I., & St Johnston, D. (2008). In vivo imaging of oskar mRNA transport reveals the mechanism of posterior localization. *Cell*, 134(5), 843–853.
- Zuker, M. (2003). Mfold web server for nucleic acid folding and hybridization prediction. *Nucleic Acids Research*, 31(13), 3406–3415.

Chapter 6: Thesis summary and future research perspectives

The work presented in this PhD thesis sheds light on the spatio-temporal dynamics of mRNAs during the stress response in human cells (Fig. 1). The application of the TRICK translation biosensor showed that mRNA can be locally repressed inside of PBs under specific conditions, such as the recovery from stress. Using single molecule imaging, tracking and colocalization approaches, the dynamical movements of mRNAs relative to PBs and SGs were quantified during stress. Reporter mRNA localization was found to depend the 5'UTR *cis*-acting TOP element. The RBP LARP1 partially controls TOP mRNA localization inside of PBs and SGs. This quantitative knowledge about mRNA localization during stress in combination with functional single molecule mRNA imaging of translation, allowed us to draw conclusions about the relevance of PB and SG localization for mRNA biology. Overall, mRNAs seem to translate well and are not subject to rapid decay during the relief from stress even though they did not spend a significant time in stress-induced granules (Fig. 1). To address potential RNA-independent functions of stress-induced mRNP complexes we performed a small molecule-based screen and identified several negative SG modulators. Most increased apoptosis when added during the stress response.

In summary, the technical approaches used and partially developed during this PhD project have the sensitivity to detect subcellular differences in mRNA decay and translation in living cells. For the majority of transcripts, the obtained evidence points towards granule-independent mRNA expression regulation during and after the stress response. Further, SGs might have important RNA-independent functions for apoptosis regulation.

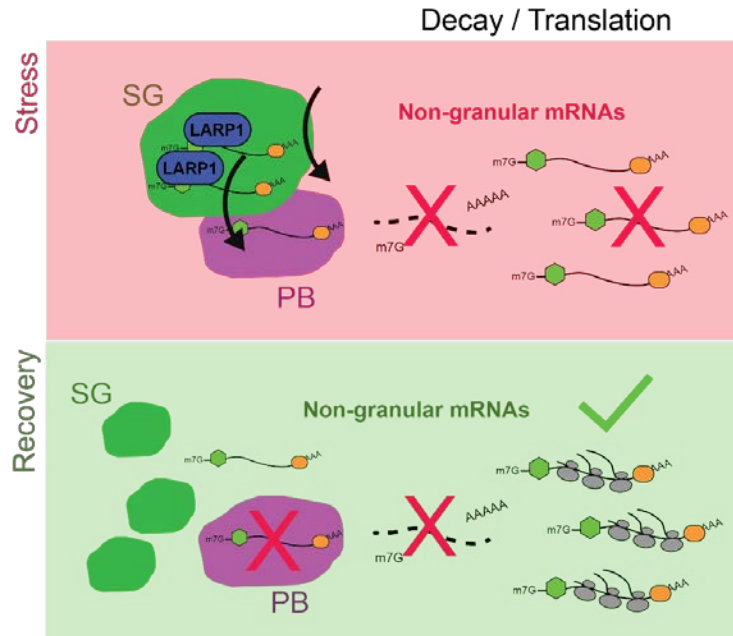


Fig. 1: mRNA interactions with stress-induced RNA-protein granules are regulated and mRNA expression regulation during stress and recovery is independent of RNA localization relative to granules. During stress, mRNAs do not undergo decay and are translationally repressed, regardless of their localization. *Cis*- and *trans*-acting factors determine RNA interaction patterns with stress granules (SGs) and processing bodies (PBs), although the majority of mRNAs localize outside of granules. During the recovery from stress, non-granule localized mRNAs do not undergo rapid decay and translate normally. mRNAs present in PBs remain translationally repressed. In summary, SGs and PBs do not seem to exert a permanent RNA storage or protection function since the majority of RNAs are unaffected by localization patterns.

Technical considerations

One key technical limitations of live cell single molecule approaches presented here are the short imaging time windows. Photobleaching becomes an important aspect of every experiment, when mRNAs are imaged for > 30 seconds. This is especially true for functional single molecule mRNA imaging where the loss of a fluorescent signal can lead to faulty conclusions. Short imaging time frames might also restrict the direct observation of transition events between SGs and PBs or the direct observation of localized decay or translation if those processes take significantly longer than the available imaging time. Furthermore, the current optical setup of most confocal or TIRF microscopes restricts fast imaging necessary for RNA tracking to a single z-plane. Rapidly diffusing RNAs, such as non-granular ones, are easily lost after a few imaging frames. Particularly in our case, it would be an enormous achievement if single mRNA could be tracked for extended periods of time. This would for example allow the direct assessment of granule effect on mRNAs. Does even brief granule localization have an effect on translation fidelity or decay rates? Do long mRNA residence times in granule correlate with a biological

effect? Such questions can currently not be answered and will require the significant improvement of chemical dyes and microscopy systems. Protein-bound chemical dyes with higher photon yield or lower activation threshold would increase brightness and therefore imaging times. Further, microscopy systems which can scan in the z-direction over extended periods of time are required. Technically the construction of such microscopes is already possible, but has not become the standard yet. Furthermore, the emergence of the CRISPR/Cas9 system will likely revolutionize live cell single molecule imaging. Although repurposed fluorescently tagged Cas9 can be used to target and image endogenous mRNAs, it currently lacks single molecule resolution (Nelles et al., 2016). Using CRISPR/Cas9 for the integration of MS2 or PP7 stemloop cassettes into endogenous genes has already been used (Pichon et al., 2016) and will further strengthen the physiological relevance of single molecule imaging studies in the future. In addition, the advent of organoid systems or intravital single molecules imaging will help to understand how different cells within solid tumors or complex organs regulate RNA biology in a spatio-temporal manner. Although single-cell RNA sequencing and ribosome profiling have made significant technical progress, single molecule imaging will remain a fractionation-, purification-, crosslinking-, and population-independent key method to assess the subcellular localization, temporal dynamics and gene expression regulation of single transcripts in their native environment.

Biological considerations

Although data concerning SGs in disease or mRNA regulation contexts exists (Anderson et al., 2015, Decker and Parker, 2012), most of it is of correlative nature and strong causal links are often missing. This limitation seems to be mainly due to two factors. First, it is technically and experimentally challenging to separate a biomolecular function from its localization. Gain of function or SG-tethering experiments often only capture a minor fraction of a molecule of interest, while the majority of non-tethered molecules might still exert a different and more dominant function in the surrounding cytosol. The high-resolution quantification of protein and mRNA localization is therefore necessary to estimate the extent to which an observed granule-related effect also occurs outside of the granule. In addition, the depletion of endogenous proteins through CRISPR/Cas9 or RNAi while at the same time expressing codon-optimized degradation-resistant reporters of the same gene might be one way to experimentally shift reaction equilibria between cytosol and SGs to study their function. For example, a given well-characterized SG-resident protein could be mutated in a way that its catalytic function is still active, while localization to SGs is inhibited. Depleting its endogenous counterpart, which is catalytically active and localizes to SGs, would then allow a clear localization-based separation of function of the candidate protein.

The second reason SG physiology is hard to study, is that loss of function experiments such as knockdowns or SG dissolution/inhibition experiments always influence secondary pathways which might drastically obscure SG functioning. Since SGs are transient structures, no RNA or protein can be regarded as “exclusively SG specific”. Knockout, knockdown or overexpression experiments to induce or inhibit SG formation can therefore easily influence other cellular processes. For example, PABP levels might influence RNA stability and translation, which will feedback to SGs causing a variation of the “chicken and egg” problem that will make it hard to deduce cause and effect. Also small molecule-induced SG formation through translation initiation blocking or the induction of SG dissolution through translation elongation blocking are unfortunately not very elegant ways to perturb granule biology. Secondary effects are difficult to control for when fundamental biological processes, such as translation, are affected. It will therefore be necessary to identify small molecules that can specifically target SG stability or formation without any or only minor off-target effects. Targeting LCD-driven phase separation processes during SG formation by shielding the molecular interactions of LCDs from each other could be one entry point.

How will the SG and PB field develop in the future? Presumably, the answer to this question will mainly revolve around the characterization of granule heterogeneity and the resulting evidences for relevant physiological functions of SGs in different biological contexts. SGs and PBs seem to be less important for the localized regulation of mRNA biology than previously thought. Despite this, studying specifically highly enriched transcripts while excluding “out-of-granule” regulation (see above) might lead to significant insights. A second promising field seems to be the role of SGs for multiple cell biological processes. Signaling (Kedersha et al., 2013), apoptosis regulation (Arimoto et al., 2008), (Grabocka and Bar-Sagi, 2016) and nucleo-cytoplasmic protein shuttling in neurological diseases (Zhang et al., 2018) have all been shown to be subject to SG-linked regulation. However, it will be crucial to establish direct and testable links with mRNP granules. Third, the phase separation and core-shell models for SG architecture will be tested more extensively in the future. In particular, it will be interesting to see to what extent RNA seeds granule cores and whether phase separation already plays a role during these early events. For an increased understanding of SG-formation, it will also be necessary to move from *in vitro* experiments into animal models. It will especially be important to study the physiologically relevant time scales for SG and PB formation and disassembly in neurons and tumors. An increased understanding of the biology of stress-induced mRNP granules could also have significant medical implications. Boosting or inhibiting SG and PB formation with combinatorial drug treatments might make viral infections and tumors more susceptible to treatment.

References

- Anderson, P., Kedersha, N., and Ivanov, P. (2015). Stress granules, P-bodies and cancer. *Biochim. Biophys. Acta BBA - Gene Regul. Mech.* *1849*, 861–870.
- Arimoto, K., Fukuda, H., Imajoh-Ohmi, S., Saito, H., and Takekawa, M. (2008). Formation of stress granules inhibits apoptosis by suppressing stress-responsive MAPK pathways. *Nat. Cell Biol.* *10*, 1324–1332.
- Decker, C.J., and Parker, R. (2012). P-bodies and stress granules: possible roles in the control of translation and mRNA degradation. *Cold Spring Harb. Perspect. Biol.* *4*, a012286.
- Grabocka, E., and Bar-Sagi, D. (2016). Mutant KRAS Enhances Tumor Cell Fitness by Upregulating Stress Granules. *Cell* *167*, 1803–1813.e12.
- Kedersha, N., Ivanov, P., and Anderson, P. (2013). Stress granules and cell signaling: more than just a passing phase? *Trends Biochem. Sci.* *38*, 494–506.
- Nelles, D.A., Fang, M.Y., O'Connell, M.R., Xu, J.L., Markmiller, S.J., Doudna, J.A., and Yeo, G.W. (2016). Programmable RNA Tracking in Live Cells with CRISPR/Cas9. *Cell* *165*, 488–496.
- Pichon, X., Bastide, A., Safieddine, A., Chouaib, R., Samacoits, A., Basyuk, E., Peter, M., Mueller, F., and Bertrand, E. (2016). Visualization of single endogenous polysomes reveals the dynamics of translation in live human cells. *J Cell Biol* jcb.201605024.
- Zhang, K., Daigle, J.G., Cunningham, K.M., Coyne, A.N., Ruan, K., Grima, J.C., Bowen, K.E., Wadhwa, H., Yang, P., Rigo, F., et al. (2018). Stress Granule Assembly Disrupts Nucleocytoplasmic Transport. *Cell* *0*.

Acknowledgements

First and foremost, I would like to thank my PhD project mentor Jeffrey Chao. I profited enormously from his technical expertise, extensive knowledge of RNA biology, and daily guidance. The door to his office is literally “always open” and I thoroughly enjoyed all the small and big scientific discussions we had. His interdisciplinary view on science and specifically on RNA biology has been an incredible driver for exciting experiments and a fantastic learning experience.

Further, I am grateful to my thesis advisory committee members Susan Gasser and Georg Stoecklin. Both were very helpful during thesis committee meetings and helped me to see the “bigger picture”. I also would like to thank Witold Filipowicz, who joined for some committee meetings. His expertise in RNA biology is an enormous resource and I am glad he shared it with me.

Importantly, I would also like to thank all current and past members of the Chao lab. The friendly, fair and collaborative atmosphere is hard to beat! Especially, I want to thank James for being a great colleague and fun collaborator during the work on the TRICK paper. I also want to thank Ivana for being such a helpful fellow PhD student and colleague. You made me feel welcome from Day 1. And thank you Franka. Working together with you during the last third of my PhD was extremely helpful and I learned a lot. The speed at which you mastered new analysis approaches, the thoroughness of your work and your positive attitude made it a pleasure to join forces with you.

I would also like to thank everyone at the FMI for providing such a stimulating and high-level environment. Caretakers, administrative staff (thank you, Elida!), and facilities take their tasks very seriously. In particular, I profited from all the expertise in the FAIM facility. Thank you Steve Bourke, Raphaël Thierry and especially Laurent Gelman and Jan Eglinger for lots of technical and analysis support even for the smallest of problems. And also the big ones were all solved. I also do not want to forget Hubertus Kohler. His expertise of FACS and meticulous approach provided the basis for all cell lines I used during this PhD. Sorry for always “sorting low”. Thank you all!

Thank you “old reps”! Organizing two PhD student retreats with more than 100 participants while being a FMI PhD student representative was great fun, some work and an enriching experience.

Next to work, all my fellow “first year” year PhD students became good friends. Someone was always available for a chat and a relaxed evening. Thank you. I would also like to thank all the sportive scientists at FMI for joining me on countless “Wiese-loop” runs, climbs in K7, bike rides or Rhine swims. Kudos to you all.

Seit meiner Kindheit ermutigten mich meine Eltern immer neugierig zu sein und alles im Detail zu erforschen. Sie unterstützten mich immer bei dem, was ich als nächstes machen wollte, auch wenn es lange Abwesenheitszeiten oder Nachrichtenmangel bedeutete. Die Erziehung, gleichzeitig offen und kritisch zu sein, hat mich zu dem gemacht, was ich heute bin. Ich bin genau da, wo ich sein möchte. Ich danke euch hierfür und freue mich auf die Zukunft!

Un vendredi soir au 5ème étage, j'ai parlé à Anaïs pour la première fois. Je pense que nous sommes très bien complétés depuis lors. Et maintenant il est temps pour un nouveau chapitre, mais ensemble.

Curriculum vitae

Johannes Wilbertz was born in Aachen, Germany in 1988. He attended high school in Stolberg (Rheinland), Germany and Big Timber, MT, USA. After graduation in 2007, he performed his civil service duty in the Alexianer Hospital for Psychiatry and Neurology in Aachen, Germany. He received his Bachelor of Science (B.Sc.) degree in Biomedicine from Radboud University in Nijmegen, The Netherlands in 2011, followed by a Master of Science (M.Sc.) degree in Molecular Biology & Biotechnology obtained from the University of Groningen, The Netherlands in 2013. He performed the first part of his master thesis research in the laboratory of Professor Arnold Driessen in Groningen on the SecA2 protein, relevant for protein export in bacteria. The second part of his master thesis was completed in the laboratory of Professor Joseph Loparo at Harvard Medical School, Boston, MA, USA using in vitro single molecule imaging of polymerase switching during the synthesis of DNA from a lesion template. In September 2013, he started his PhD project on subcellular mRNA dynamics and translation regulation during cell stress in the laboratory of Dr. Jeffrey Chao at the Friedrich Miescher Institute for Biomedical Research (affiliated with the University of Basel) in Basel, Switzerland.

Contact details:

Johannes Wilbertz

Bärenfelsenstrasse 11

CH-4057 Basel

johannes.wilbertz@fmi.ch

jwilbertz@gmail.com

